2015

The gastrointestinal uptake of titanium dioxide nanoparticles: Studies on Caco-2 cells, perfused intestine and in vivo dietary intake in the rat (Rattus norvegicus)

Gitrowski, Constantinos

Copyright Statement

The gastrointestinal uptake of titanium dioxide nanoparticles: Studies on Caco-2 cells, perfused intestine and *in vivo* dietary intake in the rat (*Rattus norvegicus*)

By

Constantinos Gitrowski

A thesis submitted to Plymouth University in partial fulfilment for the degree of

Doctor of Philosophy

School of Biological Sciences

Faculty of Science and Environment

February 2015

The gastrointestinal uptake of titanium dioxide nanoparticles: Studies on Caco-2 cells, perfused intestine and *in vivo* dietary intake in the rat (*Rattus norvegicus*)

Abstract

The use of nanomaterials (NMs) in orally ingestible products raises concerns about potential hazards. Titanium dioxide (TiO_2) particles (of which some are incidentally produced at the nanoscale) are used in cosmetics, biological remediation (photo-catalysis), toothpastes, ingestible pharmaceuticals and food products. The increased surface area to mass ratio of nanoparticles (NPs) potentially makes them more biologically reactive than their coarser (bulk) material counterparts. There is limited data available on the uptake kinetics across the mammalian gastrointestinal tract, and the potential hazard posed to humans. In this study, the uptake and accumulation of TiO_2 (nano and bulk) into and across the human intestinal cell line, the isolated perfused rat jejunum and the whole rat were evaluated. Caco-2 monolayers exhibited time-dependent, accumulation, uptake and transport of Ti/TiO_2 from TiO_2 exposures of 1 mg L^{-1} over 24 h, which was influenced by the crystal type, irrespective of cell maturity and growth substrate (Chapters 2-3). Electron micrographs of the Caco-2 monolayer showed the presence of particles inside the cells within vesicles and energy dispersive spectroscopy (EDS) confirmed the composition as TiO_2. Addition of pharmacological inhibitors altered the Ti concentration in the cells suggesting diffusion is not the primary mechanism of uptake, rather, an active process is responsible (Chapter 2). Whole gut sacs exposures of 1 mg L^{-1} bulk or nano TiO_2 demonstrated the primary regions of the gut associated with accumulation are the small and large intestine, with 70 % or more of

the TiO_2 accumulating in the mucosa rather than the underlying muscularis. Perfused intestines exposed to 1 mg L^{-1} bulk or nano TiO_2 for 4 h showed a time-dependent accumulation of Ti in the serosal perfusate with the initial rates of Ti flux from the nano exposures being 5 fold higher than the bulk form. Addition of pharmacological inhibitors caused increases in tissue Ti concentration and significantly reduced Ti serosal flux rates for NP exposures. Overall, the data suggests an active absorption mechanism is responsible for Ti uptake from both bulk and nano TiO_2 exposures across the perfused rat intestine that is drug sensitive (Chapter 4). *In vivo* work demonstrated feed status and rat age effected Ti tissue concentrations. Critically, Ti tissue concentrations reduced with increasing age and removal of Ti containing feed caused transient decreases in Ti tissue concentrations in 23 day old rats. Transient decreases in Ti tissue concentration following feed removal were not observed in older rats suggesting young rats may be more sensitive to the uptake hazards presented by titanium (Chapter 5).

Overall, the findings presented in this thesis demonstrate Ti/TiO_2 from both bulk and nano TiO_2 exposures are accumulated and transported across intestinal epithelium and these processes are drug sensitive and affected by crystal structure and particle size. The results in this thesis have contributed to a better understanding of the uptake kinetics and sub-lethal hazards presented by bulk and nano forms of TiO_2 exposed to intestinal epithelium which could be used to partially inform policy makers on human dietary risk assessments.

Table of Contents

List of figures

List of Tables

Table Description Page number

Abbreviations

Abbreviation	Glossary
%	Percent
µg	Micrograms
µL	Microlitre
µM	Micrometer
µmol	Micromole
ADI	Allowable daily intake
ANOVA	Analysis of variance
ATP	Adenosine triphosphate
BAL	Bronchoalveolar lavage
BCA	Bicinchoninic acid
BSI	Backscatter image
BUN	Blood urea nitrogen
BW	Body weight
Ca	Calcium
$CaCl_2.2H_2O$	Calcium chloride dihydrate
Caco-2	Human colon adenocarcinoma cell line
Ce	Cerium
cm^2	Centimetre squared
CME	Clathrin mediated endocytosis
CO_2	Carbon dioxide
Cu	Copper
DMEM	Dulbeccos's modified eagle media
DMT 1	Divalent metal transporter 1
DNA	Deoxyribonucleic acid
DPBS	Dulbecco’s phosphate buffered saline
DVLO	Derjaguin, Landau, Verwey and Overbeek
E171	Food grade Titanium Dioxide
EDL	Electric double layer
EDS	Energy dispersive X-ray spectroscopy
EDTA	Ethylenediaminetetraacetic acid
ENM	Engineered nanomaterial
ER	Endoplasmic reticulum
FBS	Fetal bovine serum
Fe	Iron
Fig.	Figure
g	Gram
GIT	Gastro intestinal tract
GMP	Good manufacturing practice
h	Hour

H & E	Haematoxylin and eosin
HCO_3	Bicarbonate
HEPES	4-(2-hydroxyethyl)-1-piperazineethanesulfonic acid
Hg	Mercury
Hz	Hertz
ICP-MS	Inductively coupled plasma- mass spectrometry
ICP-OES	Inductively coupled plasma- optical emission spectrometry
IU	International unit
K	Potassium
KCl	Potassium chloride
Kg	Kilogram
kGy	Kilogray
L	Litre
LM	Light microscopy
L.O.D	Limit of detection
LC50	Median lethal concentration
LDH	Lactate dehydrogenase
LOAEL	Lowest observed adverse effect level
LPS	Lipopolysaccharide
M	Molar
Mg	Magnesium
Milli-q	Ultra pure ion free water
min	Minute
mL	Millilitre
MLN	Mesentry lymphatic network
mM	Millimolar
mmol	Millimole
mol	Mole
mosm	Milliosmole
MV	Microvilli
n	Number of observations
Na	Sodium
Na_3Vo_4	Sodium orthovanadate
NaCl	Sodium chloride
$NaHCO_3$	Sodium bicarbonate
$NaH_2PO_4.2H_2O$	Sodium dihydrogen phosphate dihydryate
nm	Nanometre
nmol	Nanomole
NONS	Notification of New Substances
NP	Nanoparticle
NTA	Nanoparticle tracking analysis
O_2	Oxygen
°C	Degree Centigrade

P25	Titanium Dioxide Nanoparticles
Pb	Lead
PET	Polyethylene terephthalate
PZC	Point of zero charge
RTCA	Real time cell analyser
REACH	Registration, Evaluation, Authorization and Restrictions of Chemicals
ROS	Reactive oxygen species
S.E.M	Standard error of the mean
SEI	Secondary electron image
SEM	Scanning electron microscopy
SiO_2	Silicon dioxide
TEER	Trans epithelial electrical resistance
TEM	Transmission electron microscopy
Ti	Titanium
$Ti(OH)_4$	Titanium hydroxide
TiO_2	Titanium Dioxide
U	Unit of enzyme activity
U.V	Ultraviolet
Zn	Zinc
Ω	Ohm

Publications

Gitrowski, C., Al-Jubory, A. R. & Handy, R. D. 2014. Uptake of different crystal structures of TiO_2 nanoparticles by Caco-2 intestinal cells. Toxicology Letters*,* 226**,** 264-276.

Manuscripts in preparation from the thesis

Gitrowski, C & Handy, R. D. (Manuscript in preparation). Uptake, accumulation and transport of different crystal forms of Titanium dioxide in differentiated 21 day old Caco-2 cells (Chapter 3).

Gitrowski, C & Handy, R. D. (Manuscript in preparation). Uptake of titanium from TiO_2 nanoparticle exposure in the isolated perfused intestine of female Wistar rats (*Rattus norvegicus*) (Chapter 4).

Poster presentations and conference abstracts

Gitrowski, C and Handy, R. D. 2014. Uptake of titanium from TiO_2 nanoparticle exposure in the isolated perfused intestine of adult Wistar rats (*Rattus norvegicus*). Centre for Environmental NanoScience and Risk (CENR), CENR 9th International Conference on the environmental effects of Nanoparticles and Nanomaterials. 7- 11th September 2014, Columbia –South Carolina, USA.

Gitrowski, C., Al-Jubory, A. R. & Handy, R. D. 2013. The gastrointestinal uptake of TiO_2 nanoparticles and associated toxicity. *Toxicology Letters,* 221, Supplement**,** S162. Abstracts of the 49th Congress of the European Societies of Toxicology (EUROTOX) 1-4 th September 2013 Interlaken CH.

Gitrowski, C, Al-Jubory A. R. & Handy, R. D. 2013. The gastrointestinal uptake of TiO_2 nanoparticles and associated toxicity. Society of Environmental Toxicology and Chemistry, SETAC Europe 23rd annual meeting, “Building a better future: Responsible innovation and environmental protection”, 12-16th May 2013, Glasgow, UK. Abstract book, No. TU058, p229-230.

Gitrowski, C, Al-Jubory, A. R. & Handy, R. D. 2012. Uptake and retention of TiO_2 nanoparticles in Caco-2 cells implications for human health. Centre for Research in Translational Biomedicine (CRTB) Research Day, University of Plymouth, 2nd Annual Conference, Plymouth, 4th July 2012.

Gitrowski, C, Al-Jubory A. R. & Handy, R. D. 2012. Uptake and retention of TiO_2 nanoparticles in Caco-2 cells implications for human health. Ecotoxicology research and innovation (ERIC) April Plymouth 2012.

Al-Jubory, A. R.**, Gitrowski, C.,** Henry, T. B., Handy, R. D. 2011. The gastrointestinal uptake of metal nanoparticles and associated toxicity. Ecotoxicology research and innovation (ERIC) April Plymouth.

Al-Jubory, A. R.**, Gitrowski, C.,** Henry, T. B., Handy, R. D. 2011. The gastrointestinal uptake of metal nanoparticles and associated toxicity. April Plymouth Centre for Research in Translational Biomedicine (CRTB) Research Day, University of Plymouth, 2nd Annual Conference, Plymouth.

Platform presentations

Gitrowski C. The gastrointestinal uptake and dietary toxicology of metal nanoparticles. UoP Nano Group Meeting, University of Plymouth, 2nd Annual Meeting, Feb 2011, Plymouth, UK.

Gitrowski C. Mechanisms of TiO_2 uptake and toxicity at physiologically relevant parameters in Caco-2 cells. School of Biological Sciences seminar series, Oct 2012, Plymouth UK.

Acknowledgments

I would like to express my heartfelt thanks to my primary supervisor Professor Richard Handy, who over the last few years has encouraged helped and advised on all matters science related. Without Richard none of this would have been possible and for that I am forever grateful. His open door policy and in-human memory (for remembering obscure papers) will endlessly astound me. I would also like to thank my second supervisor Dr Ted Henry for his willingness to share his vast wealth of knowledge on all things nano, his encouragement and refreshing pragmatic scientific outlook. His opinion is highly valued. I hope the grass is greener on the other side (Heriot - Watt).

For technical support during my research, and so much more, I am greatly indebted to Lynne Cooper, Andrew Atfield, Will Vevers and Glenn Harper who have all gone above and beyond in their help during my work. Drs. Andrew Fisher, David Boyle Awantha Dissanayake, Fiona Jeganathan are also thanked for their advice and council on all things nano / thesis related. I would like to acknowledge Alia Al-Jubory who worked on the bench with me for the first Caco-2 experiment (much appreciated). I would also like to express my gratitude to all the people who supported me in one way or another who I have not explicitly mentioned (you know who you are, and there are so many of you). Thankyou.

Finally I would like to thank my family and friends for their support and encouragement during these sometimes difficult years.

Thank you all, as each and every one of you has allowed me to make it this far; and as Bernard of Chartes said (apparently) "*that we are like dwarves perched on the shoulders of giants, and thus we are able to see more and farther than the latter. And this is not at all because of the acuteness of our sight or the stature of our body, but because we are carried aloft and elevated by the magnitude of the giants.*" Sometimes Wikipedia has its place.

Author's declaration

At no time during the registration for the degree of Doctor of Philosophy has the author been registered for any other University award without prior agreement of the Graduate Committee. This study was financed by a studentship procured by Professor Richard Handy from Plymouth University. Relevant scientific seminars and conferences were attended at which work was presented and several papers prepared for publication.

Word count of main body of the thesis: 61,971 (70,487 including references).

Signed ……

Date……

Chapter 1: General Introduction

1.1 Introduction

Nanomaterials (NMs) which include nanoparticles (NPs) have existed naturally since the beginning of Earth's history (Handy *et al*. 2008). The size range of the nano scale, as suggested by the scientific committee on emerging and newly identified health risks (SCENIHR), is from the atomic level (around 0.2 nm) up to 100 nm (SCENIHR 2006). This definition is not absolute and more recent existing working definitions have stipulated materials can be regarded as 'nano' when the material is approximately between 1 and 200 nm in at least one dimension, and in the case of the UK (DEFRA) in two or more dimensions (Lovestam *et al*. 2010). These definitions fail to account for NM agglomerates/ aggregates with dimensions of a few hundred nanometres although current EU definition has stipulated that a NM is '*A natural, incidental or manufactured material containing particles, in an unbound state or as an aggregate or as an agglomerate and where, for 50 % or more of the particles in the number size distribution, one or more external dimensions is in the size range 1 nm - 100 nm*' (European-Commission, 2011). Moreover, the generic term of NM can be used to describe a NP whilst the term NP implies the particle has a spheroidal like morphology.

Of central concern for materials within the nano scale is the idea that they can have substantially different properties compared to the same substances larger size (e.g., micrometre scale and above). NMs have much larger surface area to mass ratios than courser materials. Since biological and chemical reactions often occur on the surface of materials there is an expectation that NMs will be much more reactive than the same mass of material made from larger particles (Sutariya and Pathak, 2014). Furthermore, as a result of reduced size, NMs may be able to cross biological

barriers such as the lung and gut more easily than coarser materials and consequently cause unexpected effects. In addition, quantum behaviours appear at the nanoscale. These effects prevail at sizes below 30 nm and alter basic material characteristics, including optical, magnetic and electrical properties (Lovestam *et al*. 2010).

Naturally occurring NMs can be broadly characterized into two areas, organic and inorganic compounds. Inorganic NMs include clays (aluminosilicates), metal sulphides, amorphous silica, iron oxyhydroxides; organic NMs include proteins, humic aggregates, viruses etc. (Lead and Wilkinson 2006). These naturally occurring NMs are generally found as colloidal dispersions; which can broadly be defined as substances in which microscopically dispersed insoluble particles are suspended throughout another material/solution which does not settle or takes a long time to settle appreciably (Lead and Wilkinson 2006).

NM production can occur through natural geological processes such as volcanic activity, authigenesis/neoformation and weathering of rocks (Handy *et al*. 2008). There are also biological degradation mechanisms, which typically comprise of the chemical disintegration of organic material from plant or microorganisms (Boyle *et al*. 2005). In the last decade, anthropogenic activity has become a source of NMs and intentional engineered nano material (ENM) production has occurred. Unintentional creation of NMs occurs as an incidental part of many industrial processes involving the combustion of fossil fuels, the use of diesel in vehicles, welding or smelting, polymer fabrication, and even cooking (Gwinn and Vallyathan 2006).

ENMs are deliberately manufactured with an application in mind, and ‘how the product is used’ may be more important for exposure aspects of risk assessment

than the physico chemical characteristics of the material (Hansen *et al*. 2008). Given that with no exposure there is no risk. In light of this, there is an argument that the classification of ENMs can be considered according to the industry they are used in. For example, medical prosthetics, drug delivery vehicles, cosmetics, food, water treatment and environmental remediation are likely to increase NM exposure to humans and therefore increase potential risk (Aitken *et al*. 2006). Hansen *et al*. (2007) have also suggested another method of classification based on how the ENM is incorporated into the product. For example, whether ENMs comprise the bulk of the product, whether they exist on the surface of the product, or whether they are incorporated within the product (Hansen *et al*. 2007), the material composition would likely effect exposure kinetics. For example surface bound ENMs are more likely to become freely detached in an organism in comparison to ENMs incorporated within the material matrix.

Traditionally risk assessment of new materials is based on a chemical approach, and there is debate about how to chemically classify ENMs because there is currently insufficient knowledge about the mechanisms of toxicity. However, a number of researchers involved in the NanoImpactNet environmental workshop have agreed on generally similar classifications of ENMs based on the broad chemical categories they occupy with regards to environmental studies (Stone *et al*. 2010) (although similar ideas would be useful from a human toxicological perspective). Chemical categories include, carbon-based, mineral-based, organic and composite (see Stone *et al*. (2010) and Hansen *et al*. (2014). Classification of composites is particularly problematic, (possibly due to synergistic interactions of materials that make up the composite); however, current suggestions include an initial strategy of ENM

classification based on the individual classes that make up the material (Stone *et al*. 2010).

There is a growing body of literature demonstrating that respiratory exposure to NMs/ENMs can cause adverse effects to lungs. For example respiratory exposure to TiO_2 NPs have been shown to elicit lung injury, inflammation and tumour formation in murine models (Heinrich *et al*. 1995; Chen *et al*. 2006; Kobayashi *et al*. 2009; Rossi *et al*. 2010). Moreover, a number of studies have illustrated the role of particle size in relation to toxicity, with smaller TiO_2 particles causing increased inflammatory effects compared to courser particles of the same material following acute or chronic respiratory exposure (Oberdorster *et al*. 1994; Renwick *et al*. 2004; Sager *et al*. 2008). Less is known about the risks and hazards associated with dietary exposure to NMs or ENMs. Knowledge gaps include how ENMs interact with food components; the effect of NM/food matrix on gastro intestinal tract (GIT) epithelium and gut microflora; the fate and behaviour of ENMs or NMs in the gastrointestinal tract; uptake and accumulation rates for different ENMs; the effect of ENMs or NMs on absorption and bioavailability in comparison to coarser material equivalents; and whether these changes are of toxicological significance and require lowering of the permissible limits in food (Chaudhry *et al*. 2008).

The overall aim of this review is to give a broad overview of ENMs used in the food industry with a particular focus on TiO_2 NP absorption mechanisms at the apical membrane of intestinal cells following oral exposures. The issue of hazard is approached from the view point of mammalian body systems physiology. In order to characterise mechanism of apical uptake and potential toxicity, *in vitro, ex vivo* techniques are discussed and contextualised with regard to researching NM uptake and transport in mammals.

1.1.1 The global nanotechnology market

Nanotechnology is the application of ENMs in products and processes. Early estimates of the global nanotechnology market in 2015 range from about $27 billion to $2.4 trillion (Roco and Bainbridge 2001; Global-Industry-Analysts 2012). Some of the higher estimates suggest the market may be worth more than $2.4 trillion by 2015 (Roco 2007). The variability in the estimates of global value of the market can be attributed to different analytical methods and assumptions made during each forecast, but also due to different definitions of the 'nanotechnology market' (e.g. whether to include old technologies such as carbon black, rubber reinforces and photographic silver, or whether to base the market value on nanotechnology inputs alone, as opposed to the total value of products containing NMs) (McWilliams 2010). Examples of the areas in which nanotechnology is being developed include,manufacturing, electronics, healthcare, pharmaceuticals, chemical plants, transportation, the agri-food sector, water treatment and environmental sustainability (Roco and Bainbridge 2001).

Most applications of nanotechnology in the food industry (packing and food) are outside the UK (or EU) with the majority of them in countries such as the USA, Australia, New Zealand, Taiwan, and China (Chaudhry *et al*. 2008). According to the Helmut Kaiser Consultancy, nano technology in the food market has increased from a value of $2.6 billion in 2003 to $5.3 billion in 2005; and it is expected to soar to $20.4 billion in 2015 (Helmut-Kaiser-Consultancy 2011). However, a report by the Innovative Research and Products Inc. has estimated a lower forecast growth rate to $7.30 billion by 2014, at a compound annual growth rate (CAGR) of 11.65%

(Innovative-Research-Products-Inc 2009). Nevertheless, this industry is growing, and with the increased use of ENMs in food applications the avenues of exposure and potential hazard likely to increase.

1.1.2 Current applications of nanomaterials in the food sector

The term ‘nanofood’ describes food which has been developed, manufactured, processed or packaged using nanotechnology techniques, or to which ENMs have been added (Joseph and Morrison 2006). A selection of ENMs already being used in the nanofood sector are listed in Table 1-1. Technologies are emerging aimed at improved traceability (to hold appropriate manufacturers accountable in the event of a food contaminant issue) and food nutritional value (with a view to addressing food related illness, e.g. obesity, diabetes). For example, lipid micelles, liposomes or nanospheres are used to encapsulate and protect bioactive ingredients from acid hydrolysis in the stomach with a view to improving bioavailability, increasing residence time in the GI tract and promoting efficient nutrient absorption into cells (Chen *et al*. 2006) (Table. 1-1). Another area undergoing significant research and development is smart food packaging. Such packaging can respond to changing environmental conditions such as moisture and temperature and can alert the customer via a visual cue if food is contaminated or starting to decay (Joseph and Morrison 2006). There are also some agricultural applications of nanotechnology (pesticides, fertilisers, herbicides) that could be a source of residues in the human food chain (Miller and Senjen 2008; Frewer *et al*. 2011).

It is difficult accurately estimate the amount and types of ENMs in food due to commercial confidentiality on food recipes and the absence of labelling laws that

specifically necessitate manufacturers to disclose nano forms of existing additives in food (Miller and Senjen 2008). Moreover, manufacturers of nanofood products self-promote the 'nano' nature of their products and it is unknown whether products advertised as 'nano' do in fact contain NMs. Legislators and manufacturers need to work together to ensure that claims about products are true.

There are between 150 and 600 putative nanofoods and nanofood packaging products currently available (Cientifica 2006; Miller and Senjen 2008; Helmut-Kaiser-Consultancy 2011; Woodrow-Wilson-Institute 2014). Examples of packaging incorporating ENMs include using NMs or nanocomposites (e.g., titanium dioxide, silicon dioxide, nano clay and silver) to improve the protection of food by altering the permeation behaviour of the packaging. This can include deodorising, blocking UV, scavenging ROS, improving mechanical and heat resistant properties and developing antimicrobial/antifungal surfaces (Xiao *et al*. 2004; Chau *et al*. 2007).

ENMs in food are generally either in suspension (colloidal) or an emulsion (two liquid phases; e.g., colloidal particles suspended in a gelatine matrix) (Bouwmeester *et al*. 2009). Currently available products include, synthetic lycopene (Table 1-1), which is used as an additive in soft drinks and food products aimed at promoting absorption of synthetic lycopene, which research suggests is an effective antioxidant (Vance *et al*. 2013). NovaSOL (Table1-1) from Aquanova (Aquanova 2006; Chaudhry *et al*. 2008) is a nano-based carrier system which is comprised of 30 nm (diameter) micelles that are able to solubilise hydrophobic molecules contained within them in the hope of making them more bioavailable (Aquanova 2006). By reducing the size of the encapsulate to the nano scale, opportunities for greater surface coverage, increased retention time in the GI tract and improved bio adhesion to the mucus covering the intestinal epithelium may be achieved (Medina *et al*. 2007;

Bouwmeester *et al*. 2009). Examples of solubilised substances include functional food ingredients such as vitamins A and E, omega 3 fatty acids and coenzyme Q10 (Chaudhry *et al*. 2008).

Table 1-1: A summary of currently available ENMs used in the food sector

Type of Product	Product name	Manufacturer	Nano Content	Purpose/ Claim	Reference
Beverage	Nano tea	Ph Pure health	Nanized green tea	Green tea that has been "nanized" extremely bio-available. Even those with poor digestion can rapidly absorb the "nanized" green tea	http://www.phpure.com/nutrition_products/green_tea.htm
Beverage	“Daily Vitamin Boost”	Jamba Juice Hawaii	300 nm iron (sunactive Fe)	22 essential vitamins and minerals and 100 % or more of your daily needs of 18 of them	http://jambajuiceHawaii.com/vita-boost.asp
Food additive	Nano-self assembled structured liquids (NSSL)	Nutralease	Nano micelles for encapsulation of nutraceuticals	Improved bioavailability means nutraceuticals are released into membrane between the digestive system and blood	http://www.nutralease.com/technology.asp
Food additive	Synthetic lycopene	BASF	LycoVit 10% (<200nm synthetic lycopene)	60 nm particle encapsulated in a colloid case	http://www.humannutrition.basf.com
Food additive	AquaNova Novasol	Aquanova	Product micelle (capsule) 30 nm in diameter	An optimum carrier system for hydrophobic substances for a higher and faster intestinal and dermal reabsorption and penetration of active ingredients	http://www.aquanova.de/product-micelle.htm
Food additive	E171	Shijiazhuang Tianqiu Chemicals Co.,Ltd	TiO_2	TiO_2 is a food additive that is used in over 100 products. Some of which is nano	Weir *et al*. (2012)
Food Storage	Food container NS	A-Do Global	Nano silver	99.9 % anti bacterial nanotechnology	http://www.adox.info/?doc=shop/list.php&ca_id=110
Food storage	DuPont Light Stabilizer 210	DuPont	Nano TiO_2	U.V.-protected plastic food packaging	http://www2.dupont.com/titanium_technologies/en_us/products/dls_210/dls_210_landing.html

Food storage	Adhesive for McDonald's burger containers	Ecosynthetix	50-150 nm starch nano-spheres	The adhesive requires less water and less time to dry	http://www.physorg.com/new71748835.html
Plant Growth treatment	Primo MAXX plant growth regulator	Syngenta	100 nm particle size emulsion	The extremely small particle size allows Primo MAXX to mix completely with water and not settle out in a spray tank	http://www.syngentap.com/prodrender/index.asp?nav=CHEMISTRY&ProdID=747

Regulation and legislation relating to food safety

Currently there are many different areas of legislation that apply to the food sector in which ENMs in food may be covered. For a detailed overview see (FSA 2007) Chaudhry *et al*. (2008) who performed a regulatory gap study assessing existing regulatory frameworks relevant to food and food packaging using nanotechnologies. The study concluded that existing models for risk assessment are generally applicable to ENMs, but there are major gaps in information on hazard exposure. For example:

- ‘Current legislation does not differentiate between microscale and nano forms of food additives already approved for use in food’.
- ‘There is a lack of clarity in the definition of novel foods under relevant regulations that may lead to uncertainty as to whether a food processed at the nano scale should be considered a novel food’
- There is a lack of knowledge of the effects of processes and products of nanotechnologies in food to enable adequate risk assessment’.

  (Chaudhry *et al*. 2008)

‘Of concern are existing additives such as TiO_2 that are already approved for use in food and legislation does not prescribe criteria associated with particle size which can be considered a principle issue in terms of risk and hazard presented by ENMs and NMs (Chaudhry *et al*. 2008). According to the food and drug administration (FDA) ‘Any substance that is reasonably expected to become a component of food is a food additive that is subject to premarket approval by FDA, unless the substance is generally recognized as safe among experts qualified by scientific training and experience to evaluate its safety under the conditions of its intended use, or meets

one of the other exclusions from the food additive definition' (FDA 2014). Manufacturers do not need to include TiO_2 on food labels (in most circumstances) because it meets the prescribed exclusion criteria with regards to additive labelling. For example, labelling is not required when additives perform no additive function in or make up less than 25% of the final product (Jovanović 2014). Given that TiO_2 does not have any known nutritional value and has been recognised as safe following the initial toxicological assessment performed in 1969 (JECFA 1969), it is in some cases considered a manufacturing aid rather than a food ingredient, making it exempt from labelling (Jovanović 2014).

Generic routes of exposure to ENMs and NMs

Exposure routes to ENMs and NMs, and sites of systemic accumulation are summarised in Fig. 1-1. Exposure to NMs is multifaceted and while exposure modelling for NMs has been researched (Weir *et al*. 2012; Shi *et al*. 2013), there is less information on exposure modelling from a nanofood focused perspective. Essentially, there are four modes of exposure which may result in the uptake and accumulation of NMs into systemic circulation. Inhalation/aspiration of powders aerosols and vapours; dietary exposures through eating and drinking (covered below from a nanofood related perspective); intra-body (prosthetics, IV medicines) and dermal exposures (creams, face scrubs). For example, intra-body exposures of ENMs can occur though intravenously administered ENMs for therapeutic purposes (Nazir *et al*. 2014) or through degradation of prosthetic implants. TiO_2 has long been used as a component for articulating prosthetic implants for hips and knees (Jacobs *et al*. 1991; Sul 2010). These implants can fail due to degradation of material or

through chronic inflammation in response to the implant resulting in the release of particles into the systemic circulation.

Dermal exposure studies suggest NMs contained in sunscreens and face scrubs (TiO_2) can penetrate the stratum corneum (the skin) and hair follicles (Lademann *et al*. 1999), although subsequent studies have failed to corroborate this result (Senzui *et al*., 2010, Pflucker *et al*., 2001). In more recent times research has demonstrated that hair follicles represent important routes into the skin for drugs and chemicals (Otberg *et al*. 2008). A study done on the percutanous absorption of caffeine showed that hair follicles are considerable weak spots of the skin against penetration of hydrophilic substances (Otberg *et al*. 2008). Past research has shown the potential for effective uptake of vitamins through topical application. The study concluded that topical application of a vitamin A emulsion was almost as effective in overcoming vitamin A deficiency in rats as when the vitamin was given orally (Schaefer *et al*. 1955). This route of exposure may become more relevant for manufacturers of nutritional supplements looking for novel ways to ensure vitamin exposure.

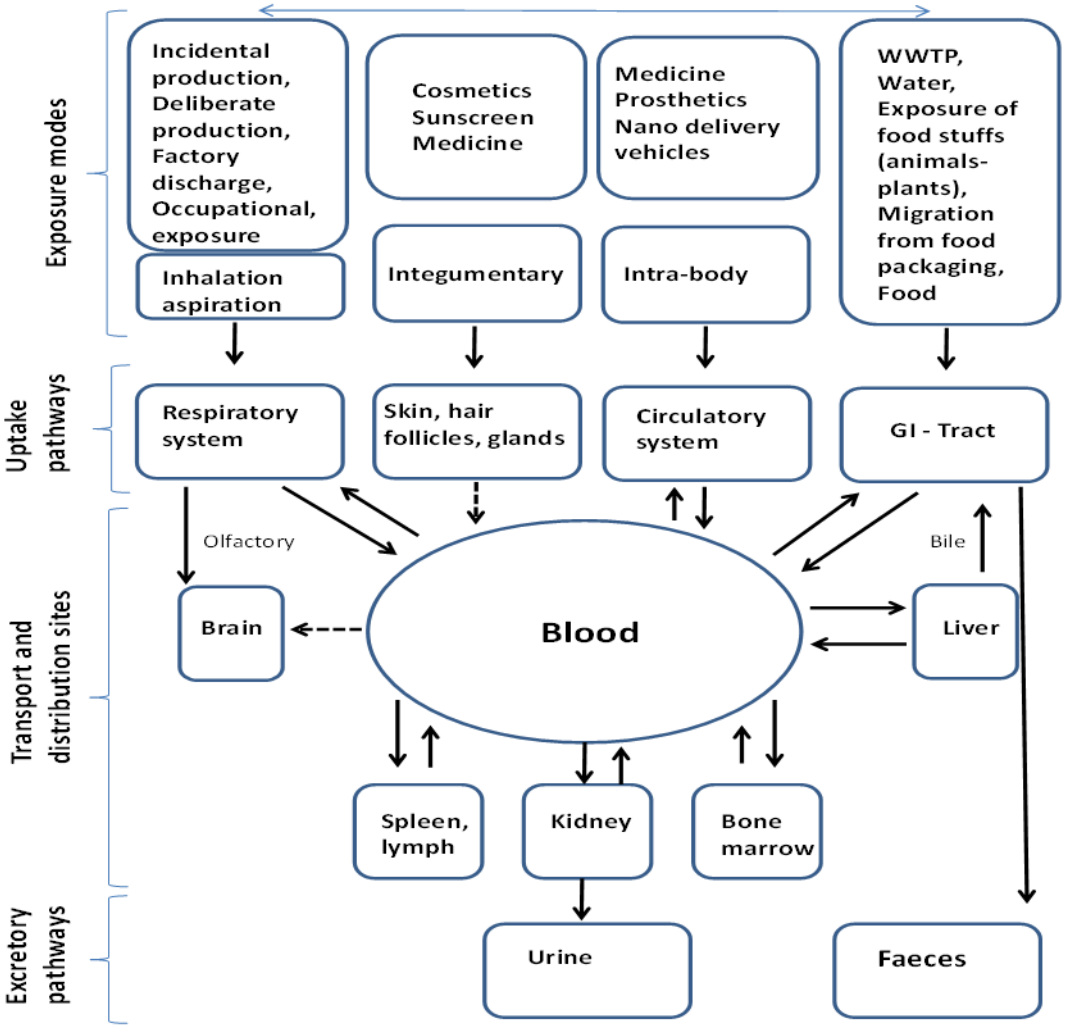

Fig. 1-1: Routes of exposure to ENMs and NMs

Adapted from Shi *et al*. (2013)

1.1.3 Routes of exposure to nanomaterials in the human food chain

ENMs and NMs can enter the food chain through a variety of processes (Fig. 1-1). ENMs in household products or in pesticides and fertiliser end up in sewage. This sewage is then processed by wastewater treatment plants. Studies have shown that particles of TiO_2 between 4 and 30 nm can be found in treated effluent from

wastewater treatment facilities (WWTP) (Kiser *et al*. 2009; Westerhoff *et al*. 2011). These particles are then re-released into the environment where they can interact with living organisms (Fig. 1-1). Exposure via ingestion is likely to occur through the consumption of food containing ENMs (TiO_2 - additive E171) in conjunction with the potential migration of ENMs into food and drinks from packaging containing ENMs (Chaudhry *et al*. 2008) (Fig. 1-1). Moreover, food and beverages containing ENMs such as herbal teas will have vapours which create NP aerosols which can be inhaled and or swallowed with mucus.

1.1.4 Occupational exposures and respiratory exposure

Historically it has been well documented that occupational exposure to food stuffs comprised of fine powders and dusts are known to be respiratory irritants. For example, ‘bakers asthma’ is an allergic asthma caused by cereal flour. In several countries baker’s asthma is reported to be one of the most frequent forms of occupational asthma (Houba *et al*. 1998; Zuskin *et al*. 1998). The addition of powdered additives could also be another risk of inhalation exposure. Diacetyl, a butter flavouring used as a liquid, paste or powder has been associated with fixed obstructive lung disease resembling bronchoilitis obliterans in microwave popcorn workers. The vapours and dust associated with diacetyl have been shown to be of respirable size with only 100 ppm (379 mg m^{-3}) required to cause acute airway injury, but diacetyl vapours have been shown to reach 1230 ppm (4.6×10^3 mg m^{-3}) in the production plants (Boylstein *et al*. 2006; Kanwal 2008; Hubbs *et al*. 2008). The food industry has routinely used fine particles of TiO_2 as a colorant in many products; with TiO_2 accounting for 70% of the total production volume of pigments worldwide (Baan

et al. 2006) of which 36% is incidentally produced at the nano scale (Weir *et al*. 2012). An elevated exposure risk and subsequent internalisation of TiO_2 may occur in people involved in its large scaled production.

In the general population, a common route of exposure is likely to occur through inspiration of vapours associated with cooking foods which contain ENMs or through the use of powdered sweeteners which could create dusts. Exposure of ENMs or NMs via the lungs can result in translocation across pulmonary epithelium to extra pulmonary sites such as the liver, heart, and brain in mammals (Kreyling *et al*. 2002; Nemmar *et al*. 2002; Oberdörster *et al*. 2004).

1.1.5 Oral/dietary exposure

Another route of direct exposure is through the gastro intestinal tract (GIT). Estimated oral doses in the form of food and drinking water for nano TiO_2 range from 5 mg day^{-1} through to 1 mg kg^{-1} bw (Lomer *et al*. 2000; Weir *et al*. 2012). In 2013 the European Commission's scientific committee on consumer safety concluded that the oral exposure lowest observed adverse effect level (LOAEL) of 5 mg kg^{-1} bw day^{-1} may be derived for nano TiO_2 (European-Commission 2013), which is close to estimated levels of consumption.

A human exposure analysis study conducted by Weir *et al*. (2012) indicated that American children between the ages of 3 and 15 years are exposed to the largest concentrations of nano TiO_2 because elevated levels occur in confectionary products in comparison to other food products (Weir *et al*. 2012) (Table 1-2). In extreme cases, just one portion of a salad dressing (225 mg TiO_2) (Table 1-2) could exceed the nano LOAEL for TiO_2 by > 2-fold for a 30 kg child. Moreover, no allowable daily intake

(ADI) for TiO_2 has been set given that the initial toxicological assessment implied low solubility, toxicity and absorption of TiO_2 (JECFA 1969).

Existing risk assessment procedures for metals assume 100% absorption and these procedures may be used for products containing ENMs. However, assessment estimates may be over zealous considering 100% absorption is unlikely for many substances. Moreover, to my knowledge there is no information on the level of absorption and the rates of uptake for TiO_2 in mammalian models.

Table 1-2: TiO_2 concentration in a selection of food products

Food group	Food product	Portion size (g)	TiO_2 (mg/portion)	Nano component /portion (mg)*	Company
Confectionery	Cake Icing	30	55	19.8	Cadbury Ltd Supercook;
	Good and plenty candy	30	81	29	Hershey foods
	Hostess powdered Donettes	2	6	2	Hostess
	Mentos Freshmint Gum	30	90	32	Perfetti Van melle corporation
Sauces	Dickinsons coconut curd	30 (1tbs)	120	43	Dickinsons family
	Mustard (min)	30 (1tbs)	225	81	Colman's of Norwich
	Italian Dressing (max)				Hellmann's
Non-dairy creamers	Teamate (max)	4·5 (1tsp)	3·5	1.3	Nestlé

*Assumed nano component based on Weir *et al*s (2012) estimate that 36% of TiO_2 in food products is within the nano size range.

Adapted from (Lomer *et al*. 2000; Weir *et al*. 2012)

1.2 Titanium dioxide physico – chemical considerations

Titanium dioxide (TiO_2) powder has been used in commercial and industrial applications since 1918 (Barksdale 1950). TiO_2 naturally exists as three distinct crystalline phases, anatase, rutile and brookite (Sayes *et al*. 2006). Pure rutile and anatase are commercially synthesised and used as a white pigment base (mostly rutile) in paints, plastics, rubber and paper, as catalysts (anatase); and as food additives (E171 anatase) (Powell *et al*. 1996).

Food grade TiO_2 in its microparticle form is widely used as a food additive for whitening and brightening food, in white sauces and dressings, powdered foods, confectionary and many ingestible pharmaceuticals (Lomer *et al*. 2000; Weir *et al*. 2012). United States (US) regulations authorize its use as a colour additive in foods at levels not exceeding 1% w/w. The EU permits its use in foods, with some specified exceptions, at *quantum satis* levels if used in accordance with good manufacturing practices (GMP) (FAO 2006).

Food grade bulk TiO_2 is generally regarded as a poorly soluble low toxicity material (JECFA 1969; Jovanović 2014). Research into the properties of bulk TiO_2 demonstrate that the mean diameter of manufactured particles are 200 nm (Lomer *et al*. 2002), although research has shown that up to 36% of 'Bulk' (food grade, E171) TiO_2 is below 100 nm in at least 1 dimension (Weir *et al*. 2012). This research has been corroborated by Yang *et al*. (2014) who assessed five different powders or paste samples of E171 from around the world by analysing primary particle size and hydrodynamic radius. The results showed average primary particle diameter was between 106 nm and 132 nm with at least 17-35% of the particles being < 100 nm in diameter (Yang *et al*. 2014). Food grade TiO_2 (E171) is composed of the anatase

polymorph which in the nano form has been shown to be the most reactive in terms of generating reactive oxygen species (ROS), and in human lung epithelial cell lines has been demonstrated to be 100 times more toxic than rutile TiO_2. Specifically, the calculated LC50 for nano anatase was 3.6 µg ml^{-1} compared to 550 µg ml^{-1} for nano rutile (Sayes *et al*. 2006). Nano (anatase) TiO_2 (10 nm diameter at a concentration of 15 mg ml^{-1}) has been shown to generate 6 times more ROS than rutile alone when irradiated by U.V through electron transfer at the surface of the TiO_2 crystal (Sayes *et al*. 2006).

The mechanisms involve the dissociative adsorption of water to titania surfaces (Sayes *et al*. 2006) and the subsequent ROS ($^{\cdot}OH^{-}$ and $^{\cdot\cdot}O_2^{-}$) react with cell constituents. It is unclear why anatase (TiO_2) is considerably more efficient at ROS production through the catalyses of water on the crystal surface compared to the other TiO_2 phases. Selloni *et al*. (1998) and Vittadini *et al*. (1998) theoretically demonstrate with first principle calculations that water molecules would dissociate to H^+ and OH^-, and then adsorb to anatase crystal surfaces; but undissociated water molecules (i.e., H_2O) adsorp to rutile surfaces (Selloni *et al*. 1998; Vittadini *et al*. 1998) (Fig.1-2). The chemistry at the surface of metal oxides are relatively unknown. The general approach to determining surface chemistry is to assume that metal oxides are ideal crytals where the atomic arrangement is maintained up to the surface plane (Diebold, 2003). This assumption is flawed considering crystals are imperfect. Crystals often contain defects (Koodali and Klabunde 2006). Defects are much more abundant at surfaces than within the lattice (Feltz 1987), and when particles become smaller, the surface area to volume ratio becomes progressively larger, increasing the likelihood of encountering a chemically reactive defect. On oxide surfaces, defects can be either cation or anion vacancies, or adatoms (Koodali

and Klabunde 2006) (atoms attached at the surface of the lattice structure – Fig. 1-2). The most predominant type of defect on metal oxide surfaces is oxygen vacancies (see review by Barteau 1996). When a metal oxide (MO) surface is exposed to water, adsorption of water molecules takes place at cationic sites through a combination of ion dipole attraction and orbital overlap (Koodali and Klabunde 2006) (Equation 1: Fig.1-2). Subsequent protonation and deprotonation of the surface hydroxyls produce a charged oxide surface (Equations 2 - 3) (Koodali and Klabunde 2006). The Gibbs free energy of adsorbative disassociation per molecule of water at TiO_2 crystal surface ranges between +0.02 and -1.56 eV; depending on the orientation and coordination of the atoms at the crystals surface. The latter is strongly influenced by crystal phase, with rutile having the lowest hydroxylation potential and anatase the greatest (Vittadini *et al*. 2010).

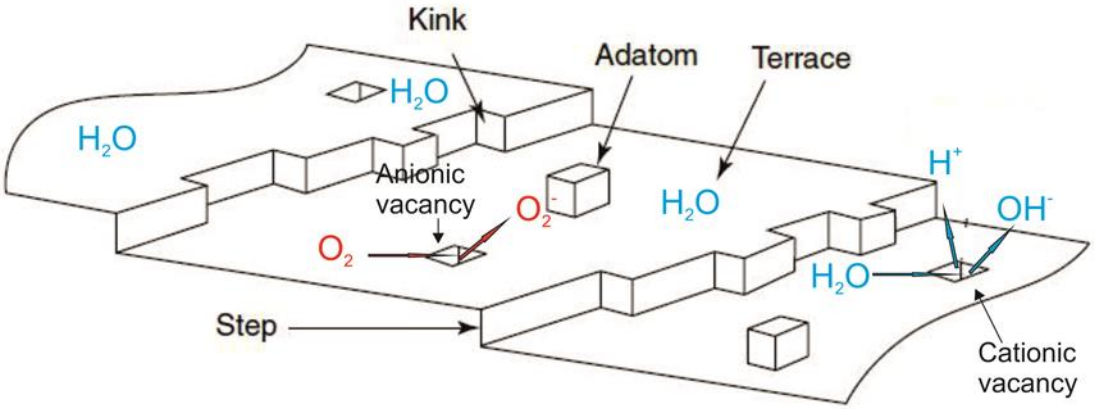

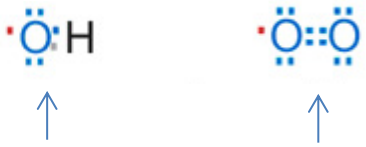

Hydroxyl radical Superoxide anion

Adapted from Brown *et al*. (1998).

Fig. 1-2:Idealised diagram of a metal oxide (MO) crystal surface. Water adsorbs to the surface through dipole attraction. Cationic vacancy acts to break apart the water molecule to form hydrogen gas and a hydroxyl radical (Equation 1). Oxygen molecule scavenges the electron in an anionic vacancy to form superoxide anion.

(Eq 1) $*MO_{surf} + H_2O \longrightarrow MO.H_2O_{surf} \longrightarrow MOH^+.OH^-_{surf}$

(Eq 2) $MOH_{surf} + H^+ \longrightarrow MOH_2^+{}_{surf}$

(Eq 3) $MOH_{surf} \longrightarrow MO_{surf} + H^+$

*Metal oxide surface (MO_{surf}).

(Koodali and Klabunde 2006).

It is important to note that equations 2 and 3 occur when TiO_2 is in an environment where the pH is below (more H^+) that of its 'point of zero charge' (PZC). Depending on the experimental method used the PZC of TiO_2 at normal body temperature is

between pH 5.97 – 5.9 (Chou and Liao 2005). Moreover, much of these hypothesised surface reactions assume the crystal is surrounded by an ideal medium (e.g. ultra pure water) which is unlikely to occur *in vivo.*

Sayes *et al* (2006) compared the ROS generation of different crystal structures (phase) of TiO_2. The results showed that anatase (TiO_2) did not require an illumination source to produce reactive oxygen species (orally ingested products will have no access to light). A higher rate of ROS production occurred when anatase (TiO_2) was sonicated (probably due to cavitation processes) (Luche 1996) and exposed to UV light (Sayes *et al*. 2006). The authors concluded that the fundamental differences between the anatase and rutile surfaces is responsible for the differences in adsorbative dissociation of water (Sayes *et al*. 2006), rather than the larger surface area associated with NMs. Chemical reactivity is fundamental to toxicity and therefore, hazard of a chemical substance. From a regulatory perspective it may be prudent to not simply extrapolate chemical reactivity of one form of TiO_2 to another.

1.3 *In vivo* toxicity of TiO_2 NPs

The toxicity of TiO_2 NPs has been the subject of a number of *in vivo* laboratory studies. Several studies (in rodents) have demonstrated TiO_2 toxicity following respiratory exposures (Table 1-3). Respiratory exposures to TiO_2 NPs have been shown to elicit lung injury, inflammation and tumour formation (Heinrich *et al*. 1995; Chen *et al*. 2006; Kobayashi *et al*. 2009; Rossi *et al*. 2010). Moreover, studies have illustrated the role of particle size in relation to toxicity, with smaller particles eliciting greater inflammatory responses in comparison to bulk counterparts following acute or chronic exposure (Oberdörster *et al*. 1994; Renwick *et al*. 2004; Sager *et al*. 2008;

Kobayashi *et al*. 2009). For example, Oberdörster *et al*. (1994) reported that TiO_2 NPs (21 nm) caused a greater pulmonary inflammatory response than bulk TiO_2 of the same mass burden. The crystal structure of TiO_2 has also been shown to play a role in the magnitude of detected bronchoalveolar lavage (BAL) inflammatory parameters related to lung tissue and cell damage (Warheit *et al*. 2007; Liu *et al*. 2009; Sayes *et al*. 2006). Moreover, P25 Degussa TiO_2 NPs (a mix of anatase and rutile 80/20) have been shown to induce greater pulmonary inflammation, cytotoxicity and adverse lung tissue effects than rutile NPs alone in rats (Warheit *et al*. 2007) supporting the idea that crystalline phase plays a role in toxicity. Given the respiratory toxicity demonstrated by TiO_2 of different sizes and crystal structures there is concern that oral and dietary exposures to TiO_2 NPs (predominantly anatase) could also elicit pathological responses.

The literature reporting the impact of TiO_2 on the GIT is scant, with the majority reporting systemic toxicity associated with intra gastric administration of TiO_2 (Table 1-3). A handful of studies have shown changes in gut morphology or parameters that are deemed to be pathological following exposures to TiO_2 NPs. For instance, Federici *et al*. (2007) demonstrated injuries to the intestine of trout, such as fusion and erosion of the villi and vacuolation of the mucosa following aqueous exposures of 1 mg L^{-1} P25 TiO_2 NPs. Wang *et al*. (2007) demonstrated an increase in inflammatory cells in the chorion and mucosa of the stomach (which he ascribed to overload of particles to the stomach) following single oral gavage of 5 g kg^{-1} TiO_2 NPs to mice. There are considerable knowledge gaps on the effects of TiO_2 NP exposures on the major physiological functions of the gut (e.g. motility secretion digestion and absorbtion) and the non-nutritional functions of the gut (e.g. endocrine and immunological functions).

1.3.1 Internal organ toxicity

The toxicity of TiO_2 NPs on internal organs of vertebrates has been well researched following many different modes of exposure (oral, intravenous, intraperitoneal intratracheal) and these pathological responses to TiO_2 exposure are described below.

1.3.2 Liver

The toxicity of TiO_2 NPs on liver function and morphology has been demonstrated in numerous studies e.g. Wang *et al*. (2007), Chen *et al*. (2009) and Wu *et al*. (2009). Hepatic injury has been demonstrated with a number of crystal phases of TiO_2 NPs at differing doses (Chen *et al*. (2009) - anatase; Nemmar *et al*. (2011) - rutile; Wu *et al*. (2009) - P25; irrespective of administration route (intragastric 5 g kg^{-1} bw: Wang *et al*. (2007); intraperitoneal between 324, and 2592 mg kg^{-1}: Chen *et al*. (2009); intratracheal between 4 and 20 mg kg^{-1}: Meng Tang *et al*. (2011); intraarticular between 2 and 20 mg kg^{-1}: Wang *et al*. (2009)) and size and shape of NPs. Significant increases in biomarkers found in the blood plasma such asaspartate aminotransferase–alanine aminotransferase (ALT/AST) ratios have been demonstrated following high doses of TiO_2 NPs (unknown crystal form) (500 mg kg^{-1} bw) via intraperitoneal injections (lower doses 200mg kg^{-1} had no effect) (Guo *et al*. 2009). Increases in the ALT/AST ratio above the upper limit of normal are indicative of hepatocellular injury (Gopal and Rosen, 2000). This result was supported by previous studies by Wang *et al*. (2007, 2009). Moreover, several experiments have

demonstrated histopathological changes and hepatocyte ultrastructural changes which would lead to impaired liver function, such as the fatty degeneration of hepatocytes, central vein infiltration of inflammatory cells in the portal area and apoptotic and necrotic cells (Wang *et al*. 2007; Duan *et al*. 2010; Cui *et al*. 2011). In contrast, some studies have reported no effects on liver function and morphology (Fabian *et al*. 2008; Liang *et al*. 2009). Fabian *et al*. (2008) demonstrated no toxic effects in a range of organs following one intravenous administration of TiO_2 (70/30 anatase rutile: 20-30 nm diameter at 5 mg kg^{-1} bw) even though detected TiO_2 levels were highest in the liver. Direct comparison between studies is problematic, although a possible explanation for the lack of effect observed in the studies by Fabian *et al*. (2008) and Liang *et al*. (2009) may be due to the dosages of TiO_2 administered (a function of concentration and time). Both studies performed single exposures whilst Wang *et al*. (2007) administered a very high dose and Guo *et al*. (2009) performed repeated exposures over a given time frame.

1.3.3 Kidneys

The literature on renal pathology following exposure to TiO_2 NPs is contradictory. Several *in vivo* studies have identified changes in renal markers such as increases in blood urea nitrogen (BUN), e.g. Wang *et al*. (2007) and Guo *et al*. (2009) following exposure to TiO_2 NPs, whilst some studies have reported the opposite (Liu *et al*. 2009). The same pattern emerges when comparing renal histopathology of animals exposed to TiO_2 NPs. Fabian *et al*. (2008) demonstrated no NP-induced nephrotoxicity following intravenous administration of anatase (< 100 nm, one dose of 5 mg kg^{-1}) and this was also demonstrated by Liang *et al*. (2009) (intratracheal

installation of anatase and rutile NPs 0.5, 5, or 50 mg kg^{-1} (one dose)). In contrast, a number of studies have observed histopathological changes in the kidneys, such as glomerula swelling, deposition of proteinic liquid in proximal tubules, apoptosis or vacuolization of the renal epithelieum, cell abscission, fatty degeneration or cell necrosis, and increased concentrations of inflammatory cells following intragastric, intrarticular and interperitonel administration of TiO_2 NPs (Wang *et al*. 2007-intragastric; Wang *et al*. 2009: intraarticular; Gui *et al*. 2013: intragastric). The aforementioned studies that demonstrate renal histopathology used repeated exposures of TiO_2 (chronic exposure) or extremely high single doses (Wang *et al*. 2007) suggesting excretion through the kidneys can become overloaded following chronic exposure or high doses of TiO_2 NPs.

1.3.4 Immune effects

TiO_2 NPs have been shown to interact with immune cells such as macrophages, monocytes, platelets, leukocytes and dendritic cells, and can trigger inflammatory responses (Skocaj *et al*., 2011, Vamanu *et al*., 2008, Palomäki *et al*., 2010). TiO_2 NP exposure to human monoblastoid cell line (U937) induced apoptosis and necrosis at concentrations similar to those found in tissues surrounding Ti implants (Vamanu *et al*., 2008). Moreover, TiO_2 NP exposure has been shown to induce the enhanced expression of a variety of pro inflammatory cytokines in murine macrophages and dendritic cells (Palomäki *et al*., 2010). For example Palomaki *et al*. (2010) reported nano TiO_2 led to an up regulation of maturation markers and activated the NLRP3 inflammasome leading to significant IL 1 B- secretion (Palomäki *et al*., 2010).

In vivo immunodulating effects have also been demonstrated. For example Larsen *et al*. (2010) that intraperitoneal exposure to TiO_2 NPs promoted a T-Helper type 2 cell

mediated response.Moon *et al*. (2011) demonstrated the intraperitoneal exposure of mice to TiO2 NPs enhanced the growth of subcutaneously implanted B16F10 melanoma through immunomodulation of B- and T- lymphocytes, macrophages and natural killer cells. Airway inflammation and increased immune activity has also been demonstrated after intranasal exposure to TiO_2 NPs (Larsen *et al*., 2010, De Haar *et al*., 2006) evidenced by an increases in eosinophils, neutrophils and lymphocytes in BAL fluid. Whether these responses are TiO_2 specific or simply inflammatory responses mediated by ROS or mechanical irritation is subject to debate and needs more research.

1.3.5 Spleen

The main functions of the spleen are to filter the blood, recycle blood cells and play a role in immunity. These functions are performed in two anatomically distinct regions, red pulp and white pulp. There is a concern that NP exposure may affect the composition and relative distribution of red and white pulp (Mebius and Kraal 2005).

The toxicity of TiO_2 NPs to the spleen following acute or chronic exposure has been demonstrated (Chen *et al*. 2009; Rossi *et al*. 2010; Sang *et al*. 2013; Tassinari *et al*. 2014). Tassinari *et al*. (2014) orally exposed female mice to 0, 1 and 2 mg kg^{-1} anatase TiO_2 per day for 5 days and showed TiO_2 aggregates in the spleen and an increase in white pulp area. Similar results were demonstrated by Sang *et al*. (2013) who exposed mice to 2.5, 5 or 10 TiO_2 NPs mg kg^{-1} body weight for 90 days via intragastric administration and demonstrated NP accumulation in the spleen and histopathological changes such as splenocyte apoptosis. In contrast Wang *et al*. (2007) administered one dose of (oral gavage) 5 g kg^{-1} TiO_2 NPs and no

histopathological changes were observed, even though substantial concentrations of Ti were detected in the spleen. Fabian *et al*. (2008) showed that Ti persisted in the spleen for 28 days following one intravenous administration of 5 mg kg^{-1} TiO_2 NPs although there were no obvious health effects and organ function remained normal (Fabian *et al*. 2008). It appears that acute exposure is fairly well tolerated by the spleen, but chronic exposures appear to cause more pathologies (Chen *et al*. 2009; Rossi *et al*. 2010; Sang *et al*. 2013; Tassinari *et al*. 2014). The reasons are unclear, although some researches attribute this to prolonged oxidative stress in overload conditions (Li *et al*. 2010; Wang *et al*. 2011). Changes in red pulp may be due to respiratory stress (Stewart and McKenzie, 2002), whilst immune responses to NMs may be responsible for changes in white pulp and the processing and mobilisation of white blood cells therein (Swirski *et al*. 2009).

1.3.6 Nervous system

The potential for NMs to elicit toxic response in the brain and nervous system is a cause for concern. From a dietary perspective the concern is whether there may be a neurological hazard following chronic exposure to TiO_2 in food and water.

Studies have demonstrated an increase in Ti concentration in the brain, suggesting Ti or TiO_2 from TiO_2 exposures can circumvent the blood brain barrier regardless of the exposure route (intranasal: Wang *et al*. (2008), intratracheal : Li *et al*. (2010), intragastric: Hu *et al*. (2010),intraabdominal: Ma *et al*. (2010) and aerosol: Oberdorster *et al* (2004)) and induce histological and biochemical changes. Wang *et al*. (2007; 2008) have demonstrated that bulk and nano TiO_2 can translocate to the central nervous system via the olfactory system in mice; and accumulate in the brain,

mainly in the hippocampal regions (Wang *et al*. 2008). Fatty degeneration of the hippocampal tissue was observed in mice exposed to 80 nm and 150 nm particles but not 25 nm particles following a single oral administration of 5 g kg^{-1} (Wang *et al*. 2007). In another study by Wang *et al*. (2007) (Table 1-3), changes in neurological biochemistry were demonstrated following exposure to TiO_2 (25 nm, 80 nm (rutile), 155 nm (anatase; intranasal instillation of 50 mg kg^{-1} every other day for 30 days). In all mice there was a significant elevation in brain Ti content, (Table 1-3) but, biochemical changes were only induced by 80 nm and 150 nm TiO_2 particles (25 nm had no significant effect). These changes included a significant increase in norepinephrine (NE) and 5-hydroxytryptamine (5-HT). The authors were unsure of why the 25 nm particles had no obvious toxicological effect (Wang *et al*. 2007). In contrast, Hu *et al*. (2010) showed a decrease in NE and 5-HT following intragastral instillation of 5 nm anatase NMs (5, 10 and 50 mg kg^{-1} every day for 60 days) (Table 1-3). Interestingly, TiO_2 exposure caused significant disturbances in electrolyte homeostasis in mouse brain (Ca^{2+}, Mg^{2+}, Na^{+}, K^{+}, Fe and Zn) and inhibition of activities of Na/K ATPase, Ca^{2+} ATPase, Ca^{2+}/Mg^{2+} ATPase (Hu *et al*. 2010). These conflicting reports maybe a function of the mode of particle administration (intranasal (Wang *et al* 2007) instead of intragastral Hu *et al*. (2010)). Nevertheless, changes in electrolyte homeostasis in brain tissue following repeated oral exposure, as demonstrated by Hu *et al*. (2010), should be a cause for concern even if the exposures used in this study are 10 fold higher than predicted human exposure scenarios.

1.3.7 Cardiovascular toxicity

The translocation of TiO_2 NPs into systemic circulation suggests that they would be free to interact with the cardiovascular system. A handful of in vivo studies have demonstrated pathological effects to the cardiovascular system following oral or intraperitoneal exposure to TiO_2 NPs (Wang *et al*., 2007, Liu *et al*., 2009, Bu *et al*., 2010). For example, oral gavage of rats with a mixture of anatase and rutile NPs (50 nm diameter) demonstrated increased levels of urine metabolites such as Aspartate aminotransferase (AST), creatine kinase (CK) and lactate dehydrogenase (LDH) in conjunction with mitochondrial swelling in heart tissue relative to control animals (Bu *et al*., 2010). Similar changes to biochemical serum parameters have been demonstrated by Wang *et al*. (2007) although histology of heart tissue demonstrated no visual pathologies. Other studies have also demonstrated pathological effects to blood vessels. For example, Nurkiewicz *et al*. (2008) observed systemic micro vessel dysfunction attributed to the adherence of polymorphonuclear leukocytes to micro vessel walls and the production of ROS following airborne exposures (1.5 -12 mg m^{-3} for 240-720 mins) of nano TiO_2 (crystal form unknown) .

1.3.8 Reproductive and developmental toxicity

A handful of studies have investigated reproductive and developmental toxicity following exposure to TiO_2 NPs. Takeda (2009) demonstrated that subcutaneous exposure of pregnant mice to TiO_2 NPs (25 and 70 nm; 16 mg kg^{-1}) at days 3, 7, 10 and 14 can damage the genital and cranial nerves by altering gene expression associated with development (Table 1-3), indicating foetal development is sensitive

to TiO_2 administrations during pregnancy. Shimizu *et al*. (2009) supported this data by demonstrating that subcutaneous injection of anatase TiO_2 NPs in pregnant mice alters a variety of genes associated with development and function of the CNS in male pups (Table 1-3). Furthermore, Yamashita *et al*. (2011) demonstrated that intravenously injected TiO_2 NPs in pregnant mice were found in the placenta, foetal liver and brain, indicative of the transplacental transfer of TiO_2 NPs. Moreover the female mice had smaller uteri and smaller foetuses than controls that were injected with the vehicle (saline) alone. There may be also be a risk of NP transfer to the GIT of the young through breast feeding, although to my knowledge no such research has explored this topic. There is limited research in this area and more needs to be performed with a view to understanding the processes underpinning maternal NP transfer to pre and post natal offspring.

The effects of TiO_2 NPs on the male reproductive system are not well understood although some experimental evidence suggests TiO_2 NPs exert some toxic effects (Guo *et al*. 2009). Guo *et al*. (2009) showed reductions in sperm density and motility and increases in sperm abnormalities and germ cell apoptosis following intraperitoneal injections of TiO_2 NPs. Interestingly histology of the testes and epididymis did not show any pathological changes.

The TiO_2 NP in food issue can best be thought of as a chronic exposure scenario. Therefore the central theme from a toxicological perspective is whether children chronically exposed to TiO_2 NP containing food will demonstrate pathological health effects in 20 years' time. Only time will tell.

Table 1-3: Selection of studies assessing the toxicity of TiO_2 NPs to *in vivo* murine models

Type of exposure	Organ/ System effected	Crystal Phase composition	Organism	Results	References
Inhalation: Dose:10 mg m^{-3} for 18 h a day for 2 years	Respiratory	P25 Degussa TiO_2 (15-40 nm)	100 female wistar rats. NMRI mice	Rats: adenocarcinomas, squamous cell carcinomas increased Mice: no effect on tumour rates	(Heinrich *et al*. 1995)
Inhalation: Dose:10, 50 and 250mg/m^3 for 2 years	Respiratory	Fine TiO_2 (< 2.5 µm)	Rats	Bronchioloalveolar adenomas and cystic keratinizing squamous cell carcinomas occurred at 250 mg m^{-3} exposure	(Lee *et al*. 1985)
Intracheal instillation: Dose: 1 – 5 mg kg^{-1} Time: 3 months	Respiratory	136, 150, 382 nm (rutile) 25 nm (80% anatase/ 20% rutile)	Rats	Pure rutile only produced transient inflammation. Anatase/rutile TiO_2 produced pulmonary inflammation, cytotoxicity and adverse lung effects.	(Warheit *et al*. 2007)
Intranasal instillation: 500 µg kg^{-1} every other day Time: 30 days	Nervous system / Kidney	80 nm (rutile) 155 nm (anatase)	Female mice	Pathological changes were observed in the hippocampus and olfactory bulb. The group exposed to anatase showed higher inflammation responses. Rutile group showed severe atrophy of the renal glomerus.	(Wang *et al*. 2008)
Intragastric administration: 5-50 mg kg^{-1} every day for 60 days	Nervous system	Anatase (5 nm)	20 female mice per group.	Changes in neurotransmitters (Increase; NE, DA, 5-HT, Dopac. Decreased Na^+/K^+, Ca^{2+}, Ca^{2+}/Mg^{2+} ATPase	(Hu *et al*. 2010)
Oral administration: (single gavage, Dose: 5 g kg^{-1} body weight Time: 2 weeks	GIT/liver/ Kidney	25, 80, 155 nm (type unknown)	Mice	25 nm and 80nm particles caused liver and kidney damage in female mice. TiO_2 accumulated in liver, spleen kidneys. inflammation of cells in the chorion and mucosa of the stomach.	(Wang *et al*. 2007)
Intragastric administration: 2.5, 5, 10 mg kg^{-1} bw every day for 90 days	Kidney	Anatase (5 nm)	120 male mice	Apoptosis, infiltration of inflammatory cells, tissue necrosis or disorganization of renal tubules, coupled with decreased body weight. Changes in gene expression: suppression of *Birc5*,*Crap2,* and *Tfrc*	(Gui *et al*. 2013)

Intragastric administration: Dose: 5-150 mg kg^{-1} for 30 days	Spleen	Anatase	20 female mice per group	Spleen O_2, H_2O_2 levels increased. Histology indicated lymph nodule proliferation	(Wang *et al*. 2011)
Intraperitoneal injections: 200 and 500 mg kg^{-1} every other day for 5 days	Reproductive/Liver/Kidney	5 nm (type unknown)	15 male mice per group	Reduced sperm density and motility, germ cell line apoptosis. Liver: Increased ALT/AST ratio Kidney: Increase in BUN	(Guo *et al*. 2009)
1 Intraperitoneal injection :324 – 2592 mg kg^{-1} bw	Liver/Kidney	Anatase (5 nm)	10 male and female mice	High dose groups- Liver: ALT and AST ratio increased. Fibrosis, necrotic and apopotic cells were detected. Kidney: severe lesions	(Chen *et al*. 2009)
Subcutanous injections: 100 µl of 1 mg mL^{-1} at days 3, 7, 10 and 14	Reproductive / developmental	Anatase (25 - 70 nm)	6 pregnant mice per group	Altered gene expression in cranial and genital nerve systems. Disorganised and disrupted seminiferous tubules, decreased sperm motility in male offspring	(Takeda *et al*., 2009)
Subcutanous injections: 100 µg $mouse^{-1}$ day^{-1} at days 3, 7, 10 and 14	Reproductive	Anatase (25 - 70 nm)	14-15 mice per group	Changes in gene expression related to development and function of the CNS in male pups	(Shimizu *et al*., 2009)

1.3.9 Genotoxicity and Carcinogenicity

In vivo genotoxicity studies are limited and there is a lack of agreement in the literature. For example, Trouiller *et al*. (2009) reported that TiO_2 NPs administered in drinking water for 5 days, induced DNA damage and genetic instability in bone marrow and white blood cells of C57Bl/6J pun/pun mice. This was supported by Sycheva *et al*. (2011) who exposed mice to bulk and nano TiO_2 (40, 200 and 1000mg kg^{-1} daily for 7 days) via oral gavage and demonstrated genetic damage in the cells of bone marrow, fore stomach, colon and testis for both treatments. In contrast Bernard *et al*. (1990) fed rats diets containing 1 2 or 5% TiO_2 (assuming adult rats eat 6 g of food per day 5% is equivalent to 300 mg day^{-1} per rat) coated mica for 130 weeks. They found no evidence that TiO_2 coated mica elicited toxicological orbiologically important changes in survival, body weight gains, hematologic or clinical chemistry parameters or histopathology.. This could simply be down to surface properties of the material considering reactions generally take place at the surface of materials. Nevertheless, there are large knowledge gaps concerning the genotoxicity of TiO_2 at physiologically relevant doses via oral exposures. The genotoxicity of a material does not necessarily imply carcinogenicity considering genetic damage can be repaired. Nevertheless a threshold level of genotoxicity is usually required carcinogenicity to occur.

In vivo TiO_2 NP induced carcinogenicity has been investigated by a number of researchers ((Bernard *et al*. 1990 and Borm *et al*. 2004), reviewed by Shi *et al*. (2013)). Lee *et al*. (1985) demonstrated that high concentrations of bulk TiO_2 particles (< 2.5 µm diameter: dose, 250 mg m^{-3} for 2 y; aerosol) have been shown to

cause respiratory tract cancer in rats, whilst Heinrich *et al*. (1995) demonstrated chronic exposure to TiO_2 NPs (15 - 40 nm diameter; exposure of 10 mg m^{-3} for 2 ye followed by a 6- month holding period) were more tumorgenic in rats than bulk TiO_2 on an equal mass dose basis. A review of the aforementioned studies by Dankovic *et al*. (2007) suggested that TiO_2 induced cancers are due to a secondary genotoxic mechanism associated with persistent inflammation.

1.3.10 Mechanisms of toxicity

Studies that demonstrate TiO_2 toxicity generally attribute the mechanism to oxidative stress mediated by free radical formation leading to persistent inflammation, and subsequent DNA damage and mutations. Oxidative stress is essentially an imbalance between the production of free radicals (ROS) and the ability of the body to counteract their harmful effects through neutralization by antioxidants (Winston and Di Giulio, 1991). ROS consist of a group of partially reduced forms of molecular oxygen, such as hydroxyl radicals ($^{\cdot}OH^{-}$), superoxide anion ($^{\cdot}O_2^{-}$), hydrogen peroxide (H_2O_2) and lipid peroxides (Buechter 1988) which are free to react with cell constituents.

Ashwood *et al*. (2007) proposed an alternative idea which suggested that TiO_2 on its own is not particularly toxic. However TiO_2 avidly binds lipopolysaccharides (LPS) with bridging calcium cations (see below). This may mimic bacterial cell surfaces thereby triggering proinflammatory responses (Ashwood *et al*., 2007). Hirayama *et al*. (2011) demonstrated this in macrophages using real time PCR. Exposures to TiO_2/LPS increased expression of proinflammatory cytokines compared to TiO_2

alone or LPS alone implying a synergistic effect of TiO_2/LPS in triggering proinflammatory responses.

Wang *et al*. (2007) suggests another mechanism of toxicity in conjunction with oxidative stress. The aggregation of rutile TiO_2 NPs observed in the kidney indicates an inability of the kidney to excrete these NPs leading to atrophy of the glomerus (Wang *et al*. (2007). Sayes *et al* (2006) showed that the aggregation of rutile TiO_2 is severe in comparison to the other crystal forms. If these aggregates can form easily in the organism than the total aggregate size may supersede the renal filtration threshold resulting in atrophy and blockage of the tissue.

Recently studies have demonstrated interference of TiO_2 NPs with electrolyte homeostasis in cells and tissue (Hu *et al*. 2010; Koeneman *et al*. 2010; Simon *et al*. 2010; Al-Jubory and Handy 2012). Exposure and internalization of anatase or P25 TiO_2 NPs appears to increase levels of intracellular calcium in various cell types (Human keratoncytes; Simon *et al*. (2010); Trout GIT tissue; Al-Jubory and Handy (2012); Mouse brain; Hu *et al*. (2010)). The mechanisms are unclear although Hu *et al*. (2010) demonstrated a reduction in activity of Ca^{2+} ATPase and Ca^{2+}/Mg^{2+} ATPase. Inhibition of calcium efflux ATPases would result in an increase of intracellular calcium down the concentration gradient. Simon *et al*. (2010) suggested TiO_2 interacts with the Golgi and this interaction is responsible for increases in intracellular free calcium considering the Golgi is thought to play an important role in calcium pool regulation (Missiaen *et al*. 2007). More research is required on the mechanism(s) of TiO_2 NP induced changes on electrolyte homeostasis.

One of the limitations of research into the adverse effects of microparticles and NPs is that *in vivo* and *in vitro* studies are usually carried out on healthy tissues. Diseased

tissue may allow for a greater absorption of NMs. This has implications for people with compromised GIT function. Research suggests that micro particles in the diet exacerbate the symptoms in conditions such as irritable bowel syndrome (IBS) and Crohn's disease (Lomer *et al*. 2000; Powell *et al*. 2000). The effects are attributed to luminal constituents adsorbing to particles (which form a corona surrounding the NP) such as LPS and calcium, mimicking bacterial cell surface and triggering an inflammatory response (Powell *et al*. 2000; Ashwood *et al*. 2007; Hirayama *et al*. 2011). Perhaps TiO_2 may act to aggravate Crohn's and IBS (Lomer *et al*. 2000; Powell *et al*. 2000; Chaudhry *et al*. 2008). The assumption that these particles are inert may not be correct and further work is required to prove beyond doubt that TiO_2 is acceptable for human consumption. With increasing applications of TiO_2 NPs in the food industry, there is an urgent need to evaluate the risk posed by chronic oral exposure to these particles, considering the demonstrated carcinogenic effects in rats following long term respiratory exposures and the toxicological responses to systemic body sites mentioned above.

1.4 Absorption, Distribution and Excretion of NMs

For systemic distribution and toxicity to occur via oral exposures, TiO_2 NPs need to be absorbed or diffuse through the GIT and into the capillaries or lymphatic networks. The usual mechanism of metal uptake across biological membranes involves carrier mediated transport on metal ion transporters (Campbell 1995). Chemically stable NMs such as TiO_2 that undergo limited dissolution are likely to be too large to use ion transporters and paracellular diffusion pathways, suggesting the most likely route of uptake will be by an endocytic mechanism at the apical membrane (Handy *et al*. 2008; Fig. 1-3, 1-4). For small NMs (< 20 nm) that have a hydrophobic surface either

through their surface chemistry or through incidental binding of anions found in the mucus (Handy and Maunder 2009) it remains possible that these NMs could passively diffuse through the cell membrane. For example Xia *et al* (2008) demonstrated that NMs with alternating surface attached hydrophilic and hydrophobic ligands could pass directly through the cell membrane and into the main cell compartment without causing membrane disruption (Xia *et al*. 2008). Given this evidence, a diffusional component for NP uptake that is both a function of particle size and particle surface hydrophobocity should be considered in particle uptake models.

For particles that undergo dissolution in the gastric environment, bioavailability is assumed to be a function of metal speciation, since only certain metals will fit relevant transport pathways (Campbell 1995), although, there are some generic metal transporters that are known to transport more than one metal as long as oxidation state remains the same e.g. divalent metal transporter 1 (DMT 1).

The absorption, systemic distribution and toxicity to systemic body sites following oral exposure to TiO_2 NPs have been demonstrated in *in vivo* studies (Table 1-3, 1-4) e.g. Jani *et al*. (1994); Wang *et al*. (2007) and Tassinari *et al*. (2014). Organs that have increased Ti levels following oral TiO_2 exposures are the mesentery and lymphatic networks (MLN), liver, kidney, spleen, brain lungs and reproductive organs (Jani *et al*. (1994) Liver, spleen, lung, MLN; Wang *et al*. (2007)- liver, kidney, spleen, lung, brain; Tassinari *et al*. (2014)- spleen, thyroid, ovaries, uterus, testes).

1.4.1 Distribution

Aside from basolateral exocytosis from enterocytes into the lymph and capillary networks within the lamina propria, NP distribution may occur via M-cell macrophages which are transported to draining lymph nodes (LeFevre *et al*. 1978). When macrophages become full of inorganic particles they make their way to the spleen and liver to be recycled (apoptotic mechanisms) (Powell *et al*. 2010) and it is during this process that the NMs enter systemic circulation where particles are free to interact with plasma proteins (Deng *et al*. 2009) and/or bind to the surface of erythrocytes (Rothen-Rutishauser *et al*. 2006). The coronal environment of NMs could have substantial effects on the distribution of NMs (Hagens *et al*. 2007) (see below – Gut lumen environment).

The liver receives blood directly from the GIT and can be considered the first internal target organ aside from the GIT itself. Following liver processing, blood will end up in the inferior vena cava (systemic circulation) where it will be redistributed to systemic body sites. Nutrient rich blood from the small intestine flows into the liver via the hepatic portal vein. Large microparticles could get stuck in hepatocytes removing them from circulation. Research by Jani *et al*. (1994) investigated the translocation of intra gastrically administered TiO_2 microparticles (500 nm diameter) and showed that accumulation of particles in the liver and spleen was elevated compared to different body sites (Table 1-4) (interestingly no particles were found in the kidneys)*et al*. Systemic distribution and retention of particles will occur if the organism is unable to excrete the dietary load fast enough.

Fabian *et al*. (2008) investigated the tissue distribution of intravenously administered (100% bioavailability) TiO_2 NPs (70/30 anatase/rutile 20-30 nm, 5 mg kg^{-1}) with

tissue Ti content being determined at days 1, 14 and 28 post exposure. Ti levels were highest in the liver > spleen > lung and kidneys at day 1 post exposure. Ti was retained in the liver and spleen for the duration of the experiment, whilst the Ti concentration of the lung and kidneys returned to control levels by day 14 and there was no detectable Ti in blood cells, plasma, brain, or lymph nodes following exposure, suggesting a rapid clearance of TiO_2 from the blood into the liver spleen lungs and kidneys. Interestingly Wang *et al*. (2007) orally exposed mice to TiO_2 and showed a small accumulation of NMs in the blood and significant accumulations in the brain (Table 1-4), suggesting route of administration (possibly coronal environment) impacts systemic distribution of particles.

1.4.2 Excretion

NMs in systemic circulation could be excreted in a number of ways. The most common/likely routes are expulsion through the urine, faeces and bile, although the possibility exists that any uptake routes may also act as excretory pathways (with the exception of injected exposures) (Fig. 1-1). Jani *et al*. (1994) calculated that 6.5% (12.5 mg kg^{-1} TiO_2 per day for 10 days 500 nm diameter primary particle size) of an oral dose is absorbed in rat small intestine whilst the rest is excreted through the bowel (Jani *et al*. 1994). In contrast to these findings, the international program on the chemical safety for TiO_2 suggests that most ingested TiO_2 is excreted with the urine (WHO 1982).

Cho *et al*. (2013) investigated and compared the distribution and excretion of TiO_2 and ZnO NPs following repeated daily oral exposures for 13 weeks in rats. had low absorption and Ti was almost entirely excreted via the faeces. None was found in the

urine. In contrast Zn was detected in the urine at high concentrations. The authors concluded absorption of Zn from ZnO exposure was much higher due to increased dissolution rates of ZnO in the acidic gastric environment in comparison to TiO_2. The maximum molecular weight for glomerular filtration is around 60 kDa (Handy *et al*. 2008) indicating that NMs only a few nano metres across would pass in to the urine.

Particles accumulated in the liver (Wang *et al*. 2007; Fabian *et al*. 2008) could migrate through hepatocytes to the gall bladder where they are re-released into the small intestine, or the particles may drain into the liver sinusoids into the hepatic vein whereby excretion through the kidneys becomes viable route. Clearance of particles from the liver via the bile duct into the small intestine is well known in pharmaceutics (Huggins and Froehlich 1966). Whether this happens in the case of insoluble NMs is subject to debate. Presumably material that is not absorbed following oral exposures will be expelled in the faeces as has been demonstrated by Jani *et al*. (1994) and Cho *et al*. (2013).

Table 1-4: Organ Ti concentrations following *in vivo* oral TiO_2 exposures in murine models

Organism	Dose (oral administration)	Liver	Kidney	Spleen	Lung	MLN	Brain	Blood (µg/ml)	Reference
Rat- Female Sprague Dawley (*n = 6*)	500 nm diameter TiO_2- 12.5 mg kg^{-1} d^{-1} for 10 days. Samples on day 11	87.34	0.005	8.09	273.17	545.92	Not measured	5.25	**Jani *et al* (1994)**
Controls	Not stated	Not stated	Not stated	Not stated	Not stated	Not stated	Not measured	Not stated	
Mice	80 nm diameter TiO_2 one dose of 5 g kg^{-1} sampled 2 weeks post exposure	19.85	2.25	2.4	3.15	Not measured	0.85	0.65	**Wang *et al* (2007)*****
Controls	Distilled water control	0.45	0.75	0.63	1.00	Not measured	0.15	0.4	
Rats (*n = 8*)	25 nm diameter anatase - 2 mg kg^{-1} for 5 consecutive days. Sampled on day 6	Not measured	Not measured	0.23	Not measured	Not measured	Not measured	Not measured	**Tassinara *et al* (2013)*****
Controls	Distilled water control	Not measured	Not measured	0.18	Not measured	Not measured	Not measured	Not measured	
Rats- Female Sprague Dawley (*n = 11*)	26 nm (Anatase/ rutile – 80/20 mix).1041.5 mg $kg^{-1}d^{-1}$ for 13 weeks. Sampled one day after final gavage	0.60	1.40	3.25	Not measured	Not measured	4.00	0.50	**Cho *et al* (2013)*****
Controls	Distilled water control	0.60	2.00	2.00	Not measured	Not measured	3.25	0.45	
Wistar Rats 9 weeks old	200 nm diameter anatase	Below LOD	Below LOD	Below LOD	Below LOD	1.0	Below LOD	Below LOD	**Geraets *et al* (2014)*****

(*n* = *6*)	10.9-12.0 mg kg^{-1} bw d^{-1} for 5 days. Sampled 24 h after last exposure							
Controls	Distilled water control	Below LOD	Below LOD	Below LOD	Below LOD	0.5	Below LOD	Below LOD

1.4.3 Gut lumen environment

Ambient chemistry has been shown to affect fate and bioavailability of NMs in all environmental and biological compartments**.** The behaviour and interaction of ENMs with the gut is influenced by a number of factors. Similar to metal chemistry, ENMs (colloids) behaviour (e.g. aggregation) are affected by abiotic factors such as pH, the presence of divalent ions, ionic strength of the surrounding matrix, concentration, collision frequency and temperature (Handy *et al*. 2008). Metal speciation models can be described as equilibrium models, whereas NP behaviour in ionic solutions can be described as a dynamic process where predicted behaviour is modelled using Derjaguin, Landau, Verwey and Overbeek (DLVO) theory (See Handy *et al*. (2008)). Factors that need to be accounted for when using DLVO to predict colloidal dispersion behaviours are particle physico-chemical properties, such as particle size, shape, surface area, concentration, surface charge (measured as zeta potentials) and surface coatings (Oberdorster *et al*. 2005; Abbott and Maynard 2010). Of primary significance to NP behaviour is surface charge and at what pH the point of zero charge (PZC) occurs for the NP in question. Outside the pH range of the PZC the electrical double bilayer will influence particle behaviour. In the context of the gut, pH changes dramatically from the oesophagus through to the colon and it can be expected, just from the view point of pH, that particle behaviour will be considerably altered.

Further complicating particle behaviour is the environment surrounding the NMs. For example, viscosity of the matrix the NMs are in, the presence of peptides (e.g. enzymes, bacterial exudates) and macromolecules (e.g. humic substances, proteins) in the gut may synergistically interact to promote or hinder particle-particle interactions. There is limited information on the interactions of NMs with food matrix

components and the effect this may have on intestinal epithelium, GIT microflora and the fate and behaviour of particles in the gastrointestinal tract.

The gut lumen can contain a myriad of different types of natural particles, including viruses, organic matter/colloids, and metal particles, which will likely influence particle behaviour. As NMs enter the luminal environment they may become covered in a corona of biomolecules which gives the NM a biological identity and differing surface chemistry which can ultimately determine the impact and fate of the particle (Hellstrand *et al*. 2009).

NP contact with the apical membrane of cells within the GIT will initially be subject to successful diffusion/migration of NMs through the mucus layer. Mucus is predominantly water (97%). The remaining constituent is composed of mucoproteins (principally the glycoprotein mucin) which contain sialic acid, carboxylic acid and sulphated residues (Creeth 1978; Handy *et al*. 2008). The mucoproteins are composed of mainly negatively charged ligands, and therefore mucus can be considered as a gel containing a fixed polyanionic matrix (Creeth 1978; Handy *et al*. 2008). The diffusion of NMs through the mucus layer has been demonstrated e.g. Saltzman *et al*. (1994); Norris and Sinko (1997); Szentkuti (1997) and Olmsted *et al*. (2001). For example, Szentkuti *et al*. (1997) demonstrated that polystyrene microspheres (14 and 415 nm diameter) placed in the distal colon of rats could be observed adjacent to the mucosa, whereas larger microspheres (1.1 μm) remained in the mucus layer and the colon. This effect of particle size on diffusion has been supported by Norris and Sinko (1997) who calculated translocation permeabilities of polystyrene NMs in purified GIT pig mucin under steady-state conditions using a modified Ussing-type diffusion chamber. They showed that diffusion of particles over 0.5 μm in size were hindered by the mucin layer. Nevertheless, the authors

concluded that although mucin may be a significant barrier to the oral absorption of particles, the rate-limiting barrier for the absorption of NMs is ultimately the intestinal mucosa (Norris and Sinko 1997). The inability of larger particles to diffuse through the mucus is likely related to the mesh spacing between mucin fibres which has been shown to be between 20 and 200 nm (Olmsted *et al*. 2001). Smaller particles would diffuse unhindered through the mucus. NMs that do become trapped in the mucus through steric hinderence by mucoproteins may agglomerate. However, this would improve residence time and possible contact with the GIT epithelium through endogenous peristaltic movements.

Food grade TiO_2 (anatase) will have an electrical double layer (EDL) following consumption due to the ionic strength and varying pH in the GIT. The surface charge of TiO_2 will change from positive (in the stomach) to negative in the intestine (due to the PZC of TiO_2 at body temperature – see above). Similar surface charge changes will also occur in the mucus lining the GIT. Assuming absorption of NMs occurs in the small intestine in mammals as demonstrated in fish (Al-Jubory and Handy 2012), TiO_2 NPs will have a negative surface charge in the small intestinal gut lumen and so will the mucoproteins lining the epithelial cells which would (from a purely chemical perspective) result in repulsive force. However, as the luminal pH increases there will be a reduction in cationic species within the mucus thereby creating larger gaps within the mucin fibres via electrostatic repulsion which in turn may facilitate direct TiO_2 NP contact with the apical membrane (Handy and Maunder 2009)

The changing pH along the GIT will act on the zeta potential (a measurement of the net charge contained within the electrical double layer (EDL)) of TiO_2 NPs. Cho *et al*. (2013) demonstrated at pH 2 (gastric pH) that the zeta potential of TiO_2 was 54.4 ± 0.7 mV and at pH 8 decreased to 7.9 ± 2.7 mV suggesting particles would be more

dispersed in the stomach and have a greater tendency to agglomerate in the intestine (assuming no other factors are involved\ this is unlikely because food matrix constituents and gut lumen environment will have an effect on particle behaviour). Nevertheless, more research is required to assess the PZC of the mucus constituents and the diffusion coefficients of metal oxide NMs through the mucus lining the epithelium.

1.5 The molecular mechanisms of uptake

The GIT has been exposed to natural NMs throughout evolution and has evolved mechanisms to take up nano scale particulates (Powell *et al*. 2010). For example, the ingestion of red meat exposes the GIT to ferritin particles which are 12 nm in diameter (including the protein shell) and contain an iron oxide core which is 6- 8 nm in diameter (Pan *et al*. 2009). Kalgaonkar and Lonnerdale (2009) showed that ferritin may be taken up by endocytosis into intestinal epithelial cells (enteryocytes). Insoluble NMs are too large to be taken up by ion or other transporters on the cell membranes (Fig. 1-3, 1-4) thereby pointing towards vesicular transport as the mechanism underpinning NP translocation (Handy *et al*. 2008).

Endocytic mechanisms at the apical membranes of cells are generally categorised into two types, broadly according to the size of the endocytic vesicle; phagocytosis and pinocytosis. In phagocytosis, large particles are ingested. In pinocytosis fluid and solutes are ingested via small pinocytic vesicles. Pinocytosis is a constitutive process; it occurs continuously, regardless of the needs of the cell (Alberts *et al*. 2008). Under the generic label of pinocytosis other endocytic process should be mentioned, such as clathrin-mediated endocytosis (CME), caveolae mediated

pinocytosis and macropinocytosis. There are also pathways that are clathrin/caveolin independent (Kirkham and Parton 2005; Cheng *et al*. 2006). Surface chemistry and particle size will influence which endocytic process is utilised for NP internalisation. Rejman *et al*. (2004) demonstrated that uptake pathways of microspheres and nanospheres (50 – 1000 nm) in non-phagocytic murine melanoma B16 cells was strongly influenced by particle size. Internalization of microspheres with a diameter < 200 nm involved clathrin-coated pits. With increasing size, a shift to a mechanism that relies on caveolae-mediated internalization occurred and became the predominant pathway of entry for particles of 500 nm in size (Rejman *et al*. (2004). The authors concluded that that particle size (ligand-devoid) can determine entry pathway. Whether different crystal phases of similar sized particles (such as anatase, rutile and brookite TiO_2) also influences route of uptake is unknown and more research is required on this topic.

1.5.1 Movement of NMs inside gut epithelium cells

Little is known about the intracellular fate of endocytosed NMs in intestinal epithelial cells. However, immunofluorescence techniques have demonstrated endocytosed NMs co-localise with a number of different organelles at different times following vesicular uptake, such as early endosomes, late endosomes, lysosomes, Golgi apparatus and the endoplasmic reticulum (ER) (Cartiera *et al*. 2009).

Depending on the endocytic process, NMs end up in endosomes, caveosomes, free floating in the cytosol or in another unlabelled type of vesicle. All the different endocytic pathways require a deformation (invagination) of the cell membrane followed by pinching off to form a vesicle. Once formed, the vesicle (dependent on

uptake pathways) merges with an early endosomes or caveosome (just beneath the plasma membrane (Fig. 1-3). If particles are not retrieved from the early endosomes and returned to the membrane by transport vesicles (or passed on to basolateral excretory transport vesicles) they are passed on to the lysosomal pathway (Alberts *et al*. 2008). NMs endocytosed by the caveolae pathway are thought to be delivered to caveosomes (similar to endosomes except they avoid lysosomal degradation (Kiss and Botos 2009)). This pathway has been shown to be targeted by small viruses such as SV40 and polyoma virus (around 45 nm in diameter) (Soldati and Schliwa 2006) which allows virus genetic material proximal access to the nucleus. NMs taken up through caveolae may be subsequently released near the nucleus where NMs co-localise with the ER and the Golgi (Cartiera *et al*. 2009). Caveosomes are thought to have some sorting properties (Parton and Simons 2007). For instance, when cholera toxin is within caveosomes it is sorted to carriers that are destined for the Golgi complex (Torgersen *et al*. 2001). It is plausible that NMs may exploit this pathway and once in the Golgi could undergo basolateral exocytosis via the Golgi excretion pathway. It is well known that copper is basolaterly excreted via this pathway and that metals such as mercury can hijack this transport pathway (Handy *et al*. 2000; Hoyle and Handy 2005). Whether this can happen for insoluble NMs is subject to debate and requires more research.

1.5.2 Alternative routes to transcellular uptake: Persorbtion and paracellular transport

NP uptake from the intestinal lumen may also occur through the villus tip in a process known as persorbtion (Powell *et al*. 2010). Persorbtion is described as a passive process which occurs at a low frequency (O'Hagen 1996). The life span of an enteryocyte is between 3 and 6 days (Saladin 2009). During this time the epithelial cell migrates from the crypt up to the tip of the villus (much like an escalator) where it is sloughed leaving a hole in the villus tip allowing particles of up to 150 µm direct access to capillary and lymphatic networks (O'Hagan 1996). This method of uptake has been demonstrated in mice following exposures through drinking water containing 2 parts per billion (ppb) gold NPs for 7 days *ad libitum* (4, 10, 28 and 58 nm diameter) (Hillyer and Albrecht 2001).

Small NMs (< 3 nm) may translocate via the tight junctions of the epithelial cell layer (paracellular diffusion). Diffusion of solutes and presumably small NMs through tight junctions are a function of the innate permeability relating to the structure of the junction and osmotic environment (salt effect on aggregation) (Handy *et al*. 2008). NMs are generally too large to diffuse through the paracellular route although this route cannot be excluded for lipophilic NMs. The Ca^{2+} and Mg^{2+} rich environment in the tight junctions imply that NMs would aggregate rather than diffuse. However, if tight junction integrity is compromised then diffusion through the paracellular route may increase (Handy *et al*. 2008).

Disorders of the gut epithelium that result in excessive inflammation (e.g. Chron' s or ulcerative colitis) could reduce tight junction integrity (see review by Arrieta *et al*. (2006)) promoting paracellular diffusion. Studies have shown that citrate can

increase the permeability of the tight junctions (Powell *et al*. 2010). Citrate is commonly used in oral food preparations (E331) and as a NP dispersant. Increasing tight junction permeability with citrate in small bowel tissue has been demonstrated by Froment *et al*. (1989). Froment *et al*. (1989) showed, under short circuit conditions, exposed tissue in the presence of citrate demonstrated a prolonged reduction in transepithelial electrical resistance (TEER), which is indicative of a reduction in tight junction integrity (Froment *et al*. 1989). Ussing (1982) put forward the idea that sodium-coupled solute transport (e.g., glucose and some amino acids) triggers contraction of the cytoskeletal elements of the enterocyte, resulting in the loosening of tight junctions (Ussing 1982; Sanderson and Walker 1993). Taken together this would suggest that both genetic and external dietary factors could alter tight junction permeability and potentially increase paracellular diffusion of NMs.

1.5.3 Immunological tissue types

Cells and tissues involved in GIT immune surveillance (M-cells of Peyer's patches) have been implicated as areas where uptake of NMs is greatest (Hillery *et al*. 1994; Jani *et al*. 1994; Janer *et al*. 2014) (Fig. 1-4). M-cells are areas which sample the contents of the lumen and present endocytosed particles to immune cells. Macrophages will phagocytose a variety of inanimate particles such as glass or latex beads, asbestos fibres and $TiO_{2,}$ amongst others (Alberts *et al*. 2008), and drain into mesenteric lymph nodes where they could enter systemic circulation. The fate of macrophages within Peyer's patches is unknown.

Dietary studies in rats and mice have shown that TiO_2 NP uptake occurs principally in the Peyer's patches (Jani *et al*. 1994; Brun *et al*. 2014; Janer *et al*. 2014). This is

supported by *in vitro* work on Caco-2 intestinal cells that had been differentiated to express M-cell characteristics. Rieux *et al*. (2005) showed that uptake of 200 nm to 500 nm (diameter) latex particles was increased 1000 fold in comparison to normal Caco-2 cells (control) (Rieux *et al*. 2005). However, an *in vivo* (mice) study performed by Hillery *et al*. (1994) using 60 nm polystyrene spheres orally administered to mice showed that 40% of non-excreted particles (composed of 10% of total particle administered) in the small bowel were in non Peyer's patch locations (Hillery *et al*. 1994) suggesting immune sampling is not entirely responsible for particle uptake in the intestine.

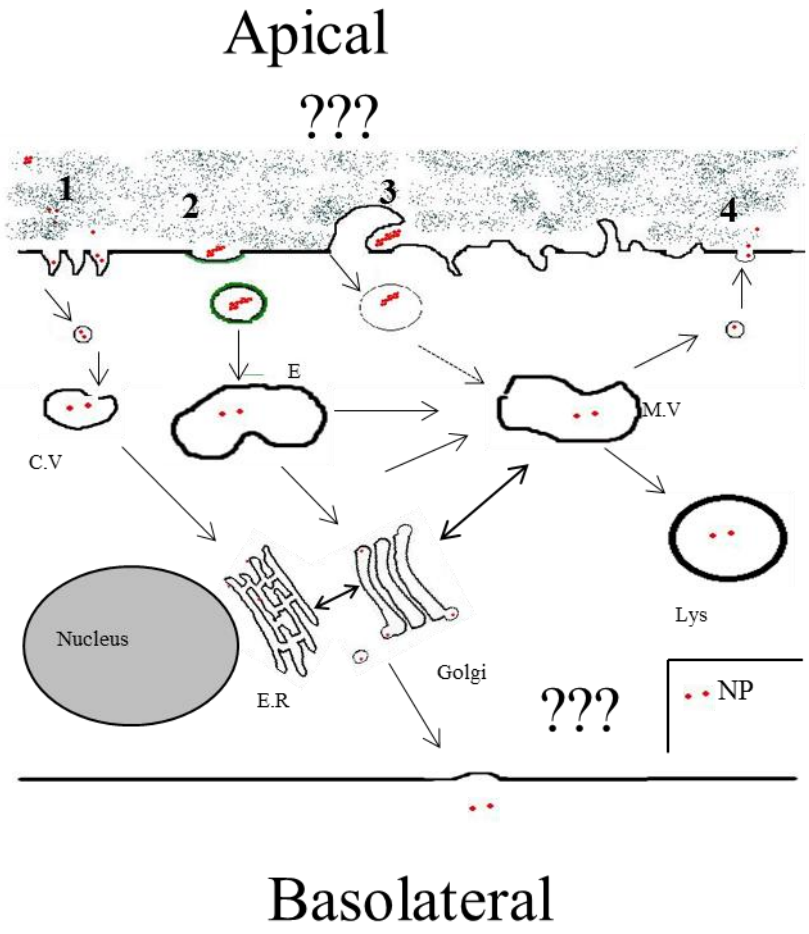

Fig. 1-3:Magnified epithelial cell highlighting possible mechanism of NP endocytosis and transport through a cell.

NP entry into the cell may be mediated by many processes. **1-2**) NMs in the extracellular space could adsorb a corona of biological molecules allowing NP's to be endocytosed through receptor mediated processes (1) calveolae and 2) clathrin) (Hellstrand *et al*. 2009). **1**) Particles taken up through calveolae dependent mechanisms end up in caveosomes (CV) (Alberts *et al*. 2008) which are ferried towards the endoplasmic reticulum (ER) and Golgi or (through an unknown mechanism) enter the nucleus (Alberts *et al*. 2008). Particles endocytosed through clathrin dependent processes end up in endosomes (E) where they are either transported to the Golgi or passed on to the Multivesicular bodies (MV) and either passed on to lysosomes, golgi, or recycled in vesicles destined for the apical membrane (**4**) pathway. Larger aggregates of Np's (<500nm) can be endocytosed through macropinocytosis ending up in macropinosomes (MP). These vesicles then mature down the degradative pathway and become multivesiclar bodies (MV) which may fuse with lysosomes be recycled or passed on to the Golgi excretory pathway.

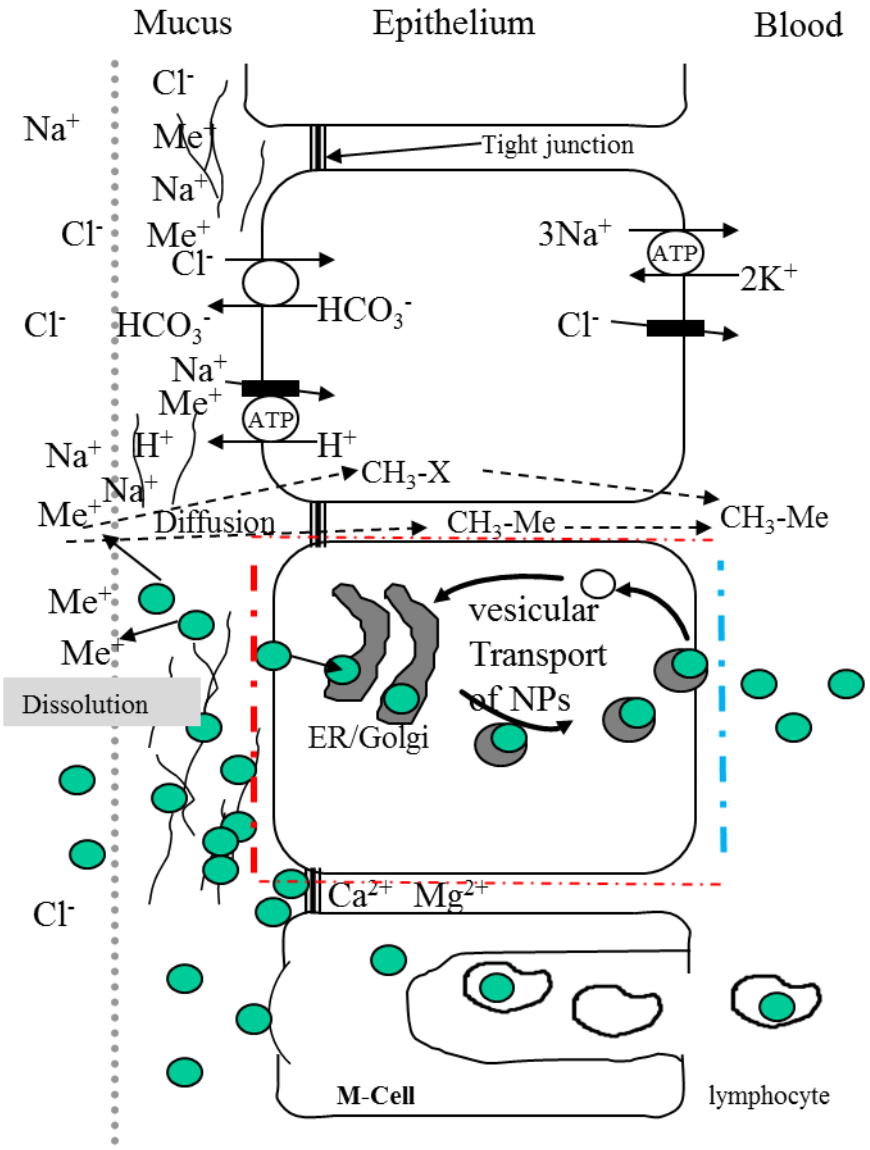

Adapted from Handy et al. (2008)

Fig. 1-4: Idealised diagram of intestinal epithelium

Substances in the gastric secretions must first diffuse into an unstirred layer comprising of water/mucus prior to transfer to the gut epithelium. NP's may aggregate to organic matter in the gut and be trapped by mucus. Metal ions usually move through the cell using ion transport pathways. In contrast, small lipophilic organic chemicals can diffuse through the cells (transcellular diffusion), or between the cells via the tight junctions (paracellular diffusion). NMs are too large to be taken up by ion or other transporters on the cell membranes, and although diffusion cannot be excluded for lipophilic NMs. The Ca^{2+} and Mg^{2+} rich environment in the tight junctions suggest that NMs would aggregate rather than diffuse through the paracellular route. If tight junction integrity is compromised then diffusion through the paracellular route may increase (Handy *et al*. 2008). Active M-cell uptake is likely to play a role in absorbing NP aggregates and when the phagocytes undergo recycling their NP contents may be released into systemic circulation.

1.6 *In vitro* techniques for studying metal uptake across GIT

In order to comply with the 3 Rs regulatory testing is moving towards the use of alternative screening methods for assessing toxicity (see European-Commission (2014)).

1.6.1 Caco-2 cell culture

Monolayers of Caco-2 cells, derived from human colorectal adenocarcinoma, have been widely accepted as an effective and efficient *in vitro* model to predict intestinal metal permeability (e.g. Copper - Arredondo *et al*. 2000; Zerounian and Linder 2002) and more recently for NMs (e.g. TiO_2 - Koeneman *et al*. 2010; Brun *et al*. 2014) (Table 1-5).

The Caco-2 cell line differentiates into polarized cells that exhibit similar morphological and functional characteristics to intestinal enterocytes such as tight junctions and well differentiated apical brush borders (Peterson and Mooseker 1992). While Caco-2 cells are a useful proxy for exploring mechanism(s) of uptake, transport, accumulation and toxicity of metals and NMs, they do not accurately represent *in vivo* uptake rates in the human gut. Primarily, monolayers do not accurately represent the whole structure of the gut. Rather, they can be viewed as just one cell type in the mucosa (enterocytes). There is no mucus on the apical side of these cells which would likely increase NP contact with the apical membrane and subsequent uptake. Moreover, Caco-2 cells were originally immortalized from colon adenocarcinoma cells. Carcinoma cells have been shown to have high trace metal uptake rates due to increased cell proliferation, membrane turnover and higher concentrations of apical membrane metal transporters, which are characteristic of carcinoma cells rather than gut cells (Brookes *et al*. 2006).

1.6.2 Isolated intestinal preparations

An important aspect of research into metal uptake is the precise location of where these processes take place in the gut. The isolated whole gut sac technique (oesophagus through to colon) can be used to determine which sections of the gut are involved in metal uptake (Handy *et al*. 2000; Al-Jubory and Handy 2012). According to Handy *et al*. (2000) gut sacs are prepared by quickly removing them from the experimental animal and filling them with the test substance for up to 4 h. Subsequent analysis of tissue metal concentration serves as a useful proxy for determining the primary regions of the gut involved in metal uptake. Further experiments using the isolated perfused intestine can be performed on the GIT section that demonstrated increased metal accumulation with a view to ascertaining metal uptake rates and potential mechanisms.

Historically the perfused intestine preparation has been used to study the uptake of water and solutes (Ando *et al*. 1986) (Table 1-5) in vertebrate gut and has also been used for measuring uptake of toxic metals (Handy *et al*. 2000; Hoyle and Handy 2005). The technique involves removing a section of intestine, carefully everting it so that the mucosal epithelium is facing outward and placing it in a physiological gut saline (Fig. 1-5). The serosal part of the gut (now on the inside) is then perfused with gut saline via a peristaltic pump. This set up allows for manipulation of either the mucosal or serosal solution (e.g., temperature, addition of NMs, addition of pharmacological inhibitors etc.) to ascertain rates of metal/particle uptake or the mechanisms involved. The viability criteria of this type of preparation are confirmed by observing normal morphology, steady perfusate flow rate, low lactate dehydrogenase (LDH) leak into the mucosal and serosal solution, normal pH fluctuations and negligible leak of Na^+ and K^+ leak into the mucosal solution. Taken

together these criteria are a robust indicator of a successful preparation. The utility of this preparation with NMs has been successfully demonstrated by Al-Jubory and Handy (2012) using trout intestine at 15°C, although it is unclear whether this preparation will work for NMs when the mucosal/ serosal solutions are heated to 37°C for mammalian preparations.

The benefits of intestinal perfusions preparations relative to cell culture models are preparations use healthy physiologically and morphologically normal tissues which is more representative of the *in vivo* situation; the quality of the data (e.g. representative uptake rates) is more relevant, assuming appropriate care has been taken during the preparation and suitable physiological saline(s) are used (species specific, isotonic solution). A weakness of the preparation is it is not particularly high throughput (in comparison to culture models) and the tissue has been removed from the animal which will effect autonomic nervous system activity.

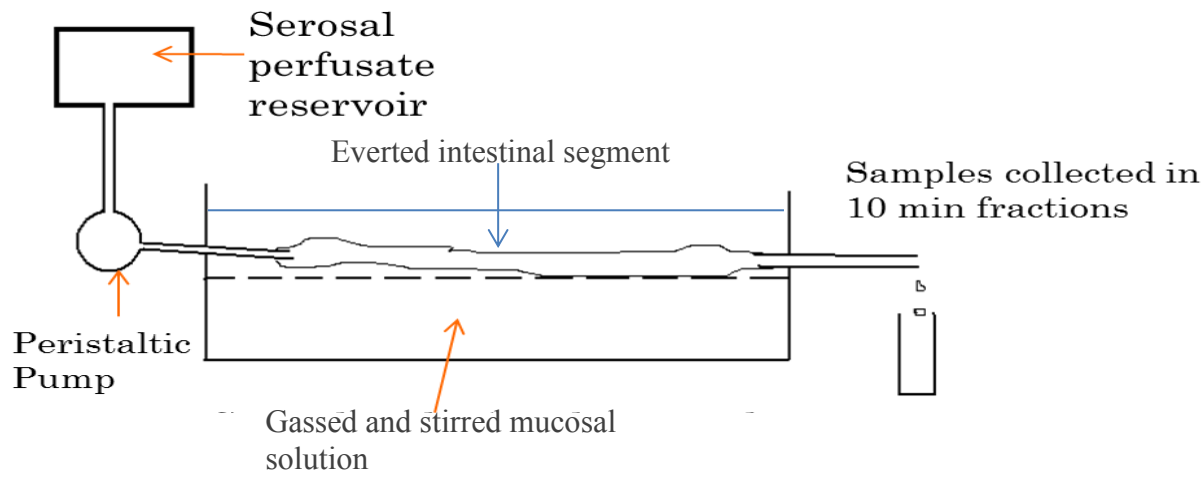

Fig. 1-5: Schematic of isolated everted intestinal perfusion

This set up allows for easy manipulation of the serosal and mucosal solutions. In this study the test material was is in the mucosal solution. Pharmacological inhibitors can be placed in the serosal perfuste or the mucosal solution to investigate pharmacological effects on uptake accumulation and transport.

Table 1-5: *In vitro* techniques for studying metal uptake and toxicity

Technique	Chemical	Concentration	Measured factors	Results	Author(s)
Caco-2 cell culture (Flat plates)	Iron, copper and zinc	5, 10, 20, and 50 µm Fe, Cu, Zn for 60 min	Effect of increasing intracellular concentrations of iron zinc and copper on iron and copper uptake	Fe uptake was reduced in the presence of high extracellular Cu and visa versa.	Arredondo *et al*. (2006)
Caco-2 cell culture (Hanging inserts)	Copper chloride, Iron sulphate	0.1-2 µm for 90 min	The effect of cellular copper availability on uptake transport and absorption of Iron	Removal of cellular Cu caused a doubling of iron uptake.	Zerounian and Linder (2002)
Caco-2 cell culture (Hanging inserts)	Iron, Manganese, Copper	0-15 µmol L^{-1} for 60 -90 min	Mechanism of iron absorption (vesiculare and ion transport across DMT1).	Endocytosis is a fundamental aspect of intestinal iron absorbtion. Excess extracellular concentration of Mn and Cu reduced uptake of Fe across DMT1.	Linder *et al*. (2006)
Caco-2 cell culture (Hanging inserts)	Anatase/ rutile mix TiO_2 NPs.	10, 100, 1000 µg mL^{-1} 24 h (acute) or 10 days (chronic).	Trans epithelial resistance, uptake and transport of TiO_2.	1000 µg mL^{-1} TiO_2 caused a significant reduction in transepithelial resistance at 7 days. Relatively more TiO_2 accumulated in cells at lower concentrations	Koeneman *et al*. (2010)
Caco-2 cell culture (Hanging inserts)	TiO_2 NPs (12 nm) Anatase	50 µg mL^{-1} 48 h exposure	Trans epithelial resistance Paracellular permeability, cell viability	TiO_2 accumulated in cells but was not present in the serosal compartment. Cell viability remained unaffected.	Brun (2014)
Perfused intestine (Rat)	Calcium/ Mannitol	0.4 mM calcium chloride and 0.025 µCi mL^{-1} ^{45}Ca. 60 mins exposure	Active transport and passive transport of calcium, transport of labelled mannitol was taken as a measure of passive permeability	High calcium increased passive transport of mannitol and calcium whilst reucing active transport of calcium.	Rao (2009)

Perfused intestine (Rat)	Copper and sodium	Cu 31.5 µmol L^{-1} in isotonic solutions	Effect of Na^{+} addition on Cu retention, effects of amiloride and furosemide	Cu retention higher in the absence of Na^{+}. Amiloride reduced copper uptake.	Wapnir (1991)
Perfused intestine Fish; African walking (Catfish)	Copper	10, 50, 100 µmol L^{-1} for 2 h at $22^{0}C$	Intestinal Cu uptake, effects of ion-transport inhibitors and manipulation of Cl^{-} gradient Water flux	Cu tissue accumulation showed a dose-dependent elevation. Inhibition of anion transport caused a 3 fold increase in copper absorption.	Handy *et al* (2000)
Perfused intestine (Fish; Rainbow trout)	Inorganic mercury	0-100 µmol L^{-1} for 4 h	Regional intestinal uptake of Hg, effects of amiloride and Ca^{2+} chelators	Luminal exposure to [Hg] between 0 and 100 µmol L^{-1} for 4 h showed a non-linear dose-dependent accumulation with a maximum Hg uptake rate of about 103 nmol g^{-1} h^{-1}	Hoyle and Handy (2005)
Perfused intestine (Fish; Rainbow trout)	TiO_2 NPs (P25) and Bulk	1 mg L^{-1} for 4 h	Intestinal Ti uptake Effects of inhibitors on uptake Water flux	Overall mucosal to serosal uptake of Ti was 0.85 ± 0.32 and 2.38 ± 0.68 nmol g^{-1} h^{-1} for bulk and nano respectively. Vanadate abolished the serosal appearance of Ti.	Al-Jubory and Handy (2012)

1.7 Hypotheses

The hypothesis of this study is that TiO_2 particles are bioavailable and can translocate through gut epithelial cells and enter the serosal compartment mediated via vesicular energy dependent processes (Fig. 1-3, 1-4). It is hypothesised that the physico-chemical properties of NPs such as particle size and crystal structure will alter uptake rates and exert different physiological effects on tissues relative to bulk versions of the same material. However, it is possible that any 'nano' effect could be offset by the propensity of NPs to form agglomerates in high ionic strength solutions, so the cells and tissues may not be exposed to primary NPs but larger agglomerates.

The following hypotheses will be tested:

i. Bulk and nano TiO_2 is taken up through intestinal cells via active processes, the rates of which are influenced by particle size and crystal structure. Pharmacological inhibitors will be used to investigate the mechanism(s) responsible (Chapters 2, 3 and 4).
ii. Uptake of bulk or TiO_2 NPs occurs without compromising epithelial layers. Viability will be assessed using LDH, histology and tight junction integrity (Chapters 2, 3 and 4).
iii. NPs will exert different physiological effects in comparison to bulk versions of the same material (Chapters 2, 3 and 4).
iv. TiO_2 uptake occurs in the mammalian small intestine (Chapter 4).
v. TiO_2 uptake occurs *in vivo* at physiologically relevant doses following normal murine eating behaviour (Chapter 5).

1.8 Aims of the Thesis

The overall aim of this research is to explore NP uptake and effects of TiO_2 on the GIT of mammals using Caco-2 cells, the perfused rat intestine and the whole rat. There is a lack of information on the effect of crystal structure on uptake processes, the mechanisms underpinning uptake processes and the rates of uptake across the GIT. There are currently large knowledge gaps on the absorption, and distribution of TiO_2 following normal eating behaviour (physiologically relevant administrations of TiO_2). This thesis will contribute to filling these knowledge gaps as well as informing the evaluation of hazards posed to humans following oral exposure to different crystal types of TiO_2 NPs at physiologically relevant concentrations.

The specific objectives of the study are:

i. To determine the effect of crystal structure and size on uptake rates and accumulation in Caco-2 cells;
ii. to assess the effect of cell maturation on uptake and accumulation;
iii. to investigate; which part of the mammalian gut is responsible for uptake of TiO_2 using the isolated whole gut sac preparation and explore the rates of particle (bulk and nano TiO_2) uptake in the perfused intestine and the mechanisms of uptake in the perfused intestine;
iv. to determine whether dietary TiO_2 can be detected *in vivo* following normal murine eating patterns; and
v. to compare the different methods of determining uptake and accumulation rates with a view to informing hazards presented to humans following exposure to physiologically relevant doses.

Chapter 2: Apical uptake and accumulation of different crystal structures of TiO_2 nanoparticles by 5 day old Caco-2 intestinal cells

2.1 Abstract

The gastrointestinal uptake of different crystal structures of TiO_2 was investigated using Caco-2 intestinal cells. The approach involved exposing cells to medium containing 1 mg L^{-1} of different forms of TiO_2. Caco-2 monolayers exhibited time-dependent uptake of Ti from TiO_2 exposures of 1 mg L^{-1} over 24 h, which was influenced by crystal type. Initial accumulation rates were 3.01, 2.75, 2.11 and 3.26 nmol mg^{-1} protein h^{-1} for bulk, P25, anatase and rutile forms respectively. All exposures caused elevations of total Ti metal in the cells relative to the control (ANOVA $P < 0.05$). Electron micrographs of the Caco-2 monolayer showed the presence of particles inside the cells, and energy dispersive spectroscopy (EDS) confirmed the composition as TiO_2. Incubating the cells with 120 IU mL^{-1} nystatin (putative endocytosis inhibitor) or 100 µmol L^{-1} sodium orthovanadate (vanadate) (ATPase inhibitor) caused a large increase in Ti accumulation for all crystal types relative to the controls (ANOVA $P < 0.05$), except for the rutile form with vanadate. Incubating the cells with 90 µmol L^{-1} genistein (tyrosine kinase inhibitor) or 27 µmol L^{-1} chlorpromazine (clathrin-mediated endocytosis inhibitor) caused a large decrease in Ti accumulation relative to the controls (ANOVA $P < 0.05$). Cell viability measures were generally good (low LDH leak, normal cell morphology), but changes were observed in the electrolyte composition (K^+, Na^+, Ca^{2+}, Mg^{2+}) of exposed cells relative to controls. A rise in total Ca^{2+} concentration in the cells was observed for all TiO_2 crystal type exposures. Overall, the data shows that Ti accumulation for TiO_2 NP exposure in Caco-2 cells is crystal structure-dependent, and that the mechanism(s) involves endocytosis of intact particles.

2.2 Introduction

There is growing interest in the use of engineered nanomaterials (ENMs) in the food sector with suggested applications including the encapsulation of essential nutrients, the inclusion of nano minerals in food; and the use of ENMs as antibacterial agents to improve the shelf life or packaging of perishable goods (Aitken *et al*. 2006; Chaudhry *et al*. 2008; Tiede *et al*. 2008). ENMs are also used in oral personal care products (e.g., tooth pastes); in drinking water technology (Handy and Shaw, 2007); and have been proposed for medicines that are intended for ingestion (Garnett and Kallinteri 2006), It is therefore clear that humans are likely to be exposed to ENMs via an oral route, but current understanding of the bioavailability and uptake mechanisms of ENMs across the gut epithelium is limited (Panessa-Warren *et al*. 2006; Bouwmeester *et al*. 2009).

Bulk forms of titanium dioxide (TiO_2) have been used in foods as a whitening agent (E171) for many years, and estimates of daily ingestion rates collectively for all forms of TiO_2 are between 5 and 50 mg in Europe and the USA (Lomer *et al*. 2000; Weir *et al*. 2012). It is likely that a fraction of the traditional ingested bulk TiO_2 was incidentally at the nano scale (estimated at around 35%, Weir *et al*. 2012), and with engineered TiO_2 nanoparticles (NPs) now being available, it seems likely that increased ingestion of nano forms of TiO_2 will occur (Weir *et al*. 2012). Studies with ultrafine (< 100 nm) TiO_2 particles have shown respiratory toxicity and epithelial inflammation of the lung in rodents (e.g., Ferin and Oberdörster 1985; Ferin *et al*. 1992; Bermudez *et al*. 2004; Warheit *et al*. 2007). Like the lung, the gut also consists of mucous epithelia and there are concerns that TiO_2 NPs may be toxic to the gastrointestinal tract.

In vivo exposures using gut gavage to administer salines containing TiO_2 NPs have confirmed oral toxicity in rodents. Wang *et al*. (2007) exposed mice to ultrafine (25 or 80 nm) or fine (155 nm) TiO_2 particles by single oral gavage. Although no clear acute mortality occurred, changes to serum biochemical parameters indicating some loss of liver function and liver pathology (inflammation, necrosis) was observed (Wang *et al*., 2007). *In vivo* studies with other metals have also shown toxicity to the internal organs with oral gavage (Cu NPs, Chen *et al*. 2006; Zn NPs, Wang *et al*. 2008). In the latter, the symptoms also included gastrointestinal tract irritation (vomiting and diarrhoea) for the first few days (5 g kg^{-1} body weight of nano scale Zn, 58 nm diameter NPs). However, the few studies where the TiO_2 has been incorporated into animal feed show little systemic toxicity (e.g., fish, Ramsden *et al*. 2009) indicating that the bioavailability of Ti in food is low.

There is some evidence for the uptake of Ti and/or TiO_2 NPs across the gut. Al-Jubory and Handy (2012) recently reported nystatin-sensitive transepithelial uptake of Ti from TiO_2 NPs across the isolated perfused intestine of trout, and found resting Ti uptake rates of around 1 - 2.4 nmol g^{-1} h^{-1}; similar to that of other non-essential divalent metals (e.g., Cu, Handy *et al*. 2002). In humans, particle size and dose-dependent increase of blood total Ti concentration following oral ingestion of anatase TiO_2 has been observed (Bockman *et al*. 2000), providing some evidence for a particle size-effect on dietary uptake. Studies using cultured monolayers of Caco-2 cells suggest some Ti uptake, possibly of intact particles, without disruption to the epithelium (Koenman *et al*. 2010; Janer *et al*. 2014).

However, the exact mechanism of TiO_2 NPs uptake by the gut epithelium is unclear. The possibilities include uptake of dissolved metal ions by dissolution of the particles

in the gut lumen or in the mucus layer on the epithelial surface; and/or direct uptake of NPs by endocytosis-related pathways at the mucosal membrane (see review by Shaw and Handy 2011 on nano metals). It is also unclear if the bulk material uses the same uptake pathway as the equivalent nano form. The situation is further complicated by the existence of several different crystal structures of TiO_2 including brookite, anatase and rutile (the latter two being more commonly produced; Chen and Mao 2007). Although cell culture studies have suggested some differences in the toxicities of the rutile and anatase forms (mostly in lung epithelial cells, Sayes *et al*. 2006; Singh *et al*. 2007), it is not clear if crystal structure influences the rate of uptake of Ti from TiO_2 NPs by gut cells, or if the different forms have different uptake mechanisms.

The overall aims of this research were to demonstrate the utility of the nascent Caco-2 cell line for Ti metal accumulation studies with TiO_2 NPs and then to compare the uptake of Ti from the bulk and nano forms (size effect), as well as the effects of different crystal structures (anatase and rutile). The approach used electrically tight, confluent monolayers of Caco-2 cells at 4 - 5 days old to enable fundamental metal uptake studies without the confounding factor of incidental nutritional uptake by non-specific processes in the aged epithelium (e.g., absorptive food vacuoles). The experiments included detailed pharmacological investigations into solute transport pathways for metals using sodium orthovanadate (a tyrosine phosphatase inhibiter and P-type ATPase inhibitor which blocks active ion transport (Cantley *et al*. 1978) and has been successfully demonstrated as an ion transport inhibitor in trout intestine (Al-Jubory and Handy 2012), as well as pharmacological studies to establish whether the different sizes or forms of TiO_2 were using different pathways to enter the cells and whether there is a cholesterol dependent component

to uptake and accumulation. For example; nystatin which sequesters cholesterol to prevent the initiation of the non-specific lipid raft formation needed for membrane invagination during calveolae-based endocytosis (Ros-Baro *et al*. 2001; Le and Nabi. 2003; Silva *et al*. 2006); chlorpromazine, which has been shown to inhibit clathrin mediated endocytosis; genistein which has been demonstrated to inhibit caveolae mediated endocytosis *in vitro* (Dos Santos *et al*., 2011); and amiloride which has been successfully used as a macropinocytosis inhibitor *in vitro* for NP uptake investigations (Koivusalo *et al*., 2010). Finally, measurements of electrolytes in the cells, biochemical measurements of cell integrity, and electron microscopy investigations were carried out to understand the physiological basis of any differences observed.

2.3 Materials and methods

Several experiments were performed using confluent monolayers of Caco-2 cells in culture medium (see below). The first series determined the total Ti metal accumulation in Caco-2 cells exposed to 1 mg L^{-1} of different forms of TiO_2 (bulk, nano P25 which was a mix of 25% rutile and 75% anatase, nano anatase, or nano rutile) over 24 hours. Effects on cell viability (LDH activity in the media, cell morphology) and electrolyte concentrations were also measured. The second series of experiments involved pharmacological investigations to determine whether or not the observed Ti metal accumulation involved either solute transport or endocytosis-related pathways for uptake at the mucosal (apical) membrane. In the third series of experiments, after having pharmacologically identified both solute transport and likely endocytosis components to Ti accumulation, pathways were probed using specific inhibitors of the possible routes involved for the different forms of TiO_2. In

the present study, the authors adopt the same precise terminology for metal accumulation as used by Al-Jubory and Handy (2012). All data on Ti accumulation were normalized as a total Ti metal concentration in the cells, expressed as nmol Ti metal mg^{-1} cell protein (not TiO_2 compound), and are distinguished from the mg L^{-1} of TiO_2 compound added to the cell culture media when confirming the exposure. The phrase “total Ti metal concentrations” refers to the total mass concentration of Ti (not TiO_2 compound) in the cells or relevant media determined by inductively coupled plasma optical emission spectroscopy (ICP-OES, Varian 725 ES, see below). It does not infer whether the Ti was present as particulate TiO_2 or as a dissolved Ti species. The term “Ti accumulation” signifies a net increase in the total Ti metal concentration in the cells over time, determined by ICP-OES of the digested cells.

2.3.1 Cell culture

A human intestinal cell line, Caco-2 (brush border expressing, European collection of cell cultures; catalogue no: 86010202; the supplier indicated that these cells were of the same origin as the ATCC HTB-37 Caco-2 cell line) was routinely incubated in 75 cm^2, 200 mL flasks (Iwaki T75, Japan) containing 15 mL of Dulbecco’s Modified Eagle Medium (DMEM) supplemented with 10% fetal bovine serum (FBS), 1% glutamine and 1% penicillin-streptomycin (100 IU penicillin and100 µg mL^{-1} streptomycin), at 37 ºC and gassed with 95% air: 5% CO_2. The DMEM, FBS, glutamine and penicillin-streptomycin was obtained from Lonza (Verviers, Belgium). For routine maintenance, the medium was changed every 48 h and the cells were sub-cultured by trypsinization. Experiments were conducted on cells between passage 60 and 75 (cells were purchased at passage 45) and antibiotics were withdrawn to avoid possible interference with ion transport ≥ 2 passages before

seeding the cells into 6-well plates (Iwaki microplates, Japan) for experiments. Preliminary trials were conducted to determine the optimum seeding density and time to confluence of the cells in 6-well plates by measuring the electrical resistance of the monolayer using an xCelligence real time label free cellular analysis system (Real-Time Cell Analyzer (RTCA), Roche Applied Science). In brief, the instrument monitors the change in electrical impedance associated with the electrical coupling of the epithelium during cell growth. Cells were grown on gold-coated wells (electrode), as cells adhered and spread across the well surface, increases in impedance were recorded. When confluence is reached, the impedance value (cell index) remains constant. A seeding density of 5×10^4 cells cm^{-2} produced confluence by 24 h (Fig.2-1). Subsequently for all experiments, cells were seeded at 5×10^4 cells cm^{-2} in the 6-well plates and, after an initial 24 h growth, the cells were left for a further 72 h to ensure both 100% confluence and that the cells were rested. The cells were also visually inspected (Phase contrast microscope, Olympus/CK30-F200, Japan) each day until they became confluent. Cell viability was checked by Trypan blue exclusion prior to seeding the flasks and 6-well plates. Briefly, 0.1 mL of a 0.4% solution of trypan blue in buffered isotonic salt solution (PBS) (pH 7.2 to 7.3) was added to 1 mL of cells and the mixture was immediately loaded onto a haemocytometer. Cells were counted and % viable cells were calculated as follows.

% viable cells = [1.00 – (Number of blue cells ÷ Number of total cells)] × 100.

Flasks with less than 90% cell viability were discarded. Lactate dehydrogenase leak (LDH) was also checked (see section 2.3.7).

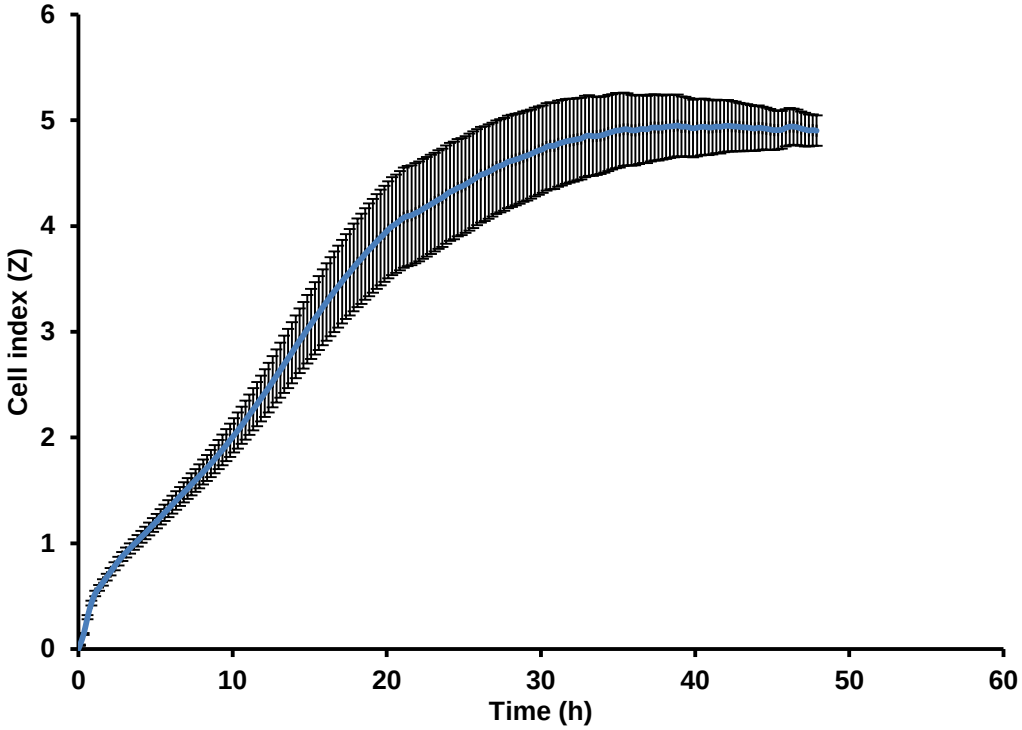

Fig. 2-1 : Change in cell index over time for Caco-2 cells seeded at a density of 5 x 10^4 cells cm^{-2}. Cell index is a surrogate measure of impedance. Steady resistance is achieved at around 35 h post seeding. Plots are means ± SEM (n = 6) from the replicate data.

2.3.2 Stock dispersions and materials characterisation

Four different types of TiO_2 were used (manufacturer's information): (i) bulk TiO_2 powder (ACROS, Titanium (IV) oxide, New Jersey, USA), composed of 75% anatase and 25% rutile crystal forms (Al-Jubory and Handy 2012), at a purity of 98.0-100.5% TiO_2. (ii) Ultrafine TiO_2 NP type "Aeroxide" P25 (DeGussa AG, supplied by Lawrence Industries, Tamworth, UK) with a crystal structure of 25% rutile and 75% anatase TiO_2 (purity was at least 99 % TiO_2 maximum impurity stated was 1% Si), the average particle size was 21 nm. (iii) Anatase TiO_2 NP form (US Research Nanomaterials, Inc, Houston, Texas, USA) with purity of 99% and 10-25 nm average particle size. (iv) rutile TiO_2 NP form (US Research Nanomaterials, Inc, Houston, Texas, USA) with high purity, 99.9% and 30 nm average particle size. A stock

dispersion of 500 mg L^{-1} for each type of TiO_2 was made by dispersing the particles in 200 mL of ultrapure water (Millipore, deionised water) in a 500 mL pyrex glass container by vigorous manual shaking for 1 - 2 min. Preliminary studies identified the materials as a source of bacterial contamination of cell cultures and subsequently all stock dispersions and the dry powder were gamma irradiated to sterilise them (Red Perspex, Turntable Irradiation Geometry, Becton Dickinson, Plymouth, England). The radiation dose used was 36.42 - 40.72 kGy for 10 h to ensure sterility before starting cell culture experiments.

The particle characterisation followed a similar protocol to our previous studies with TiO_2 NPs in the intestine (Al-Jubory and Handy 2012). Briefly, sub samples of the 500 mg L^{-1} stock dispersions made in ultrapure water were examined for primary particle size using transmission electron microscopy (TEM, JEOL-1200EX II) (Fig. 2-2). The primary particle size was 103.2 ± 16 nm (mean ± S.E.M., *particle numbers measured* = 7), 22.8 ± 0.6 nm (mean ± S.E.M., particle numbers measured *n* = 169), 16.4 ± 2.4 nm (mean ± S.E.M., *particle numbers measured* = 6) and 30.8 ± 2.5 (mean ± S.E.M., *particle numbers measured* = 7) for bulk, P25, anatase and rutile, respectively.

The particle size distribution was also determined using nanoparticle tracking analysis (NTA, Nanosight LM10, Nanosight, Salisbury, UK, laser output set at 30 mW at 640 nm). In order to achieve reliable tracks of individual particles, a 10 mg L^{-1} dilution in ultrapure water of the concentrated 500 mg L^{-1} stocks were used. The dispersions gave a mean hydrodynamic diameter of 179.3 ± 13.7, 7.1 ± 4.1, 142.3 ± 14.4 and 88.3 ± 34.1 nm (mean ± S.E.M., n = 3) for bulk, P25, anatase and rutile, respectively (Fig. 2-2). Attempts were made to determine particle size distribution of

the materials in DMEM culture media. However, the medium alone contained a high background of apparent particulates (most likely NaCl crystals) and the DMEM medium with supplements gave particle size distributions with a smallest bin size of approximately 30 nm and average hydrodynamic diameters for the whole sample around 156 nm. Furthermore, the NTA of the DMEM with supplements gave high particle number concentrations (90 x 10^6 particles) due to the presence of proteins, and completely masked the particle counts due to TiO_2 (4-10 times lower than that of the culture medium). Thus attempts to detect TiO_2 particle distributions in the culture medium gave poor reproducibility by NTA due to this high background (SeeFig. 2-3).

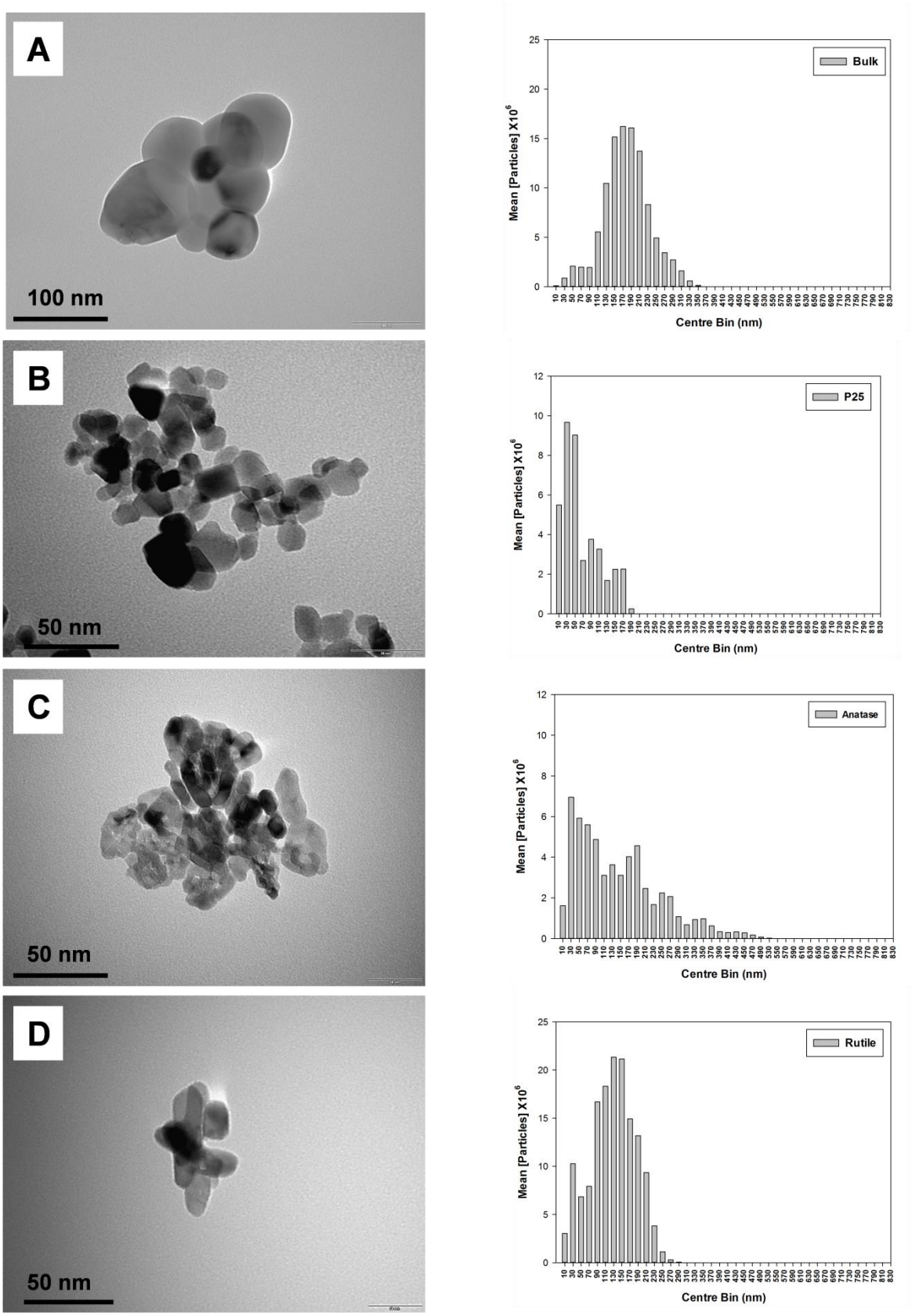

Fig. 2-2:Transmission Electron microscope (TEM) images showing primary particles, and particle size distributions by nanoparticle tracking analysis (hydrodynamic diameter, Nanosight LM10) of; (A) bulk TiO_2 particles, scale bar = 100 nm, (B) P25, scale bar = 50 nm, (C) anatase, scale bar = 50 nm and (D) rutile, scale bar = 50 nm at a concentration of 10 mg L^{-1} (dilutions of the 500 mg L^{-1} stocks) in Milliq water. Particle size distribution plots are individual examples from triplicate measurements.

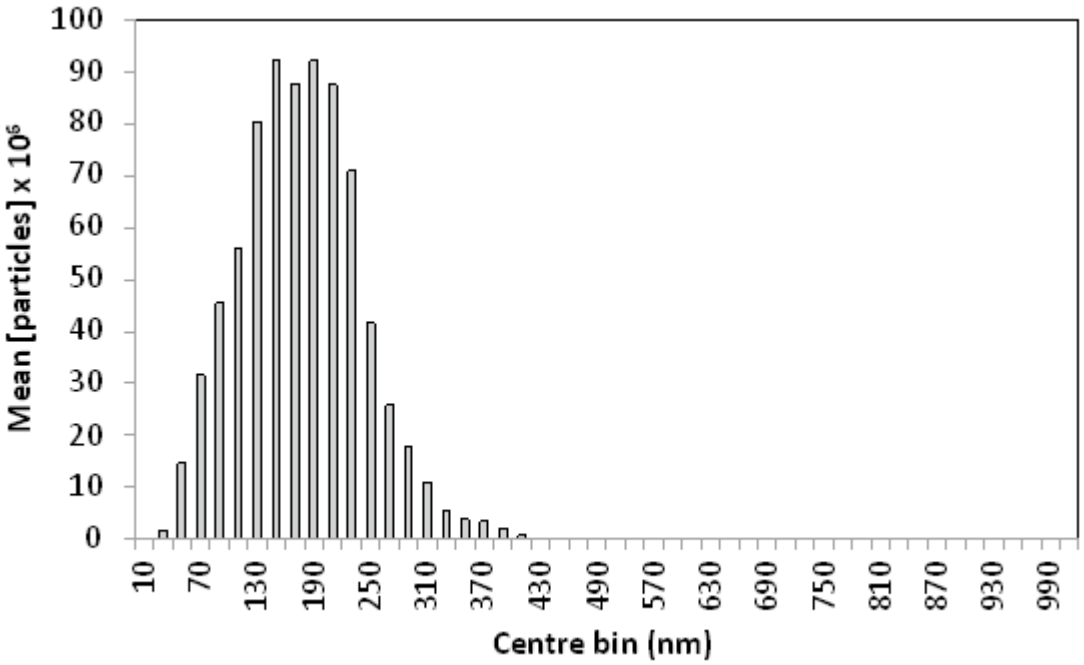

Fig. 2-3 : Nanosight particle size distributions of culture ready media. The histogram is an individual example from a triplicate of the culture medium without nanoparticles added.

2.3.3 Experiment 1: Time course of Ti accumulation from different forms of TiO_2

This experiment determined the time course of Ti accumulation for the different forms of TiO_2 in Caco-2 cells over 24 h. Confluent cells (72 h after seeding) were exposed to the cell culture medium (as described in section 2.3.1 minus antibiotics) containing 1 mg L^{-1} of no added TiO_2 (control), bulk, P25, anatase or rutile forms of TiO_2. The six-well plate was the unit of replication in the experiment, with each plate containing cells with no TiO_2 additions (2 control wells), and a well for each of the test materials. At least three plates were prepared for each time point in the experiments (*n* = 3 replicates/time point) and in order to avoid pseudo replication experiments were temporally separated and performed on different passages of cells. Dosing of the wells was performed by diluting the initial 500 mg L^{-1} stock to 10 mg L^{-1} TiO_2 in ultrapure water, and this secondary stock was mixed with fresh culture

medium (1 mL of the appropriate 10 mg L^{-1} TiO_2 stock: 9 mL DMEM) to obtain a final concentration of 1 mg L^{-1} TiO_2 for the exposures. Two mL of the appropriate media was pipetted into each well. Media and cells were then collected at 0, 2, 4, 6, 8 and 24 h of exposure for total Ti determination, electrolyte concentrations and LDH activity (see section 2.3.6 and 2.3.7).

2.3.4 Experiment 2: The effects of nystatin and sodium orthovanadate (vanadate) incubation on Ti accumulation

Having established the time course of Ti accumulation in Caco-2 cells from exposure to the different forms of TiO_2 the next stage was to assess the effect of mucosal (apical) additions of nystatin (a putative endocytosis inhibitor, Lewis *et al*. 1977) and sodium orthovanadate (a P-type ATPase inhibitor which blocks active ion transport, Cantley *et al*. 1978) on Ti accumulation. Cells were grown and exposed to 1 mg L^{-1} of the forms of TiO_2 as above, but, 1 h before to dosing with the appropriate particles, cells were pre-incubated with either 120 IU mL^{-1} of nystatin (dose to produce 100% inhibition, Lewis *et al*. 1977), or 100 µmol L^{-1} sodium orthovanadate (enough to block metal transport in the intestine, Handy *et al*. 2000), compared to drug-free controls with and without added TiO_2 (n = 6 plates/treatment, with separate drug free controls). Inhibitors were dissolved in 500 mL of DMEM. This pre-incubation enabled the drugs to have direct contact with the cells without the risk of interference from the test materials (e.g. loss of bioavailable drug due to adsorption onto particles). The inhibitors remained in the medium throughout the experiment, and the appropriate TiO_2 dose was simply added to the medium after the initial 1 h pre-incubation. After 24 h cells and media were analysed as described in section 2.3.3..

2.3.5 Experiment 3: The effects of chlorpromazine, genistein and amiloride on Ti accumulation

The second experiment above identified a nystatin-sensitive component to Ti accumulation, and the final series of experiments were carried out in order to identify which endocytosis-related mechanisms might be involved. Three different drugs were tested, and drug concentrations were selected after some range determination experiments. The drugs consisted of: 27 µmol L^{-1} chlorpromazine (a specific inhibitor of clathrin-mediated endocytosis, Wang *et al*. 1993), 90 µmol L^{-1} genistein (a tyrosine kinase inhibitor, which prevents caveolae scission and disrupts the actin cytoskeleton, Le and Nabi 2003) and 1.25 mmol L^{-1} amiloride hydrochloride hydrate. The latter is a well-characterised blocker of epithelial Na^+ channels (Handy *et al*. 2002), but may also prevent non-specific macropinocytosis (Iversen *et al*. 2011). Amiloride and chlorpromazine were dissolved in warm deionised water (to ensure all solids were in solution) at concentrations of 50 mmol L^{-1} and 3.7 mmol L^{-1} respectively. Genistein was dissolved in DMSO at a concentration of 9.25 mmol L^{-1}. The stock solutions of each drug were filter sterilised (0.22 µm, Millipore) to prevent bacterial contamination of the cell cultures, before being diluted to the appropriate working concentrations (above) in the culture medium. The experiments were conducted exactly as above (n = 6 plates/treatment, with separate drug free controls), except that cells were pre-incubated for 1 h with the appropriate drug prior to the 24 h TiO_2 exposure. Samples for Ti, electrolytes and LDH were collected at the end of the experiment.

2.3.6 Titanium and electrolyte determination in cells

Following careful removal of the culture media, the cells attached to the dish were washed twice with 2 mL of an isosmotic sucrose buffer (300 mmol L^{-1} sucrose, 0.1 mmol L^{-1} ethylenediaminetetraacetic acid (EDTA), 20 mmol L^{-1} 4-(2-hydroxyethyl)-1-piperazineethanesulfonic acid (HEPES), buffered to pH 7.4 with 2 mol L^{-1} Trizma base) to remove any residual culture medium and the external electrolytes therein. Cells were then carefully scraped off the bottom of the well (Fisher scientific cell scraper, 250 mm handle, 18 mm blade) and re-suspended in the well with 1 mL of a sucrose lysis buffer (the recipe above, but hypo-osmotic with only 30 mmol L^{-1} sucrose). The resulting homogenate was pipetted into 13 mL test tubes (Fisher Scientific) and sonicated (power 100 Watt, setting 8 on the speed dialat a frequency of 22.5 kHz, Misonix incorporated, XL2000-010, New York) for 30 seconds to ensure the lysed sample was thoroughly lysed and mixed. Each sample was then gently centrifuged for 1 min to remove debris (~160 *g*, Heraeus instruments, Biofuge *pico*, Germany) and 200 µL aliquot of the supernatant taken fresh for measurement of LDH activity and protein (see below). The remaining 800 µL of the cell homogenate was digested in 1 mL of concentrated nitric acid (7 %) at 70 ^{o}C for 4 h, and total Ti, Na^{+}, K^{+}, Ca^{2+} and Mg^{2+} determined by ICP-OES. Samples were vortexed for 20 s prior to being drawn into the instrument to ensure mixing, and calibrations were performed with matrix-matched multi-elemental standards containing Ti, Na^{+}, K^{+}, Ca^{2+} and Mg^{2+} in 38% nitric acid. In the absence of certified reference tissues for TiO_2 particle analysis, spike recovery tests were performed. Samples of cell homogenates were spiked with 200 µL of 10 mg L^{-1} of the different forms of TiO_2 and showed procedural recoveries of 80.4 ± 4.2, 82.2 ± 1.5, 76.3 ± 4.7 and 75.7 ± 1.8 % for bulk TiO_2, P25, anastase and rutile forms, respectively (mean ± S.E.M, n = 6 for

each material type). Checks on analytical precision showed low coefficients of variation within and between samples (< 5%).

Electrolyte concentrations in the cell homogenates were normalised to cell protein content. The latter was measured in triplicate using the bicinchoninic acid (BCA) method (MC155208, Pierce, Rockford, USA). Briefly, 15 µL of sample was added to 300 µL of the BCA reagents and the absorbance read at 570 nm (VERSA max, Molecular Devices, Berkshire, UK) in 96-well plates against bovine serum albumin standards. Calibrations spiked with and without 1 mg L^{-1} TiO_2 showed no interference with the assay or colour reagent (Fig. 2-4).

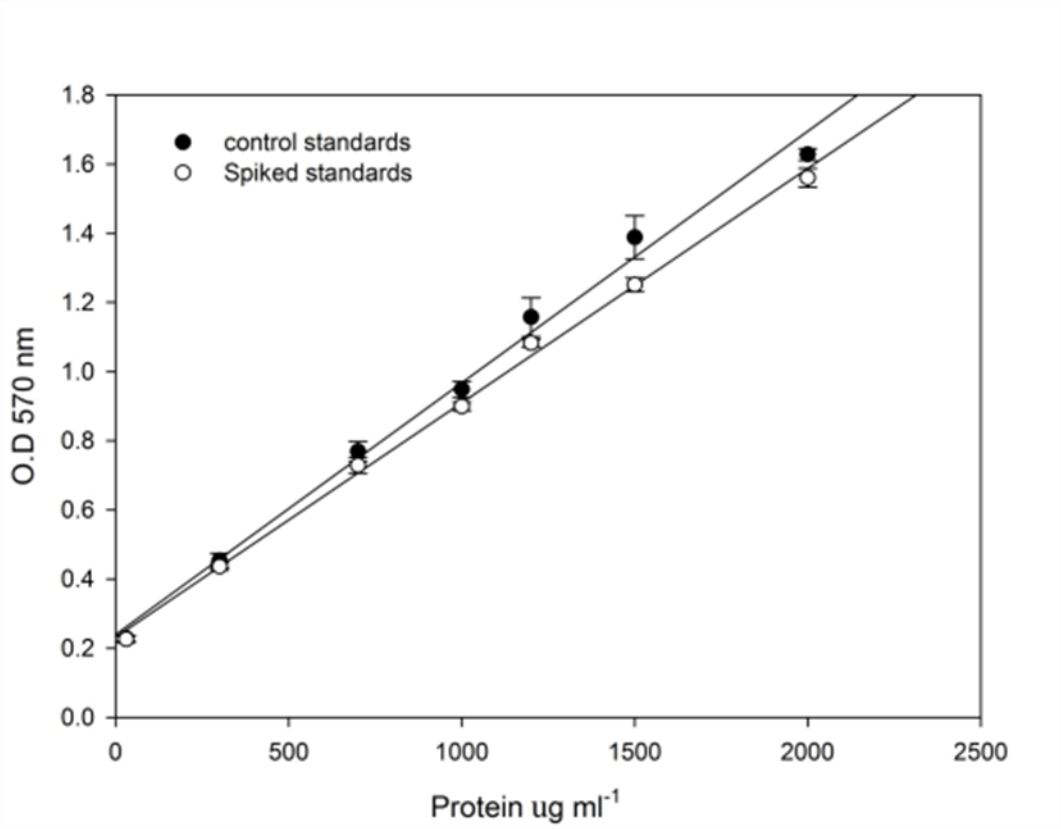

Fig. 2-4 : The effect of 1 mg L^{-1} bulk TiO_2 on BSA protein standards relative to control BSA protein standards (no TiO_2). The plots are means ± SEM (n = 3) from the replicate data. Statistical analysis showed that there were no differences between standards in the presence or absence of 1 mg L^{-1} bulk TiO_2 (Student's t-test P > 0.05 (*))

2.3.7 Lactate dehydrogenase activity

Lactate dehydrogenase activity was measured in the cell culture media overlying the cells (medium LDH) and in the cell homogenates (cell LDH). For the former, 200 µL of cell culture media from each well was gently centrifuged for 1 min to reduce any cell debris/turbidity (~160 *g*, Heraeus instruments, Biofuge *pico*, Germany) and 100 µL of the resulting supernatant was used in the LDH assay. For the latter, 200 µL of cell homogenate was sonicated and centrifuged (section 2.3.6) and then 100 µL of the cell supernatant was used in the LDH assay (Plummer, 1971). Briefly, 100 µL of sample (medium or cell supernatant) was added to a reaction mixture (2800 µL of 0.6 mmol L^{-1} pyruvate in 50 mmol L^{-1} phosphate buffer at pH 7.4, plus 100 µL of 0.6 mmol L^{-1} NADH solution), mixed directly in a 3 mL cuvette and the change in absorbance measured over 2 min at 340 nm (Helios ß spectrophotometer). The specific activity of the LDH was then calculated using an extinction coefficient of 6.22 x 10^{-3} L mol^{-1} cm^{-1} . LDH activity is expressed as U mL^{-1} (µmol min^{-1} mL^{-1}) of media. The percentage of LDH leak from the cells within each well was also estimated from the absolute total LDH activity of each well (cells + medium) divided by the LDH activity of the medium alone.

2.3.8 Cell morphology and scanning electron microscopy

Cell morphology was examined directly by phase contrast microscopy (Olympus/CK30-F200, Japan) during experiments, whilst separate runs of plates were carried out for detailed morphological investigations on fixed samples using bright field light microscopy and electron microscopy. Briefly for bright field light

microscopy, cells were washed *in situ* on the cell culture dish with Dulbecco's phosphate buffered saline (DPBS, Lonza, Verviers, Belgium), then fixed with 5 mL of fresh methanol for 5 minutes, prior to staining with Giemsa (Giemsa's stain solution, IVD, England). Plates were examined wet using light microscopy (Nikon, 803923-Japan) and photographs taken using a digital camera (Pentax, K-X) (Fig. 2-5).

For scanning electron microscopy (SEM), the cells were fixed *in situ* on the culture plates and a disk cut out of the plate wells for mounting on SEM grids. Briefly, cells were washed in sucrose wash buffer (section 2.3.6) and fixed for 1 h in 2 mL of 2.5% glutaldehyde in cacodylate buffer (0.1 M sodium cacodylate in water followed by the drop wise addition of 0.2 M HCl to a pH of 7.4). The cells were washed twice in cacodylate buffer prior to being dehydrated in a graded series of ethanol. Cells were critically point dried and carbon coated (EMITECH-K850, K450X). Samples were imaged and elementally analysed (SEM, JEOL/JSM-7001F, Oxford Instruments INCA X-ray analysis system) using a 15 KV accelerating voltage, at a working distance of 10 mm.

A separate series of culture plates was prepared for transmission electron microscope (TEM) investigations (3 plates/treatment). It was not possible to produceTEM sections from cells adhered to the plastic cell culture plates. Instead, cells were grown on well inserts (Millipore Millicell hanging cell culture insert, 0.4 µm pore size designed for 12 well plates) for up to 21 days. Then, in order to increase the chances of observing particles in the individual cells by TEM, the microplates were exposed to 10 mg L^{-1} of each form of TiO_2 for 24 h (1 mg L^{-1} used above). Inserts were fixed in 2.5% glutaraldehyde buffered in 0.1 M sodium cacodylate, pH 7.2, and post-fixed in 2% OsO_4. The specimens were then dehydrated in a graded

series of ethanol, infiltrated with Spur's resin (Agar Scientific, Essex UK), and embedded into coffin moulds using pure resin. Thin sections were cut (> 90 nm) and stained with 2% uranyl-acetate and lead citrate, and then examined by transmission electron microscope (TEM, JEOL-1200EX II). For block face analysis of the samples, specimens were viewed in backscatter imaging mode at an accelerating voltage of 10 KV and elementally analysed (SEM, JEOL/JSM-7001F, Oxford Instruments INCA X-ray analysis system).

2.3.9 Statistics

Data was analysed using StatGraphics Plus Version 5.1 and shown as means ± standard errors (S.E.M) unless otherwise stated. After checking data for kurtosis, skewedness, and unequal variance (Bartlett's test), one-way ANOVA followed by Fisher's least squares difference multiple range test was applied to analyse treatment effects, or time effects where appropriate. In the time course experiment, two-way ANOVA was used to determine treatment x time effects. Where data were non-parametric, the Kruskal–Wallis test (analysis by ranks) was used and differences were located using notched box and whisker plots. In some cases the Student's *t*-test was used to investigate the differences between pairs of data, or the Mann-Whitney U test where appropriate for non-parametric data. All statistical analysis used the default 95 % confidence limit. Curve fitting for time effects was performed using Sigma Plot Version 12.0. Curves were fitted to the raw data, although the figures show the mean values for convenience.

2.4 Results

2.4.1 Cell health and viability

The control cells (not exposed to TiO_2 or treated with drugs) showed normal morphology (day 4 - 5) during the experiments with the cells remaining confluent and attached (Fig. 2-5) to the dishes with intact apical membranes, orientated in the correct way with the presence of uniform microvilli. This was also supported by LDH activity which remained below 0.2 U mL^{-1} of cumulative LDH release over the 24 h duration of the experiments. The control cells also showed normal electrolyte levels with negligible variation in cell electrolyte concentrations. For example, in the time course experiment the electrolyte levels in control cells were (mean ± SEM, *n* = 3 plates / treatment): Na^+, 6359 ± 581; K^+, 867 ± 26 ; Ca^{2+}, 16 ± 4 ; and Mg^{2+}, 48 ± 1 nmol mg^{-1} protein. The controls across experiments and batches of cells, all had low membrane leak, and although electrolyte concentrations showed some variability when expressed per mg of cell protein, the values remained in the normal range for this cell line. For example, the control cells in the second experiment also showed cumulative LDH values (measured over 24 h) in the medium of $\leqslant$ 0.15 U mL^{-1} or less, and the ranges of electrolyte concentrations in these controls (from n = 6 plates) were: Na^+, 4518 ± 533; K^+, 718 ± 14; Ca^{2+}, 11 ± 1; and Mg^{2+}, 43 ± 1 nmol mg^{-1} protein.

Similarly for the experiments with inhibitors, the control cells incubated with drugs in the absence of TiO_2 showed normal morphology and remained adhered to the dishes. Cumulative LDH was low (mean ± SEM, n = 6 plates, 0.15 ± 0.5 U mL^{-1}) except for cells incubated with 1.25 mmol L^{-1} amiloride which exhibited a cumulative

leak of 0.354 ± 0.026 U mL^{-1} (Table 2-1). Metabolic and ion transporter inhibitors are expected to cause variations in electrolyte levels and some statistically significant changes occurred in the electrolyte concentrations relative to the appropriate no added drug controls without TiO_2 (Table 2-2). For example, additions of vanadate caused elevations of cell Ca^{2+} concentrations and depletion of K^+ consistent with ion diffusion down their respective electrochemical gradients. Additions of nystatin resulted in increases of all the major electrolytes in the cells compared to drug-free controls without TiO_2 present (Table 2-2). Conversely, additions of chlorpromazine depleted cell K^+, Na^+ and Ca^{2+} (Table 2-2). Genistein notably caused a 2.7 fold increase in cell Ca^{2+} concentration, and also lowered cell Na^+. Amiloride caused the expected Na^+-depletion consistent with block of the epithelial Na^+ channel, but also caused K^+ and Ca^{2+} to rise compared to the drug free control without TiO_2 (Table 2-2).

Cells incubated with the different forms of TiO_2 also demonstrated low cumulative LDH leak (0.15 ± 0.05 U mL^{-1}), normal morphology (confluent monolayer, orientated correctly) (Fig. 2-5 A) and reasonably consistent electrolyte concentrations within the physiological range, although there were some TiO_2-dependent changes in ion concentrations (Table 2-2).

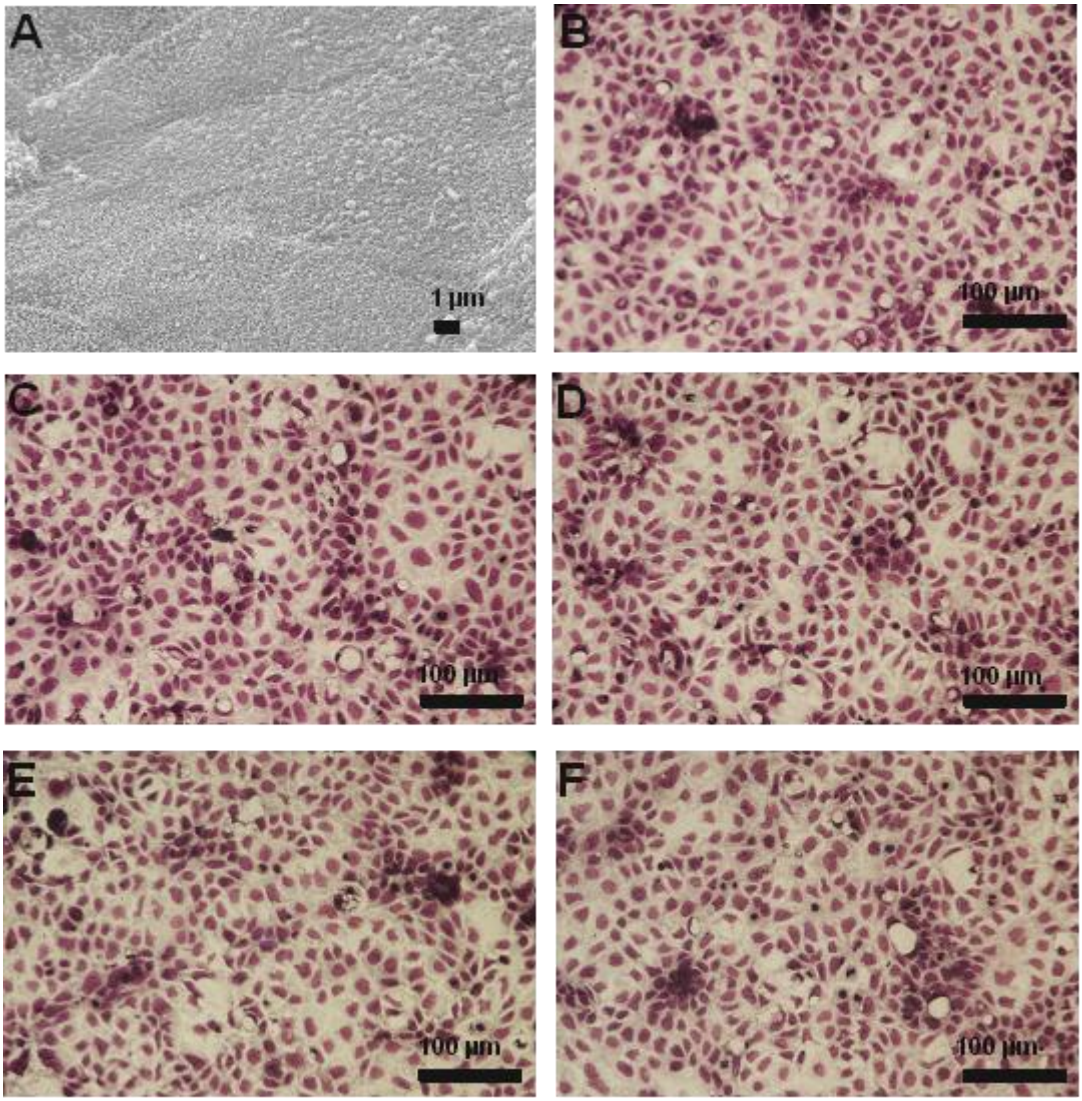

Fig. 2-5: Cell morphology after 96 h post seeding following a 24 hour exposure to 1 mg L^{-1} TiO_2 crystal forms. A) control SEM demonstrating appropriate orientation , confluence and brush border development ; B) control Light microscopy (LM); C) bulk exposure LM; D) P25 exposure LM; E) anatase exposure LM; F) rutile exposure LM. (n = 3 plates per treatment) Scale bar = 100 µm, stained with Giemsa's stain.

Table 2-1: Cumulative LDH leak from Caco-2 cells at 24 h following exposure to 1mg L^{-1} of different TiO_2 forms in the presence or absence of inhibitors

Treatment		No drug	Chlorpromazine (27 µmol L^{-1})	Genistein (90 µmol L^{-1})	Amiloride HCL (1.25 mmol L^{-1})
Control	U ml^{-1} External medium	0.129 ± 0.009[a]	0.158 ± 0.015[a]	0.184 ± 0.019[a]	0.354 ± 0.026[b]
	Uml^{-l} Cell homogenate	1.565 ± 0.034[a]	1.558 ± 0.033[a]	1.584 ± 0.023[a]	1.277 ± 0.051[b]
	% LDH leak	7.723 ± 0.522[a]	9.346 ± 0.918[a]	10.56 ± 1.08[a]	21.99 ± 1.54[b]
Bulk	U ml^{-1} External medium	0.153 ± 0.014[a]	0.143 ± 0.023[a]	0.176 ± 0.014[a]	0.407 ± 0.040[b]
	U ml^{-1} Cell homogenate	1.577 ± 0.039[a]	1.620 ± 0.017[a]	1.622 ± 0.036[a]	1.420 ± 0.054[a]
	% LDH leak	8.950 ± 0.717[a]	8.216 ± 1.270[a]	9.872 ± 0.56[a]	22.48 ± 1.39[b]
P25	U ml^{-1} External medium	0.199 ± 0.014[a]	0.177 ± 0.024[a]	0.212 ± 0.027[a]	0.404 ± 0.031[b]
	U ml^{-1} Cell homogenate	1.635 ± 0.094[a]	1.658 ± 0.109[a]	1.593 ± 0.011[a]	1.263 ± 0.109[b]
	% LDH leak	10.95 ± 0.136[a]	9.668 ± 0.686[a]	11.88 ± 1.39[a]	24.81 ± 3.15[b]
Anatase	U ml^{-1} External medium	0.159 ± 0.017[a]	0.164 ± 0.012[a]	0.196 ± 0.054[a]	0.288 ± 0.054[b]
	U ml^{-1} Cell homogenate	1.578 ± 0.031[a]	1.551 ± 0.022[a]	1.609 ± 0.018[a]	1.072 ± 0.052[b]
	% LDH leak	9.271 ± 0.947[a]	9.691 ± 0.766[a]	10.88 ± 2.703[a]	21.13 ± 2.92[b]
Rutile	U ml^{-1} External medium	0.152 ± 0.011[a]	0.138 ± 0.007[a]	0.185 ± 0.030[a]	0.413 ± 0.064[b]
	U ml^{-1} Cell homogenate	1.550 ± 0.013[a]	1.539 ± 0.044[a]	1.604 ± 0.047[a]	1.404 ± 0.054[b]
	% LDH leak	9.086 ± 0.623[a]	8.374 ± 0.578[a]	10.46 ± 1.63[a]	22.81 ± 2.11[b]

Data are expressed as means ± S.E.M. (n = 6). Values are expressed as µmol min^{-1} mL^{-1} (U mL^{-1}). Different letters indicate statistically significant differences within rows (ANOVA P > 0.05). The % leak was calculated from the absolute LDH activity of each well (cells + medium) divided by the LDH activity of the medium alone.

Table 2-2: (Experiments 2 and 3): The total intracellular K^+, Na^+, Ca^{2+}, and Mg^{2+} nmol Metal mg^{-1} protein following exposure to 1mg L^{-1} TiO_2 forms in the presence and absence of drugs (Series 2: nystatin and vanadate; Series 3, chlorpromazine, genistein, amiloride HCL) for 24 h

		Electrolytes (nmol mg^{-1} protein)				
Experiment 2		**Control**	**Bulk**	**P25**	**Anatase**	**Rutile**
K^+	No Drug	718.8 ± 14.2[a]	663.9 ± 28.3[b]	643.8 ± 19.6[b]	637.9 ± 27.6[b]	611.1 ± 11.4[b]
	Nystatin	927.9 ± 50.8[#a]	828.8 ± 62.3[#b]	815.7 ± 30.0[#b]	822.7 ± 57.9[#b]	807.1 ± 41.2[#b]
	Vanadate	466.8 ± 43.8[#a]	479.6 ± 36.9[#a]	469.3 ± 26.9[#a]	513.3 ± 16.9[#a]	490.7 ± 37.1[#a]
Na^+	No Drug	4518 ± 160[a]	4666 ± 576[a]	4793 ± 231[a]	5109 ± 624[a]	4319 ± 350[a]
	Nystatin	6303 ± 468[#a]	5253 ± 445[a]	5144 ± 308[a]	5748 ± 455[a]	5202 ± 417[a]
	Vanadate	3632 ± 427[#a]	4246 ± 406[a]	3982 ± 311[#a]	4457 ± 216[#a]	4534 ± 568[a]
Ca^{2+}	No Drug	10.6 ± 1.2[a]	14.3 ± 7.0[a]	28.0 ± 12.4[b]	20.8 ± 5.4[b]	19.1 ± 8.2[a]
	Nystatin	25.7 ± 9.4[#a]	19.8 ± 2.2[b]	27.8 ± 5.7[a]	14.4 ± 4.6[b]	17.7 ± 3.1[b]
	Vanadate	20.9 ± 3.6[#a]	25.2 ± 4.6[#a]	18.0 ± 7.2[a]	18.7 ± 4.1[a]	29.1 ± 2.4[#b]
Mg^{2+}	No drug	42.6 ± 1.1[a]	47.8 ± 2.2[b]	53.4 ± 2.7[b]	49.8 ± 1.4[b]	50.7 ± 1.5[b]
	Nystatin	56.2 ± 2.9[#a]	55.3 ± 2.8[#a]	55.0 ± 1.8[a]	56.2 ± 4.4[#a]	55.0 ± 3.1[a]
	Vanadate	30.9 ± 3.4[#a]	38.9 ± 3.1[#b]	39.4 ± 2.7[#b]	43.8 ± 2.3[b]	40.9 ± 2.8[#b]
Experiment 3						
K^+	No Drug	684.2 ± 16.8[a]	650.2 ± 31.8[b]	655.4 ± 19.7[b]	638.5 ± 25.0[b]	600.8 ± 34.4[b]
	Chlorpromazine	565.2 ± 16.2[#a]	553.3 ± 40.3[#a]	534.4 ± 22.2[#a]	561.3 ± 33.2[#a]	550.9 ± 18.5[#a]
	Genistein	642.5 ± 31.3[a]	634.6 ± 35.8[a]	686.5 ± 36.5[a]	653.7 ± 33.6[a]	663.4 ± 19.3[a]
	Amiloride	1039.8 ± 273[#a]	977.1 ± 154[#a]	771.7 ± 120[#b]	795.0 ± 199[#b]	827.1 ± 121[#a]
Na^+	No Drug	6007 ± 359[a]	5671 ± 474[a]	5654 ± 365[a]	5528 ± 477[a]	4251 ± 337[a]

	Chlorpromazine	1364 ± 160$^{\#a}$	1266 ± 136$^{\#a}$	1100 ± 73$^{\#a}$	1070 ± 50$^{\#a}$	1041 ± 45$^{\#a}$
	Genistein	3858 ± 396$^{\#a}$	4038 ± 257$^{\#a}$	4080 ± 342$^{\#a}$	4176 ± 208$^{\#a}$	4874 ± 843$^{\#a}$
	Amiloride	4118 ± 457$^{\#a}$	3708 ± 902$^{\#a}$	3318 ± 802$^{\#a}$	3358 ± 1175$^{\#a}$	3067 ± 521$^{\#a}$
Ca^{2+}	No Drug	15.5 ± 1.6^{a}	28.5 ± 5.1^{b}	32.1 ± 7.3^{b}	26.9 ± 4.9^{b}	17.9 ± 1.4^{c}
	Chlorpromazine	12.5 ± 1.3$^{\#a}$	12.8 ± 1.6$^{\#a}$	11.7 ± 1.5$^{\#a}$	12.2 ± 0.8$^{\#a}$	10.1 ± 1.2$^{\#a}$
	Genistein	48.3 ± 8.1$^{\#a}$	37.0 ± 2.9$^{\#a}$	38.2 ± 7.7$^{\#a}$	40.5 ± 2.4$^{\#a}$	36.1 ± 7.1$^{\#a}$
	Amiloride	104.1 ± 17.1$^{\#a}$	173.9 ± 69.8$^{\#a}$	86.4 ± 41.1$^{\#a}$	70.1 ± 16.2$^{\#a}$	68.6 ± 11.1$^{\#a}$
Mg^{2+}	No Drug	40.2 ± 1.1^{a}	40.7 ± 0.6^{a}	41.5 ± 2.0^{a}	39.5 ± 0.9^{a}	37.7 ± 2.1^{b}
	Chlorpromazine	37.3 ± 1.0$^{\#a}$	38.8 ± 2.9^{a}	36.2 ± 1.7$^{\#a}$	38.6 ± 2.4^{a}	38.3 ± 1.3^{a}
	Genistein	38.4 ± 1.6^{a}	40.6 ± 1.7^{b}	43.7 ± 2.7^{b}	42.4 ± 0.8^{b}	43.9 ± 0.2$^{\#b}$
	Amiloride	84.0 ± 5.0$^{\#a}$	70.4 ± 7.5$^{\#a}$	68.4 ± 3.7$^{\#a}$	71.4 ± 12.2$^{\#a}$	79.9 ± 8.3$^{\#a}$

Values are means ± S.E.M (n = 6 for each group) and are expressed as nmol mg^{-1} cell protein. Different letters indicate statistically significant differences within rows. (ANOVA $P < 0.05$). $^{\#}$ Statistically significant difference of drug controls and treatments relative to 'no drug' controls and treatments within column (ANOVA $P < 0.05$). Series 2 is the data associated with experiment 2, series 3 is the data associated with experiment 3.

2.4.2 Experiment 1 - Time course of Ti accumulation from different forms of TiO_2

The time courses of Ti accumulation for exposures to the different forms of TiO_2 are shown in Fig. 2-6. The unexposed control cells remained at a background metal concentration of around 2 nmol Ti mg^{-1} cell protein throughout. All the TiO_2 treatments showed a non-linear exponential rise of the total Ti concentration in the cells, which achieved steady-state concentrations by 24 h. This rise in net Ti accumulation by the cells occurred independently of similar elevations of cell Na^+ or K^+ concentrations which remained between 6500 and 9000 and 800 and 1000 nmol mg^{-1} protein, respectively; indicating that the Ti response was Ti-specific and not an artefact of general electrolyte changes in the cells. There were some differences in the time courses of Ti accumulation for the different forms of TiO_2 (Fig. 2-6), and these were not explained by osmotic disturbances in the cells or by differences in membrane permeability across the treatments. For the latter, the cumulative LDH activity in the medium by 24 h remained low, at 0.15 ± 0.5 U mL^{-1} (not statistically different from the control, and no material-type effect was observed, ANOVA, $P < 0.05$, Table 2-1). The net Ti accumulation by 24 h was in the following order by material-type: bulk and nano P25 > anatase > rutile > unexposed controls. The bulk material and P25 nano TiO_2 showed the largest net Ti accumulation in 24 h, saturating at 14.1 and 13.64 nmol mg^{-1} protein, respectively, but were not statistically different from each other by 24 h (ANOVA $P < 0.05$). The anatase form showed approximately 40% less Ti accumulation than either the P25 or bulk material (statistically different by 24 h, Fig. 2-6). There were also some differences in Ti accumulation from the pure anatase and rutile forms, with the latter showing saturation at a slightly lower Ti concentration (Fig. 2-6). However, the mean values at

24 h were not statistically different (ANOVA, $P < 0.05$). The initial Ti accumulation rates calculated from the curves (Fig. 2-6) followed a similar pattern with Ti accumulation from the bulk and rutile being faster than those from anatase or P25. The initial accumulation rates were 3.01, 2.75, 2.11 and 3.26 nmol mg^{-1} protein h^{-1} for bulk, P25, anatase and rutile, respectively. The times to 50% saturation were 2 h 39, 3 h 09, 2 h 17 and 1 h 01 min for bulk, P25, anatase and rutile, respectively. Initial rates were determined from the equations of each line for each treatment by multiplying a * b (Schmid and Sapunov, 1982). The time to 50 % accumulation or t ½ was calculated as follows; t ½ = ln(2) / (rate constant), for each treatment.

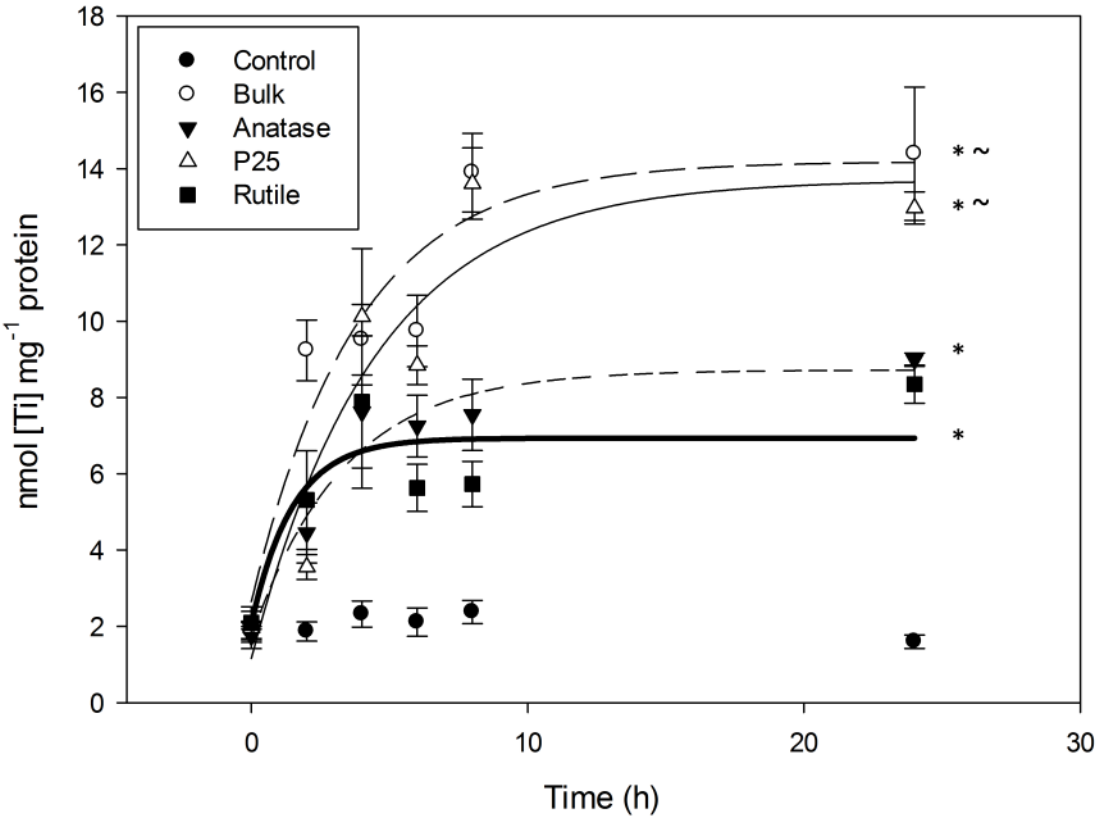

Fig. 2-6 (Experiment 1): Titanium accumulation in Caco-2 cells from exposures to 1 mg L^{-1} of different forms of TiO_2 for 24 h. Data points are means ± SEM (n = 3 replicates/treatment). Curves were fitted

using Sigma plot version 12.0 to the raw data (n = 3 observations/treatment) using the rectangular exponential rise to the maximum function (*f = y0+a*(1-exp (-b*x)*). Equations for the curve fits were as follows: For bulk *f = 2.64+11.54*(1-exp (-0.261*x)), r^2 = 0.901*; For P25, *f = 1.16+12.54*(1-exp (-0.22*x), r^2= 0.875*; For anatase *f = 1.71+7.01*(1-exp (-0.3017*x), r^2= 0.952;* For rutile *f = 2.07+4.86*(1-exp (-0.67*x)), r^2= 0.731*. The unexposed control showed no time-dependent changes and therefore a curve was not fitted. Accumulation of all titanium forms is significantly different to the controls (ANOVA $P < 0.05$ (*)) at 24 h. Accumulation of Bulk and P25 titanium forms at 24 h is significantly greater than the anatase and rutile forms (ANOVA $P < 0.05$ (~)).

2.4.3 Experiment 2 - The effect of nystatin and vanadate on Ti accumulation at 24 h

Nystatin and vanadate incubation increased the level of Ti accumulation for exposures to all the forms of TiO_2 (ANOVA $P < 0.05$), except for rutile TiO_2 when incubated with vanadate (Fig. 2-7). This net Ti accumulation occurred without changes in cell membrane integrity (e.g. no membrane blebs were observed) and cells remained adhered to the culture dishes throughout. Apical incubations of 100 μmol^{-1} vanadate caused the largest increases in Ti accumulation relative to the no drug equivalent control (all statistically significant, except for the rutile treatment, $P < 0.05$), resulting in increases above the control value of 10, 12, 12 and 0.9 nmol Ti mg^{-1} cell protein for bulk, P25, anatase and rutile, respectively. Similarly, cells incubated with 120 IU mL^{-1} nystatin showed a statistically significant increase in Ti accumulation for all forms of TiO_2 (ANOVA $P < 0.05$) with subsequent increases being 3, 4, 2 and 4 nmol mg^{-1} cell protein for bulk, P25, anatase and rutile respectively, above the equivalent no drug control with TiO_2 (Fig. 2-7).

2.4.4 Effect of titanium dioxide, nystatin and vanadate exposure on cell electrolytes concentrations at 24 h

There were some TiO_2-dependent changes in electrolyte concentrations in the cells. For example, all forms of TiO_2 (no drugs present) caused some depletion of K^+ and elevation of cell Mg^{2+} concentrations compared to the no added TiO_2 controls (Table 2-2). There were also some crystal structure effects without drugs, notably a statistically significant elevation of Ca^{2+} following P25 or the anatase treatments, but not with the other materials (Table 2-2). These TiO_2-dependent changes in

electrolyte concentrations in the cells were all with the electrochemical gradient, but were not associated with non-specific membrane leak (LDH leak remained low).

Incubations of nystatin or vanadate in the absence of TiO_2 caused some changes in cell electrolyte concentrations relative to the drug-free control (Table 2-2), but there were also some effects observed with drugs plus TiO_2. For example, in the presence of nystatin, all TiO_2 treatments showed an increase in cell K^+ concentrations. There was a material-type effect with nystatin causing some decrease in cell Ca^{2+} concentrations in the anatase and rutile treatments compared to the nystatin control (Table 2-2). Cells incubated with vanadate plus TiO_2 exposure showed increases in cell Mg^{2+} for all types of TiO_2.

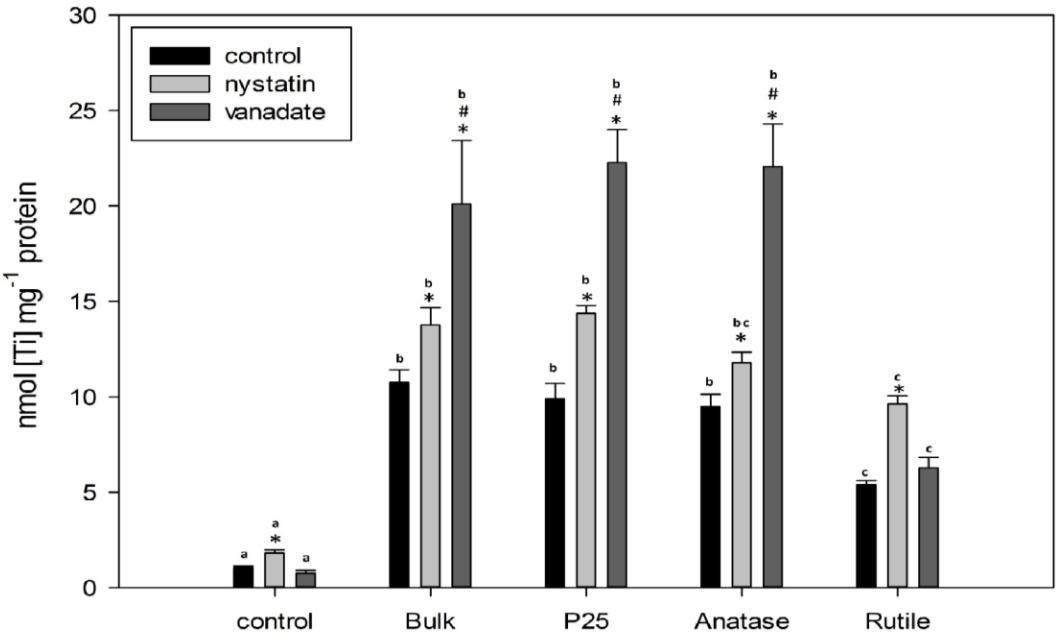

Fig. 2-7 (Experiment 2): Effect of nystatin and vanadate on Ti accumulation in Caco-2 cells incubated with 1 mg L^{-1} titanium forms at 24 h. The plots are means ± SEM (n = 6) from the replicate data and are expressed as 'nmol [Ti] mg^{-1} protein'. Statistical analysis at 24 h time point showed that the levels of accumulation relative to the no drug controls were different (ANOVA $P < 0.05$ (*)). # indicates statistical differences between vanadate and nystatin (ANOVA $P < 0.05$). Letters represent differences between materials within drug treatment (material-type effect) (ANOVA $P < 0.05$)).

2.4.5 Experiment 3: The effect of chlorpromazine, genistein or amiloride on Ti accumulation at 24 h

Following the primary pharmacological experiments with nystatin and vanadate to broadly determine any involvement of endocytosis or active transport, respectively, in Ti accumulation, more detailed studies were performed with selective inhibitors (Fig. 2-8). Incubating the cells with genistein in the presence of TiO_2 caused a statistically significant reduction (ANOVA $P < 0.05$) in Ti accumulation relative to the TiO_2 exposure without the drug regardless of material-type (Fig. 2-8); indicating that genistein may block Ti uptake from all forms of TiO_2. In contrast, incubations with 27 µmol L^{-1} chlorpromazine only caused a reduction of Ti accumulation relative to TiO_2 exposure without the drug (ANOVA $P < 0.05$) for the bulk and anatase forms of TiO_2 (Fig. 2-8). Cell viability with TiO_2 and chlorpromazine or genistein was as expected, with cumulative LDH activity remaining low (0.15 ± 0.5 U mL^{-1} for both drug trials) and not statistically different from the no drug controls, or the drug controls without TiO_2 (Table 2-1). Cells showed no membrane blebs and did not detach from the dishes, suggesting the chlorpromazine and genistein effects on Ti / TiO_2 accumulation were physiological.

Amiloride had no effect on Ti accumulation from TiO_2 exposures, except for the bulk material which caused a relative increase in the total Ti metal concentration in the cells (Fig. 2-8). However, the apparent absence of an effect of amiloride on the cells during exposure to the nano forms of TiO_2 may be due to some membrane leak. Amiloride-treated cells exhibited some of the highest cumulative LDH activity values with or without TiO_2 present (between 0.35 and 0.45 U mL^{-1} in the external medium (Table 2-1), being significantly higher than the leak in cells without amiloride

(ANOVA $P < 0.05$). Furthermore, visual inspection confirmed the presence of membrane blebbing on the cells. Protein content of the amiloride treated cells was lower than expected (< 150 mg cell protein well $^{-1}$ compared to values of 400-500 mg cell protein well^{-1} for other treatments) which is likely responsible for the impression of increased or normal Ti accumulation in the cells.

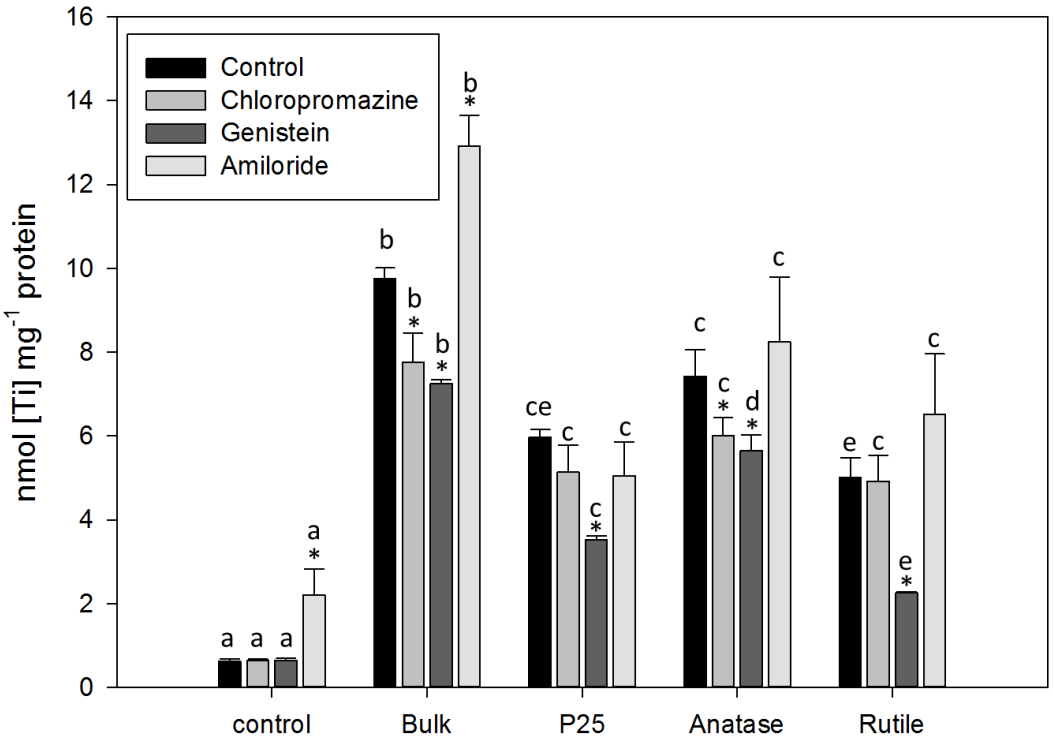

Fig. 2-8 (Experiment 3): Effects of chlorpromazine, genistein and amiloride on Ti accumulation in Caco-2 cells incubated with 1 mg L^{-1} titanium forms at 24 h. The plots are means ± SEM (n = 6) from the replicate data and are expressed as 'nmol [Ti] mg^{-1} cell protein'. Statistical analysis at 24 h showed that the levels of accumulation relative to the no drug controls were different (ANOVA $P <$ 0.05 (*)). Letters represent differences between materials within drug treatment (material-type effect) (ANOVA P <0.05).

2.4.6 Effect of chlorpromazine, genistein or amiloride on cell electrolytes at 24 h

Although incubations of the cells with drugs in the absence of TiO_2 caused some changes in electrolytes (Table 2-2, experiment 3), the addition of the different forms

of TiO_2 generally had no extra effect on the electrolyte concentrations. However, one notable exception was the effect of genistein on cell Mg^{2+} concentrations which increased in the presence of all forms of TiO_2 compared to TiO_2 exposure without the drug (ANOVA $P > 0.05$, Table 2-2, experiment 3). The relative increases in Ti accumulation above the control value were 2.2, 5.3, 4.0 and 5.5 nmol Ti mg^{-1} protein for bulk, P25, anatase and rutile, respectively, but there was no material-type effect on total Mg^{2+} concentrations in the cells.

2.4.7 Electron microscopy studies to determine TiO_2 particles inside the cells

Electron micrograph images show particles within cells beneath the apical membrane in vesicles or in process of being endocytosed following a 24 h exposure to anatase or P25 TiO_2 forms in the absence of drugs (Fig. 2-9 A, C, D and Fig. 2.9 B, C, D). The particles were of the same crystalline morphology as the equivalent electron micrographs from the stock dispersions (Fig. 2-2), and the presence of Ti being confirmed by EDS (Fig. 2-9 and 2-10). Neither particles nor Ti were present in control cells (Fig. 2-10 A) and there did not appear to be any observable intracellular pathological differences in cells exposed to all forms of 1 mg L^{-1} TiO_2 relative to control cells. Fig. 2-9 A, C and D show electron dense material in the scanning electron micrographs, and EDS confirms that these are Ti-rich electron dense areas underneath the apical membrane (i.e., inside the cells) and not between or basolaterally located underneath the cells.

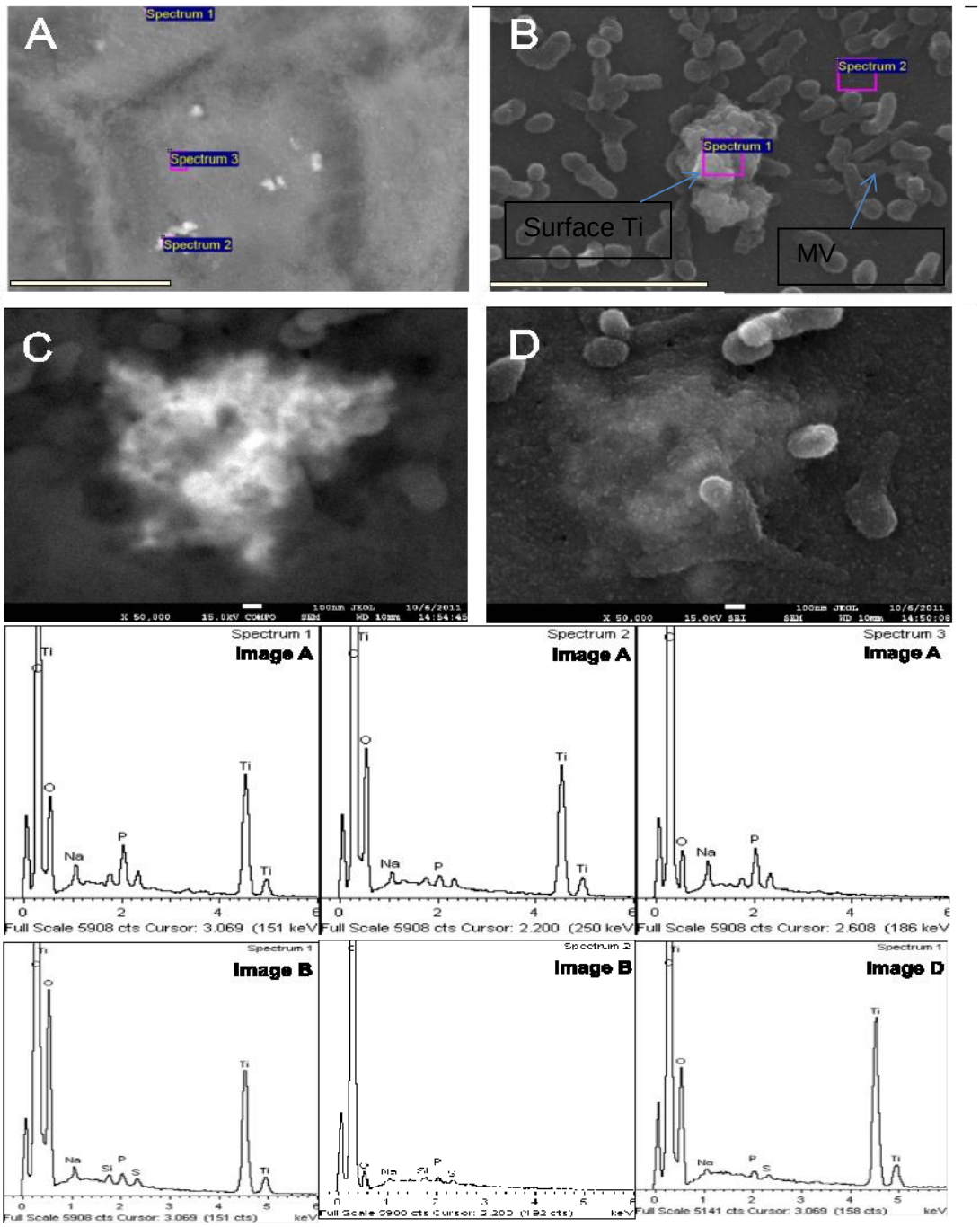

Fig. 2-9: (A- D) SEM images of Caco-2 cells 96 h after seeding having been exposed to 1 mg L^{-1} TiO_2 forms. A) Backscatter image (BSI) of Caco-2 cells exposed to 1 mg L^{-1} 'anatase' TiO_2'A' showing sub-surface Ti with EDS spectra below ; B) Secondary electron image (SEI) of surface bound anatase TiO_2 (scale bar represents 2 µm); C) BSI of 'D' showing subsurface Ti ; D) SEI image of cell surface exposed to P25 TiO_2. The cell membrane appears to have covered the TiO_2 (projections are microvilli, scale bar represents 100 nm); Spectra are labelled according to which image they belong to. The spectrum labelled Image D is the spectra associated with an EDS map of the entire image D.

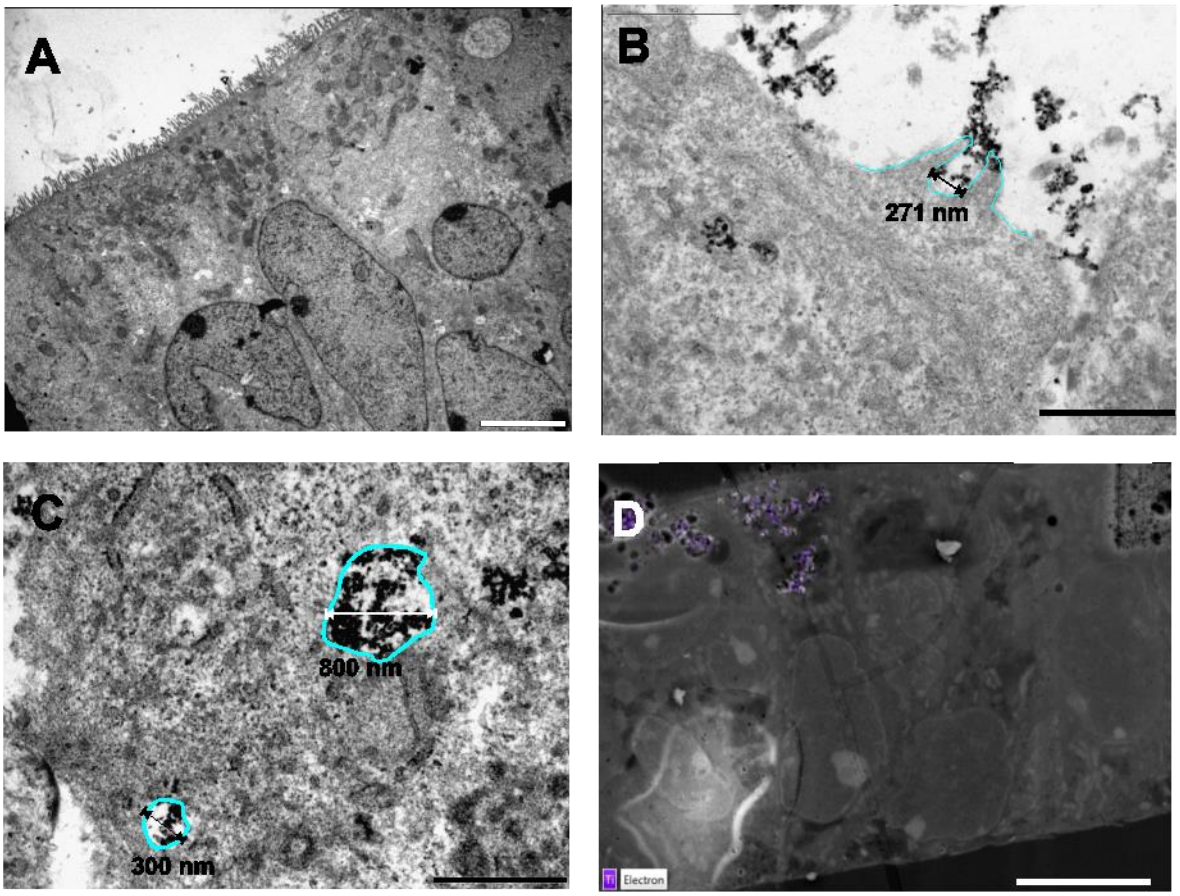

Fig. 2-10: (A-D) TEM images of cells grown for 21 days in culture inserts; A) TEM of control cells ; B) TEM image of cells following exposure to 10 mg L^{-1} P25 TiO_2 NPs (Note the invagination in progress (measuring 271 nm across)) (scale bar represents 1 µm; C) TEM image of intracellular matrix comprising of two vesicles containing NPs (Vesicles are of differing sizes 300 nm and 800 nm diameter, Scale bar represents 1 µm); D) SEM block face image in backscatter mode with EDS showing intracellular Ti underneath the apical membrane (scale bar represents 10 µm) The thickness of the monolayer is between 30 and 40 µm.

2.5 Discussion

The present study demonstrates that confluent and electrically tight Caco-2 cells are capable of Ti metal accumulation within a few days of the epithelial forming. The cells will accumulate Ti from TiO_2 particle exposures, and the occurrence of deposits rich in elemental Ti and oxygen underneath the apical (mucosal) membrane suggests at least some of the TiO_2 entered the cells in the particulate form. Caco-2 cells show drug-sensitive Ti accumulation which is indicative of an active uptake

mechanism(s). Critically, the Ti accumulation rate is dependent on the crystal structure of the material, with the nano rutile form being taken up the least. The differential drug sensitivity of the Ti accumulation suggests more than one pathway is involved in Ti accumulation from TiO_2 exposures, and given the ability of Caco-2 cells to exclude the rutile form, the possibility of crystal-structure specific pathways cannot be excluded.

2.5.1 Accumulation of titanium from TiO_2 exposures

The present study showed time-dependent accumulation of total Ti metal in Caco-2 cells which reached steady state from exposures to TiO_2 particles (Fig. 2-6). This is indicative of an active accumulation mechanism(s) and cannot be easily explained by passive uptake of dissolved Ti metal down the electrochemical gradient, or by incidental uptake of intact particles through damaged cell membranes. The absence of an appreciable diffusive leak through the apical membrane is confirmed by the consistently low LDH activity in the external medium (0.1-0.2 U mL^{-1}) in the presence of the different forms of TiO_2. The incidental passive uptake of dissolved Ti metal by solvent drag with the major electrolytes is also extremely unlikely, as the cell Na^+ concentrations did not change, and the K^+ gradient is outward, in the opposite direction to that of the net Ti accumulation. In any event, TiO_2 particles are poorly soluble at neutral pH in NaCl-rich gut lumen salines (Al-Jubory and Handy, 2012) or defined NaCl solutions (Schmidt and Vogelsberger 2009), releasing only picomolar concentrations of Ti metal that would be insufficient to support the accumulation rates observed here from the external medium (Fig. 2-6).

An active accumulation mechanism is also supported by the effects of addition of inhibitors such as vanadate or nystatin which both increased the net Ti accumulation in the cells (Fig. 2-7). The rate limiting step in metal uptake by epithelial cells is usually at the basolateral (serosal) membrane where efflux into the blood compartment must occur against the electrochemical gradient; and this is also true for metals like copper (Cu) that have a vesicular trafficking system which exudes Cu-containing vesicles at the basolateral membrane by exocytosis (Arrendondo *et al*,, 2000; Handy *et al*. 2000; Dameron and Harrison 1998; Kaplan and Lutsenko, 2009; Bury and Handy 2010). Blockage of the primary ion transporting ATPases on the basolateral membrane, or the ATPases involved in vesicular trafficking to the serosal compartment, will result in the observed net increase in Ti accumulation by the cells (Fig. 2-7). Similarly, nystatin which sequesters cholesterol to prevent the initiation of the non-specific lipid raft formation needed for membrane invagination during calveolae-based endocytosis (Ros-Baro *et al*. 2001; Le and Nabi. 2003; Silva *et al*. 2006) should at least slow vesicular trafficking through the cell leading to the observed increase of total Ti in the cells (Fig. 2-7). Al-Jubory and Handy (2012) also showed that nystatin prevented transepithelial uptake of Ti from exposures of TiO_2 particles, and although the form of the Ti was not verified in the cells, this occurred with a concomitant increase of total Ti content of the gut epithelium. Nystatin does not block all modes of endocytosis (clathrin-based processes may continue, Chen *et al*. 2011). Regardless, the observed nystatin-sensitive Ti accumulation (Fig. 2-7) is indicative of active mechanism(s) for handling either Ti metal or TiO_2 particles by Caco-2 cells.

The total Ti accumulation was between 6 and 14 nmol Ti mg^{-1} cell protein in 24 h for Caco-2 cells for an exposure to 1 mg L^{-1} TiO_2, depending on the form of the material

(Fig. 2-6). This is broadly similar to previous reports on this cell line in DMEM exposed to 1 mg L^{-1} TiO_2 particles (e.g., Koeneman *et al*. 2010, 160 ng over 24 h). Initial uptake rates, which represent the maximum accumulation rate when the experimental system is not at steady-state, appear not to have been previously reported for Caco-2 cells. The initial rate of uptake for Ti accumulation was 3-5 nmol mg^{-1} protein h^{-1}, depending on the form of TiO_2 (Fig. 2-6). This maximum rate of accumulation is broadly similar to that for other metals; notably for copper (trout intestinal cells, 1.8 nmol mg^{-1} protein h^{-1}, Burke and Handy 2005; Caco-2 cells, 0.1 nmol mg^{-1} protein h^{-1} (the maximum rate of influx using radio labelled copper, Arrendondo *et al*. 2000)). The initial accumulation rates in the present study are also broadly consistent with the notion of nanomole rates of uptake in the perfused trout intestine (initial rates of around 1 nmol Ti g^{-1} tissue h^{-1} (Al-Jubory and Handy 2012). This similarity in Ti metal uptake rates with intact intestinal tissue may be fortuitous. While the Caco-2 cell line is a useful model for exploring relative differences between metal treatments, and the mechanisms involved, they are not intended to represent *in vivo* uptake rates in the human gut. Indeed, it is important to note that Caco-2 cells were originally immortalized from colon cancer cells. Subsequently, carcinoma cells have been shown to have high trace metal uptake rates due to increased cell proliferation, membrane turnover and higher concentrations of apical membrane metal transporters, which are characteristic of carcinoma cells rather than gut cells (Brookes *et al*. 2006).

2.5.2 Membrane maturity and the absorption of intact TiO_2 particles

It is well established that Caco-2 cells of only a few days old can be used for metal transport studies, provided the cells are confluent as a polarised monolayer with a steady measurable transepithelial resistance of around 250 Ω cm^2 and/or have demonstrable unidirectional ion fluxes. Indeed, all of these parameters have been shown to occur within four days (Peterson *et al*. 1993; Yamashita *et al*. 2002; Zerounian and Linder 2002; Arrendondo *et al*. 2000; Moriya and Linder 2006; Linder *et al*. 2006; Sonnier *et al*. 2011). It is perhaps no surprise that electrolyte and trace element transport mechanisms are the first features of intestinal cells to mature (Dharmsathaphorn and Madara, 1990); for without these mechanisms in place, fundamental process to cell survival such as cell volume control would not occur. However, this is the first time that 4 - 5 day old confluent monolayers of Caco-2 cells have been used to study the accumulation of nano metals. For 'intact' nano particle uptake there may be some concern that the proteins necessary for vacuole formation and vesicular uptake are not yet localised to the apical membrane. This is not the case. Particles can be clearly seen directly under the apical membrane on the inside of the cell (Fig. 2-9 - 2-10), with the presence of TiO_2 confirmed by EDS. Moreover, several of the electron micrographs captured the process of vesicular formation and membrane invaginations with particles being captured by the folding membrane (Fig. 2-10; B-D). This strongly suggests active processes, with large folds being reminiscent of macropinocytosis (Fig. 2.-10; B-D) and the smaller vesicles likely a form of endocytosis (Fig. 2-10; C). Peterson *et al*. (1993) also showed F-actin and villin are localised to the apical membrane by day 2-3 in Caco-2 cells. Moreover, Peterson *et al*. (1993) also showed no statistical differences in the concentration of fodrin and myosin between day 3 and 21 in Caco-2 cells. In short,

all the molecular machinery for endocytosis are present in Caco-2 cells early on after the monolayer is formed and visual evidence of membrane invaginations are present in the current study. Thus Caco-2 cells of 4 days old (post seeding) can be used for both dissolved metal and NP metal studies. It was not possible to perform a quantitative analysis of the number of crystals or type within each vesicle from the electron micrographs (Fig. 2-10 B, C), but there appeared to be more aggregates composed of rounded particles rather than striated particles (rutile) in the invaginations and vesicles, tentatively suggesting that the anatase crystal form may be preferentially accumulated by cells. In contrast to research on metals, nutrient absorption studies (e.g., Au and Reddy 2000) tend to use cells around 21 days old since these express enzymes involved in digestive processes (e.g., alkaline phosphatase activity continues to rise; sucrose-isomaltase localises to the apical membrane (Peterson and Mooseker 1993). However, the advantage here is that metal transport can be studied without the confounding factors of nutritional processes, and for example the non-specific digestive vacuoles associated with feeding fully matured cells.

2.5.3 Effect of particle - size and crystal structure on Ti accumulation

Notably, the type of the TiO_2 influenced the total Ti accumulation over 24 h with the bulk material showing the greatest uptake, and nano rutile TiO_2 the least (Fig. 2-6). The bulk material effect may simply be explained on a mass basis. For every particle taken up by the cells, the larger bulk TiO_2 would inevitably contain more Ti metal. However, the bulk material stock dispersions did have one of the higher particle number concentrations and mean aggregate sizes (Fig. 2-2), and it is possible that

the bulk material was more bioavailable in the experiments. Al-Jubory and Handy (2012) also noted this behaviour for the same bulk material in gut salines. Another explanation may be associated with the increased settling rate demonstrated by larger particles which would increase the contact time of bulk particles with the epithelial surface in this particular experimental set up (Teeguarden *et al*., 2007).

There is also some evidence of a true-particle size effect on total Ti accumulation by the cells. In the present study, both the bulk and P25 materials were 25% rutile: 75% anatase (Al-Jubory and Handy 2012). In the time course study, there was generally a lag in uptake of P25 compared to the bulk material (Fig. 2-6), and the third series of experiments (Fig. 2-8) showed a clear statistical difference with less Ti accumulation from the P25 compared to the bulk material. There was also a trend of less Ti accumulation from P25 compared to bulk material in the second experiment although it was not a statistically significant difference (Fig. 2-7). Particle-size effects on TiO_2 uptake by Caco-2 cells have been controversial. Unlike, the present study, some reports have used high doses of TiO_2 that caused toxicity (Liu *et al*. 2006; Trouiller *et al*. 2009; Koeneman *et al*. 2010; Ryabchikova *et al*. 2010), and are therefore unlikely to be measuring true physiological uptake. Whilst others have used a bulk material of unspecified crystal structure, perhaps not the same as the nano form, making it problematic to separate a true size-effect from any crystal-structure effect in the experimental design (Liu *et al*. 2006; Wang *et al*. 2007; Kobayashi *et al*. 2009; Koeneman *et al*. 2010).

There was a crystal-structure effect within the nano forms of TiO_2, with the rutile being accumulated less than the anatase or P25 (Fig. 2-6). This is not readily explained by poor availability of rutile particles in the stock dispersions. Indeed, the

rutile form gave the highest particle number concentrations (Fig. 2-2). Unfortunately, it was not possible to reliably determine the total Ti metal concentrations in the medium over the cells for each crystal structure, as particle settling was observed during the experiments especially for the rutile form. Any settling would increase the contact of each test material with the cells. Nonetheless, there may be a biological reason for less Ti accumulation from the rutile TiO_2 NP exposure. One possible explanation is that the Caco-2 cells are using different pathways to take up TiO_2, depending on the form of the material (see below on pharmacology). Alternatively, there may be some aspect of cell surface recognition that excludes one crystal form over another. Interestingly, Ryabchikova *et al*. (2010) found that brookite and rutile forms of TiO_2 NPs produced different morphologies of membrane invaginations in MDCK cells by electron microscopy. The authors tentatively interpreted these observations as a possible crystal-structure effect on plasma membrane fluidity. However, Ryabchikova *et al*. (2010) also noted a substantial loss of cell viability that was crystal structure-dependent (up to 60% of the cells staining with trypan blue at 100 µg ml^{-1} of brookite TiO_2), which could confound their data interpretation as non-physiological.

2.5.4 Pharmacological investigation and the accumulation of Ti from exposures to different crystal structures

Having demonstrated that Ti accumulation was sensitive to vanadate or nystatin, more detailed experiments were performed with specific inhibitors (Fig. 2-8) to determine the pathways involved. These pharmacological investigations were intended to be physiological without causing damage to the cells. This was confirmed by the low LDH activity in the medium in the presence of drugs with/

without TiO_2 present (Table 2-1), and the normal morphology of the (adherent) cells in the presence of the drugs. The only exception was a small (0.3 U mL^{-1}, Table 2-1), but statistically significant increase in medium LDH activity following exposure to 1.25 mmol L^{-1} amiloride. However, this occurred without loss of cell K^+ (Table 2-2) suggesting the effect was modest.

Chlorpromazine is arguably a selective inhibitor of clathrin-mediated endocytosis and the drug prevents the formation of clathrin lattices at the plasma membrane which are essential to initiating the membrane invagination (Wang *et al*. 1993). In the present study, chlorpromazine caused a statistically significant decrease in Ti accumulation in Caco-2 cells for exposure to the bulk (contains anatase) and the nano anatase form, but not the P25 and rutile materials (Fig. 2-8). This could suggest that the anatase form is somehow better detected for uptake by the clathrin-mediated endocytosis pathway. Such a hypothesis would require a specific receptor-mediated detection of anatase TiO_2 crystals by clathrin-coated pits, but how this might occur is unclear.

Genistein is a tyrosine kinase inhibitor that can be used to manipulate cell volume control via its effects on the actin-cytoskeleton (Akiyama *et al*. 1987; Wodnicka and Burridge 1994), and for similar reasons also blocks caveolae-mediated endocytosis pathways (Razani.*et al*. 2002; Van der Ma *et al*. 2007). In contrast to chlorpromazine, genistein decreased the accumulation of Ti from all forms of TiO_2, but had the largest effects on the rutile and P25 materials (Fig. 2-8). This might suggest that the rutile form especially is preferentially taken up through caveolae-mediated endocytosis, but the mechanism for this selection is unknown. There is also some cross-talk between the endocytosis pathways in mammalian cells, so secondary effects cannot

be excluded. For example, genistein may also inhibit F-actin recruitment to clathrin-coated pits and therefore causes a secondary inhibition or delayed uptake via the clathrin-mediated pathway (Zhang and Monteiro-Riviere 2009). This might explain why genistein also has some effects on the anatase form of TiO_2. A component of clathrin-dependent endocytosis also seems to occur without the involvement of specific receptors (Kirchhausen 2009).

An alternative hypothesis to crystal structure-specific pathways of endocytosis is incidental size selection into each pathway by particle type. However, this idea is not easily explained by the data. For example, on a size basis, the bulk material might be expected to have its own pathway, but the drug-sensitivity profile (Fig. 2-8) does not support this. Nonetheless, it is curious that within the nano scale materials, the nano anatase TiO_2 with the smallest primary particle size (16 nm) is the most sensitive to chlorpromazine, and the largest nano material (rutile, 30 nm) is affected the most by genistein.

Alternative methodologies for investigating mechanisms of uptake such as SiRNA to specifically reduce concentrations of proteins associated with particular endocytic pathways (e.g. caveolin, dynamin) could be used to corroborate data produced from pharmacological inhibitor trials in light of recent evidence that suggests commonly used pharmacological inhibitors (chlorpromazine, genistein, amelirode) show poor specificity for inhibiting distinct endocytic pathways (Vercauteren *et al*., 2010).

2.5.5 Ionic regulation in Caco-2 cells during TiO_2 exposure

One of the functions of the gut epithelium *in vivo* is the absorption of nutritionally required electrolytes. Dissolved forms of toxic metals are known to interfere with ion uptake across the gut, and for example, Cu interference with Na^+ homeostasis (Handy *et al*. 2002). This interference in physiologically functional cells is usually explained by competition for ion uptake down the electrochemical gradient through ion channels, and/or selective inhibition of specific ion transporters. In the present study, direct competition from dissolved Ti^{2+} is unlikely. Although, the Ti^{2+} ion has a crystalline ionic radius smaller than all the electrolytes reported here, except possibly for the Mg^{2+} ion (in order of size: Mg^{2+}, 86 pm; Ti^{2+}, 100 pm; Ca^{2+}, 114 pm, Na^+, 116, K^+, 152 pm, (Shannon 1976), the appearance of appreciable dissolved Ti^{2+} in the cell culture medium by dissolution is extremely unlikely (solubility reasons above at neutral pH). In any event, the likely picomolar concentrations released would be easily out competed by the millimolar concentrations of the other ions in the media. Nonetheless, TiO_2 exposure resulted in increases of the total Ca^{2+} concentrations in the cells (Table 2-2). The reasons for this are unclear, but TiO_2 is reported to interfere with Ca homeostasis in keratinocytes (Simon *et al*. 2010). There were also some increases in the Mg^{2+} content of the cells during the TiO_2 exposures, and with most of the intracellular Mg^{2+} being normally bound to membranes inside the cell (Romani and Scarpa 1992; Juttner and Ebel. 1997) this may be incidental Mg^{2+} accumulation with endocytosis of TiO_2 particles. The depolarising effect of the small decrease of the cellular K^+ during TiO_2 exposure (Table 2-2) would also slow active Mg^{2+} efflux on the Na^+/Mg^{2+} exchanger (see Handy *et al*. 1996 for the latter).

The combined effects of ion transport inhibitors in the presence of TiO_2 particles on cell electrolyte contents appear not to have been previously reported. In the present study, the combined effect of TiO_2 plus nystatin caused a decrease of cell K^+ concentration compared to the drug alone. The combination of nystatin plus TiO_2 also caused less disturbance to cell Ca^{2+}, with the presence of TiO_2 counteracting the effect of the drug (Table 2-2). The combined effect of genistein plus TiO_2 also ameliorated the effect of genistein alone to raise Ca^{2+}. The reasons for these interactions require further investigation, and remain unknown.

2.5.6 Conclusion

This study shows that Caco-2 cells accumulate Ti from TiO_2 exposures with characteristics that are most easily explained by active uptake of Ti-containing particles in physiologically competent cells. Critically, there is a crystal structure-effect with the anatase form of TiO_2 being absorbed faster than the rutile in time-matched cultures of the Caco-2 cells, indicating this was not a cell maturation effect. From a regulatory perspective, it is therefore not safe to simply extrapolate from one form of TiO_2 to another, and at least some correction factor for the accumulation rates of the different crystal structures should be included in dietary exposure hazard assessments for human health. Moreover, TiO_2 also appears to disturb some aspects of electrolyte status in Caco-2 cells, and like other metals, health effects assessments should consider interference with the nutritionally required minerals.

Chapter 3: Uptake, accumulation and transport of different crystal forms of Titanium dioxide in differentiated 21 day old Caco-2 cells

3.1 Abstract

The gastrointestinal uptake of different crystals of TiO_2 was investigated using mature Caco-2 intestinal cells cultured on hanging inserts or in flat-bottomed plates. Monolayers exhibited time dependent uptake of Ti or TiO_2 from TiO_2 exposures of 1 mg L^{-1} over 24 h, influenced by crystal type, irrespective of the cell growth substrate (plates or inserts). The initial and overall accumulation rates were (initial) 1.39, 1.24, 1.39, 1.10 nmol mg^{-1} cell protein h^{-1} and (overall) 0.28, 0.25, 0.19, and 0.09 nmol mg^{-1} cell protein h^{-1} for Bulk, P25, anatase and rutile respectively, for cells cultured in flat plates. Similarly initial and overall accumulation rates were (initial) 1.54, 1.08, 1.02 and 0.40 nmol mg^{-1} cell protein $h^{-1}$and (overall) 0.40, 0.34, 0.30 and 0.20 nmol mg^{-1} cell protein h^{-1} for Bulk, P25, anatase and rutile respectively in cells cultured on hanging inserts. The overall rates of Ti or TiO_2 transport (Apical to Basolateral) from 1 mg L^{-1} TiO_2 were 0.11, 0.09, 0.08 and 0.02 nmol mg^{-1} cell protein h^{-1} for Bulk, P25, anatase and rutile respectively. The appearance of detectable Ti in the basolateral media occurred at 6 and 8 h for nano P25 (75% anatase, 25 % rutile) and nano anatase whilst Ti from bulk particle exposures (75% anatase, 25 % rutile) was first detected at 24 h. TiO_2 exposures had a negligible effect on apical membrane morphology, transepithelial electrical resistance and media LDH activity suggesting that TiO_2 was well tolerated and did not acutely damage the cells. There were some changes in the electrolyte composition of exposed cells relative to controls. A rise in the total Ca^{2+} concentration in the cells was observed for all TiO_2 crystal exposures irrespective of cell growth substrate. Overall the data demonstrates that accumulation and basolateral transport of Ti or TiO_2 from TiO_2 apical exposures is unlikely to be due to passive diffusion through leaky damaged cells or paracellular pathways. Rather the data advocates an active process through intact epithelial cells.

3.2 Introduction

Titanium dioxide (TiO_2) particles are widely used in a variety of food based consumer products such as chewing gum, sweets and bulking agents in over the counter medicines labelled as the ingredient, E171 (Weir *et al*. 2012). Moreover, it is estimated that approximately 36% of the particles in these food grade powders are less than 100 nm in diameter (Weir *et al*. 2012). Chen *et al*. (2013) showed that the (NP) fraction of TiO_2 in chewing gum reached 93% and that the majority of this is swallowed upon chewing. Surprisingly, literature on the effects and translocation of TiO_2 NPs through the gut is scarce (Bergin and Witzemabb 2013).

Caco-2 monolayers cultured on permeable inserts are widely used as an *in vitro* model to predict oral absorption and transport of organic compounds and metals (Artursson *et al*. 2001; Zerounian and Linder 2002; Linder and Moriya. 2006) because this cell line has been demonstrated to express the structural characteristics of human enterocytes (Peterson and Mooseker 1992). Recently, this model has been used as a test system for investigating TiO_2 NP accumulation (Chapter 2, this work) and transport across gut epithelium (Koeneman *et al*. 2010; Janer *et al*. 2014). The studies on Caco-2 cells so far have demonstrated the effect of NPs on the Caco-2 gut cell system using, either fully differentiated (Koeneman *et al*. 2010; Brun *et al*. 2014; Janer *et al*. 2014) or partially differentiated cells (Gerloff *et al*. 2012; Gitrowski *et al*. 2014). For transport studies on nutrients, it is generally accepted that fully differentiated cells are required, to ensure maximal tight junction integrity and brush border development. However, for metal accumulation studies there is some debate regarding the appropriate time point at which partially differentiated cells can be used for measurements of net ion influx. For particle

uptake studies there is concern that partially differentiated cells will accumulate atypical amounts of particles because apical remodelling during enterocyte differentiation is more amenable to larger scale endocytic events (Hansen 2009). According to Hansen (2009), mature enterocytes are unable to undergo the invagination process leading up to endocytosis because microvilli morphology sterically hinders the process. In spite of this suggestion, a handful of studies have demonstrated TiO_2 NP accumulation in vesicles within cells (Brun *et al*. 2014 - Exposures of 50 µg mL^{-1}; Janer *et al*. 2014 – Exposures of 100 µg mL^{-1}; Gitrowski *et al*. 2014- Chapter 2 – Exposures of 1 µg mL^{-1}). Koeneman *et al*. (2010) demonstrated apical to basolateral transport of Ti following apical administration of 1 µg mL^{-1} TiO_2 NPs (mixture of anatase and rutile) to differentiated Caco-2 cells. In contrast, Fisichella *et al*. (2012) demonstrated no internalisation or transport of TiO_2 NPs following 24 h exposure to 100 µg mL^{-1} in differentiated Caco-2 cells. This disparity in results for what is considered to be the same cell type may be due to cell heterogeneity, which has been demonstrated to occur in Caco-2 cells (Herold *et al*. 1994), or to arise from differences in the crystal phases of TiO_2 NPs used in exposures. NP surface chemistry is well known to alter particle-membrane interactions (Rivera Gil *et al*. 2010). It is also unclear whether morphologically different Caco-2 cells differ with regards to functional and biochemical parameters.

Due to the conflicting reports in the literature regarding NP uptake and translocation in Caco -2 cells, there is a need to characterise the morphology of such cell lines and the form of TiO_2 used in exposures to ensure comparability with the wider literature. The aim of the present study was to assess the effect of TiO_2 crystal structure on uptake, accumulation, apical to basolateral transport, and epithelial integrity on fully differentiated Caco-2 cells and gauge whether this is comparable to partially

differentiated Caco-2 cells (Chapter 2 – Gitrowski *et al*. 2014). Secondary objectives were to assess whether cell growth substrate affected brush border differentiation and subsequent TiO_2 accumulation rates. Moreover biochemical endpointsand cell electrolyte concentrationswere measured to assess whether exposure to different forms of TiO_2 have subtle effects on mature cell physiology.

3.3 Materials and methods

Several experiments were performed using fully differentiated confluent monolayers of Caco-2 cells. The first experiment determined the total Ti metal accumulation in 21 day old Caco-2 cells exposed to 1 mg L^{-1} of different forms of TiO_2 over 24 hours cultured in flat bottomed 6 well plates. The second experiment involved growing Caco-2 cells for 21 days on polyethylene terephthalate (PET) inserts and determining the total Ti metal accumulation and transport (apical to basal) of different crystal forms of TiO_2 (identical to those used in Chapter 2). Maturation of cells was evaluated using SEM and TEM micrographs in conjunction with monitoring tight junction integrity by measuring transepithelial electrical resistance (TEER). Cell health was assessed using inverted light microscopy observations and measuring LDH activity (leak) in culture media. Cellular electrolyte concentrations were examined using ICP-OES in order to determine whether subtle biochemical changes occured following TiO_2 exposures.

3.3.1 Cell culture

The human intestinal cell line, Caco-2 (brush border expressing, European collection of cell cultures; catalogue no: 86010202 HTB-37) was cultured as previously described (Chapter 2) with the following modifications. Cells cultured in flat bottomed 6 well plates were incubated for 21 days post seeding to ensure complete cell maturation and brush border development. For the second series of experiments, cells were cultured for 21 days on BD Falcon cell culture inserts (PET, 1.0 µM pores, 0.9 cm^2 effective growth area) in 12 well plates (only 5 wells were used per plate). Cells were seeded at 5 x 10^{-4} cells cm^{-2} and experiments were conducted on cells between passage 60 and 75. The basolateral side (serosal) and apical side (mucosal) compartments contained 1.5 and 0.5 mL of culture medium, respectively. The culture medium was replaced every two days until the 21st day.

3.3.2 TiO_2 Stock dispersions and materials characterisation

Stocks and materials were the same as those used in Chapter 2, section 2.3.2.

3.3.3 Time course of Ti accumulation and apical to basolateral transport from different forms of TiO_2

The first experiment determined the time course of Ti accumulation for the different forms of TiO_2 in mature Caco-2 cells over 24 h in flat bottomed six well plates. This experiment followed the same method as previously described (Chapter 2 section 2.3.3) with the following modifications. Cells were cultured as described in section 3.3.1. Fully mature confluent monolayers (21 days post seeding) were exposed to

the cell culture media containing 1 mg L^{-1} of either no added TiO_2 (control), bulk, nano P25, nano anatase or rutile forms of TiO_2. The six-well plate was the unit of replication in the experiment with each plate containing cells without TiO_2 additions, and a well for each of the test materials (5 wells were used per plate). Dosing of the well was the same as previously described (Chapter 2, section 2.3.3) with three plates per timepoint being used. Media and cells were then collected at 0, 2, 4, 6, 8 and 24 h for total Ti determination, electrolyte concentrations and LDH activity (see below).

The second series of experiments demonstrated the time course of Ti accumulation and transport from the mucosal solution (apical) to the serosal solution (basolateral) for the different forms of TiO_2 in Caco-2 cells cultured on inserts. Similar to the previous experiment, the 12-well plate was the unit of replication (only 5 wells were used in each plate). As in the previous experiment at least three plates were prepared for each time point (*n* = 3 replicates/time point) temporally separated to avoid pseudo replication and take into account passage effects. Insert experiments did not start until the cells were 21 days old allowing the TEER resistance to be > 250 Ω cm^2 (See below). Dosing of the wells was performed by diluting the initial 500 mg L^{-1} stock to 10 mg L^{-1} TiO_2 in ultrapure water, and this secondary stock was mixed with fresh culture media (1 mL of the appropriate 10 mg L^{-1} TiO_2 stock: 9 mL DMEM) to obtain a final concentration of 1 mg L^{-1} TiO_2 for the exposures. Exactly 0.5 mL of the appropriate medium was pipetted into the apical compartment of each insert. Media and cells were then collected at 0, 2, 4, 6, 8 and 24 h of exposure for total Ti determination, electrolyte concentrations and LDH activity (see below).

3.3.4 Transepithelial electrical resistance (TEER)

TEER is widely used as an indicator of tight junction integrity (Pohl *et al*. 2009), although under short circuit conditions the electrical resistance of the entire epithelium is measured and is assumed to be a surrogate of the net resistance of all the paracellular pathways (not just tight junctions). TEER was measured using an EVONTM voltohmmeter (World Precision Instruments, Sarasota, FL) and the voltage resistance through monolayer cells was recorded as $\Omega.cm^2$. Measurements were obtained by pipetting 1500 µL PBS (NaCl - 137 mmol L^{-1}, KCl - 2.7 mmol L^{-1}, Na_2HPO_4 - 10 mmol L^{-1}, KH_2PO_4 - 1.8 mmol L^{-1}) into the basolateral chamber of the EVONTM voltohmmeter, inserting a culture insert and pipetting 500 µL PBS into the apical chamber. An insert containing PBS and no cultured cells was used as a blank and the resistance reading was subtracted from the sample readings. The readings were multiplied by the insert surface area (0.9 cm^2). Monolayers of cells were incubated with PBS for 5 mins at room temperature to equilibrate samples before each reading. Readings for each insert were performed twice to ensure voltages were stable and three inserts were analysed per timepoint (day 3, 7, 10, 14 and 21 post seeding)

3.3.5 Titanium and electrolyte determination in cells

For the flat bottomed 6 well plate experiment, exactly the same protocol was followed as previously described in Chapter 2 (Section 2.3.6).

A similar protocol was used with the following modifications for the insert experiments. At each time point mucosal (apical) and serosal (basolateral) medium

was carefully collected and stored in 13 mL tubes for elemental analysis. Inserts were carefully washed twice with 1.5 mL PBS prior to measuring TEER. Following TEER measurements inserts were carefully washed twice more with isotonic sucrose buffer (as described in Chapter 2 section 2.3.6) in order to remove residual electrolytes left over following the PBS wash. Filters were carefully removed from the insert and placed in 1 mL of sucrose lysis buffer (similar to the sucrose wash buffer, but hyp osmotic with only 30 mmol L^{-1} sucrose) to detach and lyse the cells attached to the insert. After 10 min lysed cells were carefully scraped of the filters and the resulting 1 mL of homogenate pipetted into 13 mL test tubes and sonicated (power 100 Watt, setting 8/ frequency 22.5 kHz, Misonix incorporated, XL2000-010, New York) for 30 sec to ensure lysed samples were well mixed. A 50 µL aliquot was taken for protein determination (BCA assay as described in Chapter 2 section 2.3.6) and the remaining 950 µL of the lysed sample containing the cells was digested in 1 mL of nitric acid (70%) at 70 ^{o}C for 4 h. Then, total Ti, Na^{+}, K^{+}, Ca^{2+} and Mg^{2+} was determined using inductively coupled plasma - optical emission mass spectroscopy (ICP – OES, see below). The remaining cell free filter insert was gently washed once more in order to remove any residual cells using 1 mL sucrose lysis buffer prior to being placed in a test tube and digested in 1 mL of concentrated nitric acid (70%) at 70 ^{o}C for 4 h, and total Ti determined by ICP-OES.

3.3.6 Trace metal analysis

All samples were sonicated for 1 h (Branson 2800, Frequency 40 kHz, Danbury, USA) and vortexed for 20 s prior to being drawn into the instrument to ensure mixing, and calibrations were performed with matrix matched multi elemental standards

containing Ti, Na^+, K^+ Ca^{2+} and Mg^{2+} in 38% nitric acid. Instrument detection limits (3 x standard deviation of the blank + the mean of the blank) (Thomsen *et al*. 2003) were 0.0014, 0.6448, 0.0653, 0.0050 and 0.0086 mg L^{-1} for Ti, Na^+, K^+, Ca^{2+} and Mg^{2+} respectively.

In the absence of certified reference tissues for TiO_2 particle analysis, spike recovery tests were performed both in the cell homogenate following the above protocol and in culture media. Exactly 1 mL samples of medium and cell homogenates (in sucrose lysis buffer) were spiked with 200 µL of 10 mg L^{-1} of the different forms of TiO_2 and then the acid digestion protocol was followed (addition of 1 mL of concentrated nitric acid (70%) then heated 70 ^oC for 4 h prior to total Ti determination, total volume 2.2 mL) and showed procedural recoveries for the cell homogenate of 94 ± 3.2, 82 ± 2.8, 82 ± 1.2, 72 ± 3.6 and 71 ± 1.6% (Fig. 3-1 panel A) and for the medium 93.7 ± 2.4, 75 ± 1.8, 71 ± 2.2, 69 ± 2.4, and 72 ± 3.7% for dissolved Ti, bulk, P25, anatase and rutile, respectively (Data presented as mean ± SEM, n = 6 for each material type) (Fig. 3-1 panel B). Electrolyte concentrations in the cell homogenates were normalised to cell protein content as described previously (Chapter 2, section 2.3.6).

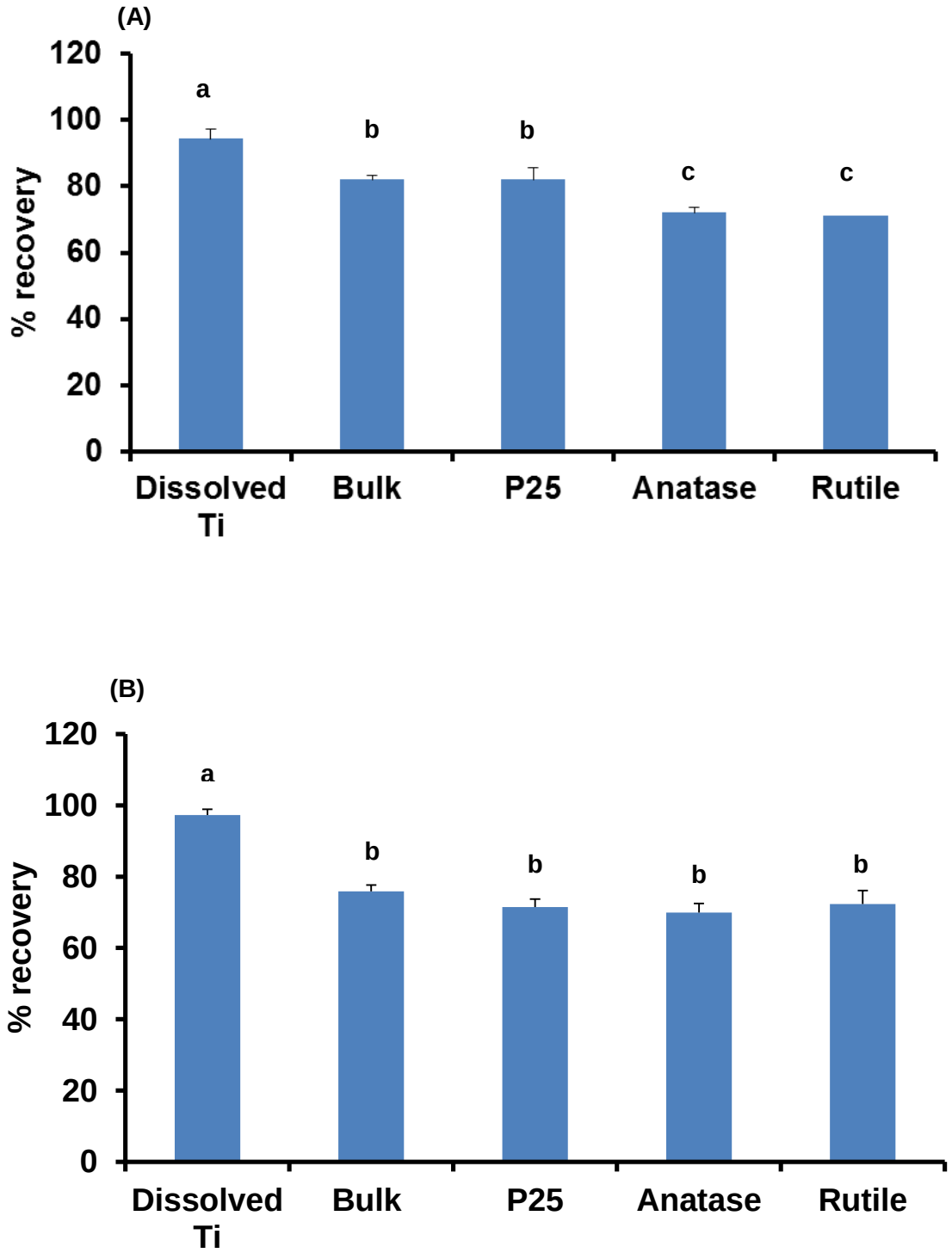

Fig. 3-1**:** Procedural recovery of Ti in (A) cell homogenate and (B) culture ready medium spiked with 200 µL of 10 mg L^{-1} TiO_2 or 6 mg L^{-1} Ti metal before digestion by nitric acid. Data are mean ± SEM, % recovery of Ti metal or TiO_2 particles spike, *n = 6*; Different letters indicate statistically different recoveries for the spiked material (ANOVA *P* > 0.05).

3.3.7 Lactate dehydrogenase activity

Lactate dehydrogenase (LDH) activity is widely used to determine levels of cell damage, by assessing the activity of LDH released into the medium following cell leakage or rupture. In this study, the culture medium and samples of cell homogenate were collected and immediately frozen at -80 ^{0}C until later biochemical analysis. LDH was measured as described by Bergmeyer and Bernt (1974). The reaction mixture contained 250 µL of 0.169 mmol L^{-1} NADH and 4.45 mmol L^{-1} pyruvate in 50 mmol L^{-1} of potassium phosphate buffer at pH 7.4 and was added to 50 µL of samples. The LDH activity was determined by the measuring the decrease in absorbance at 340 nm (VersaMaxTM, Molecular Devices, Sunnyvale, CA) due to the oxidation of NADH, and was allowed to proceed for 15 min with readings taken every 11 s. Measurements were carried out in triplicate and enzyme activity was calculated using an extinction coefficient of 6.22 x 10^{-3} L mol^{-1} cm^{-1}. LDH activity is expressed as U mL^{-1} (µmol min^{-1} mL^{-1}, where one unit causes the oxidation of one µmol of NADH per minute). The percentage of LDH leak from the cells within each well was estimated from the absolute total LDH activity of each well (cells + media) divided by the LDH activity of the medium alone.

3.3.8 Cell morphology and electron microscopy

Cell morphology and brush border differentiation was examined using both transmission and scanning electron microscopy. Three culture inserts per time point were processed. Cells were fixed *in situ* on the filter inserts. Briefly, cells on the cell culture inserts were washed in isotonic sucrose buffer (Described in Chapter 2, section 2.3.6) and fixed for 1 h in 2 mL of 2.5% glutaraldehyde in cacodylate buffer

(0.1 M sodium cacodylate in water at pH 7.4). The cells were then washed twice in cacodylate buffer prior to the insert being carefully cut away from the insert base. The insert was cut in half and one half was embedded for ultrathin sectioning and subsequent TEM analysis, while the other half was prepared for SEM. For SEM the filter was dehydrated in a graded series of ethanol and then critically point dried and carbon coated (EMITECH-K850, K450X). Samples were imaged using a 15 kV accelerating voltage, at a working distance of 10 mm (SEM, JEOL/JSM-7001F).

For TEM the insert was post fixed in 2% OsO_4 prior to being dehydrated in a graded series of ethanol, infiltrated with Spur's resin (Agar Scientific, Essex UK) and embedded into coffin moulds using pure resin. Ultrathin sections were cut (> 90 nm) and stained with 2% uranyl-acetate and lead citrate and then examined by transmission electron microscopy (TEM, JEOL- 1200 EXII).

3.3.9 Image analysis

For quantitative estimation of microvilli (MV) coverage in developing Caco-2 cells SEM images were collected and digitally analysed using Image J software (W. Rasband, National Institutes of Health, Bethesda, MD, USA, http://rsb.info.nih.gov/ij) as follows.

1. - SEM images of 8000 x magnification were imported into image J and the cropping tool was used to remove microscope generated text. The cropped image was then autocorrected for brightness and contrast (Fig. 3-2).

2. - The images were then auto thresholded (creating a binary image) (Fig. 3-3). Image binarization or thresholding is a widely used method (González and Woods 2001) that determines a grey threshold and assigns each pixel of a digital image to

one class (image objects). An automated binarization (black and white) was applied to each SEM image (Fig. 3-3). The automated thresholding function used by the Image J command Image/Adjust/Threshold applies Otsu's method (Otsu 1979) which is based on analysis of the shape of the image histogram. The Otsu method turns an image with different grey levels (e.g. SEM micrograph) into a black and white one, separating the objects from the background. By using binarization it is possible to separate the pixels which represent microvilli (brighter pixels) from those that represent the rest of the cell membrane (darker zones in an original image), allowing quantification cell surface microvilli coverage by calculating the percentage area fraction that is black and white (Julio *et al*., 2008) . Measurement settings were altered to measure the percentage area fraction that is black (which corresponds to areas with no microvilli) (Fig.3-4). The remaining fraction (white) is microvilli coverage. Occasionally the auto threshold function failed to appropriately distinguish microvilli from the background of the cell. In these cases the threshold settings were manually configured to give a true representation of the villi density. This was achieved by having the original image next to the binary image and making the background spaces match up. Three cell inserts were imaged per time point with two distinct areas imaged per insert ($n = 6$ images per timepoint).

Cell height was also calculated from TEM micrographs; a minimum of 12 cells per time point where measured. Only cells whose full length (including microvilli) was in the plane of the section and approximately 90^{o} to the filter were included.

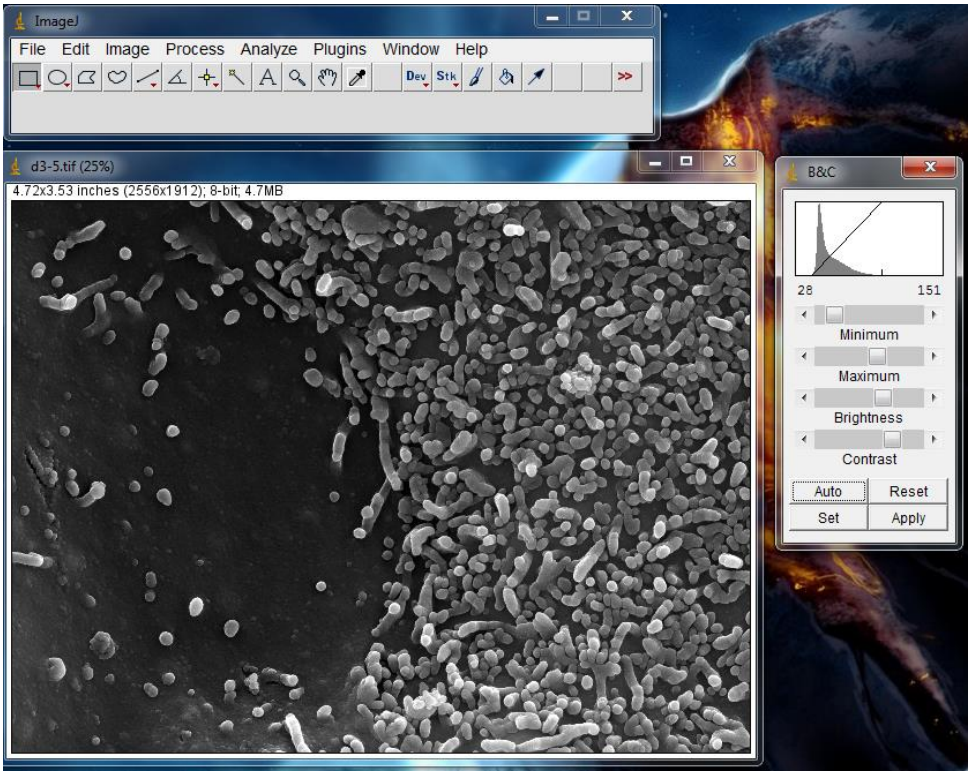

Fig. 3-2: Screenshot of SEM image of 3 day old Caco-2 cell using image J to auto correct brightness and contrast.

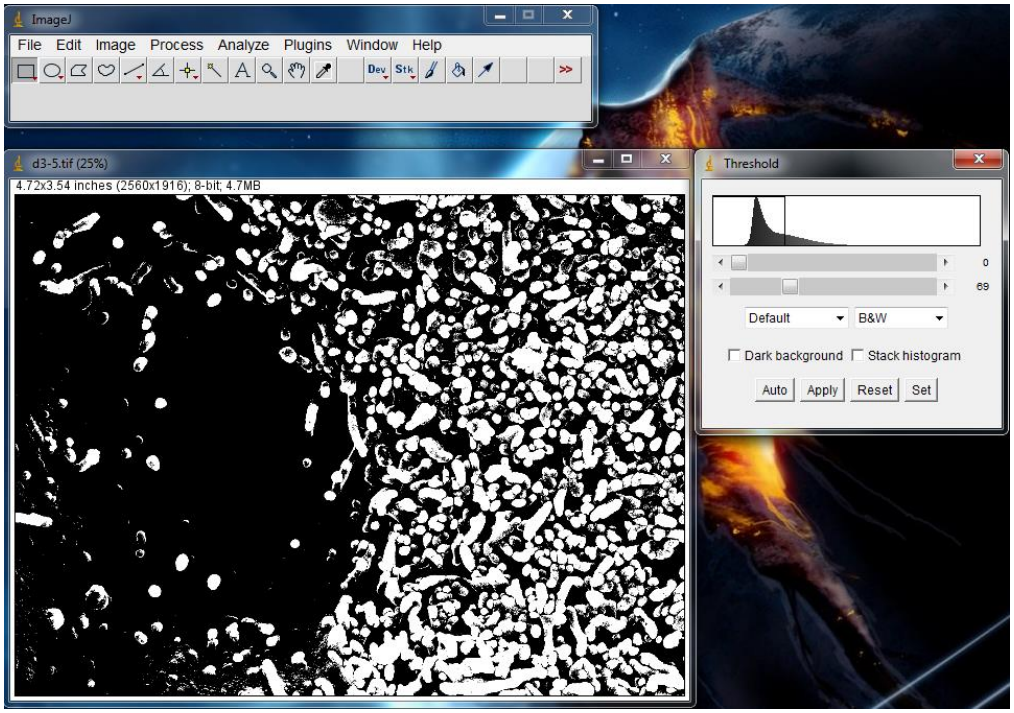

Fig. 3-3: Screenshot of SEM image of 3 day old Caco-2 cell using image J to auto threshold (black areas correspond to no micro villi areas whilst white areas represent microvilli).

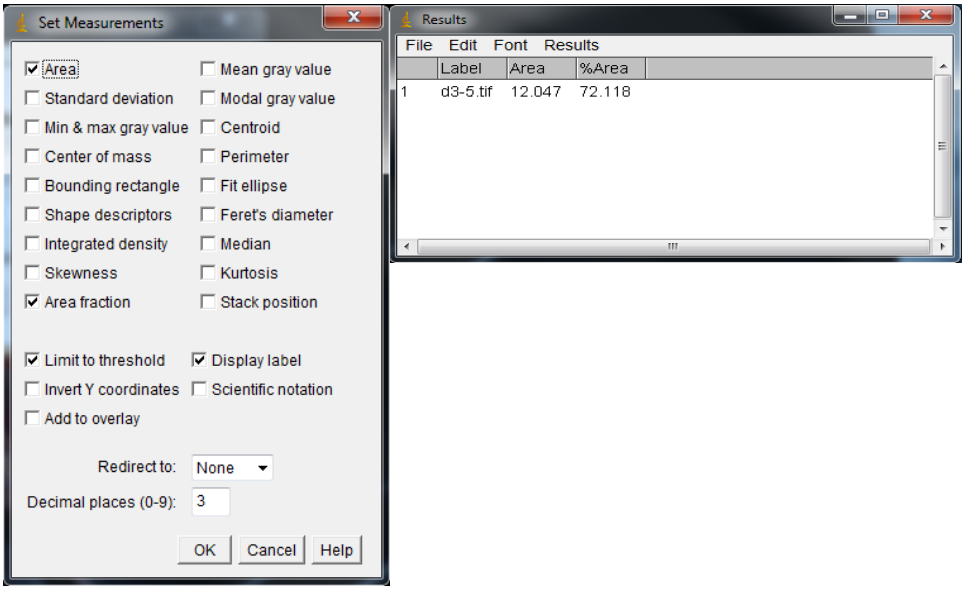

Fig. 3-4: Screenshot of selected measurement options for analysing binary image. To the right of the image the percentage area of the image which is black is shown (in the above example the % area of microvilli coverage is (100 – 72.1 = 27.9%).

3.3.10 Statistics

The statistics applied were the same as those used in Chapter 2, section 2.3.9.

3.4 Results

3.4.1 Cell health and viability

The control cells (not exposed to TiO_2) grown on 6 well plates showed normal morphology during the experiments with the cells remaining confluent and attached to the dishes with intact apical membranes orientated correctly with the presence of dense MV. This was supported by LDH activity which remained below 0.1 U ml^{-1} of cumulative LDH activity over the 24 h duration of the experiments and was equivalent to a mean LDH leakage of 1.4% ± 0.27% (Fig. 3-7) The control cells showed normal electrolyte concentrations. For example, in the time course experiment performed on 6 well plates the electrolyte levels in control cells at 24 h were (mean ± SEM., *n = 3* plates per treatment): Na^+, 7690 ±1543; K^+, 838 ± 95; Ca^{2+}, 34 ± 4; and Mg^{2+}, 60 ± 10 nmol mg^{-1} protein.

In the second experiment (cells grown on inserts) control cells exhibited normal morphology and the expected TEER (between 250 – 350 Ω cm^2 (Moriya and Linder 2006)) readings for fully differentiated cells which was (mean ± SEM., *n = 3* plates per treatment) 313 ± 4 Ω cm^2 (Fig. 3-9). Moreover electrolyte concentrations were similar to cells grown on plates (no significance ANOVA *P > 0.05* for all electrolytes), with the values for control cells being (mean ± SEM., *n = 3* plates per treatment): Na^+, 7429 ±118; K^+, 886 ± 65; Ca^{2+}, 32 ± 7; and Mg^{2+}, 52 ± 2 nmol mg^{-1} protein at 24 h.

Cells incubated with different forms of TiO_2 in experiments performed in flat culture plates (experiment 1) demonstrated low cumulative medium LDH activity (Fig. 3-7) and normal apical morphology (Fig. 3-5). Cells cultured on inserts demonstrated negligible changes in TEER. Cells grown on both substrates (plates and inserts) had reasonably consistent electrolyte concentrations within the physiological range, although there were some TiO_2 dependent changes in ion concentrations (Table 3-1, Series 1 and 2).

Table 3-1: (Series 1 and 2): The total intracellular K^+, Na^+ Ca^{2+} and Mg^{2+} Metalnmol mg^{-1} protein of 21 day old Caco-2 cells cultured in plates (Series 1) or inserts (Series 2) following exposure to 1 mg L^{-1} TiO_2 forms for 24 h.

		Electrolytes (nmol mg^{-1} protein)				
Series 1	**Time (h)**	**Control**	**Bulk**	**P25**	**Anatase**	**Rutile**
Electrolyte						
K^+	**0**	1020.6±58.4	988.2±95.9	1034.6±18.53	976.7±86.8	1009.9±63.8
	2	1072.3±100.9	955.5±152.9	829.2±37.8*	843.3±90.8	942.4±171.4
	4	1069.3±101.5	966.5±113.0	961.8±107.5*	965.9±9.4	755.7±123.5
	6	934.4±108.5	853.3±40.8	790.5±54.3*	750.2±24.6*	765.9±40.9
	8	920.9±70.5^{a}	816.7±2.1^{b}	771.5±72.6^{a*}	748.2±46.8^{a*}	668.9±51.7^{b*}
	24	985.4±95.8	689.8±77.8	781.8±41.8*	700.9±37.8*	569.4±63.1*
Na^+	**0**	8545±764	8421±859	7872±412	8016±925	8045±757
	2	9611±1567	7289±1381	6651±430	6391±1292	7616±1981
	4	7720±113^{a}	6543±1065^{a}	8783±2795^{a}	6742±136^{b}	5459±865^{b}
	6	6396±325	5932±642	6363±1215	5155±405*	5065±262
	8	5906±1163	9355±3536	6619±1435	5000±398*	6012±1434
	24	7690±1543	4850±719	5272±431	4321±478*	4175±545
Ca^{2+}	**0**	20.0±5.9	23.7±3.1	39.6±4.7	22.5±7.9	22.3±9.7
	2	25.2±6.9	47.3±3.0	39.5±2.8	38.6±7.9	41.4±16.3
	4	21.2±7.8^{a}	25.3±7.3^{a}	45.6±2.1^{b}	42.1±3.9^{b}	30.1±5.6^{a}
	6	28.4±4.2	30.5±9.2	30.3±3.8	24.4±1.0	53.1±28.0
	8	25.0±6.4	43.8±10.2	30.6±2.2	52.6±9.2	31.3±12.1

	24	31.8±4.2[a]	41.9±10.1[a]	68.8±5.4[b*]	43.8±12.2[a]	57.7±2.1[b*]
Mg^{2+}	**0**	66.0±7.4	62.1±5.9	64.7±2.7	61.4±3.9	62.9±4.9
	2	49.4±8.5	44.5±6.8	45.7±5.7	45.8±15.2	49.4±16.6[*]
	4	40.5±4.7	45.1±6.1	43.7±5.8	50.6±5.3	37.6±1.8[*]
	6	43.7±7.2	41.1±8.5	37.0±10.3	33.5±6.8	34.9±7.4[*]
	8	47.9±4.9	57.0±8.8	46.2±6.9	41.0±5.8	43.6±6.1[*]
	24	60.4±10.0	54.8±4.6	48.2±7.2	38.5±5.9	42.8±0.7[*]

Series 2

		Control	**Bulk**	**P25**	**Anatase**	**Rutile**
Electrolyte						
K^+	**0**	1049.6±104.6	1110.5±120.1	1038.5±139.6	1216.5±51.4	1125.4±71.1
	2	865.5±69.3	890.1±95.4	863.3±112.0	820.5±56.9	835.8±63.6
	4	1110.4±36.5	1085.7±48.5	1044.7±24.7	1175.2±79.8	1200.5±58.5
	6	883.9±34.8	816.3±25.2	960.6±54.4	945.9±68.5	854.3±79.1
	8	979.5±51.3	895.3±17.8	959.642.0	907.9±61.9	942.3±37.2
	24	886.9±65.2	965.8±39.4	979.2±18.8	835.1±10.9*	907.2±32.1
Na^+	**0**	9352±1363	9521±1280	7893±1115	9981±892	8964±844
	2	6745±411	7992±881	8204±883	6679±311	7006±612
	4	8660±372	8777±643	8404±237	8469±123	9863±473
	6	9041±611	8125±671	8939±872	8257±638	7340±587
	8	9245±785	8679±671	8595±309	8430±761	7451±380
	24	7429±118	7325±335	7006±157	6339±287	7107±521
Ca^{2+}	**0**	19.8±5.5	20.5±5.1	29.7±7.2	26.8±6.9	24.8±10.8
	2	22.4±4.9	47.2±14.0	27.9±6.3	42.7±7.4	32.3±5.8
	4	33.1±3.0	45.5±6.0[*]	34.7±14.9	33.8±2.2	50.9±17.5
	6	23.9±5.8	33.3±5.3	31.6±4.5	41.1±8.0	30.9±5.3
	8	30.1±4.4	35.3±2.9	40.8±2.5	33.6±5.0	32.9±8.7
	24	31.8±2.8	51.4±2.9[*]	49.1±3.0*	42.9±3.3	51.3±11.6*
Mg^{2+}	**0**	74.7±14.2	70.0±8.5	64.9±9.2	76.9±3.6	70.2±5.4
	2	59.1±3.9	65.9±9.1	66.1±6.8	52.5±2.3*	57.2±4.0
	4	63.8±1.8[a]	73.6±3.9[b]	67.6±4.0[a]	73.2±2.2[b]	78.3±1.6[b]
	6	61.9±4.7	62.8±3.3	68.5±7.2	73.7±8.5	64.0±5.7
	8	63.1±4.5	71.6±5.1	78.4±4.9	66.4±3.4	69.1±2.9
	24	52.3±2.0	60.7±2.1	62.6±2.1	49.8±0.6*	58.0±2.2

Values are means ± S.E.M. (n = 3 for each group) and are expressed as nmol Metal mg^{-1} cell protein. Different letters indicate statistical significance within rows. Symbols represent statistical significance within columns and electrolytes (ANOVA or Kruskal-Wallis test, $P < 0.05$).

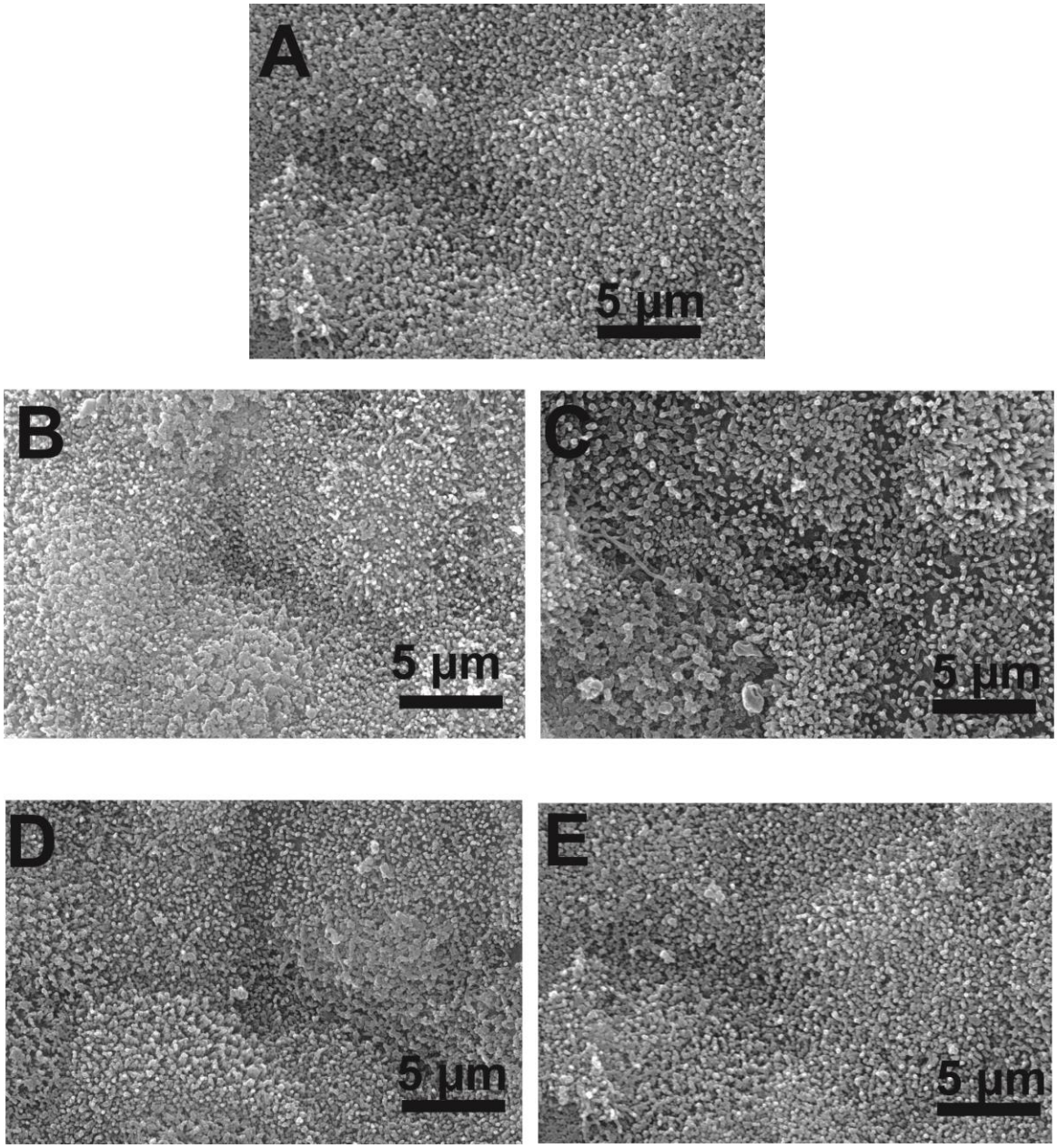

Fig. 3-5: Brush border morphology of cells cultured in 6 well plates (experiment 1) following 24 h exposure to 1 mg L^{-1} different forms of TiO_2. A) control, B) bulk, C) P25, D) anatase, E) rutile. Scale bar = 5 µm

3.4.2 Time course of Ti accumulation from different forms of TiO_2 in 21 day old cells cultured in conventional 6 well plates

The time course of Ti accumulation for exposures to different forms of TiO_2 is shown in Fig. 3-6. Unexposed control cells remained at a background metal concentration of between 0.5 and 1 nmol Ti mg^{-1} cell protein throughout. All the TiO_2 treatments showed a non-linear exponential rise of the total Ti concentration in the cells, which achieved steady state concentrations by 8 h. This rise in net Ti accumulation occurred without elevations in Na^+ (Table. 3-1), indicating that the accumulation was not an artefact of solvent drag. There were some differences in the time courses of Ti accumulation for the different forms of TiO_2 which were not explained by changes in membrane permeability. Cumulative LDH leak at 24 h in the media remained low and did not exceed 5% (not statistically different from the control, and no material–type effect was observed (Fig. 3-7). The net Ti accumulation by 24 h was as follows by material-type: Bulk > nano anatase> P25> nano rutile > unexposed controls. The bulk material and nano anatase showed the largest net Ti accumulation in 24 h saturating at 7.3 and 6.0 nmol mg^{-1} protein respectively, but were not statistically different from each other at 24 h (Kruskal Wallis $P < 0.05$). The P25 nano form showed approximately 20% less accumulation than either bulk or nano anatase at 24 h saturating at 4.9 nmol mg^{-1} cell protein (statistically different to rutile form, Fig. 3-6). The nano rutile form demonstrated much lower accumulation at 24 h saturating at 2.6 nmol mg^{-1} protein (significantly different to all the other treatments, Kruskal Wallis $P < 0.05$). Initial Ti accumulation rates calculated from the curves (Fig. 3-6) followed a similar pattern, with Ti accumulation from the bulk and anatase being faster than those from P25 and rutile. The initial and overall accumulation rates were (initial) 1.54, 1.08, 1.02 and 0.40 for nmol mg^{-1} cell protein h^{-1} and (overall) 0.28, 0.25, 0.19,

and 0.09 nmol mg^{-1} cell protein h^{-1}. The times to 50% saturation were 2 h 28, 2 h 42, 2 h 06 and 1 h 3 min for bulk, anatase, P25 and rutile, respectively.

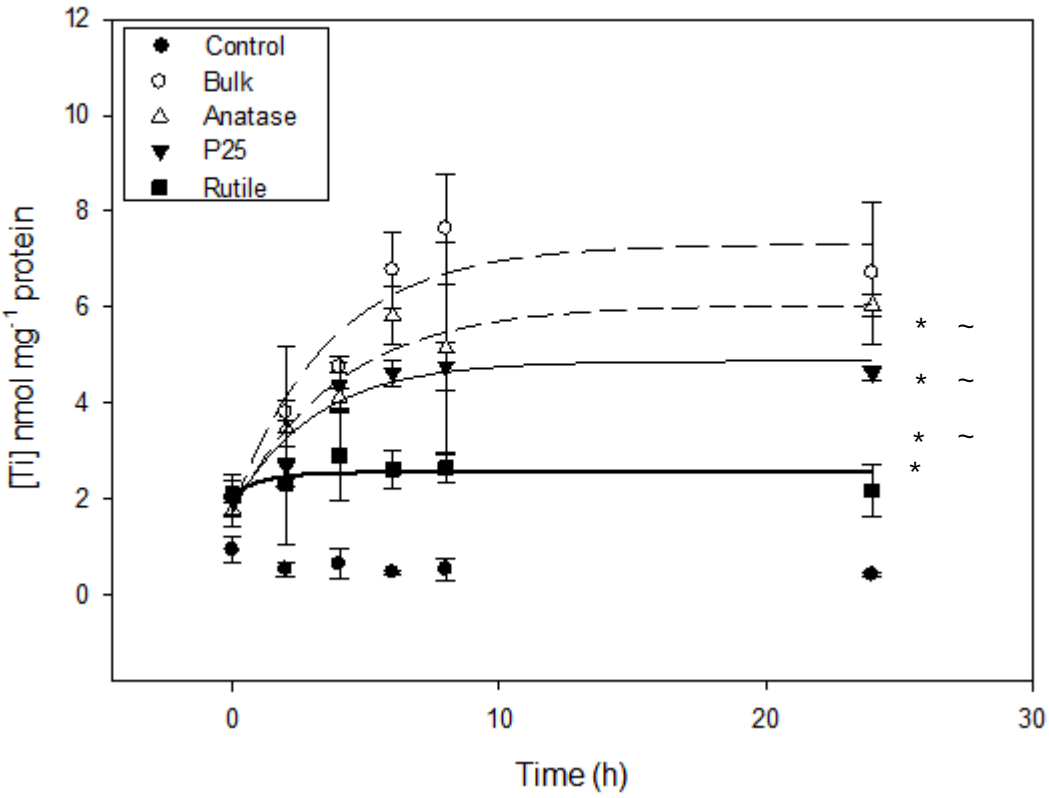

Fig. 3-6: Titanium accumulation in 21 day old Caco-2 cells cultured in conventional 6 well plates from exposures to 1 mg L^{-1} of different forms of TiO_2 for 24 h. Data points are mean ± SEM (n = 3 replicates/ treatment). Curves were fitted using Sigma plot version 12.0 to the raw data (n = 3 observations / treatments) using the exponential rise to the maximum function *f = y0+a*(1-exp(-b*x))*. Equations for the curve fit were as follows: For Bulk *f = 1.18+5.53*(1-exp(-0.28*x))*, r^2 *= 0.905;* For Anatase *f = 1.73+4.32*(1-exp(-0.25*x))*, r^2 *= 0.941*; For P25 *f = 1.78+3.09*(1-exp(-0.33*x))*, r^2 *= 0.917;* For Rutile *f = 2.08+0.48*(1-exp(-0.84*x))*, r^2 *= 0.362.* The unexposed control demonstrated no time dependent changes and therefore a curve was not fitted. Accumulation of all titanium forms is significantly different to the controls (Kruskal Wallis P < 0.05) at 24 h (*). Different symbols indicate statistically significant differences between treatments (Different TiO_2 form exposures).

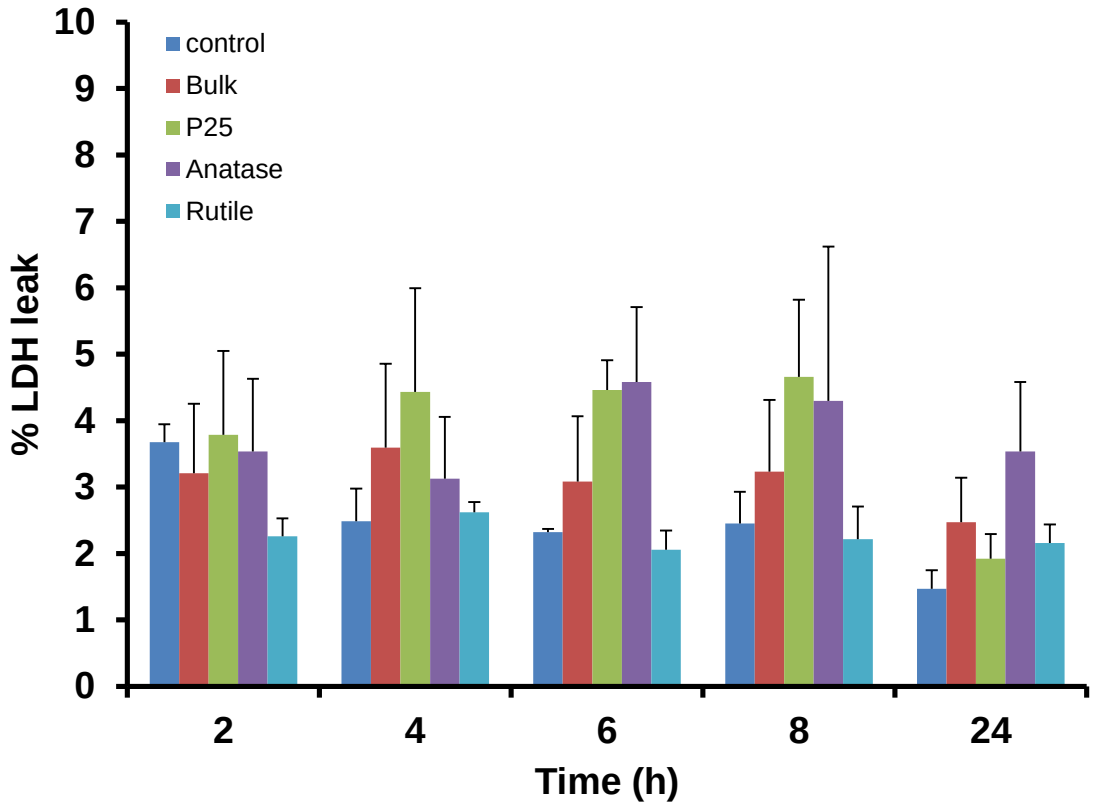

Fig. 3-7: Time course of % LDH leak from 21 day old confluent Caco-2 cells cultured in 6- well plates incubated with 1 mg L^{-1} different forms of TiO_2. At the indicated times post TiO_2 incubation media and cell homogenate were analysed for LDH activity. The percentage of LDH leak from the cells within each well was calculated from the absolute LDH activity of each well (cells + medium) divided by the LDH activity of the medium alone. Data are means ± SEM *n = 3*. Absence of annotation indicates no statistically significant differences between treatments.

3.4.3 Time course of Ti accumulation and transport across cells from exposures to different forms of TiO_2 in 21 day old cells cultured in inserts

The time course of Ti accumulation for exposures to different forms of TiO_2 in cells cultured in hanging inserts is shown in Fig. 3-8. Culturing cells on inserts appeared to have a negligible effect on the pattern of Ti accumulation in comparison to cells cultured in flat bottom plates. All the TiO_2 treatments showed a non-linear exponential rise of the total Ti concentration in the cells, which achieved steady state

concentrations by 8 h (similar to the previous experiment). TEER showed negligible changes following exposure to different forms of TiO_2 (not statistically different from the control, and no material–type effect was observed (Fig. 3-9). The net Ti accumulation at 24 h was as follows by material type: Bulk > P25> nano anatase > nano rutile> unexposed controls (Table 3-3) which was different to the previous experiment, but this order was similar to previous experiments carried out using 4 day old cells cultured in flat bottomed plates (Chapter 2, Fig. 2-6). Mean Ti saturation occurred at 9.6, 8.5, 7.3 and 4.7 nmol mg^{-1} following exposure to bulk , P25, anatase and rutile, respectively for 24 h with the latter being significantly less than the other material exposure (ANOVA, P > 0.05). P25, anatase and rutile accumulation at 24 h in inserts was significantly more than cells cultured in normal plates (ANOVA *P* > 0.05). Initial and overall accumulation rates calculated from the curves were (initial) 1.39, 1.24, 1.39, 1.10 nmol mg^{-1} cell protein h^{-1} and (overall) 0.40, 0.34, 0.30 and 0.20 nmol mg^{-1} cell protein h^{-1} for Bulk, P25, anatase and rutile, respectively. The times to 50% saturation were 3 h 51, 3 h 38, 3 h 18, and 1 h 13 for Bulk, P25, anatase and rutile, respectively.

TiO_2 particles could freely move through the insert membrane in the absence of cells (Table 3-2) and a small proportion was able to cross the insert when cultured cells were present. There was a gradual appearance of Ti in the basolateral compartment (Fig. 3-10) with Ti being detectable above background media concentrations at 6 h for P25, 8 h for anatase and at 24 h for bulk and rutile. Overall transport rates (apical to basolateral) and the absolute amount (µg) of apically administered Ti that was in or on the cells that managed to cross the cell monolayer and culture inserts by 24 h is presented in Table 3-3 for the different TiO_2 crystal types. As a percentage of total administered dose, cells exposed to bulk had the highest Ti concentrations and the

highest overall Ti transport into the basolateral medium (Table 3-3). Rutile TiO_2 exposure demonstrated the lowest uptake and overall transport rates at 24 h and was statistically different from all the other TiO_2 forms assessed (Fig.3-8, Table 3-3).

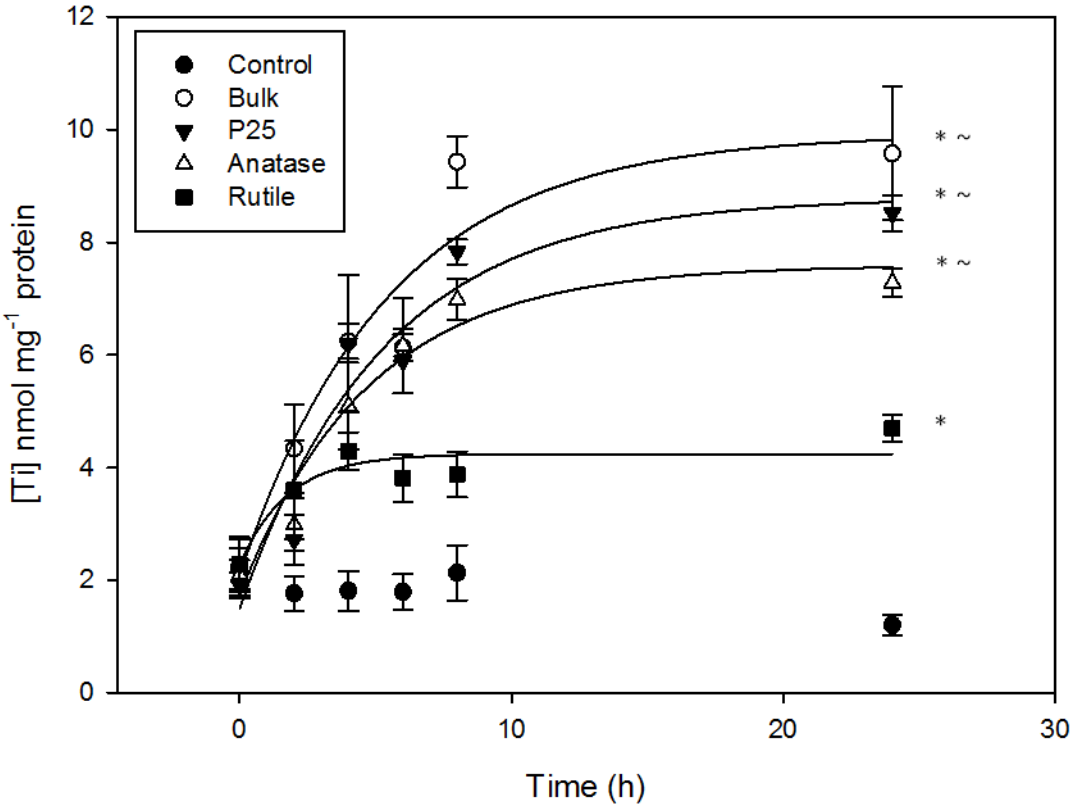

Fig. 3-8: Titanium accumulation in 21 day old Caco-2 cells grown in culture inserts following exposures to 1 mg L^{-1} of different forms of TiO_2 for 24 h. Data points are means ± SEM (n = 3 replicates/ treatment). Curves were fitted using Sigma plot version 12.0 to the raw data (n = 3 observations / treatments) using the exponential rise to the maximum function *f = y0+a*(1-exp(-b*x))*. Equations for the curve fit were as follows: For Bulk *f = 1.18+7.822 *(1-exp(-0.18x))*, r^2 *= 0.905;* For Anatase *f = 1.73+5.86*(1-exp(-0.21*x))*, r^2 *= 0.941*; For P25 *f = 1.78+7.30*(1-exp(-0.1.9*x))*, r^2 *= 0.917;* For Rutile *f = 2.08+1.96*(1-exp(-0.56*x))*, r^2 *= 0.362.* The unexposed control showed no time dependent changes and therefore a curve was not fitted. Accumulation of all titanium forms is significantly different to the controls (Kruskal Wallis P < 0.05 differences located using a notched box plot) at 24 h (*). Different symbols indicate statistically significant differences between treatments at 24 h (Different TiO_2 form exposures).

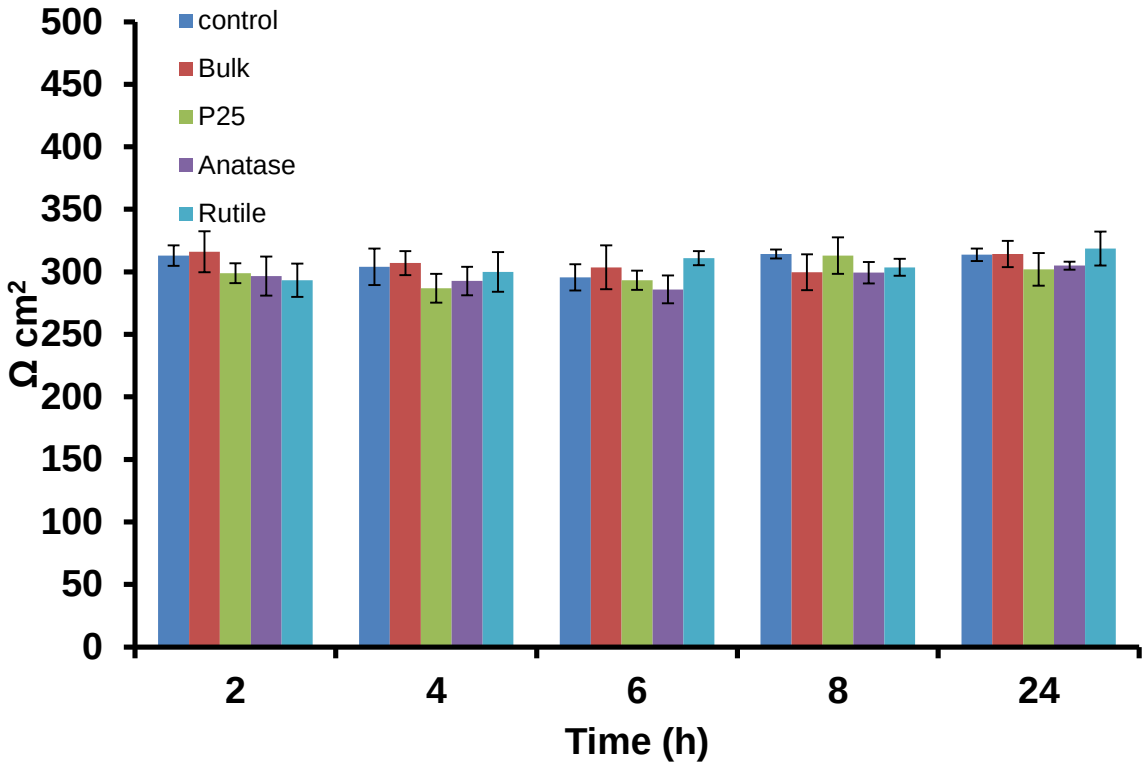

Fig. 3-9: TEER following the administration of 1 mg L^{-1} TiO_2 forms over 24 h. Data are mean ± S.E.M (*n = 3* replicates per treatment per time point).

Table 3-2: Levels of Ti present in the basolateral compartment at 24 h after apical administration of 1 µg mL^{-1} in the absence of cells

Material	Total Ti in mucosal compartment at 0 h (µg)	Total Ti in basolateral compartment at 24 h (µg)	% Ti in basolateral compartment at 24 h
Bulk	0.3	0.161 ± 0.005	53.9 ± 1.4
P25	0.3	0.178 ± 0.006	59.6 ± 1.9
Anatase	0.3	0.181 ± 0.007	60.5 ± 2.2
Rutile	0.3	0.184 ± 0.010	61.6 ± 3.2

Values are means means ± S.E.M.. (n = 2 for each material). Absence of annotation indicates no statistically significant difference between treatments. There were no material type differences.

Table 3-3: Absolute Ti in the cells and basolateral compartment at 24 h following exposure to 1 µg mL^{-1} TiO_2

Material	Mean absolute Ti in the cells at 24h (Ti in cells-background in control cells) (µg).	Mean % of exposure in/on cells	Mean absolute Ti in basolateral compartment (Ti in basolateral compartment – background in controls) (µg)	Mean % of exposure in basolateral compartment	Mean overall transport (apical to basolateral) rates of Ti (nmol mg^{-1} h^{-1})
Bulk	0.0179[a]	5.9712	0.0057[a]	1.8889	0.1118[a]
P25	0.0155[a]	5.1687	0.0048[a]	1.5901	0.0961[a]
Anatase	0.0148[a]	4.9381	0.0047[a]	1.5560	0.0833[a]
Rutile	0.0079[b]	2.6245	0.0014[b]	0.4627	0.0269[b]

Values are means of the triplicate data. Mean % of exposure in/on the cells was calculated from the mean absolute Ti in the cells / by total Ti metal dose in the apical compartment (0.3 µg Ti metal). Likewise, mean % of exposure in basolateral compartment was calculated from the mean absolute Ti in the basolateral compartment / by total Ti metal dose in the apical compartment (0.3 µg Ti metal). Mean overall transport of Ti (apical to basolateral) were calculated from Ti in basolateral media at 24 h following exposures(converted to nmols) / cell protein content and expressed as nmol mg^{-1} h^{-1}. Letters indicate statistical differences within columns (ANOVA *P* > 0.05).

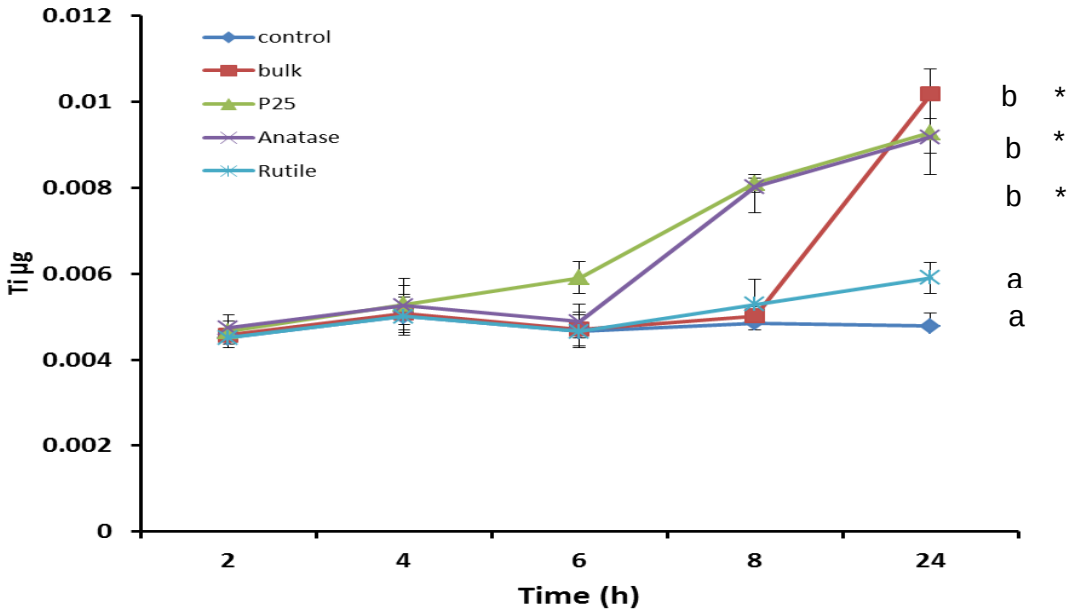

Fig. 3-10: Absolute total Ti metal appearance in the basolateral media in µg (Mean ± SEM *n* = *3*). * indicates statistically different to the control value at 24 h (ANOVA P > 0.05). Letters represent statistically significant differences due to materials at 24 h.

3.4.4 Effect of Titanium dioxide on cell electrolyte concentrations

There were some TiO_2 dependent changes in electrolyte concentration in the cells. For example all the nano forms of TiO_2 caused some depletion in K^+ (Table 3-1 series 1). This trend was apparent in the second experiment although it was only regarded as significant in the cells treated with anatase TiO_2. Exposure to all forms of TiO_2 appeared to increase mean total cellular Ca^{2+} over time and this was regarded as significant for P25 and rutile in the first experiment and for bulk, P25 and rutile in the second experiment (Table 1, Series 1 and 2). Low LDH leak, negligible changes in TEER and a general trend of cell Na^+ depletion (against the concentration gradient) suggests that the changes are material specific, rather than attributed to non-specific membrane leak.

3.4.5 Morphological characterisation of differentiating Caco-2 HTB 37 cells grown on culture inserts – SEM analysis

Morphological changes in differentiating Caco-2 cells were investigated using SEM and TEM. Complete monolayers had already formed by day 3 and previous work (Chapter 2, Fig. 2-1) confirmed cell confluence occurs by 35 h following a seeding density of 5×10^4 cells cm^{-2}. MV density appeared to steadily increase over time (Fig. 3-11, Panel C). At day 3 MV density was heterogeneous with some regions exhibiting dense packing whilst other regions were more sparsely populated with MV. By day 7 MV density continued to increase although the development was heterogeneous in terms of organisation, density and length. By day 10, MV density was still increasing and the development of dome regions in the monolayer had become apparent (Fig. 3-12, E). By day 14 MV density was approaching maximal

packing with MV appearing to be getting longer, but the occasional cell still appeared sparsely covered. At day 21 MV had reached maximum packing density and apical membranes displayed many dome like regions (Fig. 3-11 H). Similarly, cells grown on plastic flat bottomed plates exhibited the same apical morphological characteristics to cells grown in inserts at day 21 (Fig. 3-11 I).

3.4.6 TEM analysis

TEM analysis revealed considerable differences in internal cell morphology and development. Cell differentiation was not homogeneous. Even by day 21 cell morphology displayed heterogeneous characteristics. Cell height increased in a step like manner over time (Fig. 3-11 Panel B). Approximately 70% of the TEM images demonstrated cells growing as monolayers, although even at day 21 there were patches of cells that were not a monolayer, rather cells were clearly growing on top of each other (Fig. 3-13 I). In these situations the most apical cells had sparsely populated areas of MV.

By day 3 cells had formed a flat monolayer (mostly) and cell apical junctional complexes were visible between neighbouring cells (Fig. 3-13 A, B, C). Cells were dominated by a large nucleus which was positioned in the middle of the cell, with organelles occupying the entire space around the nucleus. Microvilli demonstrated the heterogenous patchiness noted in the SEM micrographs. Cells that were seven days old were indistinguishable from 3 day old cells. At day 10 cells also appeared similar to days 3 and 7 except microvilli density had increased and the mitochondria were predominantly located above the nucleus. Monolayer height remained the same. SEM images of 10 day old cells indicated the development of dome like

regions suggestive of more cuboidal like epithelial cells; this was not visualised in the TEM micrographs. At day 14 junctional complexes were clearly visible on most adjacent cells. Microvilli density had increased and organelles appeared to be orientated above the nucleus. There were also clear pseudopodia anchoring the cells to the growth substrate within the pores of the insert. Cells were taller than previous days (Fig. 3-13).

By day 18 the cells were starting to take on a cuboidal appearance and were generally taller than less mature cells (measured from insert to MV, Fig.3-11 and 3-13 EF). MV appeared to be maximally packed on most cells although there was still the occasional sparsely populated cell. Moreover, there appeared to be an increase in non-specific vacuoles occupying the space in between the apical membrane and the nucleus. By day 21 cells appeared to be more columnar (Fig.3-13). MV were longer, straighter and more organised. Organelles appeared to be congregated above the nucleus and junctional proteins extended further into the cells. There were still areas where the cells were growing on top of each other with heterogeneous microvilli development (Fig. 3-13).

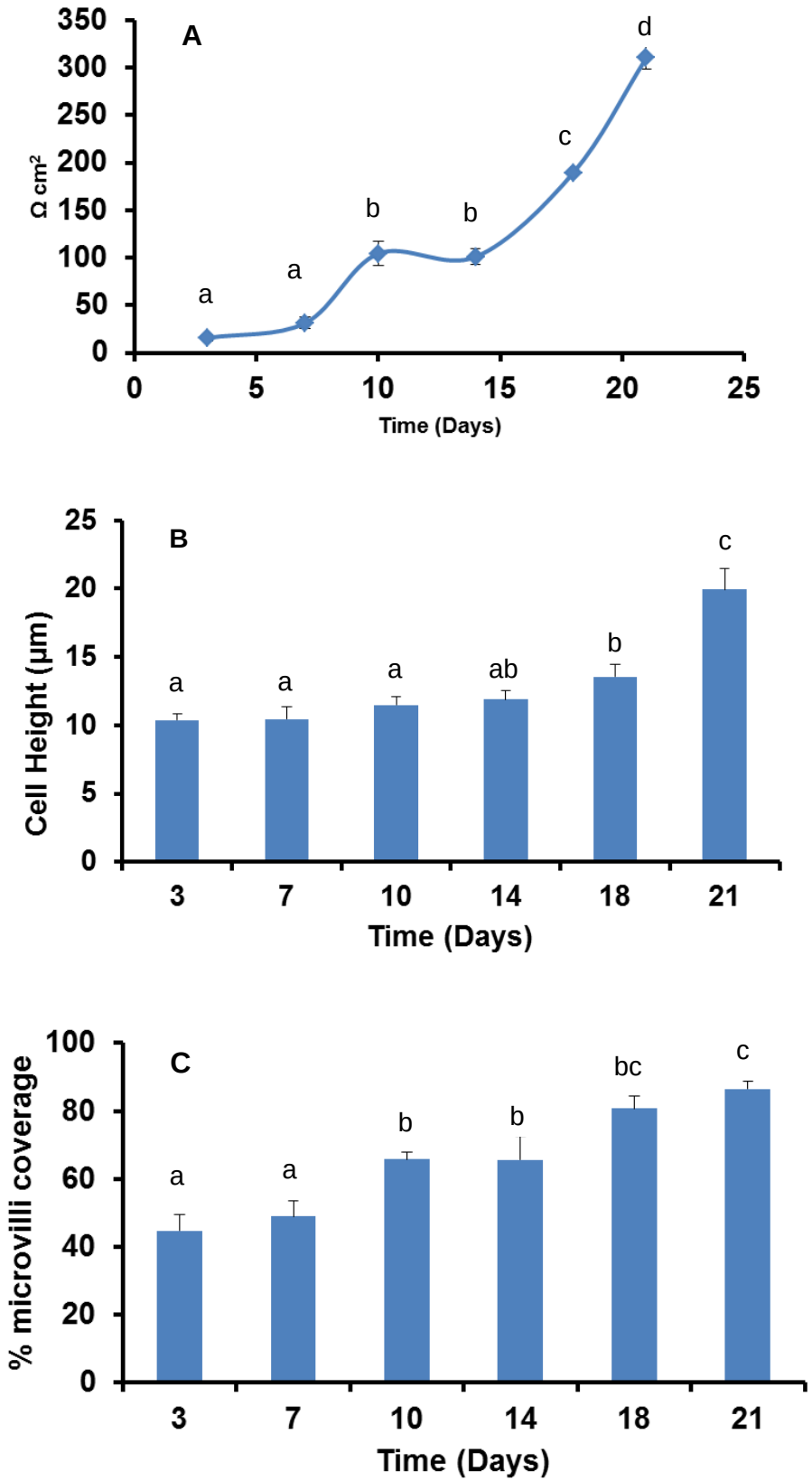

Fig. 3-11;Panel A: Trans-epithelial electric resistance (TEER) was measured during Caco- 2 cell differentiation. Data represents mean ± SEM (n = 3). Panel B: Quantitation of cell height increase over time. A minimum of 12 cells per time point was measured in TEM micrographs. Data shown represents the mean ± SEM. Panel C: Quantitation of the increase in microvilli density over time. Microvilli were quantified using SEM micrographs. Data represents mean ± SEM of 6 images taken from 3 separate inserts (n = 6). Different letter indicate significant differences between time points within graph panels (ANOVA $P > 0.05$)

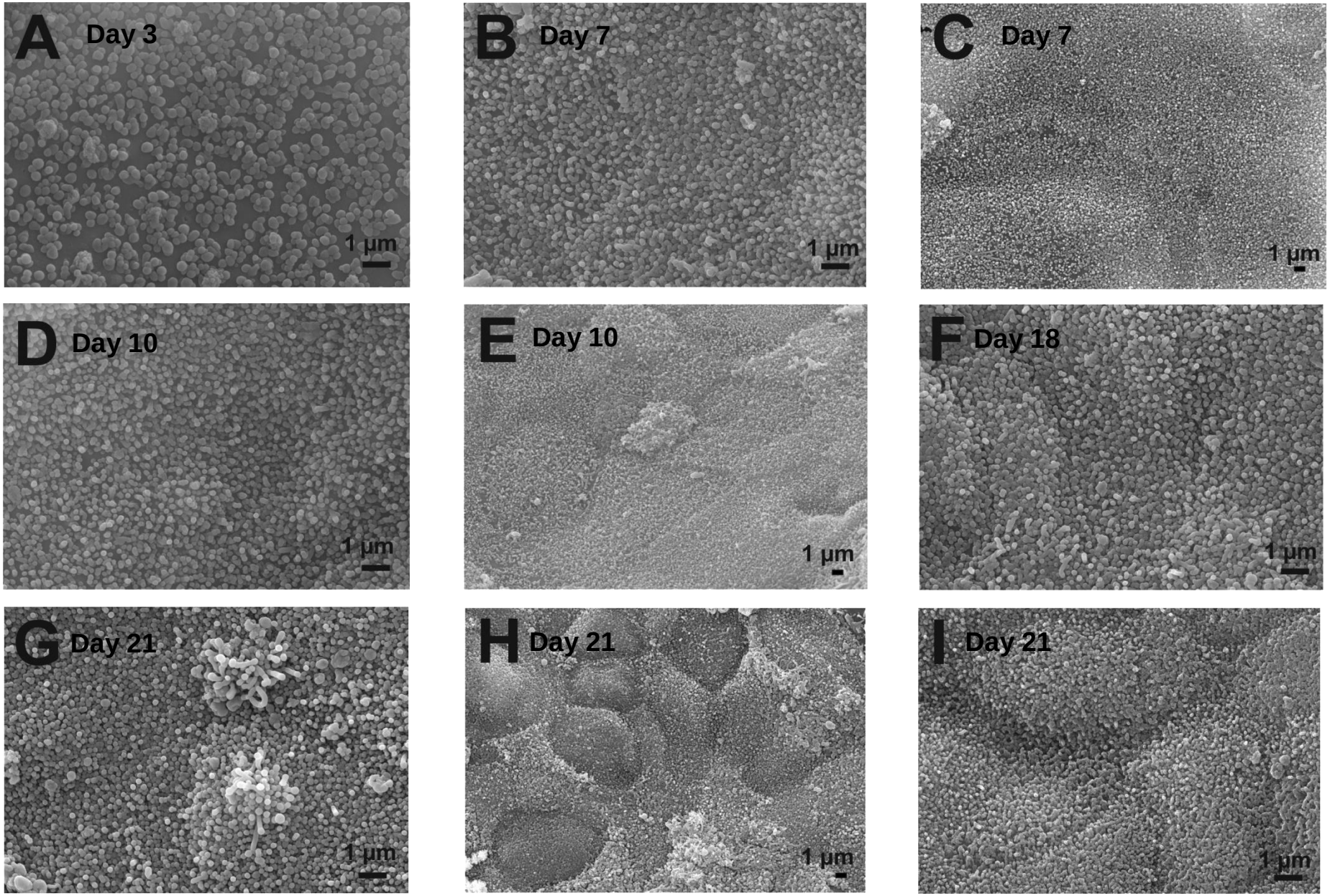

Fig. 3-12: SEM sequence of apical brush border development in unexposed cells. Villi density increases over time as do the amount of dome like regions. Multiple images of the same day aim to show the extent of the MV coverage. Image I: 21 day old cells cultured in flat bottomed plates. Apical morphology is indistinguishable from 21 day old cells cultured in inserts. Scale bar represents 1 µm.

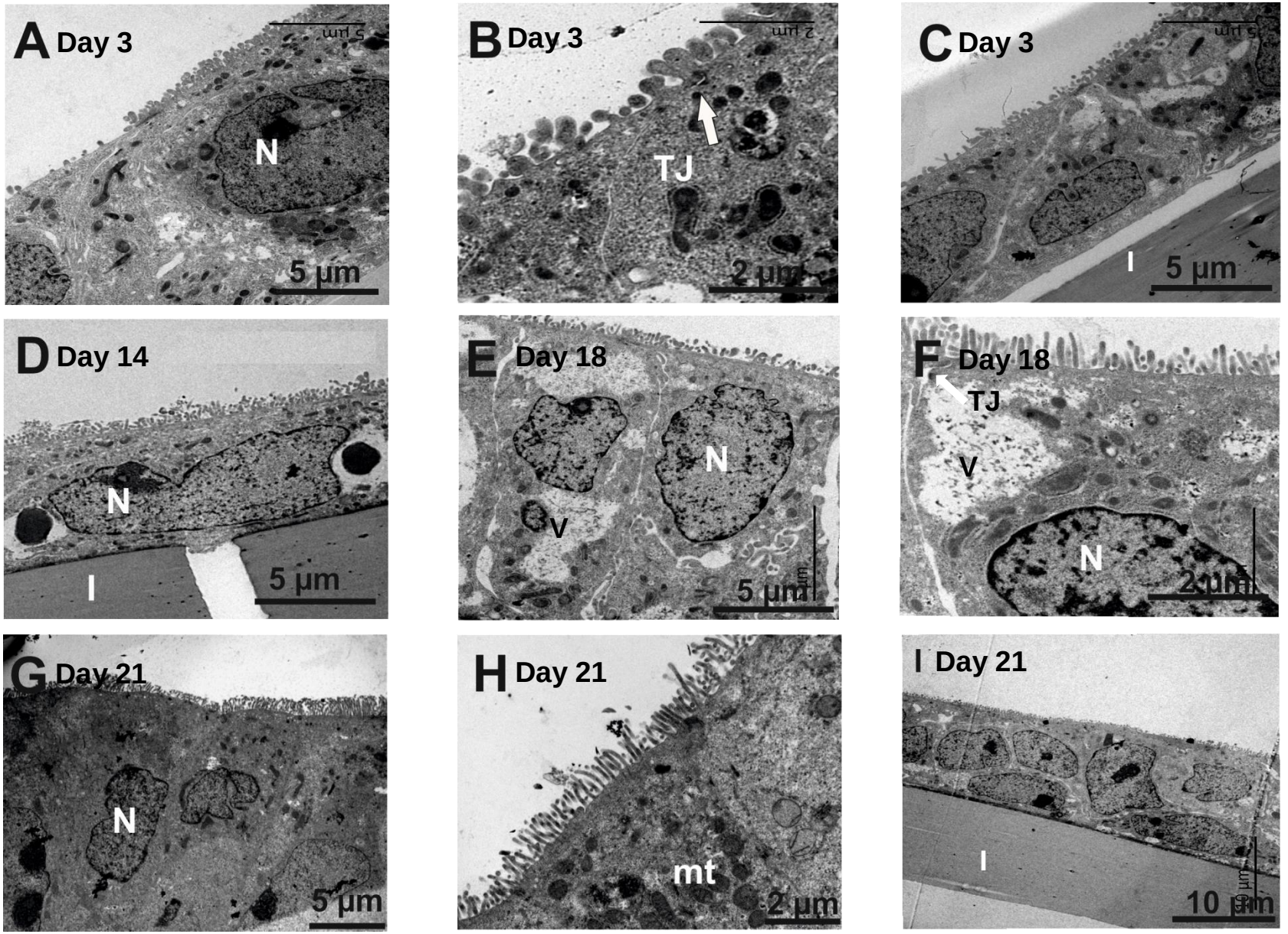

Fig. 3-13: TEM sequence of cell maturation in unexposed cells cultured on inserts (I). 3 day old cells showing, A) heterogeneous MV development, B) junctional complex (TJ), C) and monolayer formation, D) 14 –day old cells are still flat, however mv density is increasing, E) cells beginning to appear cuboidal, F) appearance of nonspecific vacuoles (V) and clear junctional complexes, G) cells are more columner with central nucleus (N) and dense MV, H) mitochondria situated below the apical membrane, uniform MV, I) Day 21 showing areas of under-developed cells growing on top of each other.

3.5 Discussion

The present study demonstrates that mature, confluent Caco-2 cells with fully differentiated brush borders are capable of accumulating and transporting Ti from TiO_2 particle exposures. However, the precise form of the Ti taken up by the cells and/or translocated to the serosal compartment was not determined. Similar to immature Caco-2 cells (4 day old, Chapter 2), the mature cells show Ti accumulation which is influenced by the crystal structure of TiO_2 with the rutile form being taken up the least irrespective of cell growth substrate. These novel experiments were used to determine the rate of apical to serosal appearance of total Ti metal from exposures to different forms of TiO_2 in addition to assessing cellular electrolyte concentrations of fully differentiated Caco-2 cells following 24 h exposures to TiO_2. The main findings were that accumulation occurs irrespective of cell maturation and culture substrate and that TiO_2 crystal structure influences uptake and transport.

3.5.1 Brush border morphogenesis

Batch related morphological heterogeneity of Caco-2 cell differentiation has been well illustrated (Herold *et al*. 1994). Moreover, it is uncertain whether morphologically distinct Caco-2 cells also differ with respect to functional and biochemical parameters. In order to reliably compare studies using differentiated cells, it is important to characterise the development of the cell line in addition to defining culture conditions. This study has demonstrated (for this batch) that monolayer formation occurs in less than 3 days and that microvilli density and TEER increase steadily over time. Development of cuboidal epithelial cells appears to happen relatively late (day 18) and is not homogenous across the cell population. Moreover,

by day 21 the cells did not have homogenous morphology and there were still patches of cells that appear to be growing on top of each other. Growing cells on culture inserts provides a more natural environment than normal culture plates, with better basolateral accessibility, ideally allowing for better enterocyte differentiation. Nevertheless, this batch of cells had the same apical morphology and similar intracellular electrolyte concentrations irrespective of the culture matrix conditions which conforms to previous research (Herold *et al*. 1994).

Interestingly TEER values reported for Caco-2 cells range from 200 > 3500 Ω cm^2 (for the latter see Johannessen *et al*. 2013). There appear to be contradictions in the unitary expression of TEER in the literature (Ω cm^2 Koeneman *et al*. 2010 or Ω/ cm^2 Janer *et al*. 2014). Firstly, values of 3500 Ω cm^2 are considerably high for epithelial resistance readings in gut epithelial cells, considering the tightest epithelial cells (freshwater fish gill) in culture conditions have resistance readings of 1000–5000 Ω cm^2 (Wood *et al*. 1998); secondly, resistance is inversely proportional to the cross sectional area of the insert, i.e. the larger the insert the less resistance, so the resistance reading is multiplied by the area of the insert (usually in cm) to normalise the reading to Ω cm^2. If units are plotted as Ω / cm^2 when expressing TEER values they are implying a proportional relationship of resistance to insert size which is incorrect.

3.5.2 Accumulation and basolateral appearance of Ti from TiO_2 exposures in 21 day old Caco-2 cells

Similar to the previous study (Chapter 2) this study demonstrated a time dependent accumulation of total Ti metal in mature Caco-2 cells from exposures to TiO_2

particles (Fig. 3-6; 3-8) regardless of culture conditions (flat plates or use of cell culture inserts). Gradual reduction in cell Na^+ (against the concentration gradients) and the gradual depletion of K^+ in the opposite direction to the net Ti accumulation in conjunction with low medium LDH activity and healthy cell appearance suggest Ti accumulation is not due to passive diffusion through leaky cells or via solvent drag, rather, it is an active process.

The presence of Ti in the basolateral medium suggests transport of Ti or TiO_2 from TiO_2 particle exposures across the epithelial layer. The potential mechanisms of transport are 1) through the paracelluller route in between tight junctions; 2) by damaging cells thus creating a hole in the monolayer; 3) or through an epithelial cell (Koeneman *et al*. 2010). For paracellular transport through intact tight junctions individual particles would need a diameter smaller than 5 nm to diffuse in between the monolayer, furthermore, a high divalent ion concentration in the tight junction would likely result in increased particle aggregation and diffusion would be hindered by junctional proteins. TEER was unaffected by TiO_2 exposures suggesting tight junctions maintained their integrity. Characterisation of the materials (Chapter 2, Fig. 2-2) demonstrated < 0.5% of the particles were in the 5 nm size range. The results of this present study demonstrate more than 0.5% of the administered concentration was detected in the basolateral compartment. Penetration through a hole in the monolayer is also unlikely considering the cells were healthy and there were negligible changes in TEER (ion leak) and media LDH leak relative to control cells. Overall the data suggest paracellular transport and/or transport of particles through holes in the epithelial layer are unlikely thereby implying transport through intact epithelial cells as the most probable transport route. This conclusion is in line with previous conclusions of Koeneman *et al*. (2010).

The main purpose of this study was to assess the effect of TiO_2 crystal structure on uptake, accumulation, apical to basolateral transport, and epithelial integrity on fully differentiated Caco-2 cells and gauge whether this is comparable to partially differentiated Caco-2 cells. The form in which TiO_2 crosses the epithelial layer was not assessed. However, given the similarity of the results with the previous work on 4 - 5 day old Caco-2 cells (Chapter 2) one could tentatively assume the majority of Ti which accumulated (in the cells) and crossed the epithelium was in the form of intact particles. A number of researchers (Koeneman *et al*. 2010; Brun *et al*. 2014; Gitrowski *et al*. 2014, Chapter 2) have demonstrated intact particle accumulation in Caco-2 cells. Moreover, Brun *et al*. (2014) revealed, using X-ray absorbtion spectroscopy (XAS), Ti rich intracellular regions of the cell contained Ti still in the TiO_2 NP state and the crystalline phase and speciation remained identical to stocks, indicating no partial dissolution had occurred (Brun *et al*. 2014). In contrast, Schmidt and Vogelsberger (2009) demonstrated TiO_2 can undergo picomolar rates of dissolution at neutral pH in 100 mM NaCl solution. This level of Ti dissolution would be insufficient to support the accumulation and transport observed here, suggesting a large percentage of the detected Ti is in particulate form (TiO_2).

The overall apical to basal transport rates of Ti from exposures to different forms of TiO_2 appear not to have been previously reported for the individual forms of TiO_2 exposed to fully differentiated Caco-2 cells. These rates, between 0.02 (Rutile) and 0.11 (Bulk) nmol mg^{-1} protein h^{-1} are broadly similar to previous reports using mixtures of TiO_2 forms (Koeneman *et al*. (2010) reported 0.141 nmol $insert^{-1}$ h^{-1} mixture of anatase and rutile). Moreover, this is broadly similar to other metals known to have active transport mechanisms (Iron 0.036 nmol mg^{-1} protein h^{-1} Linder *et al*. (2006) ; Copper 0.003 nmol $insert^{-1}$ h^{-1} Arrendondo *et al*. 2000). It is important

to note values reported in this study are likely to be lower than actual transport rates. Spike recoveries demonstrated between 20% and 30% reduction in detectable Ti from different forms of TiO_2 spiked into culture medium (Fig .3-1).

3.5.3 Effect of particle size and crytal structure on accumulation and transport

The form of TiO_2 influenced the total Ti accumulation over 24 h with the bulk material showing the greatest accumulation and the nano rutile the least (Fig. 3-6; 3-8). This pattern has been demonstrated in 4 day old cells grown in plates (Chapter 2) and 21 day old cells grown in plates and inserts (Fig. 3-6; 3-8). Bulk uptake may be explained on a mass basis. For every particle of bulk taken up would inevitably contain more Ti metal then the NP. The reason for the greatly reduced uptake of rutile is unclear. This is not explained by poor availability of the particles in the stock dispersions (Chapter 2) or by the ability to detect the particles using ICP- OES in the cell homogenate or media (Fig. 3-1). It remains possible that the surface properties of rutile TiO_2 are the cause for reduced uptake; however, more research would be required to confirm this (See Chapter 2, section 2.5).

The appearance of Ti in the basolateral medium appeared to be influenced by particle size and form. Ti from P25 TiO_2 exposures was the first to be detected in the basolateral medium, followed by anatase and finally bulk. Ti from the rutile form was detected by 24 h but the amount was negligible in comparison to controls (Fig. 3-10). Interestingly the crystal composition of the bulk TiO_2 used in this trial contained the same percentages of anatase and rutile crystal types as the nano P25 (75% anatase, 25% rutile) (Al-Jubory and Handy 2012), suggesting a size effect on apical to basal transport. A simple reason for the disparity in Ti appearance between bulk and nano

P25 TiO_2 could be due to the porosity of the cell insert. The filter membrane itself represents a barrier for TiO_2 diffusion. Steric constraints due to narrow pores and available area for diffusion will affect different sized particles to a different extent. In this present study between 53 and 61% of the apically administered material was detected in the basolateral media at 24 h in the absence of cells (Table 3-2) Similarly Janer *et al*. (2014) demonstrated that only 44.5 ± 16% of a 100 mg L^{-1} NP (anatase NPs mean diameter of 18 nm) solution administered to the apical chamber of an insert perforated with 1 µm pores could migrate into the basolateral compartment in the absence of cells. It would be reasonable to assume that larger particles would migrate through the insert at a reduced rate and the data herein shows bulk particle apical administrations have the lowest recovery from the basolateral medium relative to the NPs (not statistically significant). Fortuitously, filter inserts taken from the bulk trial appeared to have the highest Ti concentration from 6 h (just below the detection limit) compared to the other TiO_2 forms. Moreover, Ti from bulk TiO_2 exposures was only detectable in the basolateral media by 24 h suggesting a slower rate of migration through the inserts.

3.5.4 Cell maturity and the effect of culture matrix on accumulation

Previous work on 4 day Caco-2 cells demonstrated higher rates of accumulation in comparison to the present study (Chapter 2, Fig. 2-6). A possible reason for reduced uptake may be due to apical membranes with dense microvilli having a reduced ability to undergo the invagination process preceding large endocytic events (Hansen *et al*. 2009). The actin core bundles innervating the MV are anchored bellow the apical membrane and hinder the invagination process. Nevertheless,

endocytic processes can continue unabated in areas between neighbouring microvilli and in areas where limited brush border differentiation has taken place.

Interestingly, there appears to be an effect of culture matrix on total Ti accumulation (Fig. 3-6; 3-8). Cells cultured in plates demonstrated lower accumulation of Ti from TiO_2 exposures in comparison to cells cultured in inserts. The reasons for this are unclear and would merit further investigation. Interestingly the effect of crystal structure on the pattern accumulation remained the same (rutile was taken up the least) independent of cell maturation status and culture matrix.

3.5.5 Ionic regulation

Similar to the previous study (Chapter 2) TiO_2 exposure caused increases in total cellular Ca^{2+} and decreases in K^+ over the 24 h exposure period. This occurred irrespective of growth substrate and material. The reasons for this are unclear although potential mechanisms are reviewed in Chapter 1, section 1.3.8. The similarity of electrolyte changes over time when comparing mature cells (21 day old) with 4 day old cells (Chapter 2) suggests cell ion regulatory functions are set early in the maturation of cells, supporting the notion that immature cells are a useful proxy for metal accumulation studies without the need to wait for cells to mature fully.

3.5.6 Conclusion

This study shows that fully differentiated Caco-2 cells accumulate Ti from TiO_2 exposures in a manner indicative of active uptake which is similar to 4 day old cells. Cells cultured on inserts demonstrated accumulation and transport of Ti and/or TiO_2

from TiO_2 exposures. Critically, there is a crystal structure effect with the anatase form being absorbed and transported faster than the rutile form in mature cells cultured on inserts. Similarly, this pattern of accumulation was observed in mature and immature cells cultured on flat bottom plates. Short term exposure of TiO_2 appears to disturb some aspects of electrolyte status in Caco-2 cells, without affecting membrane integrity (LDH and TEER) and apical morphology, similar to 4 day old cells (Chapter 2).

Calculated human daily exposures to TiO_2 NPs have been shown to be in the region of 1.8 – 4.5 ng cm^2 of intestine (Brun *et al*. 2014). This study exposed 1 cm^2 of Caco-2 cells to 0.55 µg TiO_2 particles which is 125 fold higher than calculated expected exposure scenarios. This exposure could be considered as a worst case acute exposure scenario. Modelling chronic exposure scenarios to different forms of TiO_2 NPs which reflect dietary concentrations needs to be completed in order to inform dietary exposure assessments for human health. Moreover, standardization of the filter materials, experimental procedures and analytical techniques in combination with documenting cell line development (age and differentiation) in NP accumulation and transport studies would improve the comparability of results between laboratories and allow for a better understanding of NP cell interactions.

Chapter 4: Uptake of titanium from TiO_2 nanoparticle exposure in the isolated perfused intestine of female Wistar rats (*Rattus norvegicus*)

4.1 Abstract

In vivo studies have raised concerns that titanium dioxide nanoparticles (TiO_2 NPs) may be taken up across the gut of mammals, but there is limited information on the uptake mechanism(s) and kinetics of NPs across the gastrointestinal tract. Whole gut sacs and the isolated perfused intestine of rat (*Rattus Norvegicus*) were used to determine the parts of the gut involved in absorption, and the intestinal uptake rates of Ti from both bulk and nano TiO_2 exposures across rat gut. Pharmacological inhibitors were used to explore mechanisms of Ti uptake from TiO_2 exposures. Luminal exposure of whole gut sacs to 1 mg L^{-1} TiO_2 NP for 4 h caused accumulation of Ti in the small and large intestine, with 70% or more of the Ti in the mucosa, rather than underlying muscularis. Perfused intestines exposed to 1 mg L^{-1} nano TiO_2 or the equivalent bulk powder in the mucosal solution for 4 h showed a time-dependent accumulation of Ti in the serosal perfusate with a mean initial flux rates into the serosa (mean ± S.E.M n = 5) of 4.402 ± 0.461, 25.08 ± 2.545, and 2.814 ± 0.929 nmol g^{-1} h^{-1} for TiO_2 bulk, nano, and controls (no-added TiO_2), respectively. This demonstrates that Ti from TiO_2 exposures can cross the gut and enter the serosal solution with the nano form being faster than bulk. The addition of 100 µmol L^{-1} sodium orthovanadate, (P-type ATPase inhibitor) or 120 U mL^{-1} nystatin (putative endocytosis inhibitor) to the serosal solution increased mean Ti tissue concentrations for both bulk and nano TiO_2 exposures compared to the no drug exposures (e.g., from 0.265 ± 0.044 to 0.673 ± 0.133 and 0.447 ± 0.081 µmol g^{-1} dry weight for bulk TiO_2 exposures in the no drug, nystatin and vanadate treatments, respectively. Similarly for nano TiO_2 exposures tissue Ti concentrations were 0.293 ± 0.048 to 0.403 ± 0.062 and 0.388 ± 0.064 µmol g^{-1} dry weight for no drug, nystatin and vanadate treatments, respectively) and reduced Ti serosal flux for the nano exposures. Overall, the data suggests an active absorption mechanism is responsible for Ti uptake from both bulk and nano TiO_2 exposures across the perfused rat intestine that is drug sensitive.

4.2 Introduction

The mechanism(s) of NP uptake across the intestinal epithelium of mammals remains poorly understood (Handy *et al*. 2008; Shaw and Handy 2011). Handy (2008) argued that apical uptake of intact NPs in fish is unlikely to occur through ion transport pathways or paracellular diffusion (tight junctions) because NPs are too large. Transport through vesicular mediated processes seems more likely, with analogous arguments having been made for mammalian gut exposed to carbon NPs (Panessa-Warren *et al*. 2006), which is unsurprising considering the functional and structural similarities of intestinal epithelium within vertebrates. NPs have been shown to cross cell membranes in Caco-2 cells following apical exposures of 1 mg L^{-1} (Koeneman *et al* 2010) and traverse entire cells (apical to basal) without disrupting junctional complexes (Koeneman *et al*. 2010; Chapter 3). Furthermore work by Gitrowski *et al*. (2014) (Chapter 2) and Brun *et al*. (2014) have shown intact TiO_2 particles occupying vesicles within Caco-2 intestinal cells, suggesting that, at least at the apical membrane, the majority of TiO_2 NPs are taken up in particulate form.

The translocation of Ti or TiO_2 from TiO_2 NP exposures to systemic body sites has been demonstrated in a number of species. (e.g. mice – Wang *et al*. 2007; rats - Tassinari *et al*. 2014; trout - Ramsden *et al*. 2009). For example, Wang *et al*. (2007) demonstrated an increase in organ Ti concentration (liver, spleen, kidney, lungs and brain) 2 weeks after a single oral exposure of 5 g kg^{-1} bw. Ramsden *et al*. (2009) demonstrated an increase in spleen Ti concentration in trout following 8 week exposures of diets containing 10 – 100 mg kg^{-1} of TiO_2. Data on the rates of Ti translocation *in vivo* or *ex vivo* are sparse, nevertheless, mucosal to serosal transport rates of Ti or TiO_2 from TiO_2 NP exposures of 1 mg L^{-1} in perfused trout

intestines have been shown to be in the order of 2 nmol g^{-1} (dry weight) h^{-1} (Al-Jubory and Handy 2012) whilst rates for bulk particles were 0.85 nmol g^{-1} h^{-1}. *In vitro* Caco-2 intestinal cell transport rates (apical to basolateral) have been shown to be between 0.11 and 0.02 nmol mg^{-1} (cell protein) h^{-1} (Chapter 3), depending on TiO_2 crystal structure or 0.141 nmol $insert^{-1}$ h^{-1} (Koeneman *et al*. 2010) for a mixture of TiO_2 NP crystal types. The overall translocation rates of Ti or TiO_2 from TiO_2 exposures in Caco-2 cells are considerably greater than demonstrated translocation rates for the perfused trout intestine (for the same exposure dose), suggesting that cell lines may not accurately reflect the situation *in vivo*. There are a number of limitations that need to be considered when extrapolating uptake and transport data from immortalized cell lines to *in vivo* or *ex vivo*. For instance, Caco-2 cells only represent a monolayer of mucous-free enterocyte-like cells and are likely to express characteristics of carcinoma cells rather than normal gut enterocytes. Further, the *in vivo - ex vivo* situation is quite different. There are four layers of intestinal tissue (mucosa, submucosa, muscularis and serosa) and a thick layer of anionic mucus protecting the absorptive surface. Furthermore, luminal pH and digesta matrix varies considerably with anatomical location, and at the absorptive interface there are a number of different cells types (e.g. goblet cells, enterocytes, paneth cells and M cells). With this in mind, it remains uncertain whether the processes mediating particle uptake are the same in cell lines as they are *in vivo* or *ex vivo*.

The aim of this study was to determine which part of the mammalian gut is most likely involved in uptake and accumulation of TiO_2 NPs by using isolated whole gut sacs from rats. Having determined which areas are likely associated with particle uptake, precise measurements of total Ti uptake rates (mucosa - serosa) using the perfused intestine preparation were performed and the results interpreted in the

context of particle behaviour in the gut lumen. These *ex vivo* preparations allow manipulations of the mucosal or serosal solutions to measure concentration-dependent uptake rates, or can be used to investigate uptake mechanisms through the addition of pharmacological inhibitors. Mechanism(s) of uptake were explored with pharmacological agents and involved using nystatin (a putative inhibitor of lipid raft caveolae endocytosis) and sodium orthovanadate, which is a P-type ATPase inhibitor, which non-specifically blocks the ATPase family of ion pumps including the Na^+- K^+ ATPase. In order to accurately interpret whether apparent uptake had any surface-bound components of Ti, some rapid solution dipping experiments were performed with a view to measuring the instantaneous adsorption of TiO_2 to the intestine. *Ex vivo* preparations of trout intestine have been successfully used to explore TiO_2 NP uptake (Al-Jubory and Handy 2012) at 15°C but, it is uncertain whether the preparation would be successful with more delicate rodent gut performed at 37°C.

4.3 Materials and methods

4.3.1 Stock animals

Adult Wistar female rats (*Rattus norvegicus albinus*) weighing 185 ± 5 g (mean ± S.E.M., *n* = 42) were purchased from Harlan Laboratories and placed in suitable cages (no more than 6 animals per cage), maintained at a constant temperature (18-23°C), appropriate humidity (40 – 50%) and photoperiod (12 h light: 12 h dark). Rats were fed a standard formulation (2018 Teklad 18% protein rodent diet, Harlan Laboratories) comprised of 18, 5 and 5% of protein, fat and fibre, respectively. Animals had access to drinking water *ad libitum*. ICP-OES analysis for total metal

concentrations in the feed revealed a total Ti concentration of 3.28 ± 0.61 mg g^{-1} dry feed (mean ± S.E.M., *n = 5*). Prior to beginning the experiments, all rats were starved for 48 h to let the gut empty of residual food, to facilitate eversion of the gut and to minimise incidental binding of titanium from undigested food on the gut epithelium.

4.3.2 Preparation of gut sacs

Whole gut sacs were used to determine which parts of the gastrointestinal tract are mainly involved in Ti absorption from TiO_2 exposures and prepared according to Hoyle and Handy (2005) derived from the original method of Handy *et al*. (2000). This physiological technique involves removing the whole gut from the animal, filling the lumen with the test substance of interest, and then suturing closed the different anatomical parts of the gut so that regional uptake into the tissue can be measured over a few hours. Rats were humanely sacrificed by cervical dislocation (in compliance with ethical approval in the UK). The weight of the rat was measured; then the entire gastrointestinal tract was carefully removed, washed and flushed through with the physiological saline which contained (in mmol L^{-1}): NaCl, 117.5; KCl, 5.7; $NaHCO_3$, 25.0; $NaH_2PO_4.2H_2O$, 1.2; $CaCl_2.2H_2O$, 5.0; $MgSO_4$, 1.0; glucose, 5.0; mannitol, 23.0; osmolarity 320 mOsm (Osmomat 030, Gonotec) adjusted to pH 7.4 with a few drops of 10 mol L^{-1} HCl. The length of the rat gut required a slight modification of the Handy and Hoyle (2005) technique due to anatomical differences. In brief, the gut was cut where the stomach meets the duodenum and where the ileum meets the caecum. Physiological saline was flushed through each gut section followed by ligating the posterior end of the tissue sections prior to filling the lumen with physiological saline with a concentration of 1 mg L^{-1} TiO_2 (Bulk, NP, or no

added TiO_2 control as appropriate). The remaining parts of the gut were ligated with surgical silk around the upper end of the oesophagus, duodenum and caecum and further sutures applied to separate each region of the gut (oesophagus, stomach, duodenum, jejunum, ileum, caecum and large intestine). The gut was then placed in a bath containing 700 ml of the same physiological saline (no added TiO_2). The bath (serosal side) was continuously stirred and gassed with 95% O_2: 5% CO_2 at 37°C for 4 h. The 4 h duration time for this experiment was chosen following previous metal perfusion studies which indicated saturable uptake within 4 h (e.g. Cu in catfish gut, Handy *et al*. 2000; Hg in trout gut, Hoyle and Handy 2005; TiO_2 in trout gut, Al-Jubory and Handy 2012). After each experiment the gut was carefully opened and washed with deionised water to remove excess TiO_2, then divided into sections of intact oesophagus, stomach, duodenum, jejunum, ileum, caecum and large intestine for metal analysis and histology (see below). In some experiments, each part of the gut was further divided longitudinally into two equal parts; one part was stripped of the mucosa, while the other part was left whole, to enable calculation of the relative proportion of Ti in the mucosa and underlying muscularis (Hoyle and Handy 2005).

4.3.3 Surface binding experiment

To aid data interpretation on Ti accumulation in the mucosa, some rapid solution dipping experiments were done to quantify surface binding of Ti. The approach followed a well-established method for tissue (Handy and Eddy 2004) and is well known for metal salts (Shaw and Handy 2011) and has previously been reported for TiO_2 NPs in trout intestine (Al-Jubory and Handy 2013). The technique involves allowing the tissue to instantaneously adsorb metal onto the surface of the

epithelium over a few seconds (i.e., before true uptake can occur) and then determine the metal concentration on the tissue. Measurements were made on jejunum segments. Briefly, rats were sacrificed and the intestinal tract was quickly removed, everted, and then rinsed in clean saline (as above). Pieces of everted jejunum were then dipped (mucosa facing the solution) in 500 ml of fresh physiological saline for 15 s (control dip to equilibrate the surface of the tissue with the saline), then dipped in to 1 mg $L^{-1}$of TiO_2 bulk or NPs in 500 ml physiological saline for 30 s. Finally, tissues were rinsed of excess TiO_2 by dipping in two consecutive 500 ml beakers of clean physiological saline (total of 15 srinsing). Tissues were then digested in nitric acid and analysed for total Ti metal content (see below).

4.3.4 Preparation of the isolated perfused intestine

The isolated perfused intestine technique has been used in mammalian physiology for many years to study the uptake of ions and water (e.g., Rao 2009; Wapnir 1991), and has also been used for measuring the uptake of toxic metals like copper and mercury (e.g., Handy *et al*. 2000) and more recently TiO_2 uptake in trout (Al-Jubory and Handy 2012). The approach involves removing the intestine from the animal, carefully turning it inside out (everted) so that mucosal epithelium is on the “outside” and can be directly bathed in the external media (usually in a static, stirred bath of a gut saline). This enables the experimenter to change the composition of the bath (i.e., the mucosal or luminal-side solution) so that uptake mechanisms can be investigated (e.g., by adding different concentrations of the test substance to the bath, or by adding inhibitors). Uptake of substances by the preparation is generally recorded in

two ways: (i) measurement of the test substance in the gut tissue at the end of the experiment, (ii) measurement of the appearance of test substance on the blood side of the preparation (i.e., transepithelial uptake to the serosal perfusate). The perfusate usually flows constantly in the preparation (via a peristaltic pump) to prevent the system from coming into a diffusional steady-state so that true uptake rates can be measured. In this study the isolated perfused intestine was prepared according to Handy *et al*. (2000). The rats were sacrificed (as above) and the entire intestinal tract (from oesophagus to the rectum) was quickly removed. The length of the small intestine (duodenum to ileum) was measured and divided into three equal segments. A 10 cm segment was cut from the jejunum portion of the small intestine (anatomically it is difficult to distinguish the jejunum section from the rest of the small intestine externally, however, its position can be noted prior to excision of the gastrointestinal tract). The jejunum segment was then everted, connected to the perfusion apparatus, and bathed in 700 mL of the physiological saline (described above), at 37°C, gassed with 95% O_2: 5% CO_2 (a standard gas mixture used for gut perfusion work). The intestine was serosally perfused (1 mL min^{-1} via an Ismatec peristaltic pump) using the gut saline described above 4 h. Perfusions were conducted in parallel to eliminate time-dependent artefacts with a control (no added TiO_2 and two treatments (e.g., + TiO_2 NPs or bulk powder) performed each day. The eluted serosal perfusate was collected manually in 10 min fractions, and the volume determined gravimetrically. Five ml of the mucosal solution (bath samples) were collected every 30 min for Ti, Na^+ and K^+ analysis (see below), and to monitor pH. At the end of each experiment the guts were carefully washed in deionised water to remove excess TiO_2 and residual electrolytes from the saline. Samples of each gut were also taken for histopathology and electron microscopy. In separate experiments,

the effects of adding 100 µmol l^{-1} sodium orthovanadate (a P-type ATPase inhibitor; Kuhlbrandt 2004) to the serosal perfusate was tested in order to discover whether Ti uptake had an energy - dependent component or additions of 120 IU ml^{-1} nystatin (a putative endocytosis inhibitor) to the mucosal solution to explore if cholesterol is involved in uptake processes.

4.3.5 Lactate dehydrogenase (LDH) assay

The routine viability criteria for the perfused intestine preparation are the presence of steady perfusate flow, net efflux of water across the gut, and negligible LDH leak from the tissue (Handy *et al*. 2000). LDH activity was determined by the same method described in Chapter 3, Section 3.3.7. Typically, in perfused organ preparations, the maximum LDH activity in the medium from a normal healthy tissue would not exceed 1 U ml^{-1} (1 µmol min^{-1} ml^{-1}) with the data for all samples below this value (see Results).

4.3.6 Trace metal analysis

The methodology for trace metal analysis in tissues was based on the original nitric acid digestion method of Handy *et al*. (2000) for fish intestine, but with some novel modifications that enable detection of Ti from intact TiO_2 NPs dispersed in the tissue digest without the need for hydrofluoric acid or hot sulphuric acid digestion (see Lomer *et al*. (2000) for the traditional H_2SO_4 method for foods). The modification presented here involved adding Triton X-100 to dilute the nitric acid digest, and with mixing/shaking it was possible to get good nebulisation of the sample in the spray

chamber of the ICP-OES to detect both the total Ti metal concentration from the NP exposure and other dissolved trace metals in the sample (Shaw *et al*. 2013). Briefly, tissues from all experiments were oven dried to a constant weight at 100°C for up 48 h (Gallenkamp Oven BS Model OV-160), then the samples were transferred into 20 mL scintillation vials (VWR International Ltd, Poole, UK) and digested in 1 or 4 mL (depending on tissue weight) of concentrated nitric acid for 3 h at 70°C in a water bath. The digested samples were allowed to cool, and then Triton X-100 was slowly added to each digest with Milli-Q water (ultra-pure ion free water) to achieve a final concentration of 2% Triton X-100 in each sample. Typically this involved adding 3.2 or 0.8 mL of 10% Triton X-100 and diluting to a final volume of 16 or 4 mL (for tissue weights of 1 g or 0.1 g, respectively). Digests were then analysed for total Ti metal, Na^+, K^+, Ca^{2+} and Mg^{2+} concentrations by ICP-OES. Critically, samples were sonicated (Bransonic 60 Hz) for 2 h prior to being vortexed (10 s) and immediately introduced to the instrument (IKA MS2 Minishaker; set at 2500 r min^{-1}). The instrument detection limit (3 x standard deviation of the blank + the mean of the blank (*n* = 6) (Thomsen *et al*. 2003)) for measuring the gut salines or matrix matched standards was calculated as 1.7 µg L^{-1}, equivalent to 35 nmol L^{-1} of Ti metal, and for the entire digestion protocol 1.9 µg L^{-1}, equivalent to 40 nmols L^{-1} of Ti metal (for a typical 0.5 g tissue sample this equates to 0.001 µmol Ti metal g^{-1} dry weight of tissue). The optimised protocol gave good spike recovery for rat tissue (e.g., mean ± SEM, n = 6; 97.5 ± 2.9% for spiking with Ti metal, and 90.2 ± 1.4% for spiking with TiO_2 NPs) and low coefficients of variation within and between tissue samples from different rats (around 5% or less for repeats of the entire protocol). Spike recovery of mucosal bath (physiological saline) solutions was (mean ± S.E.M, n = 5); 89 ± 4% 78 ± 1.5% for spiking with Ti metal and nano TiO_2, respectively. Calibrations with

different concentration of Triton-X100 in standards had a negligible effect (no problems with instrument calibration with metals standards or TiO_2 dispersions (Shaw *et al*. 2013)). Tissue Ti levels are reported as µmol of Ti metal g^{-1} dry weight. The bath solution was measured for Ti to confirm the TiO_2 exposure and for convenience the data are reported as mg L^{-1} of TiO_2 (for the bath solution only) after correcting the Ti metal data using the stoichiometry of the compound (Ti content of TiO_2 as 60% of the mass). All other data are reported as total Ti metal concentrations (in the tissues and eluted perfusates).

4.3.7 TiO_2 bulk and NP stock solutions

A 0.5 g L^{-1} dispersion of bulk TiO_2 was prepared from 0.5 g of TiO_2 powder (ACROS, Titanium (IV) oxide, New Jersey, USA; manufacturer's information: purity of 98.0-100.5% TiO_2). The manufacturer's technical support indicated a crystal structure mixture of anatase (75%) and rutile (25%) (Al-Jubory and Handy 2012). The powder was dispersed and stirred (Stuart magnetic stirrer, set at half speed) in 1 litre of ultrapure (ion free) Millipore water for 20 min. The particle size was determined by two independent methods. First, sub samples of the 0.5 g L^{-1} stock dispersion were examined for primary particle size using transmission electron microscopy (TEM, JEOL-1200EX II) and examples of the particles are shown in (Fig. 4-1 A) with a primary particle size measurement of 115.4 ± 13 nm (mean ± S.E.M., n = 6) for bulk TiO_2. The second approach was for particle size distribution using NP tracking analysis (NTA, Nanosight LM 10, Nanosight, Salisbury, UK, laser output set at 30 mW at 640 nm). In order to measure particle size distribution by NTA the initial stock dispersion (0.5 g L^{-1}) was diluted to 1 mg l^{-1} in the physiological saline used for gut

perfusions (see below) to account for matrix effects on aggregation (1 ml of the initial stock made up to 500 ml of saline, stirred as above), and the resulting dispersion gave mean values of 213 ± 23 nm for the average particle size with 10% of the particles being smaller than 148 ± 7.17 nm (bin size, mean ± S.E.M., n = 3) for bulk TiO_2 (Fig. 4-1 C).

The TiO_2 NPs used here was the same as that used by Federici *et al*. (2007) and Al-Jubory and Handy (2012). The powder form of ultrafine titanium dioxide NP type "Aeroxide" P25 (DeGussa AG, supplied by Lawrence Industries, Tamworth, UK) with (revised manufacturer's information): a crystal structure of 25% rutile and 75% anatase TiO_2, purity was at least 99% TiO_2 (maximum impurity stated was 1% Si), the average particle size was 21 nm with a specific surface area of 50 ± 15 m^2 g^{-1}. Chemical analysis of stock dispersions revealed no metal impurities (data not shown), and the batch purity was high.

A stock dispersion containing 0.5 g L^{-1} was made as above. Transmission electron microscopy showed the structure and the primary particle size of P25 NPs to be 22.8 ± 6 nm (mean ± S.E.M., n = 6), while the mean aggregate size of the NPs was 148.8 ± 18 nm (mean ± S.E.M., n = 6; Fig. 4-1 B). The dosing of the bath was the same as that reported for the bulk material (above), and the distribution of the 1 mg L^{-1} TiO_2 NPs in the physiological saline prior to the start of experiments was also confirmed by NTA. The mean values for particles (primary and aggregates) were 146 ± 15 nm with 10% of the particles being smaller than 58 ± 6 nm (mean ± S.E.M., n = 3; Figure 1 D). Prior to administering TiO_2 to the mucosal bath saline (and saline for Nanosight analysis) both stocks were dispersed with sonication in a bath-type sonicator (500 ml of stock, 35 kHz frequency, Fisher brand FB 11010, Germany) overnight.

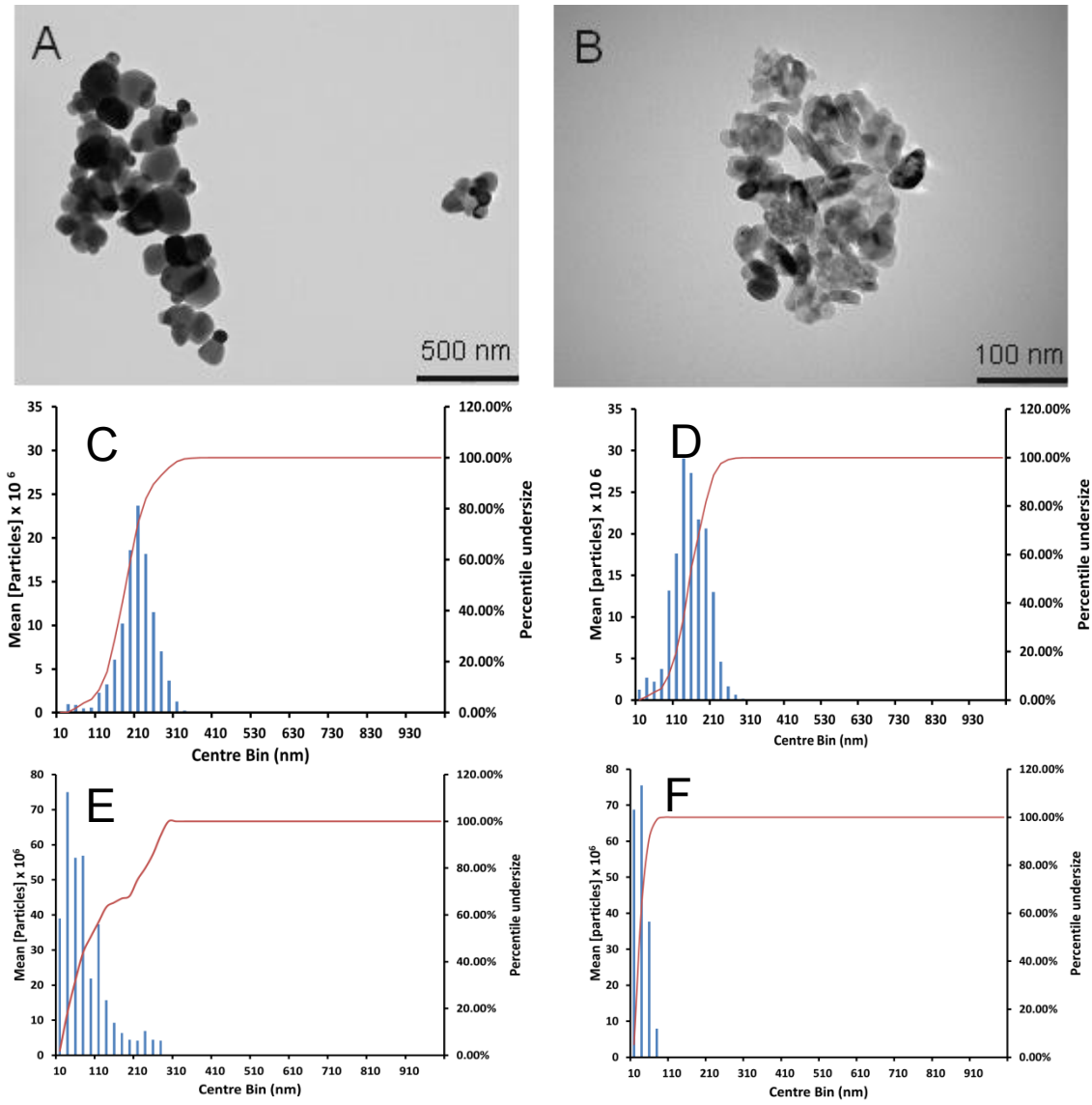

Fig. 4-1: Electron micrographs showing (A) bulk and (B) nano TiO_2 particles in a 0.5 g L^{-1} stock dispersion. Particle size distributions measured by nanoparticle tracking analysis (NTA) are shown below; (C) bulk TiO_2 and (D) TiO_2 NPs in a 1 mg L^{-1} stock dispersion in physiological saline (without the gut present); (E) bulk TiO_2; and (F) and nano in the mucosal solution following a 4 h perfusion graphs are individual examples from triplicate measurements of each.

4.3.8 Histology and transmission electron microscopy

After each perfusion, a piece of tissue from the middle of each preparation was carefully collected for light microscopy. Briefly, tissues were rinsed and fixed in 10% buffered formal saline for at least 48 h, dehydrated in graded series of ethanol, and cleared in xylene prior to embedding in paraffin blocks. Seven micrometre sections were stained with haematoxylin and eosin. Slides were examined using light microscopy (Olympus Vanox - TAH2) and photographs were taken using a digital camera (Olympus camedia C-2020 Z). For scanning electron microscopy (SEM), briefly, tissue was washed in physiological saline (above) and fixed in 2.5% glutaldehyde in cacodylate buffer (0.1 M sodium cacodylate, pH of 7.2, for 2 h). Tissues were then washed twice in cacodylate buffer prior to being dehydrated in a graded series of ethanol. Tissues were critically point dried and carbon coated (EMITECH-K850, K450X). Samples were imaged and elementally analysed (SEM, JEOL/JSM-7001F, Oxford Instruments INCA X-ray analysis system) using a 15 KV accelerating voltage, at a working distance of 10 mm. For the transmission electron microscope investigations, small fragments from the centre of the jejunum were fixed in glutaraldehyde (2.5%), buffered in 0.1 M sodium cacodylate, pH 7.2, and post-fixed in osmium tetra oxide 2% (OsO_4). The pieces were then dehydrated in a graded series of ethanol and infiltrated with a graded series of Spur's resin. Embedding as a small capsule was performed using pure resin. Thin sections were cut (70 - 90 nm) and stained with 2% uranylacetate and lead citrate, then examined by transmission electron microscope (TEM, JEOL-1200EXII).

4.3.9 Calculations and terminology

All calculations on uptake rates were performed according to Handy *et al*. (2000). Briefly, data were graphically presented as the cumulative appearance of Ti metal in the perfusate, plotted against exposure time for example perfusions; and with cumulative perfusate flow shown on the same graph. The absolute Ti content of each 10 min fraction (µg) was calculated by multiplying the total Ti metal concentration in each tube (µg mL^{-1}) by the total volume of perfusate/tube (mL). Ti contents of each fraction were summed for the cumulative plots (reported as nmol absolute Ti metal). The initial (first 10 min) and overall (240 min) net Ti flux rates (J_{net},Ti, in nmol g^{-1} dry tissue h^{-1}) to the serosal perfusate were calculated from the perfusate Ti content (in nmol) divided by the tissue dry mass and corrected to 1 h, while the initial (first 10 min) and overall (240 min) net water flux rates (J_{net}, H_2O, in mL g^{-1} dry tissue h^{-1}) to the eluted perfusate were calculated from the differences between the rates of cumulative perfusate and effluent flow divided by the tissue dry mass and corrected to 1 h. The moisture content of tissues was determined by taking the weight of the tissue before and after oven drying and calculated as:((wet weight - dry weight)/wet weight) x 100. In the present study, we therefore use precise terminology for the absolute amounts of Ti metal in the perfusates (nmols, not a concentration), the concentration of total Ti metal in the tissue (µmol g^{-1} dry weight of Ti metal, not TiO_2 compound), and distinguish this from the mg L^{-1} of TiO_2 compound added to the bath when confirming the exposure. The phrase “total Ti metal concentrations” is used to mean the total mass concentration of Ti (not TiO_2 compound) in the tissue or relevant salines determined by ICP-OES; it does not imply anything about whether the Ti is present as particulate TiO_2 or as a dissolved Ti species. The term “Ti accumulation" is used to mean a net increase in the total Ti

metal concentration in the tissue over time, determined by ICP-OES of the tissue digests. The phrase “Ti uptake” is used specifically to mean the net uptake of total Ti metal to the serosal compartment in relation to the flux calculations above.

4.3.10 Statistical analysis

All data were presented as mean ± S.E.M and analysed using Stat Graphics Centurion XVI Plus while figures were drawn using Excel (2010). The data (treatment or time effects) were tested after checking for kurtosis, skewedness, and unequal variance (Bartlett’s test). Parametric data were tested by one-way ANOVA or general linear model (for time/treatment interactions) followed by the Tukey’s HSD multiple range test. Non-parametric data that could not be transformed were tested using the Kruskal-Wallis test (analysis by ranks) and differences were located using notched box and whisker plots. The Student’s t-test was used as well to investigate the differences between pairs of data, or the Mann-Whitney U test where appropriate for non-parametric data. All statistical analysis used a 95% confidence limit, so that *p* values equal to or greater than 0.05 were not considered statistically significant.

4.4 Results

4.4.1 Ti accumulation in whole gut sacs

The whole gut sac preparation was used to determine which regions of the gut were accumulating Ti from TiO_2 exposures (Fig. 4-2). All regions of the intact gut except the oesophagus, stomach and caecum showed statistically significant elevations of total Ti metal concentrations in the tissues from exposure to bulk or nano TiO_2 compared to the unexposed controls, with the greatest increases in the small intestine (duodenum, jejunum and ileum) and the large intestine. There were no statistically significant differences between the regions of the gut that accumulated TiO_2 (ANOVA, $P < 0.05$) nor were there any material-type effects (comparison of bulk versus nano treatment, Kruskal-Wallis, $P > 0.05$) on the tissue total Ti concentration. Comparisons of the proportions of total Ti metal concentrations in the mucosa relative to the intact gut confirmed that most (65% or more) of the background Ti in the small intestine of control animals was in the mucosa. Similar observations were made for the guts exposed to both bulk and nano TiO_2 (Table 4-1). The percentage of Ti retained in the mucosa for bulk exposures was 77, 77, 67 and 59% for the duodenum, jejunum, ileum and large intestine, respectively. For nano TiO_2 exposure, the percentage of Ti retained in the mucosa was 69, 82, 72, and 79% for the duodenum, jejunum, ileum and large intestine, respectively.

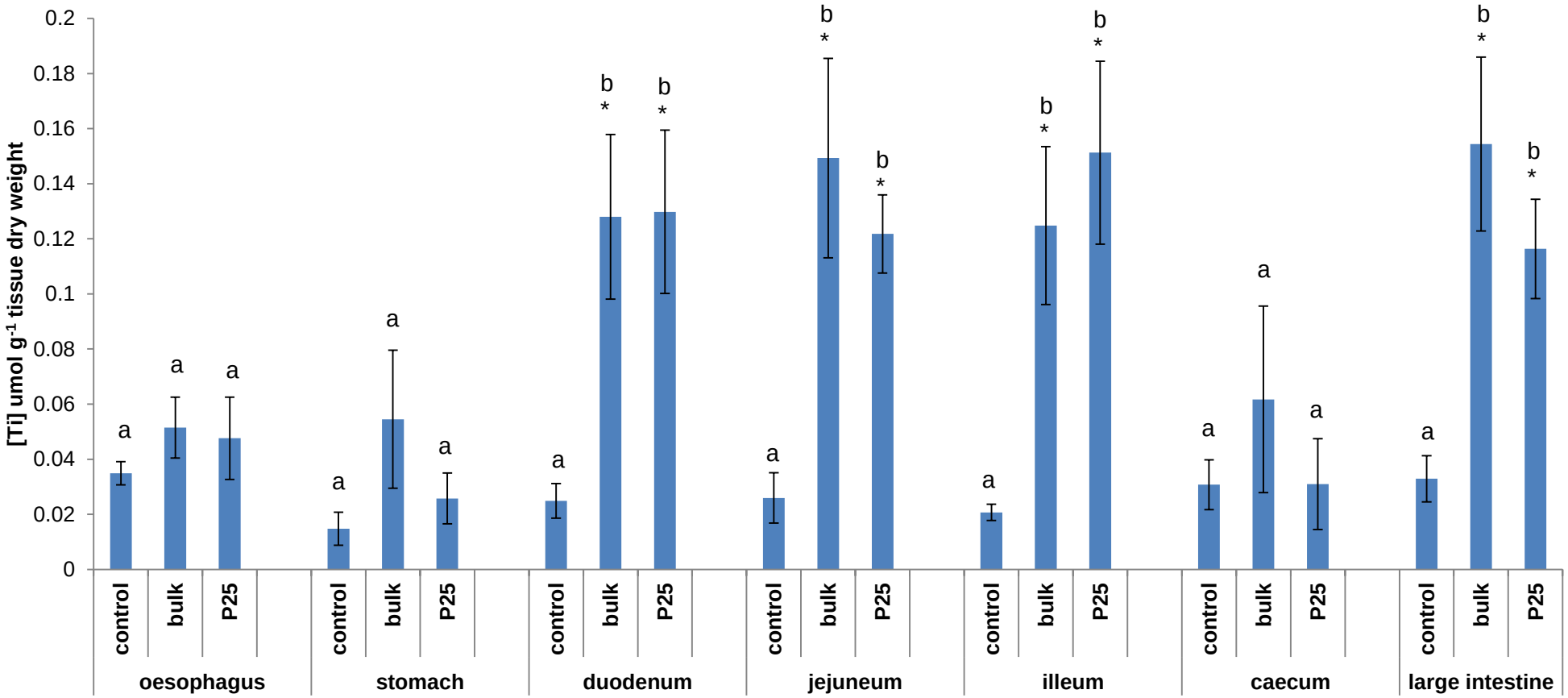

Fig. 4-2: Total Ti metal concentrations µmol g^{-1} tissue dry weight following exposure of isolated whole gut sacs to 1 mg L^{-1} TiO_2 in the gut lumen for 4 h (Values are means ± S.E.M. (n = 5 for each group)). *Statistically significant difference from the control (Kruskal-Wallis or ANOVA $P < 0.05$). Different letters within treatments indicate a statistically significant difference between regions of the gut (Kruskal-Wallis or ANOVA $P < 0.05$).

Table 4-1: Absolute Ti metal concentrations in intact gut and corresponding mucosa following exposure of isolated whole gut sacs to1 mg l^{-1} TiO_2 in the gut lumen for 4 h.

		Absolute [Ti] (μg) in tissue section and corresponding mucosal scraping			
Treatments		**Duodenum**	**Jejunum**	**Ileum**	**Large intestine**
Control	Intact gut	0.055 ± 0.019	0.050 ± 0.015	0.043 ± 0.010	0.075 ± 0.023
	Mucosa	0.028 ± 0.008	0.032 ± 0.013	0.021 ± 0.002	0.029 ± 0.009
	% in mucosa	65.7 ± 16.2	77.9 ± 17.2	61.2 ± 13.3	46.9 ± 14.4
Bulk TiO_2	Intact gut	$0.266 \pm 0.061^*$	$0.261 \pm 0.061^*$	$0.263 \pm 0.047^*$	$0.401 \pm 0.177^*$
	Mucosa	$0.190 \pm 0.032^*$	$0.187 \pm 0.038^*$	$0.176 \pm 0.058^*$	$0.190 \pm 0.055^*$
	% in Mucosa	77.5 ± 6.3	77.5 ± 7.3	67.2 ± 13.6	59.6 ± 8.2
Nano TiO_2	Intact gut	$0.338 \pm 0.077^*$	$0.249 \pm 0.046^*$	$0.215 \pm 0.034^*$	$0.240 \pm 0.014^*$
	Mucosa	$0.235 \pm 0.051^*$	$0.191 \pm 0.020^*$	$0.157 \pm 0.027^*$	$0.190 \pm 0.018^*$
	% in Mucosa	69.3 ± 2.4	82.0 ± 7.5	72.8 ± 5.6	79.1 ± 5.1

Values are means ± S.E.M. (n = 5 for each group) expressed as absolute Ti content in μg^{-1} except Ti % in mucosa. Whole gut sacs were filled with physiological saline (control), 1 mg l^{-1} bulk TiO_2 and 1 mg l^{-1} TiO_2 NP at 37°C for 4 h.% Ti in mucosa is calculated for each region of the gut, % Ti in mucosa = [Absolute [Ti] in mucosa / Absolute [Ti] in corresponding intact gut section] x 100. * Statistically significant difference from the control value within columns (Kruskal-Wallis or ANOVA, $P < 0.05$).There were no gut region effects on [Ti] content. There were no material- type effects (bulk versus nano) within each region of the gut. Data was not normalised to dry weight because the moisture content of the mucous skewed the normalisation.

4.4.2 Histology of the whole gut sac

Morphological examination of different gut sections (stomach, jejunum and large intestine) following a 4 h incubation with 1 mg L^{-1} bulk or nano TiO_2 in physiological saline demonstrated that the preparation was well tolerated. The gut sections exhibited normal morphology (Fig. 4-3) with no obvious pathologies in the tissues. The tissues exposed to bulk and nano TiO_2 appeared to show aggregates of 'particles' in contact with the mucosa, the morphology of the aggregates and the lack of similar aggregates in the control treatments tentatively suggest that these may be TiO_2 (Fig.4-3 D-I).

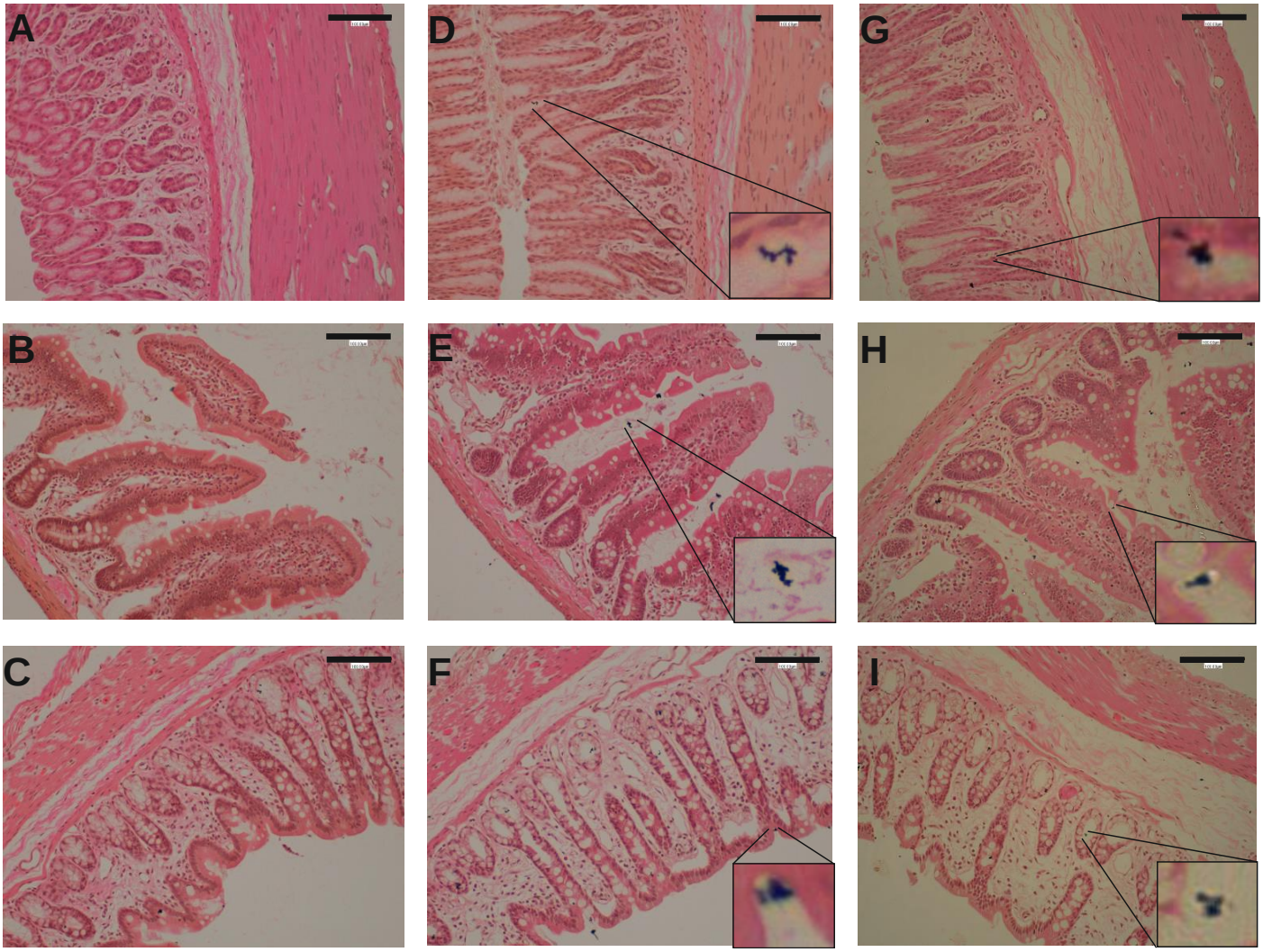

Fig. 4-3: Histology of gut sections following 4 h gut sac experiment. A) Control stomach, B) Control jejunum, C) Control large intestine, D) 1 mg L^{-1} Bulk TiO_2 stomach, E) 1 mg L^{-1} Bulk TiO_2 jejunum, F) 1 mg L^{-1} Bulk TiO_2 large intestine, G) 1 mg L^{-1} Nano TiO_2 stomach, H) 1 mg L^{-1} Nano TiO_2 jejunum, I) 1 mg L^{-1} Nano TiO_2 large intestine. Scale bar represent 100 µm, sections were 7 µm thick and stained with haematoxylin and eosin (n = 5 rats per treatment).

Table 4-2:Total Ti metal, Na^+, K^+, Ca^{2+} and Mg^{2+} concentrations of gut tissue segments from whole gut sacs following luminal exposure to 1 mg L^{-1} of TiO_2 for 4 h.

		[Metal] μmol g^{-1} dry mass						
Parameter	**Treatment**	**Oesophagus**	**Stomach**	**Duodenum**	**Jejunum**	**Ileum**	**Caecum**	**Large intestine**
Na^+	Control	110.7 ± 16.9^{a}	314.7 ± 21.7^{b}	753.6 ± 97.9^{c}	866.3 ± 121.0^{c}	656.6 ± 90.9^{c}	193.3 ± 51.2^{a}	625.4 ± 25.4^{c}
	Bulk TiO_2	166.9 ± 23.8^{a}	344.3 ± 83.8^{b}	686.6 ± 131.5^{c}	722.7 ± 88.2^{c}	747.8 ± 132.0^{c}	420.2 ± 69.6^{cd}	450.9 ± 49.8^{cd}
	Nano TiO_2	$304.9 \pm 32.5^{!*a}$	289.4 ± 38.42^{a}	622.8 ± 77.9^{b}	696.6 ± 44.2^{b}	671.4 ± 119.0^{b}	284.4 ± 56.6^{a}	482.2 ± 34.8^{c}
K^+	Control	74.5 ± 10.2^{a}	140.9 ± 7.6^{b}	155.8 ± 13.3^{b}	155.2 ± 8.4^{b}	109.7 ± 9.6^{c}	41.5 ± 15.8^{d}	179.8 ± 18.0^{b}
	Bulk TiO_2	82.7 ± 17.5^{a}	123.7 ± 18.7^{b}	175.0 ± 17.4^{b}	134.8 ± 22.8^{b}	93.0 ± 15.7^{a}	72.4 ± 6.2^{a}	145.4 ± 28.8^{b}
	Nano TiO_2	$190.5 \pm 24.3^{!*a}$	117.9 ± 4.6^{b}	126.6 ± 14.3^{b}	110.6 ± 14.5^{b}	98.5 ± 8.6^{b}	59.8 ± 9.6^{c}	132.4 ± 14.7^{ab}
Ca^{2+}	Control	12.9 ± 1.6^{a}	13.0 ± 2.4^{a}	57.6 ± 10.6^{b}	65.4 ± 10.5^{b}	61.9 ± 16.1^{b}	$17.6 \pm 0.96a$	40.7 ± 3.1^{c}
	Bulk TiO_2	12.6 ± 2.2^{a}	12.5 ± 2.7^{a}	41.1 ± 6.9^{b}	53.7 ± 7.1^{b}	56.5 ± 10.4^{b}	37.7 ± 11.4^{b}	28.3 ± 4.96^{ac}
	Nano TiO_2	$30.9 \pm 3.4^{!*a}$	18.0 ± 6.6^{b}	37.8 ± 4.6^{c}	53.7 ± 4.8^{cd}	56.7 ± 7.4^{cd}	24.8 ± 5.2^{ace}	27.6 ± 3.6^{ace}
Mg^{2+}	Control	7.0 ± 0.7^{a}	16.6 ± 1.1^{b}	18.7 ± 1.7^{b}	18.7 ± 1.1^{b}	14.1 ± 1.6^{b}	9.0 ± 2.0^{a}	16.1 ± 1.4^{b}
	Bulk TiO_2	7.9 ± 1.6^{a}	18.1 ± 1.7^{b}	18.6 ± 1.9^{b}	15.7 ± 1.9^{b}	13.0 ± 2.2^{b}	$18.3 \pm 4.3^{*b}$	13.4 ± 2.3^{b}
	Nano TiO_2	$18.1 \pm 2.9^{!*a}$	17.4 ± 0.9^{a}	15.0 ± 1.0^{a}	14.2 ± 1.4^{a}	13.0 ± 0.9^{a}	13.3 ± 1.7^{a}	12.8 ± 1.0^{a}
Moisture(%)	Control	51.5 ± 3.5^{a}	81.3 ± 1.2^{b}	84.8 ± 2.5^{b}	87.2 ± 0.6^{b}	79.2 ± 5.8^{b}	78.3 ± 3.0^{b}	86.0 ± 0.9^{b}
	Bulk TiO_2	52.3 ± 11.2^{a}	80.6 ± 0.9^{b}	84.1 ± 1.8^{b}	84.4 ± 1.6^{b}	78.9 ± 7.8^{b}	86.2 ± 1.8^{b}	78.0 ± 1.6^{b}
	Nano TiO_2	$71.6 \pm 9.4^{!*a}$	82.6 ± 0.7^{b}	83.9 ± 1.2^{b}	85.3 ± 1.1^{b}	84.7 ± 1.6^{b}	84.1 ± 2.5^{b}	79.9 ± 2.7^{b}

Values are means ± S.E.M. (n = 5) for each group expressed as µmol g^{-1} dry mass of intestinal tissue, except moisture content (%). Whole gut sacs were filled with physiological saline (control), 1 mg l^{-1} bulk TiO_2 and 1 mg l^{-1} TiO_2 NP at 37°C for 4 h. * Statistically significant difference from the control value within columns and electrolytes (Kruskal-Wallis or ANOVA, $P < 0.05$). ! Statistically significant difference from bulk TiO_2 values within columns and electrolytes (Kruskal-Wallis or ANOVA, $P < 0.05$). Different letters (within rows) indicate a statistically significant difference between regions of the gut (Kruskal-Wallis or ANOVA, $P < 0.05$).

4.4.3 Electrolyte and moisture composition of whole gut sacs

The tissue electrolyte concentrations are shown in Table 4-2. There were some differences in the electrolyte composition of different gut regions, which is to be expected, but, there were no treatment-dependent effects of either bulk or nano TiO_2 on the Na^+, K^+, Ca^{2+} or Mg^{2+} concentrations in the whole gut sacs, with the exception of the oesophagus treated with nano TiO_2, which caused an increase in all of the measured tissue electrolyte concentrations (ANOVA $P < 0.05$). This is likely attributed to the differences in moisture content compared with the bulk and control treated oesophagus (71.6 % ± 1.4 (Nano), 51.5 % ± 3.5 (Control) 52.3 % ± 11.2 (Bulk)).

4.4.4 The effect of TiO_2 on the viability of the perfused intestine

All the perfused intestine preparations were within the normal ranges for the selected viability measurements. Individual perfusions all displayed steady cumulative perfusate flow (Fig. 4-11), and LDH activity in all experiments remained below 1 μmol min^{-1} mL^{-1} (1 U mL^{-1}). The maximum LDH activities in the serosal perfusate at a given time point for the control, bulk TiO_2 and nano TiO_2 were 0.04, 0.02 and 0.04 U mL^{-1}, respectively. There were no statistically significant differences between treatments in either cumulative perfusate or mucosal salines LDH activities (Fig. 4-4). There were no TiO_2 treatment dependent effects on $[K^+]$, $[Na^+]$, $[Mg^{2+}]$, $[Ca^{2+}]$ and pH of the mucosal solution, which is indicative of a normal leak free intestine. The measured concentrations of $[K^+]$, $[Na^+]$, $[Mg^{2+}]$, $[Ca^{2+}]$ and pH in the fresh mucosal saline were 6.59 ± 0.22, 162.6 ± 4.00, 0.8 ± 0.016, 3.26 ± 0.035 mmol L^{-1} and 7.47 ± 0.01, respectively (means ± S.E.M, n = 5). Following the 4 h treatment there were

only minor increases in the mucosal saline electrolyte concentrations for all experiments. For example, the average increase of [K^+] and [Na^+] in the control runs was 0.34 ± 0.074 and 4.5 ± 3.4 mmol L^{-1} respectively (means ± S.E.M, n = 5). The bulk and nano TiO_2 treatments exhibited a similar pattern to the control with the average increase of [K^+] and [Na^+] being 0.47 ± 0.076 and 9.4 ± 3.9 for bulk and 0.61 ± 0.22 and 16.9 ± 6.1 for nano TiO_2, respectively, over the course of the experiment. The grand mean change in pH (grand means of controls and treatments) for all experiments was 0.256 ± 0.023 which is representative of the expected base secretion of the intestine. The pH changes for each of the treatments was 0.226 ± 0.033, 0.260 ± 0.039 and 0.282 ± 0.049 for the control, bulk and nano treatments, respectively (Table 4-3).

Ultrastructural examination of the perfused intestine after 4 h indicated that tight junction integrity and brush border morphology were maintained throughout the experiment. The addition of 1 mg L^{-1} bulk or nano TiO_2 to the mucosal solution appeared to cause no appreciable changes in enterocyte ultrastructure (Fig. 4-5 and 4-6). Taken together, all the perfused intestine viability measurements were met which is indicative of a structurally and physiologically normal intestine following a 4 h perfusion.

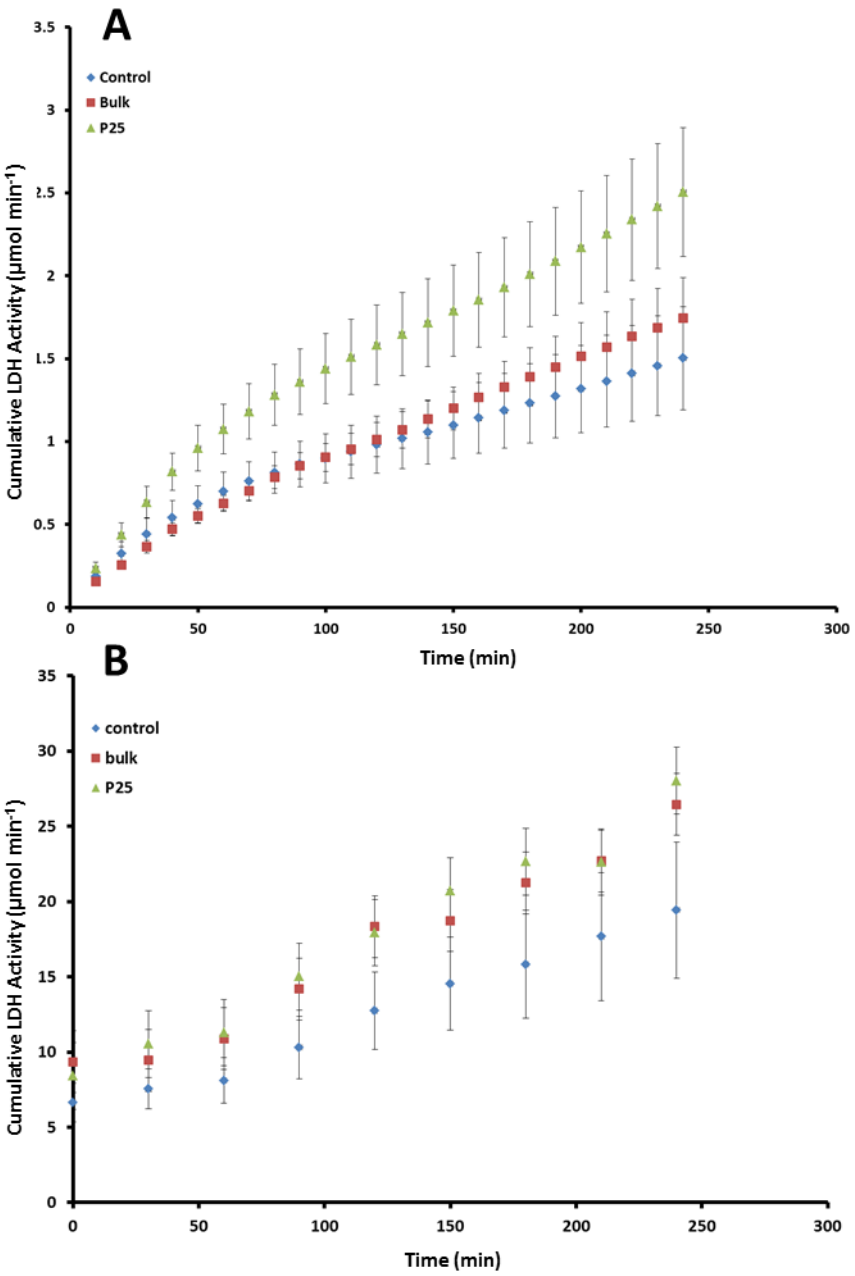

Fig. 4-4: (A); The effect of 1 mg L^{-1} TiO_2 exposure on the cumulative perfusate LDH activity (cumulative sum of units of LDH activity per minute) over 4 h in perfused intestine at 37 °C, gassed with 95% O_2: 5% CO_2 gas mixture. Values are means ± S.E.M (n = 5). Statistical analysis for the 4 h time point showed no differences between cumulative totals between treatments (ANOVA *P* = 0.1102). (B); Cumulative absolute LDH activity in the mucosal solution over 4 h. Statistical analysis at 4 h showed no differences between cumulative totals between treatments (ANOVA *P* = 0.5504).

Table 4-3: pH and total Na^+ and K^+ concentrations in the mucosal solution during exposure of the isolated perfused jejunum to 1 mg l^{-1} of TiO_2.

	Control			Bulk			Nano		
Time (min)	pH	Bath Na^+ (mmol l^{-1})	Bath K^+ (mmol l^{-1})	pH	Bath Na^+ (mmol l^{-1})	Bath K^+ (mmol l^{-1})	pH	Bath Na^+ (mmol l^{-1})	Bath K^+ (mmol l^{-1})
0	7.47 ± 0.03	148.44 ± 20.24	6.59 ± 0.22	7.48 ± 0.03	160.87 ± 2.83	6.42 ± 0.14	7.47 ± 0.03	155.40 ± 2.41	6.39 ± 0.16
30	7.66 ± 0.02	162.60 ± 4.04	6.63 ± 0.21	7.74 ± 0.04	162.62 ± 3.13	6.58 ± 0.14	7.77 ± 0.04	160.92 ± 4.48	6.54 ± 0.14
60	7.72 ± 0.03	160.72 ± 2.99	6.58 ± 0.23	7.79 ± 0.05	163.64 ± 2.29	6.64 ± 0.13	7.81 ± 0.04	160.94 ± 4.44	6.57 ± 0.18
90	7.75 ± 0.04	165.81 ± 4.82	6.77 ± 0.18	7.82 ± 0.07	164.03 ± 3.92	6.56 ± 0.18	7.85 ± 0.04	162.94 ± 3.83	6.66 ± 0.12
120	7.77 ± 0.05	167.19 ± 3.54	6.79 ± 0.14	7.81 ± 0.06	163.05 ± 4.67	6.59 ± 0.19	7.84 ± 0.05	168.58 ± 5.99	6.85 ± 0.23
150	7.76 ± 0.05	166.52 ± 2.99	6.81 ± 0.14	7.80 ± 0.05	167.75 ± 3.65	6.72 ± 0.10	7.84 ± 0.05	165.71 ± 7.01	6.67 ± 0.24
180	7.71 ± 0.02	167.76 ± 4.28	6.85 ± 0.12	7.75 ± 0.03	166.11 ± 4.05	6.83 ± 0.15	7.81 ± 0.05	172.06 ± 9.34	6.90 ± 0.29
210	7.66 ± 0.02	168.76 ± 2.49	6.86 ± 0.13	7.71 ± 0.02	166.39 ± 2.57	6.77 ± 0.16	7.77 ± 0.03	173.98 ± 9.43	7.03 ± 0.30
240	7.70 ± 0.04	162.58 ± 4.01	6.01 ± 0.94	7.74 ± 0.03	170.25 ± 3.28	6.90 ± 0.11	7.75 ± 0.03	172.39 ± 8.27	6.99 ± 0.31

Values are means ± S.E.M. (n = 5) for each group expressed as mmol L^{-1} for both Na^+ and K^+ in the mucosal solution. There were no significant difference between treatments nor were there any time effects (ANOVA, $P > 0.05$).

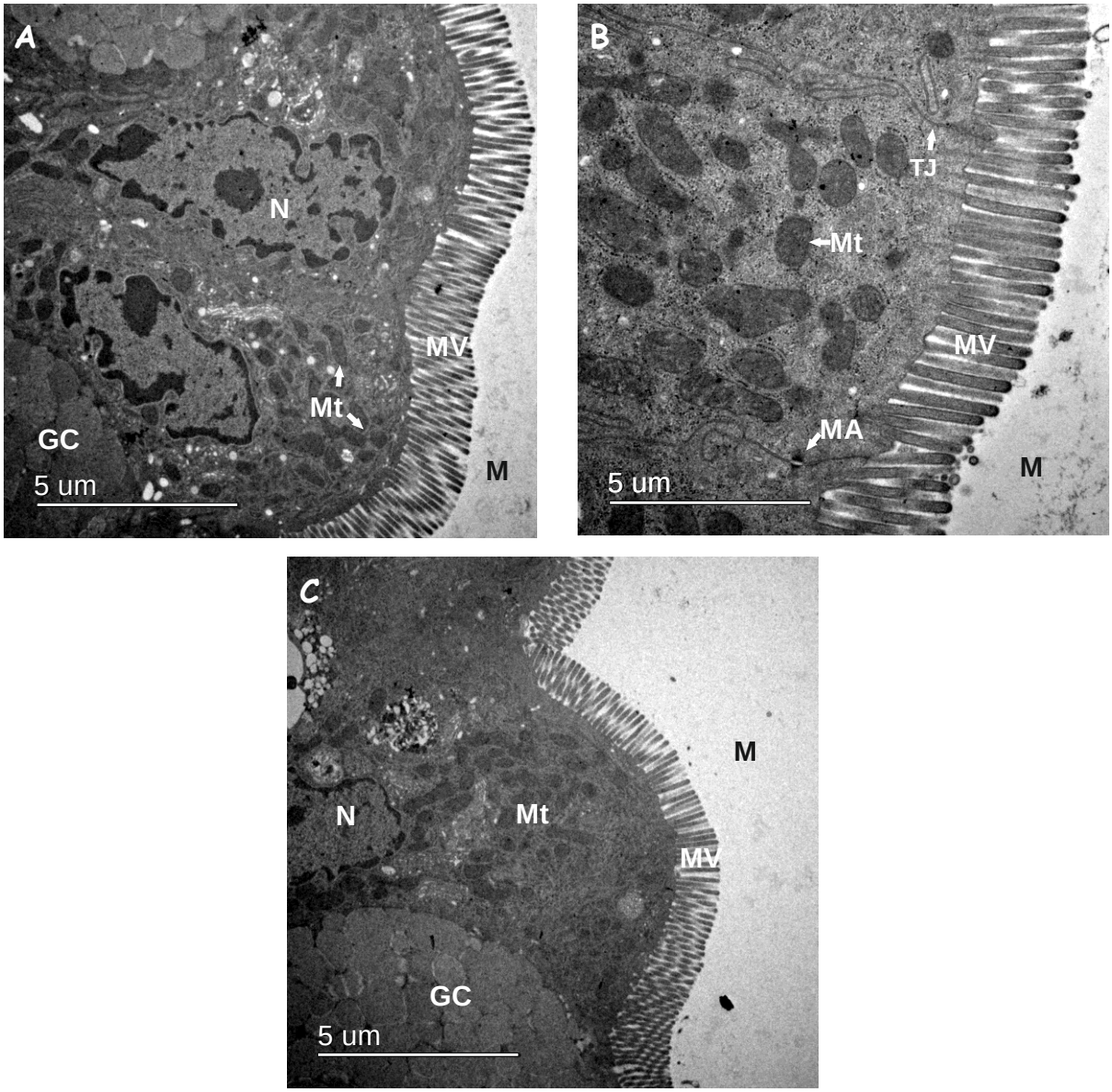

Fig. 4-5: TEM of the everted perfused intestine (Jejunum) following a 4 h perfusion. A) Everted control showing normal morphology with densely packed uniform microvilli; B) Everted jejunum exposed to 1 mg L^{-1} Bulk TiO_2 showing normal morphology intact mitochondria and intact tight junctions; C) Jejunum exposed to 1 mg L^{-1} nano TiO_2 showing normal morphology. Images are representative of individual animals from replicated experiments (n = 5). Scale bars represent 5 µm). (N) Nucleus, (MV) Microvilli, (Mt) Mitochondria, (GC) Goblet cell, (M) Mucous, (TJ) Tight junction, (MA) Macula Adherens.

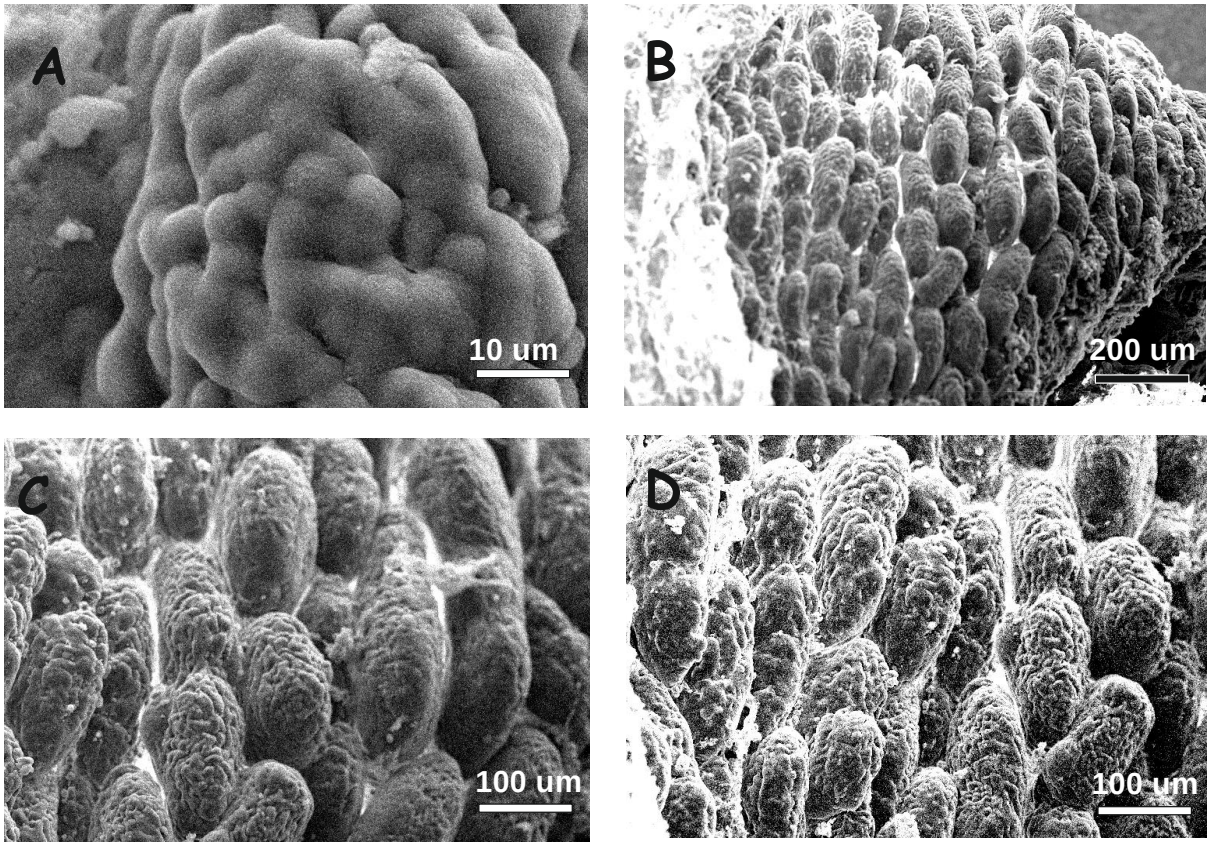

Fig. 4-6: SEM of the everted perfused intestine (Jejunum) following a 4 h perfusion. A) A villus from the control group covered in mucous showing normal morphology. Scale bar represents 10 µm; B) Control treatment showing densely packed villi which is indicative of a healthy gut. Scale bar represents 200 µm; C) Perfused intestine exposed to 1 mg L^{-1} bulk TiO_2 exhibiting normal villi morphology. Scale bar represent 100 µm; D) Jejunum exposed to 1 mg L^{-1} nano TiO_2 showing normal morphology. Scale bar represents 100 µm. Images are representative of individual animals from replicated experiments (n = 5).

4.4.5 The effect of pharmacological agents on the viability of the perfused intestine

Addition of 120 IU mL^{-1} nystatin to the mucosal solution or 100 µmol L^{-1} sodium orthovanadate to the serosal solution had little effect on the viability criteria. Individual perfusions all displayed steady cumulative perfusate flow (Fig. 4-12), and LDH activity in all experiments remained below 1 µmol min^{-1} mL^{-1} (n = 5) (Fig. 4-7). The maximum LDH activity at a given time point in the nystatin trial for the control, bulk and nano TiO_2 exposures was 0.03, 0.03 and 0.02 U ml^{-1} respectively (Fig. 4-7). Similarly for the sodium vanadate trials the maximum LDH activity at any given time point for the control, bulk and nano exposures where 0.02, 0.02 and 0.01 U ml^{-1}, respectively (Fig. 4-7). There were no statistically significant differences between treatments in either cumulative perfusate LDH activity or mucosal saline LDH activity; nor where there any differences in these measurements between the drug and no drug trials (ANOVA, $P < 0.05$).

The 4 h perfusions in the presence of drugs had negligible effects on mucosal saline electrolyte concentrations. For example, in the nystatin treatment the average change of $[K^+]$ and $[Na^+]$ in the control trials (no added TiO_2) over 4 h was -0.001 ± 0.114 and 2.621 ± 3.149, (S.E.M. n = 5) respectively. Addition of bulk or nano TiO_2 treatments in the presence of nystatin exhibited a similar pattern to the control, with the average increase of $[K^+]$ and $[Na^+]$ (mmol l^{-1}) being 0.025 ± 0.158 and 3.4 ± 3.9 for bulk and -0.007 ± 0.167 and 3.99 ± 2.52 for nano TiO_2, respectively, over the course of the experiment. There were no drug treatment-dependent effects on the mucosal bath pH. The grand mean change in pH (grand means of controls and treatments) for all experiments in the presence of nystatin was 0.11 ± 0.024. The pH

change for each of the treatments was 0.182 ± 0.044, 0.064 ± 0.026 and 0.084 ± 0.043 for the control, bulk and nano treatments, respectively (Table 4-4).

Addition of 100 µmol L^{-1} sodium orthovanadate to the serosal perfusate had little effect on [K^+] and [Na^+] leak into the mucosal solution. The increases in mucosal solution [Na^+] concentrations were 5.66 ± 2.45, 8.81 ± 3.39, and 9.49 ± 1.632 mmol L^{-1} for the control, bulk and nano TiO_2 treatments, respectively, over the 4 h perfusion. [K^+] leak into the mucosal solution at the end of the 4 h perfusion was as 0.277 ± 0.096, 0.415 ± 0.198 and 0.39 ± 0.07 mmol L^{-1} for the control, bulk and nano treatments respectively. The pH change followed a similar pattern to the other experiments. The grand mean change in pH for all the experiments perfused with 100 µmol L^{-1} sodium vanadate was 0.186 ± 0.022. Ph change for each of the treatments was 0.213 ± 0.053, 0.183 ± 0.003 and 0.163 ± 0.012 for the control, bulk and nano exposures, respectively (Table 4-5) none of which was regarded as statistically significant. The data indicates that gut integrity and viability was maintained throughout the perfusion experiments for all treatments and exposures (drugs and TiO_2).

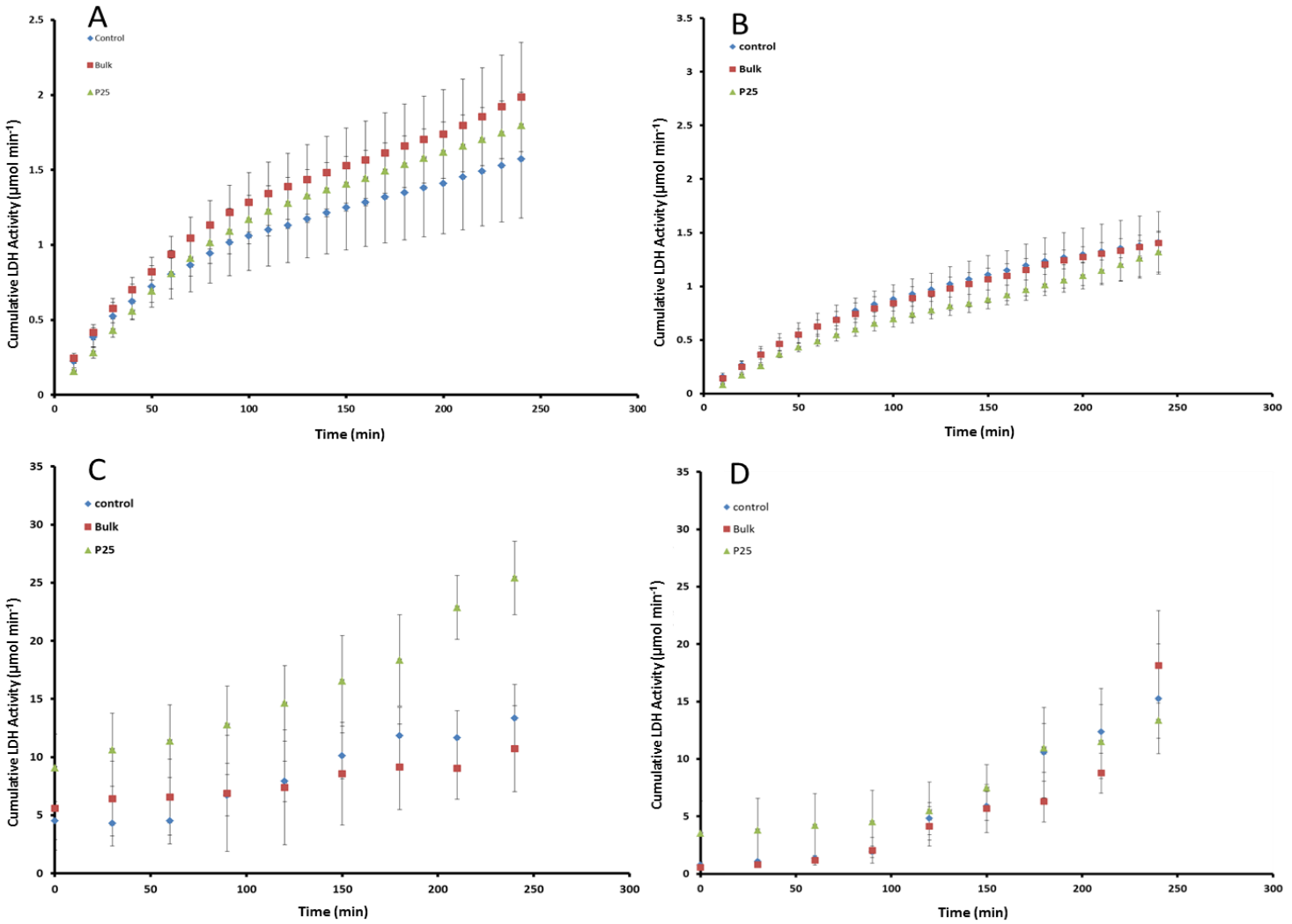

Fig. 4-7: Panel; A) The effect of 120 IU mL^{-1} nystatin in the mucosal solution on the cumulative perfusate LDH activity over 4 h; C) Cumulative absolute LDH activity in the mucosal solution over 4 h in the presence of nystatin; B) The effect of 100 µmol L^{-1} vanadate in the serosal perfusate on the cumulative perfusate LDH activity over 4 h; D) Cumulative absolute LDH activity in the mucosal solution over 4 h in the presence of vanadate. Values are means ± S.E.M (n = 5). Addition of 1 mg L^{-1} TiO_2 (bulk or nano) to the mucosal solution had no effect on the cumulative perfusate LDH activity (cumulative sum of international units of LDH activity per minute) or the cumulative absolute LDH activity in the mucosal solution at 4 h within groups or between groups relative to the controls (ANOVA or Kruskal wallis $P > 0.05$). All baths were maintained at 37°C gassed with 95% O_2: 5% CO_2 for 4 h.

Table 4-4: pH and total Na^+ and K^+ concentrations in the mucosal solution during exposure of the isolated perfused jejunum to 1 mg l^{-1} of bulk or nano TiO_2 in the presence of 120 IU ml^{-1} nystatin.

	Control			Bulk			Nano		
Time (min)	pH	Bath Na^+ (mmol l^{-1})	Bath K^+ (mmol l^{-1})	pH	Bath Na^+ (mmol l^{-1})	Bath K^+ (mmol l^{-1})	pH	Bath Na^+ (mmol l^{-1})	Bath K^+ (mmol l^{-1})
0	7.412 ± 0.01	130.59 ± 9.32	4.35 ± 0.59	7.46 ± 0.01	129.05 ± 8.01	4.31 ± 0.52	7.46 ± 0.02	127.69 ± 10.05	4.27 ± 0.627
30	7.63 ± 0.03	131.24 ± 8.64	4.37 ± 0.57	7.62 ± 0.03	132.39 ± 8.96	4.43 ± 0.51	7.62 ± 0.02	129.49 ± 10.85	4.29 ± 0.64
60	7.68 ± 0.03	131.86 ± 9.03	4.31 ± 0.52	7.63 ± 0.05	131.56 ± 9.28	4.32 ± 0.51	7.65 ± 0.01	129.63 ± 10.20	4.28 ± 0.064
90	7.70 ± 0.05	131.02 ± 9.14	4.29 ± 0.53	7.61 ± 0.06	131.27 ± 9.44	4.29 ± 0.53	7.64 ± 0.02	131.15 ± 9.87	4.29 ± 0.58
120	7.68 ± 0.04	130.41 ± 8.65	4.25 ± 0.49	7.63 ± 0.04	132.13 ± 9.02	4.37 ± 0.52	7.63 ± 0.03	132.07 ± 9.85	4.35 ± 0.58
150	7.65 ± 0.04	131.71 ± 9.12	4.27 ± 0.53	7.56 ± 0.03	133.83 ± 9.47	4.39 ± 0.55	7.60 ± 0.04	133.47 ± 10.56	4.42 ± 0.61
180	7.60 ± 0.04	132.83 ± 9.78	4.34 ± 0.55	7.54 ± 0.03	134.34 ± 10.04	4.33 ± 0.54	7.58 ± 0.04	131.46 ± 9.08	4.26 ± 0.45
210	7.59 ± 0.04	132.57 ± 9.41	4.29 ± 0.52	7.56 ± 0.03	134.51 ± 10.76	4.42 ± 0.61	7.57 ± 0.03	131.98 ± 8.71	4.32 ± 0.50
240	7.59 ± 0.04	133.21 ± 9.01	4.35 ± 0.50	7.52 ± 0.02	132.48 ± 10.19	4.34 ± 0.60	7.54 ± 0.02	131.67 ± 9.16	4.26 ± 0.48

Values are means ± S.E.M. (n = 5) for each group expressed as mmol L^{-1} for both Na^+ and K^+ in the mucosal solution. There were no significant differences between treatments nor were there any time effects (ANOVA, $P > 0.05$).

Table 4-5: pH and total Na+ and K+ concentrations in the mucosal solution during exposure of the isolated perfused jejunum to 1 mg L^{-1} of TiO_2 in the presence of 100 µmol L^{-1} sodium orthovanadate.

	Control			Bulk			Nano		
Time (min)	pH	Bath Na^+ (mmol l^{-1})	Bath K^+ (mmol l^{-1})	pH	Bath Na^+ (mmol l^{-1})	Bath K^+ (mmol l^{-1})	pH	Bath Na^+ (mmol l^{-1})	Bath K^+ (mmol l^{-1})
0	7.41 ± 0.01	136.58 ± 3.10	4.91 ± 0.70	7.45 ± 0.02	136.60 ± 2.82	4.88 ± 0.66	7.50 ± 0.02	134.97 ± 1.14	4.96 ± 0.603
30	7.58 ± 0.08	138.77 ± 2.66	5.10 ± 0.72	7.68 ± 0.07	130.82 ± 6.21	4.43 ± 0.51	7.74 ± 0.05	134.27 ± 2.15	4.93 ± 0.61
60	7.64 ± 0.07	139.83 ± 3.05	5.15 ± 0.76	7.80 ± 0.02	135.90 ± 1.11	4.90 ± 0.60	7.71 ± 0.05	138.46 ± 2.12	5.10 ± 0.066
90	7.74 ± 0.06	139.72 ± 2.95	5.04 ± 0.74	7.77 ± 0.05	137.75 ± 1.61	4.97 ± 0.64	7.77 ± 0.07	141.09 ± 1.47	5.26 ± 0.66
120	7.66 ± 0.03	141.64 ± 3.17	5.09 ± 0.76	7.68 ± 0.07	140.10 ± 2.72	5.01 ± 0.73	7.66 ± 0.04	141.95 ± 2.69	5.30 ± 0.74
150	7.72 ± 0.04	140.89 ± 2.49	5.07 ± 0.73	7.64 ± 0.06	143.27 ± 2.73	5.19 ± 0.70	7.70 ± 0.02	144.69 ± 2.76	5.32 ± 0.72
180	7.57 ± 0.05	142.64 ± 2.38	5.18 ± 0.70	7.60 ± 0.05	144.34 ± 3.22	5.32 ± 0.70	7.70 ± 0.03	143.09 ± 2.77	5.31 ± 0.68
210	7.58 ± 0.07	143.69 ± 2.42	5.15 ± 0.68	7.66 ± 0.04	145.61 ± 2.55	5.31 ± 0.73	7.66 ± 0.05	142.38 ± 2.35	5.31 ± 0.67
240	7.62 ± 0.06	140.77 ± 3.10	4.83 ± 0.78	7.64 ± 0.03	143.80 ± 1.31	4.87 ± 0.69	7.66 ± 0.03	142.82 ± 1.76	4.99 ± 0.71

Values are means ± S.E.M. (n = 5) for each group expressed as mmol L^{-1} for both Na^+ and K^+ in the mucosal solution. There were no significant differences between treatments nor were there any time effects (ANOVA, $P > 0.05$).

4.4.6 Confirmation of 1 mg L^{-1} TiO_2 exposure in mucosal saline solution

The exposure to TiO_2 was confirmed by a number of procedures;1) measuring the mass concentration of TiO_2 and particle size distributions in the mucosal solution (Fig. 4-8); 2) using nanoparticle tracking analysis (NTA, Fig. 4-1); 3) measuring total Ti metal concentration in the intestinal tissue (Table 4-6). NTA measurements were made on samples collected a 0 and 240 min during the experiments using triplicate measurements for a sample each time. TiO_2 concentrations of 1 mg L^{-1} in the mucosal solution (bulk and nano) produced an unstable colloidal dispersion. The mean size distribution of the particles were smaller at the end of the 4 h perfusion (Fig. 4-1 - E-F) changing from 213 to 90 nm for the bulk material, and from 146 to 30 nm for the NPs and is probably a reflection of the faster settling rate of larger aggregates (Keller *et al*. 2010) rather than selective uptake of larger particles by the tissue. Analysis of the concentration of Ti from mucosal saline samples taken throughout the experiment implied that bulk TiO_2 settles out of suspension at a much faster rate than the nano form (ANOVA $P < 0.05$) (Fig. 4-8). Addition of drugs (nystatin and sodium orthovanadate) to the mucosal or serosal solutions had little effect on the mass concentration of TiO_2 in the mucosal solution in comparison to no drug treatments. The nano TiO_2 dispersion in the mucosal solution maintained a relatively consistent concentration, diminishing by (grand means) 0.160 ±0.027 mg L^{-1} for the duration of the experiment (equivalent to a 20% loss of TiO_2 from the starting concentration at 4 h). In contrast, 1 mg L^{-1} bulk TiO_2 dispersions settled much faster resulting in an average loss of 0.494 ± 0.0498 mg L^{-1} suspended TiO_2 by the end of the experiment (equivalent to a 62% loss of suspended TiO_2 from the starting concentration at 4 h (Fig. 4-8) (means ± S.E.M, n = 15)).

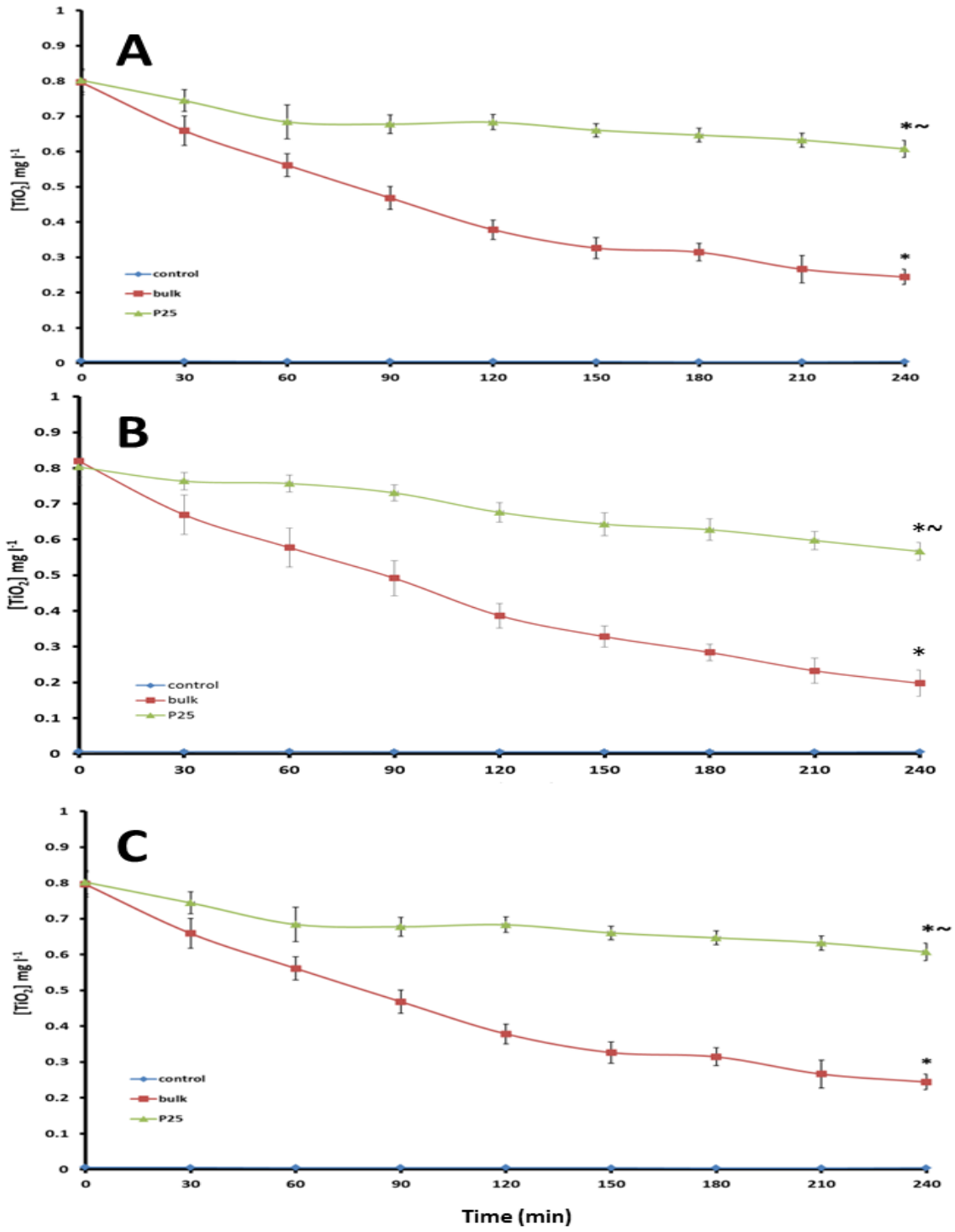

Fig. 4-8: The concentration of TiO_2 in the gassed and stirred mucosal solution over 4 h in the presence of the intestine. A) No drug; B)120 IU mL^{-1} nystatin added to the mucosal saline; C) 100 µmol L^{-1} sodium orthovanadate added to the serosal perfusate. Values are means ± S.E.M., n = 5 * indicates statistical significance at 4 h relative to the control. ˜indicates a statistical significance between materials at 4 h (ANOVA $P < 0.05$).

4.4.7 Titanium accumulation from TiO_2 exposures in the perfused rat jejunum in the presence or absence of pharmacological agents

The accumulation of Ti in the tissue following the perfusions is shown (Table 4-6). Total Ti metal concentrations in the tissues were higher in both of the TiO_2 treatments compared to the no added TiO_2 controls (ANOVA $P < 0.05$). These were 0.265 ± 0.044 and 0.293 ± 0.048 µmol g^{-1} dry weight for bulk and nano TiO_2 respectively, compared to 0.027 ± 0.08 µmol g^{-1} dry weight in the control.

Mucosal applications of 120 IU mL^{-1} nystatin caused a mean increase in tissue Ti concentration for bulk and nano TiO_2 exposures relative to the no drug treatments. Tissue Ti concentrations following the 4 h exposure to TiO_2 in the presence of nystatin were 0.673 ± 0.133 and 0.403 ± 0.06 µmol g^{-1} dry weight for bulk and nano TiO_2, respectively. The increase in Ti for the bulk exposure was statistically significant compared to the no drug bulk TiO_2 exposure (t test, $P < 0.05$) and significant at the 90% confidence level compared to the no drug nano exposure (t-test, $P = 0.061$). Similar to the nystatin treatment, addition of 100 µmol L^{-1} vanadate to the serosal perfusate caused a mean increase in tissue Ti concentrations. Ti tissue concentrations after 4 h were 0.447±0.08 and 0.388 ± 0.06 µmol g^{-1} for bulk and nano TiO_2, respectively. These increases were not statistically different to the no drug TiO_2 treatments nor where than any material type differences (Table 4-6).

TEM images of the jejunum epithelium in the no drug trials are shown in Fig. 4-9. For the TiO_2 treatments electron dense particles of similar morphology to the TEM characterised stocks were observed in vesicles (Fig. 4-9). Moreover, cells were intact relative to the controls implying accumulation is not due to incidental leak into damaged epithelium (Fig. 4-5 and 4-9).

Table 4-6: Total Ti, K^+, Na^+, Ca^{2+} concentrations and % moisture of jejunum tissue following exposure to 1 mg L^{-1} TiO_2 with or without drugs for 4 h.

	[Metal] μmol g^{-1} dry mass					
Treatment	**Ti**	**Na^+**	**K^+**	**Ca^{2+}**	**Mg^{2+}**	**% Moisture**
Control	0.027 ± 0.008	359.01 ± 56.81	71.18 ± 15.17	15.65 ± 1.01	8.05 ± 1.22	82.38 ± 1.94
Bulk TiO_2	$0.265 \pm 0.044^*$	316.59 ± 39.08	63.27 ± 10.68	17.89 ± 2.64	7.39 ± 0.64	79.54 ± 1.53
Nano TiO_2	$0.293 \pm 0.048^*$	301.77 ± 53.78	67.68 ± 12.58	18.67 ± 1.97	8.88 ± 0.78	83.88 ± 1.57
Nystatin Control	0.034 ± 0.008	473.30 ± 39.18^a	87.44 ± 16.10	205.91 ± 13.26^a	12.24 ± 1.93	80.93 ± 1.77
Nystatin Bulk TiO_2	$0.673 \pm 0.133^{*a}$	434.21 ± 59.31^a	78.59 ± 10.21	185.45 ± 26.89^a	11.43 ± 1.52^a	79.45 ± 3.03
Nystatin Nano TiO_2	$0.403 \pm 0.062^*$	338.46 ± 48.03	58.42 ± 11.38	140.32 ± 19.83^a	8.14 ± 1.18	75.57 ± 2.66
Vanadate Control	0.038 ± 0.008	459.36 ± 84.03^b	42.22 ± 4.03^b	229.94 ± 44.30^b	7.36 ± 0.91	78.72 ± 2.58
Vanadate Bulk TiO_2	$0.447 \pm 0.081^*$	509.61 ± 33.39^b	47.17 ± 4.65^b	281.76 ± 59.21^b	$8.28 \pm 0.62^\dagger$	79.64 ± 2.57
Vanadate Nano TiO_2	$0.388 \pm 0.064^*$	402.63 ± 50.23^b	35.20 ± 5.47^b	237.93 ± 15.39^b	6.80 ± 0.99	72.82 ± 2.95

Values are means ± S.E.M. (n = 5) expressed as total Metal µmol g^{-1} dry mass of intestinal tissue, except for moisture content (%).* Statistically significant difference from the control value within columns. [a] Statistically significant difference of nystatin values relative to the no drug trials within columns, treatments and electrolytes. [b] Statistically significant difference of vanadate values relative to the no drug trials within columns, treatments and electrolytes. [†] Statistically significant difference of vanadate values relative to nystatin values within columns, treatments and electrolytes (all data was tested using either ANOVA or Kruskal Wallis t-test or mann whitney U where appropriated and significance determined by, $P < 0.05$ or notched box whisker plots).

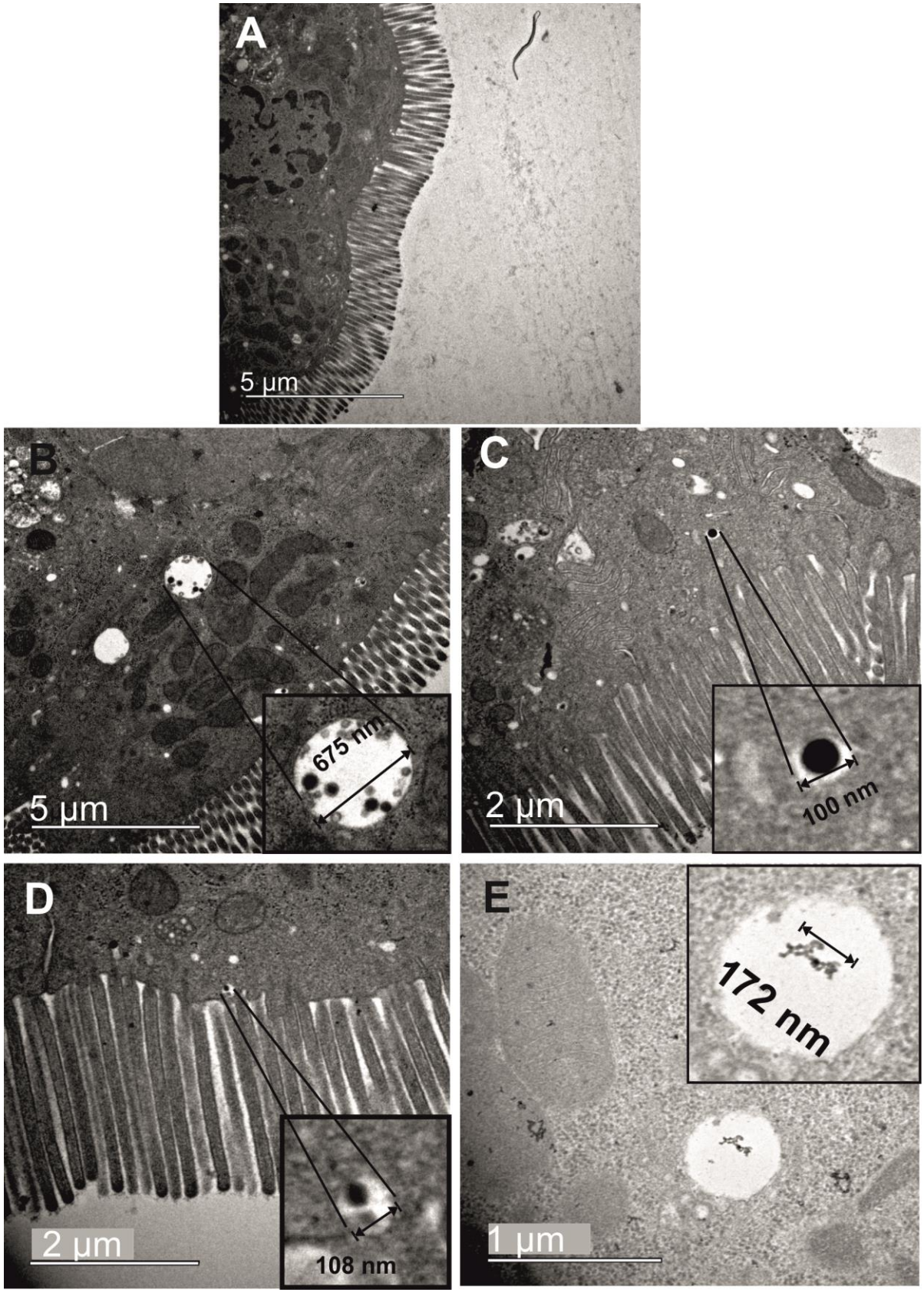

Fig. 4-9: TEM of the everted perfused intestine (Jejunum) following a 4 h perfusion. A) Control; B-C) 1 mg L^{-1} bulk TiO_2 exposures showing intact cells with vesicles containing morphologically similar particles to the characterised stocks.; D-E) 1 mg L^{-1} nano TiO_2 exposures showing intact cells with particle containing vesicles. The composition of the particles was not confirmed in the electron micrographs.

4.4.8 Instantaneous surface adsorption

Measurements from the rapid solution dipping protocol to determine surface-bound Ti on everted jejunum segments revealed low insignificant amounts of Ti metal instantaneously bind to the tissue surface (before true uptake can occur). The Ti metal concentration of the dipped everted jejunum segments was (means ± S.E.M, n = 6) 39.6 ± 9.0, 55.5 ± 6.9 and 73.0 ± 15.0 nmol g^{-1} dry weight for the control, bulk and nano TiO_2 exposures, respectively (Fig. 4-10). The Ti concentrations in jejunum segments exposed to the bulk or nano TiO_2 were not statistically different from the unexposed control (ANOVA P = 0.138). Furthermore 'dipped' tissue concentrations of total Ti metal were also significantly lower than those reported in the whole gut sacs (small intestine and large intestine) and perfusions treated with TiO_2 (t-tests, P values all < 0.05). The instantaneous adsorption of Ti represents 33 and 50 % of the total tissue Ti reported for the jejunum segment of the gut sac experiment and 20 and 24 % of the total tissue Ti reported for the intestinal perfusions for bulk and nano treatments respectively.

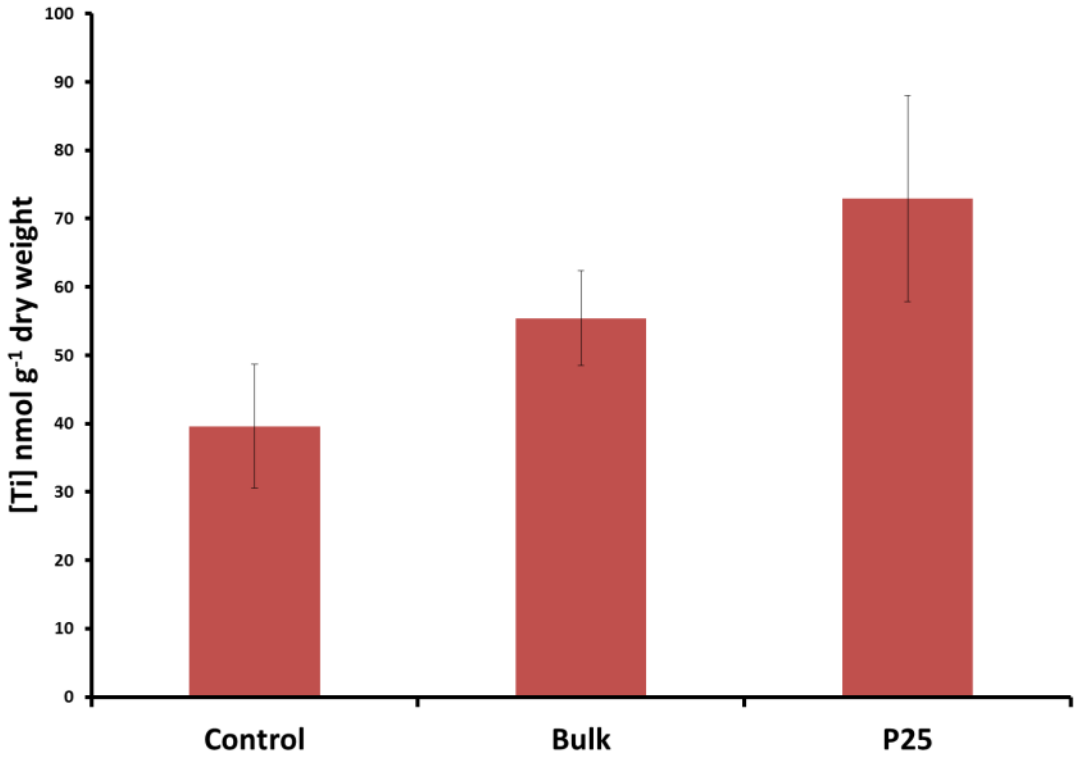

Fig. 4-10: Tissue concentration of Ti (nmol g^{-1} dry weight) following a 20 s dip in 1 mg L^{-1} bulk or nano TiO_2 in physiological saline (means ± S.E.M. n = 6). There were no statistically significant differences between treatments.

4.4.9 Tissue electrolytes and moisture content of the perfused intestine in the presence or absence of pharmacological agents

The tissue electrolyte concentrations and moisture content of the perfused jejunum are shown in Table 4-6. There were no TiO_2 treatment effects on tissue electrolyte levels (Na^+, K^+, Ca^{2+} and Mg^{2+}). Although not significant, mean tissue Ca^{2+} concentration appeared to be consistently higher for both treatments relative to the control whilst tissue K^+ was lower (none of these were significant though). Metabolic and ion transport inhibitors are expected to cause changes in the electrolyte status of tissues and in both the no-added TiO_2 controls and the TiO_2 NP treatments nystatin and vanadate treatment caused elevated Ca^{2+} tissue concentrations (ANOVA, $P < 0.05$). In the nystatin treatments mean Na^+ and K^+ tissue concentrations increased and this was significant within controls and bulk exposures relative to the no drug counterparts. Vanadate exposure caused a mean increase in tissue Na^+ and decrease in K^+ concentrations for all the exposures relative to the no drug trials (ANOVA, $P < 0.05$*)* and a significant reduction in tissue K^+ compared to the nystatin treatments (ANOVA, $P < 0.05$*)*. Mg^+ levels were largely unaffected. There were no significant drug or treatment effects on tissue moisture content (Table 4-6).

4.4.10 Net Ti and water flux across the perfused intestine

The cumulative appearance in the serosal compartment for representative experiments is shown in Fig. 4-11. All treatments maintained a steady perfusate flow and both the TiO_2 exposures demonstrated a steady increase in the appearance of total Ti metal in the serosal perfusate compared to the controls. Calculated net Ti uptake rates and water fluxes across the intestine are shown (Table 4-7). Only the

nano TiO_2 exposure showed a statistically significant elevation of Ti flux to the serosal compartment compared to the control treatment (Table 4-7). The mean initial and overall flux rates for the nano TiO_2 exposures were 10 and 2 times higher, respectively, compared to the control values and 5 and 1.5 times higher than the bulk initial and overall flux rates. Moreover, initial and overall flux rates were different from each other, indicating that there may have been a saturation of the nano Ti uptake mechanism with respect to the overall flux rate, but not the initial flux rate. Bulk Ti flux was regarded as significant at the 90% confidence interval (t-test P = 0.059) for initial flux rates compared to the control initial flux and for overall flux rates (t-test) P = 0.062).

All treatments demonstrated a net outward flux of water across the intestine. Addition of both bulk and nano TiO_2 caused a significant increase in initial and overall rates of water flux compared to the control (ANOVA, $P < 0.05$; Table 4-7). The initial net outward water flux was -6.017 ± 10.68, -31.316 ± 14.321 and 33.989 ± 14.731 ml g^{-1} h^{-1} for the control, bulk and nano exposures respectively. Overall water flux rates for the bulk and nano treatments remained similar to the initial flux rates and there were no statistically significant material-type effects on water flux rates (Table 4-7). The control showed a statistically significant difference between initial and overall water flux rates ($P < 0.05$) with values of. -6.017 ± 10.68 to -27.618 ± 3.184 mL g^{-1} h^{-1} for initial and overall rates, respectively.

4.4.11 Effect of inhibitors on Ti and water flux on the perfused intestine

Addition of either nystatin or vanadate to the preparation had effects on the appearance of Ti in the serosal perfusate. Perfusate flow remained unaffected in the

presence of drugs (Fig. 4-12). The initial and overall Ti flux rates for the Bulk TiO_2 treatment in the presence of either inhibitor appeared to be unaffected relative to the no drug treatment. In contrast to the bulk treatment, the nano treatments exhibited marked reductions in initial and overall Ti flux rates relative to the no drug treatments, suggesting a particle size sensitive drug effect (ANOVA, $P < 0.05$). There was a 5 fold decrease in initial Ti flux rates for both the nystatin and vanadate nano treatments relative to the no drug treatment (ANOVA, $P < 0.05$). Overall Ti flux rates were also reduced relative to the no drug treatment albeit by a lesser amount than the initial Ti flux reduction. For example, overall Ti flux rates decreased from 7.846 ± 0.808 to 3.857 ± 0.284 nmol g^{-1} h^{-1} for the no drug nano compared to the vanadate nano treatment, respectively (ANOVA, $P < 0.05$) (Table 4-7).

The effects of these two drugs on the perfused intestine preparation caused a statistically significant increase in outward water flux in the controls (no added TiO_2). The nano TiO_2 treatment with vanadate appeared to cause a decrease in the overall net outward water flux relative to the no drug treatment, -48.731 ± 5.034 to -39.015 ± 3.705 mL g^{-1} h^{-1}. In contrast, the bulk vanadate treatment caused an increase in net outward water flux relative to the no drug treatment (-41.731 ± 5.034 to -52.766 ± 3.914 mL g^{-1} h^{-1} for the no drug bulk TiO_2 and vanadate bulk TiO_2 treatment, respectively) (Table 4-7).

Table 4-7: Effects of exposure to 1 mg L^{-1} TiO_2 with or without inhibitors on the Ti and water fluxes across the isolated perfused jejunum segment of rat intestine

	Net Ti flux, *Jnet Ti* (nmol $g^{-1}h^{-1}$)		Net water flux, *Jnet* H_2O (ml $g^{-1}h^{-1}$)	
Treatment	**Initial rate**	**Overall rate**	**Initial rate**	**Overall rate**
Control	2.814 ± 0.929	3.030 ± 0.241	-6.017 ± 10.68	$-27.618 \pm 3.184^{\dagger}$
Bulk TiO_2	4.402 ± 0.461	5.082 ± 1.257	$-31.316 \pm 14.321^{*}$	$-41.731 \pm 5.034^{*}$
Nano TiO_2	$25.08 \pm 2.454^{*d}$	$7.846 \pm 0.868^{*\dagger}$	$-33.989 \pm 14.731^{*}$	$-48.261 \pm 14.84^{*}$
Nystatin Control	3.373 ± 0.972	2.789 ± 0.664	-55.733 ± 14.767^{a}	-64.374 ± 10.51^{ac}
Nystatin Bulk TiO_2	4.589 ± 1.380	5.655 ± 1.198	-36.261 ± 3.848	-49.060 ± 7.420
Nystatin Nano TiO_2	5.330 ± 1.641^{a}	$5.751 \pm 1.669^{*!a}$	-46.990 ± 19.862	-49.206 ± 17.096
Vanadate Control	2.728 ± 0.483	2.464 ± 0.403	-30.501 ± 5.512^{b}	-32.701 ± 5.521^{c}
Vanadate Bulk TiO_2	$4.228 \pm 0.735^{*}$	4.799 ± 0.359	-51.918 ± 8.630	$-52.766 \pm 3.914^{*b}$
Vanadate Nano TiO_2	$5.965 \pm 1.489^{*c}$	3.857 ± 0.284^{b}	-43.455 ± 4.637	-39.015 ± 3.705^{bc}

Values are means ± S.E.M. (n = 5) expressed per gram dry mass of intestine per hour. Negative values indicate a net loss from the serosal solution. Initial and overall rates were calculated from cumulative perfusate data at 10 min and 4 h respectively.* Statistically significant difference from the control within drug groups and treatments; [a]Significant difference of nystatin trial compared to no drug trial within treatment; [b]Significant difference of vanadate trial compared to no drug trial within treatment; [c]Significant difference between nystatin and vanadate trials within treatments. [d] Significant difference between bulk and nano within drug treatments within columns [†]Significant difference between initial and overall flux rates (Kruskal-Wallis, ANOVA, and/or t-test $P < 0.05$).

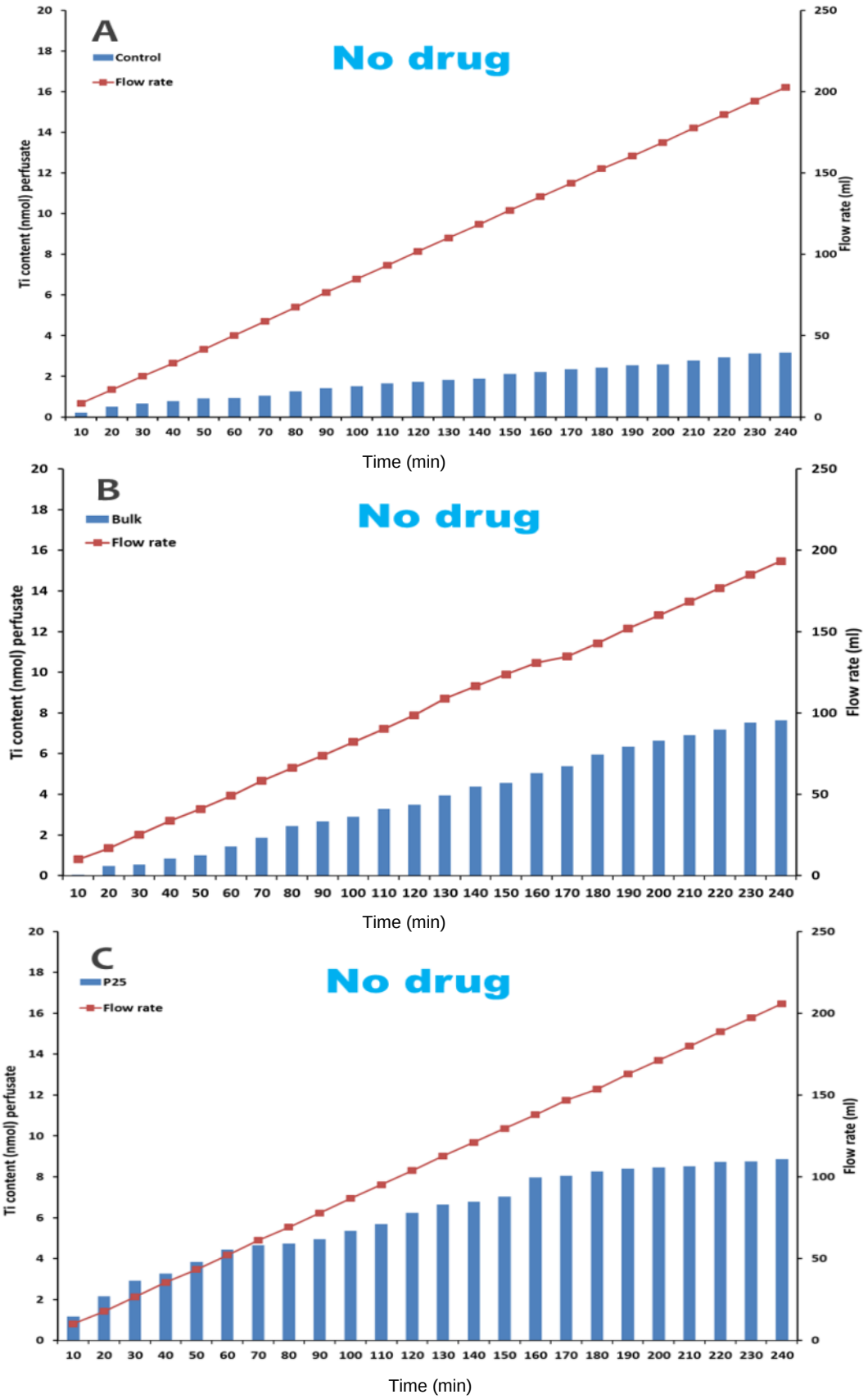

Fig. 4-11: The cumulative appearance of total Ti metal in the serosal compartment (blue bars, nmol Ti metal) of perfused intestine preparations from rat exposed to 1 mg L^{-1} of TiO_2 in the mucosal saline. Cumulative perfusate flow (red squares, mL) is also shown. Graphs are representative examples of individual perfusions from replicated experiments (all groups, n = 5 perfusions). (A) Control with no added TiO_2, (B) bulk TiO_2, (C) nano TiO_2. Rat weights (g) in the examples are 200, 190 and 220, respectively.

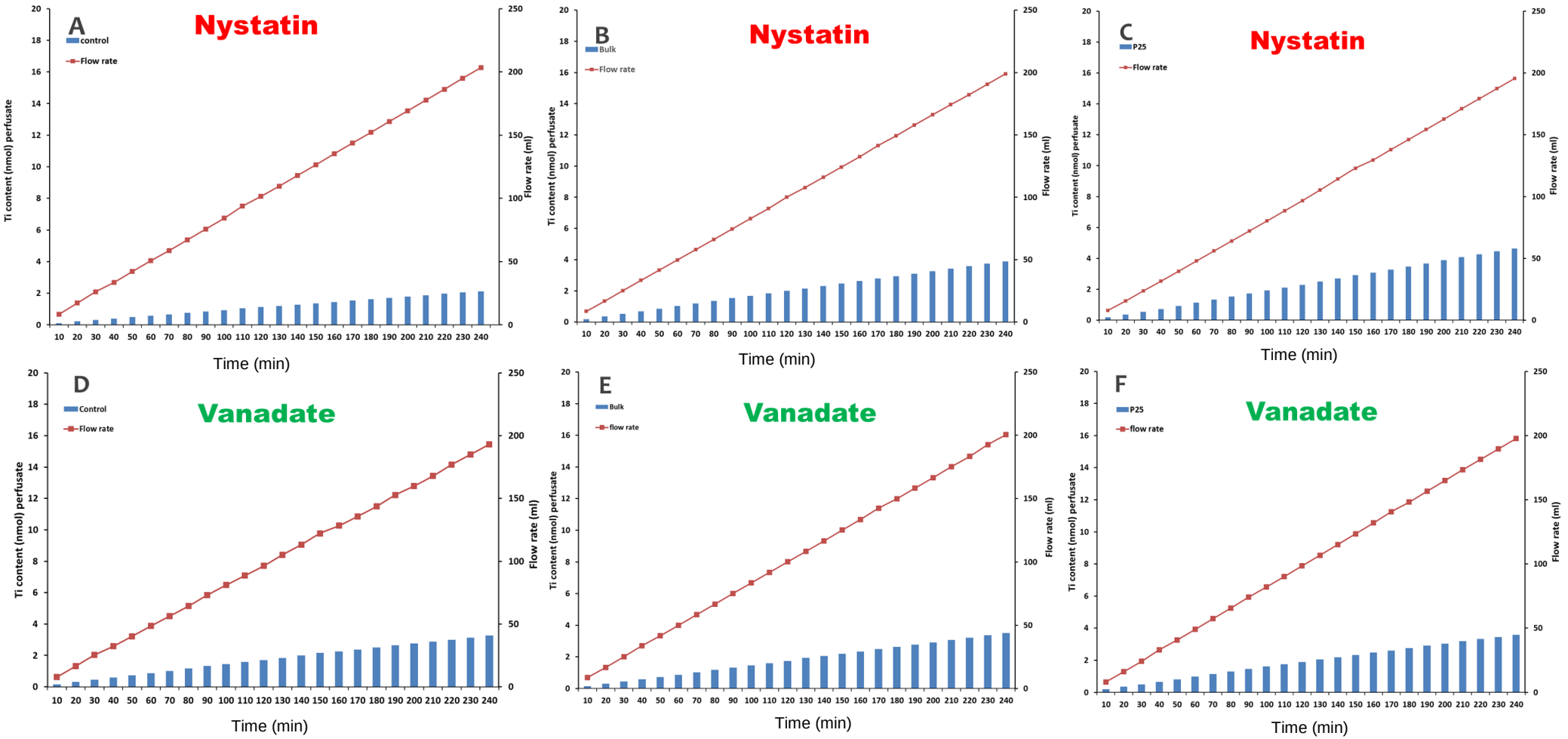

Fig. 4-12: The cumulative appearance of total Ti metal in the serosal compartment (blue bars, nmol Ti metal) of perfused intestine preparations from rat exposed to 1 mg L^{-1} of TiO_2 in the mucosal saline in the presence of either 120 IU mL^{-1} nystatin (mucosal solution) or 100 µmol L^{-1} sodium orthovanadate (serosal perfusate). Cumulative perfusate flow (red squares, ml) is also shown. Graphs are representative examples of individual perfusions from replicated experiments (all groups, n = 5 perfusions). (A) Control Nystatin treatment with no added TiO_2, (B) bulk TiO_2 in the presence of nystatin, (C) nano TiO_2 in the presence of nystatin, (D) Control vanadate treatment with no TiO_2, (E) bulk TiO_2 in the presence of vanadate, (F) nano TiO_2 in the presence of vanadate. Rat weights (g) in the examples are 180, 210 and 170, 190, 220, 190, respectively.

4.5 Discussion

This study is the first to show Ti tissue accumulation and Ti flux across the rat gut from bulk and nano TiO_2 exposures that are drug sensitive and in the opposite direction to water flux, implying that an active uptake mechanism is responsible. The presence of particles in the cells implies that at the apical membrane there is some particle internalisation. The key findings of this study are that Ti accumulation mainly occurs in the small and large intestine of the rat gut following exposure to TiO_2 particles (bulk or nano) with the majority of this Ti (ions or particles) found in the mucosa and not in the muscularis (Fig. 4-2, Table 4-1). There were material size effects on initial and overall Ti flux rates between nano and bulk TiO_2 exposures. The former was much greater than the latter (Table 4-7) suggesting that transport rate appears to be affected by particle size.

4.5.1 Where is TiO_2 absorbed along the gut?

To our knowledge regional differences in Ti accumulation along the whole rat gut have not been previously reported. In this study, treatment with either the bulk or nano TiO_2 resulted in Ti accumulating in all the regions of the gut, from the oesophagus to the hind intestine, but, this was only deemed significant along the whole of length of the small intestine (duodenum, jejunum, ileum) and the large intestine (Fig. 4-2). Importantly, the majority of the Ti in both nano and bulk TiO_2 treatments was in the mucosa rather than the muscularis (usually 70% or more, Table 4-1), indicating that some of the accumulated Ti was associated with the epithelial cells (see below).

The tissue appeared to be healthy with expected tissue water contents (water %), and there did not appear to be any major departures from normality for the major electrolytes (Table 4-2), particularly Na^+ which plays an essential role in maintaining osmoregulatory processes in tissues. The viability criteria for the whole gut sac were met suggesting that the tissue was not leaking and that Ti accumulation was not an artefact of osmotic solvent drag. Rather, the data suggests that the intestine (small and large) is the primary region of the gut involved in the uptake of Ti (particles or dissolved Ti) following TiO_2 exposures. The idea that the small intestine is involved in the uptake of metal (particles or dissolved species) in vertebrates is consistent with much of the literature on metal uptake in the vertebrate gut (Hoyle and Handy 2005, Handy *et al*. 2000, 2002, Al-Jubory and Handy 2013, Onishchenko *et al*. 2012). Approximately one third of the apparent accumulation of Ti metal in/on the gut sacs can be accounted for by surface adsorption, with about 55 nmol g^{-1} dry weight being instantaneously bound (Fig. 4-10), compared to 150 nmol g^{-1} dry weight in the gut sacs exposed to bulk TiO_2. Handy and Eddy (2004) found that dissolved ions can be detected in the blood after 90 s, and thus the binding experiment has to be shorter than this to measure true binding. A longer exposure may have resulted in a slightly elevated surface bound Ti component although the instantaneous surface binding of metals is not linear over time with the majority of the binding occurring in the first 30 s (Handy & Eddy 2004). Therefore, it is likely that only a small fraction of the Ti found in/on the gut sac (or perfused intestine) over 4 h is due to surface binding and that the Ti tissue measurement is reflective of Ti concentration in (accumulation) rather than on (adsorption) the tissue.

4.5.2 Viability of the perfused intestine

The viability criteria applied for the perfusion technique in this study were the same as previous research (Al-Jubory and Handy 2012, Handy *et al*. 2000). In brief, the histological integrity of the gut; perfusate and mucosal LDH activity; the leak of ions ($[K^+]$, $[Na^+]$) into the mucosal solution and the perfusate flow.

Histological and ultrastructural examination of the gut following the perfusions for all treatments showed normal morphology (Fig. 4-5, 4-6, 4-9) indicating a structurally sound intestinal barrier. LDH activity is regarded as a sensitive viability indicator (Campbell *et al*. 1999) and in this this study perfusate and mucosal LDH activity were below that found *in vivo* (< 2.2 U mL^{-1}, Gershbein and Raikoff 1977) in all experiments (Fig. 4-4). Electrolyte leak from the tissue into the mucosal solution was low with only statistically insignificant micromolar changes in Na^+ and K^+ concentrations (Table 4-3). Moreover, perfusate flow rates remained steady in all experiments (Fig. 4-11,). Similarly, addition of 120 IU mL^{-1} nystatin to the mucosal solution or 100 µmol L^{-1} sodium orthovanadate had little effect on the assessed viability parameters (Fig. 4-7 (LDH), 4-12 (Perfusate flow) and Table 4-4, 4-5 (mucosal solution electrolyte concentration)).

The pH of the mucosal solution fluctuated slightly with a net increase of 0.256 ± 0.023 (grand means of controls and treatments) suggesting either the uptake of H^+ ions by the tissue, or the efflux of bicarbonate (HCO_3^-) resulting in a more alkaline pH. The intestine is involved in osmoregulation and acid base balance. A net secretion of water and bicarbonate is expected without dramatic changes in tissue Na^+ and K^+, which was demonstrated suggesting that the physiological performance of the gut remained intact.

When viewed together the above criteria indicate thatthe perfused intestines remained in a viable condition throughout the experiments. Furthermore, this technique can be effectively used to measure Ti uptake (accumulation and uptake) from bulk or nano TiO_2 exposures in the delicate rat intestine at 37°C.

In order to clarify what is meant by 'expected' gut secretions it would have been useful to perform a positive control perfusion by administering a detergent to the mucosal solution. This information would have provided a bench mark for a non-viable gut prepartion. For example, the lack of histological integrity, reversing of water flux and the concomitant decrease of Na^+ and K^+ from the mucosal solution would have provided useful information about a failed preparation. The use of detergents to assess LDH leak however would likely give a gross underestimate of the bath LDH leak and subsequent tissue damage because of the expected reversal of water flux (from the bath into the tissue). Nevertheless a positive control would aid in data interpretation and have provided histological evidence of a damaged gut.

4.5.3 TiO_2 exposure and distribution of the particles in the mucosal solution

TiO_2 exposures were confirmed during gut perfusions by measuring the mass concentration of TiO_2 in the mucosal solution (Fig. 4-8) and by the detection of elevated total Ti metal concentrations in/on exposed tissues (Table 4-6). The concentrations measured by ICP-OES showed a decrease of Ti over time (Fig. 4-8). At the end of the 4 h perfusions the grand % loss of suspended TiO_2 were 62% and 20% for the bulk and nano treatment, respectively (Fig. 4-8), indicating a loss of Ti from the mucosal solution. This occurrence is well known for dissolved metals and is associated with the normal protective role of mucus secreted by the preparation

which will chelate and then precipitate metal ions (e.g., for Cu perfusions, 77% of the added Cu is lost at exposures of 100 µmol L^{-1}, Handy *et al*. 2000) or in the case of particles bind and promote settling. Moreover, the gravimetric settling of particles and the effect of a high ionic strength mucosal solution will enhance aggregation and subsequently, particle settling over time. The particle size distribution measures support the idea that at the end of the perfusion smaller particles remain suspended in the perfusate (Fig. 4-1) which may be why NPs maintain a more stable dispersion. Similar losses of Ti from mucosal solutions have been reported by Al-Jubory and Handy (2012) for TiO_2 particles in mucosal salines.

4.5.4 Ti accumulation and efflux in the perfused intestine

Total tissue Ti concentration increased in all intestines exposed to either bulk or nano TiO_2 in comparison to the control. There were no material type differences on tissue Ti concentration (Table 4-6). Nevertheless, because Ti accumulates in the tissue this suggests that the efflux of Ti from mucosa to serosa is slower than apical uptake of Ti. Interestingly, the mean values reported herein for tissue Ti accumulation are three times higher for the bulk treatment in perfused rat intestine (0.265 µmol g^{-1} dry weight) than in trout intestine (0.094 µmol g^{-1} dry weight (Al-Jubory and Handy 2012) and 15 times higher for the nano treatment (0.293 µmol g^{-1} dry weight herein compared to 0.019 µmol g^{-1} dry weight (Al-Jubory and Handy 2012). Overall Ti flux rates are also considerably higher (for bulk Ti flux in rat intestine 5.082 ± 1.257 whilst in trout intestine 0.85 ± 0.32 nmol g^{-1} h^{-1} (Al-Jubory and Handy 2012); for nano exposed rat intestine 7.846 ± 0.868 for trout intestine 2.38 ± 0.68 nmol g^{-1} h^{-1} (Al-Jubory and Handy 2012). Possible explanations for this observation include anatomical differences and differences in the perfusion temperature, and the metabolic rate of trout in comparison to rats. Metabolic rates in endotherms are typically higher than ectotherms and the temperatures at which the perfusions were performed would exacerbate these differences (15°C- trout, 37°C rat). It would be interesting to see whether reducing rat intestinal perfusion temperature to 15°C would reduce uptake (Ti flux) and tissue accumulation of Ti to the levels demonstrated in trout perfusions.

The form of detected tissue Ti is unknown, although TEM images of enterocytes following perfusions showed particles of similar morphology to those characterised in the stock solutions beneath the apical membrane in vesicles (Fig. 4-1 and Fig. 4-9). Analogous observations have been made in rat and mouse gut associated lymphoid

tissue (rat - 12.5 mg kg^{-1} for 10 days - Jani *et al*. (1994); mouse – 12.5 mg kg^{-1} - Brun *et al* (2014)) and trout intestinal enterocytes (Al-Jubory and Handy 2012) suggesting (at least at the apical membrane) that the Ti is still in particulate form.

Perfused intestine exposed to both bulk and nano TiO_2 (no pharmacological inhibitors) demonstrated a cumulative increase of total Ti in the serosal perfusate (Fig. 4-11), suggesting transepithelial uptake of Ti or TiO_2 from TiO_2 exposures. The possibility of some dissolved Ti into the serosal compartments cannot be excluded (Al-Jubory and Handy 2012). In a cellular environment at physiological pH (7.4) the majority of free Ti would likely complex with chloride ions then water prior to binding oxygen and precipitating back into TiO_2. Stable ionic $Ti^{(+)}$ species would only be found in miniscule concentrations and in physiological conditions these species would be found at the centre of anionic complexes such as $Ti(OH)_4$ (Schmidt and Vogelsberger 2009). Interestingly Al-Jubory and Handy (2012) showed that the dissolution rate of particles in a high KCl solution (typical of intracellular environments) is between 18-26 nmol Ti metal h^{-1}, which represents around 0.01% loss of metal from the particles every hour (Al-Jubory and Handy 2012. Therefore, it remains possible that a small percentage of detected serosal Ti is ionic.

The nano TiO_2 exposures resulted in higher amounts of Ti in the serosal perfusate than the bulk material, and initial and overall flux rates of Ti for nano TiO_2 exposures were much greater than both the control and bulk treatment Ti flux rates (Table 4-7). A possible explanation for this observation may simply be that the particle size influences uptake and efflux rate and that smaller particles are taken up and transported faster than larger particles. This has been demonstrated in a number of different models, for example, SiO_2 transport in HepG2 cells (Hu *et al*. 2011); and in the Desai *et al*. (1996) rat in situ intestinal loop preparation which demonstrated a 15

– 250 fold increase in uptake for 100 nm polylactic polyglycol particles compared to 500 nm and 1 µm. Moreover, initial Ti flux rates in the nano treatment were considerably larger than the overall flux rates (Table 4-7). A possible explanation may be due to saturation of the processes mediating particle translocation (possibly ATP availability or vesicle scission proteins) which is indicative of active transport systems.

4.5.5 Mechanism(s) of TiO_2 transepithelial uptake

The appearance of Ti in the eluted perfusate in conjunction with the outward net water flux (from tissue to mucosal bath (Table 4-7)) and negligible changes in mucosal and tissue electrolytes (K^+, Na^+) imply that a carrier mediated mechanism(s) is responsible for Ti translocation rather than a passive mechanism such as solvent drag associated with osmotically stressed tissue.

This is also supported by the effect that addition of inhibitors such as vanadate or nystatin had on the perfused intestine. Both drugs caused mean increases in Ti tissue concentrations (Table 4-6). There was a significant decrease in the serosal efflux of Ti from nano TiO_2 exposures relative to the no drug trials (Table 4-7) whilst Ti flux rates from bulk particle exposures were unaffected by both drugs even though mean Ti tissue concentration was elevated relative to the no drug bulk TiO_2 exposure. This tentatively suggests that there may be different uptake pathways for different sized particles.

Vanadate increases the rate of apical caveolae budding into the cell (Parton *et al*. 1994) through tyrosine phosphatase inhibition which results in the unregulated

activation of a tyrosine kinase signalling pathway leading to increased rates of caveolae budding (Parton and Richards 2003; Nucifora and Fox 1999) and subsequent apical uptake. The reduction of Ti efflux into the serosal compartment in the presence of vanadate in the nano treatment suggests some differential drug sensitivity which may be due to increased dissolution potential of nano TiO_2 in intracellular fluid (Al-Jubory and Handy 2012) due to an increased material surface area. Inhibition of ATPases is known to be involved in loading metal ions into vesicles destined for exocytosis at the basolateral membrane (For example, Cu ions are loaded into the trans Golgi network through the action of Cu-ATPase (Dameron and Harrison 1998)) would reduce efflux of Ti. Ti could potentially cross the cell using similar ATP-ase trafficking systems to Cu, which are known to be hijacked by other non-essential toxic metals like mercury (Hoyle and Handy 2005). Inhibition of metal-transporting ATPases on the basolateral membrane may result in the observed net increase in tissue Ti concentrations (Table 4-6). Further work elucidating the exact mechanism by which vanadate interferes with uptake and transport is required.

Similarly, Ti efflux was reduced in nano exposures in the presence of nystatin suggesting differential drug sensitivity influenced by particle size. Nystatin has been shown to sequester cholesterol, which is thought to be involved in the production of exocytic vesicles in cells (Chintagari *et al*. 2006; Salaun *et al*. 2004). Reduction of exocytosis apically or basolaterally would result in a net increase of tissue Ti. Al-Jubory and Handy (2012) showed that nystatin prevented transepithelial uptake of Ti from exposures of TiO_2 particles and this occurred with a concomitant increase of total Ti in the intestinal tissue. Curiously flux rates from bulk Ti seemed unaffected even though there was a significant increase in tissue Ti (bulk nystatin exposure

tissue Ti concentration of 0.673 ± 0.133 compared to 0.265 ± 0.044 µmol g^{-1} for the bulk no drug exposure - Table 4-6). More research is required to assess particle size effects on uptake. Regardless, the observed nystatin/vanadate - sensitive Ti accumulation (Table 4-6) is indicative of active mechanism(s) for handling either Ti metal or TiO_2 particles by intestinal tissue.

4.5.6 The effect of TiO_2 on water flux and tissue electrolytes in the perfused intestine

Exposure to either bulk or nano TiO_2 caused an increase in initial and overall net outward water flux (Table 4-7) in comparison to the control without dehydrating the tissue or significantly altering tissue Na^+. A possible explanation for this includes an increase in the oncotic (colloidal osmotic pressure) pressure of the mucosal saline through the addition of TiO_2 particles. Significant increases in colloidal osmotic pressures have been demonstrated in solutions containing 1 g L^{-1} silicon dioxide NP dispersions in comparison to pure water (Quant *et al*. 2008). Moreover, colloidal pressure increased by 30% when temperature of the dispersion was increased from 26 to 36°C (Quant *et al*. 2008).

Tissue electrolyte concentrations were not significantly affected following TiO_2 exposures in the absence of drugs relative to controls, but, there were some trends which should be mentioned. The increase in net water efflux was accompanied by reduced mean tissue K^+ levels relative to the control (probably due to solvent drag associated with water efflux), and increased mean tissue calcium levels. Although not significant this pattern of electrolyte changes following exposures to TiO_2 has

been demonstrated in previous studies (Chapter 2, Section 2.4.4, Chapter 3, Section 3.4.4).

The mechanisms responsible for these changes are uncertain although passive solvent drag of K^+ out of the tissue and reduced Na^+/K^+ ATPase activities may provide a tentative explanation for these changes. Reduction of intestinal Na^+/K^+ ATPase activity has been demonstrated in fish exposed to 1 mg L^{-1} TiO_2 (Federici *et al*. 2007). Ramsden *et al*. 2009 also demonstrated a 50% reduction in brain Na^+/K^+ ATPase activity in trout brain following 8 week dietary exposures in trout to 100 mg kg^{-1} TiO_2 NP diets.

Elevation of intracellular calcium in epithelial cells or whole tissues exposed to TiO_2 particles has also been demonstrated (Gitrowski *et al*. 2014- Caco-2 cells-Chapter 2 and Chapter 3, Al-Jubory and Handy 2012- Trout intestine, Simon *et al*. 2011 Lung epithelium cells). The mechanisms underpinning these changes in calcium homeostasis are also unclear, although, inhibition of, Ca^{2+} ATPase, Ca^{2+}/Mg^{2+} ATPase in mouse brain following oral TiO_2 exposures has been demonstrated (Hu *et al*. 2010). TiO_2 interference with electrolyte homeostatic mechanisms would be worthy of further investigation.

4.5.7 Effects of inhibitors on tissue electrolytes

Metabolic ion transporters are expected to cause changes in the electrolyte cocnetrations in cells and tissues. 100 µmol L^{-1} serosal administration of vanadate caused an increase in tissue Na^+ and a decrease in K^+ concentrations in comparison to the no drug treatments. This is to be expected, considering vanadate inhibits

Na^+/K^+ ATPase activity resulting in tissue Na^+ increases due to passive influx and concomitant decreases in tissue K^+ via passive efflux (with the concentration gradient). Tissue calcium levels increased in the presence of vanadate compared to no drug controls. This is most readily explained through vanadate's inhibitory effect on Ca^{2+} ATPase (Barrabin *et al*. 1980) and the subsequent reduction in efficacy of the sodium calcium exchanger (Blaustein and Lederer 1999) which hinders the efflux of calcium that has entered the cells down the extreme diffusion gradient (10^{-3} M outside, 10^{-6} M inside) resulting in the increase observed herein. Similar changes in electrolytes have been demonstrated in trout intestine in the presence of vanadate (Al-Jubory and Handy 2012). Likewise 120 IU ml^{-1} mucosal administrations of nystatin caused increases in Na^+ and Ca^{2+}. Nystatin is well known for increasing cell membrane permeability to monovalent cations (e.g. Na^+) (Eilam and Grossowicz 1982), which in turn will reduce the efficacy of the sodium calcium exchanger (reduces the concentration gradient of Na^+) resulting in an increase in cellular calcium (Blaustein and Lederer 1999).

4.5.8 Concluding remarks

This study shows that the primary areas of Ti absorbtion from TiO_2 exposures (bulk and nano) are the small and large intestine. Moreover, the isolated perfused intestine preparation works with NPs in rat jejunum and the expected viability criteria are met with these materials. Additionally, this work demonstrates that Ti or TiO_2 from TiO_2 exposures can cross the mammalian intestine. There is a material-type effect with much higher Ti flux in to the serosal compartment from the nano form. Ti or TiO_2 absorption and transport from both bulk and nano TiO_2 exposures are time-

dependent, saturable and in the opposite direction to water flux, with tissue accumulation being affected by pharmacological inhibitors. Taken together this suggests an active absorption mechanism is responsible rather than passive diffusion. From a regulatory perspective, a dietary exposure hazard to human health should be considered in risk assessments. The overall net uptake rates reported here for Ti are between 5-7 nmol g^{-1} h^{-1} depending on particle size roughly double those reported for copper (Handy *et al*. 2000), but about 10 fold less than Hg uptake rates (40-50 nmol g^{-1} h^{-1} for 0.2-2 mg L^{-1} of Hg metal, Hoyle and Handy 2005) in the perfused intestine. The fact that Ti or TiO_2 from the nano form is transported faster than bulk TiO_2 also implies that risk assessments based on the bulk material will underestimate the nano systemic distribution hazard. The assumption that the traditional bulk forms of TiO_2 powders are not absorbed via the small intestine should also be reconsidered. The risk of dietary exposure to NPs is likely to increase through a number of avenues (toothpaste, food) with the major exposure route associated with drinking water processed through wastewater treatment plants (Westerhoff *et al*. 2011). Long term chronic exposure scenarios to nano TiO_2 need to be performed in order to clarify whether an increased uptake risk is associated with an increased risk of developing pathological conditions.

Chapter 5: Age and feed status effects on tissue Ti concentration in female Wistar rats (*Rattus norvegicus*): A pilot study

5.1 Abstract

Titanium dioxide nanoparticles (TiO_2 NPs) have potential applications as food additives, but concerns persist about their safety, absorption and subsequent systemic distribution following oral exposures. Children are identified as having the highest exposure and may face the greatest health risks. The toxicological sensitivity of TiO_2 in different aged mammals following oral exposure is not clear.

The aim of this pilot study was to determine whether animal age influences Ti tissue concentration in secondary target organs (kidney, liver, spleen) following *ad libitum* food consumption of a standard maintenance diet known to contain Ti; and to assess whether Ti tissue concentrations in rats changes in the absence of food. Young (23 day old) female rats demonstrated significant decreases in brain, spleen, lung tissue and whole blood Ti concentrations following the removal of feed (Mean Ti concentration of feed was 3.28 mg g^{-1} dry weight) for 48 h. For example, whole blood Ti concentrations decreased from 19.1 to 6.2 nmol mL^{-1} in fed and food deprived animals, respectively (Student's *t*-test, $P < 0.05$). Older (3 - 6 months) rats demonstrated no differences in tissue Ti concentration associated with feed status. Critically, there was an age effect with older rats demonstrating lower tissue Ti concentrations in liver, kidney and spleen following long term chronic dietary exposures to relatively large concentrations of Ti in comparison to young rats. Overall the data demonstrate that young rats show rapid decreases in whole blood and tissue Ti concentrations when standard laboratory feed is removed. The implications of this study suggest *in vivo* chronic oral exposure studies with TiO_2 need to assess the Ti concentration of control feed.

5.2 Introduction

The European Union allows TiO_2 to be applied in food products at *quantum satis* levels under good manufacturing procedures (European Union 2003). Worldwide human consumption of food grade TiO_2 in 2012 was estimated to be almost 6 metric tonnes (USGS 2013). Moreover, TiO_2 is permitted for use in animal food stuffs at *quantum satis* levels, and because it is not a nutritionally required mineral, the concentration and form does not need to be explicitly mentioned in animal diet formulations (European Union 2003).

The FAO/WHO Expert committee of food additives tasked with evaluating the toxicity of TiO_2 historically concluded that there was no need to establish daily intake levels due to its insolubility, lack of absorption and lack of accumulation (JECFA 1969). Since this original toxicological assessment, numerous *in vivo* and *in vitro* studies have demonstrated Ti/TiO_2 uptake and translocation from TiO_2 exposures across vertebrate GIT epithelium following oral exposures (Jani *et al*. 1994; Wang *et al*. 2007; Cui *et al*. 2010; Al-Jubory and Handy 2012; Tassinari *et al*. 2014). Interestingly, Ti/TiO_2 from both nano and bulk TiO_2 particle exposures has been detected in systemic body sites or the serosa following exposures to vertebrate intestinal epithelium (Jani *et al*. 1994; Al-Jubory and Handy 2012, Chapter 4).

For example Al-Jubory and Handy (2012) confirmed the appearance of Ti from 1 mg L^{-1} nano and bulk TiO_2 (aggregate diameter of bulk 1124 ± 331 nm) in the serosal fluid following mucosal administration of TiO_2 particles (bulk and nano) to perfused trout intestine and this occurred in a saturable time dependent fashion. Pharmacological evidence implied this was an active process (Al-Jubory and Handy 2012), and TEM evidence indicated a proportion of the Ti within enterocytes was in

particulate form (TiO_2). Jani *et al*. (1994) demonstrated *in vivo* gastrointestinal absorption and translocation of Ti from (liver, kidney, spleen) TiO_2 particle (500 nm diameter) exposures following daily oral gavage of 12.5 mg kg^{-1} TiO_2 particles for 10 days. SEM evidence implied at least some of the Ti was still in particulate form (TiO_2). More recently, Tassinara *et al*. (2014) orally exposed rats to TiO_2 NPs (< 25 nm diameter) for 5 days at a concentration of 2 mg kg^{-1} b.w day^{-1}, and reported a significant mean tissue Ti increase of 0.01 µg g^{-1} wet weight in the spleen. In contrast, Cho *et al*. (2013) demonstrated no changes in organ or whole blood Ti concentrations relative to controls animals following daily TiO_2 NP exposures of 1073.5 mg kg^{-1} b.w day^{-1} for 13 weeks. This lack of agreement in the literature may be due to a number of factors. For example, the crystal structure of theTiO_2 particles used was different. Tassinara *et al*. (2014) used a pure anatase (< 25 nm diameter), while Cho *et al* (2013) used an 80/20 % anatase/rutile mix (26 nm diameter). Moreover, the age of the rats used in both studies was different. In the Tassinara *et al*. (2014) study the rats were 8 weeks old, whilst in the Cho *et al* (2013) study the rats were 19 weeks old at the time of sampling.

The effect of age on metal uptake metabolism and toxicity for non-nutritionally required metals is poorly understood. A recent study by Wang *et al*. (2013) assessing the comparative toxicity of TiO_2 NPs in 3-week (youth) and 8-week (adult) old Sprague-Dawley rats following oral exposure of 10, 50, 200 mg kg^{-1} bw day^{-1} TiO_2 NPs for 30 days demonstrated increased intestinal permeability to TiO_2 NPs in younger rats. Moreover severe liver oedema, heart injuries and non-allergic mast cell activation in stomach tissue were reported in 3 week old rats. In contrast 8 week old rats exhibited only slight toxic effects (Wang *et al*. 2013). There is limited information on the toxicological sensitivity and accumulation potential of TiO_2 in different aged

animals which is of concern considering children are thought to preferentially consume food products that contain more TiO_2 than their adult counterparts (Weir *et al*. 2012). Historically, increased metal accumulation and tissue distribution in younger animals relative to older animals has been well demonstrated for some metals e.g. lead, iron (Forbes and Reina 1972), cerium (Inaba and Lengemann 1972) and copper (Terao and Owen 1977), whilst the opposite has been shown to occur for other metals (e.g. mercury- Weiner and Nylander 1993; Cadmium -Wong *et al*. 1980). These age differences in metal uptake are attributed to differences in ADME. For instance copper and iron are readily taken up across the placenta leading to an increase in metal tissue concentrations in prenatal animals and post natal animals. As the animal develops, metal handling mechanisms are able to excrete some nutritionally and non nutritionally required metals. In contrast mercury and cadmium tissue concentration increases with age because these metals are poorly excreted and accumulate over the life time of the animal. Given this, it is unclear where TiO_2 sits in terms of accumulation profiles compared to other non-nutritionally consumed metals.

Chapter 4 Section 4.3.1 demonstrated that standard laboratory rodent feed had a mean Ti concentration of 3.28 mg g^{-1} of feed. Assuming rats consume 5 g of food per 100 g of body weight (Bogdanske *et al*. 2011) rats are exposed to 164 mg kg^{-1} bw day^{-1} Ti through their normal diet. This is considerably higher than concentrations used in recent studies aimed at assessing the Ti tissue distribution following TiO_2 oral exposures (e.g. 6.8-8.6 mg kg^{-1} bw day^{-1} for 5 days (Geraets *et al*. 2014); 1-2 mg kg^{-1} bw day^{-1} for 5 days (Tassinari *et al*. 2014); single oral dose 12.5 mg kg^{-1} (Brun *et al*. 2014)). A number of recent studies assessing absorption and distribution of Ti from TiO_2 exposures have failed to evaluate, or specify the Ti concentration of

the food that animals are fed during experimental procedures (Wang *et al*. 2007; Cho *et al*. 2013; Geraets *et al*. 2014; Tassinari *et al*. 2014). Moreover, the primary method for detecting tissue Ti in these studies is though total metal concentration determined by ICP-OES or ICP-MS; which makes it difficult to differentiate newly acquired Ti from the experimental exposure compared to that derived from the food of the animals. This problem of detecting newly acquired metal against an existing tissue background is well known for nutrients such as iron and copper (Que *et al*. 2008; Niwa *et al*. 2014), but has not been previously considered for TiO_2.

The primary objectives of this pilot study were to assess whether Ti could be detected in a variety of primary target organs in rats and then determine whether animal age influences Ti tissue concentration in these target organs (kidney, liver, spleen) following *ad libitum* food consumption of a standard maintenance diet known to contain Ti; and to assess whether Ti tissue concentrations in rats change in the absence of food. Further aims included assessing the physiological effects of acute food deprivation on tissue electrolytes and proximal carcass composition in young rats.

5.3 Materials and methods

5.3.1 Stock animals and diet

Female Wistar rats of different ages (21, 110 and 172 days, respectively) bred in the University of Plymouth animal facilities were used for this study. The standard living conditions and feed were the same as those described in Chapter 4 Section 4.3.1. Rats were fed a standard formulation (2018 Teklad Global 18% protein rodent diet,

Harlan Laboratories) comprised of 18, 5 and 5 % of protein, fat and fibre respectively. ICP-OES analysis of total metal concentrations in the feed revealed a measured Ti concentration of 3.28 ± 0.61 mg g^{-1} dry feed (mean ± S.E.M., n = 5). Characterisation of the form of Ti in the feed was not possible. SEM with concomitant X-ray analysis (SEM, JEOL/JSM-7001F Oxford instruments INCA X-ray analysis system) of feed samples revealed no discrete particles of Ti amongst the food matrix.

5.3.2 Treatments

The first pilot experiment determined the effect of age on trace element and electrolyte concentrations in a selection of target organs in rats. The concentration of Ti, K^+, Na^+, Ca^{2+} and Mg^{2+} in the spleen liver and kidneys of rats of different ages (23, 110 and 172 days old, respectively) were compared with unfed (48 h without food) rats of the same age. The weight (g) of each group of rats (in age order) at the beginning of the experiment was 75 ± 1.3, 186 ± 2.5 and 202 ± 2.3 g (Means ± S.E.M, n = *12*), respectively.

The second pilot experiment investigated the effect of 48 h without food on carcass, tissue and whole blood electrolytes in 23 day old rats. Moreover, proximate carcass composition analysis was also performed with a view to assessing changes in protein, lipid and energy composition in 23 day old unfed rats in comparison to rats fed the standard diet *ad libitum*. The weight (g) of the rats at the beginning of the experiment was 79 ± 2.1 (means ± S.E.M, *n = 10*).

5.3.3 Tissue sampling

Rats were humanely sacrificed by cervical dislocation (in compliance with ethical approval in the UK) following asphyxiation with CO_2. Tissues/organs were carefully removed for electrolyte analysis in the following order; brain, liver, kidney, spleen, intestine and skinned muscle from the *bicep femoris* and then processed for ion analysis. Contents of the gastrointestinal tract were removed by rinsing the lumen with physiological saline (as described in Chapter 4, Section 4.3.2). The skinned eviscerated carcasses, and excised tissues, were separately weighed (wet weight) and then all the separate tissues were dried to a constant weight at 100°C for up 48 h (Gallenkamp Oven BS Model OV-160). The moisture content of tissues was determined by taking the weight of the tissue before and after oven drying and calculated as: ((wet weight - dry weight) / wet weight) x 100.

Dried tissues were subsequently transferred into separate 20 ml scintillation vials (VWR International Ltd, Poole, UK) and digested in 1 or 4 ml (depending on tissue weight- See Chapter 4, Section 4.3.6) of concentrated nitric acid for 3 h at 70°C in a water bath before following the same exact digestion protocol mentioned previously (Chapter 4, Section 4.3.6).

5.3.4 Proximate analysis of eviscerated carcasses and diet

Carcasses and diet were subjected to analysis for determination of moisture, protein, lipid, ash and gross energy. Samples were ground into a fine powder and analysed on a dry matter basis. Analysis was conducted in duplicate for each sample according to AOAC (2007) guidelines and is described in the following sections.

5.3.5 Crude protein

Determination of total crude protein in the diets and feed ingredients was performed in duplicate for each animal by the Kjeldhal method, which determines total nitrogen content of samples which is assumed to come from protein (McDonald 2009). Total nitrogen is multiplied by a factor of 6.25 (a definition assuming that animal protein contains 16% nitrogen) to calculate the crude protein content. Briefly, ~100 mg of dried sample was weighed directly into a micro Kjeldahl tube along with one catalyst tablet (3 g K_2SO_4, 105 mg $CuSO_4$ and 105 mg TiO_2; BDH Ltd. Poole, UK) and 10 ml low nitrogen 98% sulphuric acid (H_2SO_4) (Sp. Gr. 1.84, BDH Ltd. Poole, UK). Digestion of samples was performed with a Gerhardt Kjeldatherm digestion block (Gerhardt Laboratory Instruments, Bonn, Germany) using the following protocol; 100 ºC for 30 min, 225 ºC for 45 min (1 h if samples had high lipid content) and 380 ºC for 1 h. Once digestion was complete and following a cooling period, the samples were distilled using a Vodapest 40 automatic distillation unit (Gerhardt Laboratory Instruments, Bonn, Germany), the distillate was neutralised with 0.1 M H_2SO_4 and from the titration value the crude protein value was determined using the following formula: (McDonald 2009).

% Nitrogen = (ml sample Titrant – ml Blank Titrant) x (Acid Normality) x (MW of Nitrogen) / Sample wt.

5.3.6 Lipid

Lipid content was determined in duplicate for each sample using the Soxhlet extraction method (Sukhija and Palmquist 1988). Briefly, ground carcasses and diets were weighed (~3 g) and placed into a cellulose thimble lightly plugged with cotton wool and inserted into the condensers and raised into the 'rinsing' position of a SoxTec™ extraction system (Tecator Systems, Högnäs, Sweden; model 1043 and service unit 1046). Pre-weighed glass cups containing 40 ml of petroleum ether (to dissolve the fat) were clamped into the condensers and extraction levers were moved to 'boiling' position for 30 min. Following this, the extraction levers were set to 'rinsing' position for 45 min (to evaporate the ether). The glass cups containing the extracted lipid were then left to cool for 30 min and weighed. Total lipid was determined by the following formula:

Total lipid (%) = ((final weight of beaker – initial weight of beaker) / initial sample wt.)) x 100

5.3.7 Ash

Ash (total mineral or inorganic content) content was determined in duplicate for each sample by adding a known sample weight (~500 mg) to a pre-weighed ceramic crucible. The crucibles and samples were then incinerated in a muffle furnace (Carbolite, Sheffield, UK) at 550°C for 12 h. After cooling in a dehumidification chamber, percentage ash was determined from the sample residue by:

Ash (%) = ((Sample residue (g) – crucible wt. (g)) / (initial sample wt. (g))) x 100

5.3.8 Gross energy

Gross energy was determined in duplicate for each sample in MJ kg^{-1} with a Parr Adiabatic Bomb Calorimeter model 1356 (Parr Instrument Company, IL, USA). Briefly, ground carcasses were compressed into a 1 ± 0.5 g pellet and weighed. The pellet was then placed into a nickel crucible with a 10 cm length fuse wire, which was formed into a 'U' shape to touch the pellet. The crucible was then carefully placed into the chamber and filled with oxygen to complete the loading process. The bomb was then placed in a vessel containing 2 kg of water to determine the released heat energy. Prior to initiating the reaction the sample weight was keyed into the calorimeter for determination of MJ gross energy per kg as calculated by the instrument algorithm.

5.3.9 Trace metal analysis

The same protocol described in Chapter 4, Section 4.3.6 was followed. The instrument limit of detection (L.O.D) (calculated using - 3 x standard deviation of the blank + the mean of the blank (n = 6)) (Thomsen *et al*. 2003) using matrix matched standards were calculated as 3.3 µg L^{-1} which is equivalent to 70 nmol L^{-1} of Ti metal, and for the entire digestion protocol (procedural blank) 4.05 µg L^{-1}(equivalent to 0.084 µmol L^{-1} of Ti metal, and for a typical 0.5 g tissue sample equates to 0.003 µmol Ti metal g^{-1} dry weight of tissue. L.O.D for matrix matched blanks and procedural blanks for Na^{+}, K^{+}, Mg^{2+}, Ca^{2+}, Fe, Cu and Zn are listed in Table 5-1. All analysed sample data was above the detection limits calculated from procedural blanks.

Given that the form of Ti in the food was unknown, spike recoveries were performed on rat liver with Ti metal, Bulk TiO_2 and P25 TiO_2 NPs. Liver tissue was selected as the spiking medium because research by Shaw *et al*. (2013) has demonstrated that tissues with a high lipid concentration give reduced Ti recovery rates following spiking of TiO_2 NPs relative to other organs. The digestion protocol (Chapter 4, Section 4.3.6) gave good recoveries for rat liver spiked with 200 µL of 6 mg L^{-1} Ti metal (which for a 16.2 ml sample is equivalent to a spiked Ti concentration of 74 µg L^{-1} Ti metal) and average recoveries for liver spiked with 200 µL of 10 mg L^{-1} Bulk or nano P25 TiO_2. Percentage recoveries were (Mean ± S.E.M, n = 6): 67.4 ± 6.9, 65.8 ± 1.8 and 92.5 ± 6.8% for bulk, nano P25 and Ti metal, respectively, for spiking at the end of the digestion protocol (analytical spikes) (Fig. 5-1). Tissue Ti is reported as nmol Ti metal g^{-1} dry weight and tissue and blood electrolytes are reported as µmol Ti metal g^{-1} dry weight or µmol mL^{-1}, respectively.

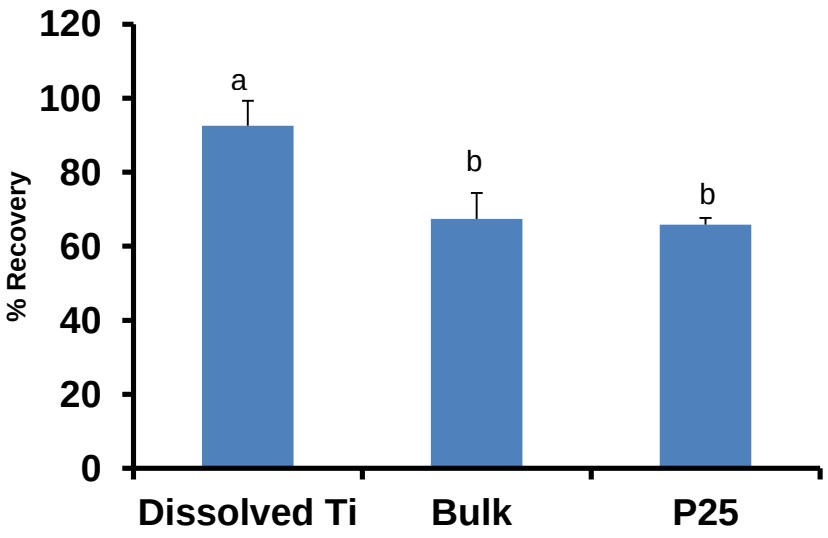

Fig. 5-1: Analytical recovery of Ti in liver tissue digests spiked with 200 µL of 10 mg L^{-1} TiO_2 or 6 mg L^{-1} Ti metal. Data are mean ± S.E.M % recovery of Ti metal or TiO_2 particles spike, *n = 6*; Different letters indicate statistically different recoveries for the spiked material (ANOVA *P* > 0.05)

5.3.10 Statistics

Routine statistics were the same as those described previously (Chapter 4, Section 4.3.10).

Table 5-1: ICP –OES matrix matched and procedural blanks limit of detection

	Matrix matched		Procedural matrix matched		L.O.D. for a 0.5 g tissue sample
Element	**µg L^{-1}**	**µmol L^{-1}**	**µg L^{-1}**	**µmol L^{-1}**	**Metal µmol g^{-1} dry weight**
Na	69.89	3.042	77.87	3.386	0.108
K	514.14	13.18	601.33	15.419	0.493
Mg	5.19	0.225	5.1	0.213	0.007
Ca	6.54	0.164	8.17	0.204	0.007
Fe	4.46	0.173	5.11	0.197	0.006
Cu	5.39	0.085	6.24	0.098	0.003
Zn	4.17	0.064	5.33	0.081	0.003
Ti	3.3	0.069	4.05	0.084	0.003

Values are means *n = 6*. L.O.D is calculated using the following formula: 3 x Std deviation of the blank + the average of the blank. Estimated detection limits for a 0.5 g sample are calculated from procedural matrix matched detection limits in µmol L^{-1}. Briefly (0.016 (L) * L.O.D Metal (µmol L^{-1})) / 0.5 g (Dry tissue) = µmol Metal g^{-1} dry weight. Procedural blanks have been subjected to the full digestion protocol (Chapter 4, Section 4.3.6).

5.4 Results

5.4.1 Pilot study 1: The effect of feed status and age on tissue Ti and electrolyte concentrations

Removing feed for 48 h had the expected effects on weight loss, with younger animals losing relatively more weight as a % of body mass than older animals. The mean weight loss as a % of initial body weight post removal of food was 9.7 ± 1.3, 4.4 ± 1.1 and 2.9 ± 0.6% for 23, 110 and 172 day old rats, respectively. Rats fed until sampling had a mean % weight increase of 4.5 ± 0.7, 2.0 ± 0.6 and 0.3 ± 0.3% for 23, 110 and 172 day old rats, respectively (Fig. 5-2).

The mean Ti concentrations of rat spleen, liver and kidney for different aged animals that had been fed for 48 h or fed *ad libitum* until sampling is shown in Fig. 5-3; Panel A, B, C. Young fed rats demonstrated higher mean Ti tissue concentrations than unfed rats. These differences reduced with increasing age.

The mean concentration of Ti in the spleen of fed 23 day old rats was significantly greater than unfed animals (t-test, $P < 0.05$). The values were (Mean ± S.E.M) 98.2 ± 17.6 and 40.9 ± 7.8 nmol g^{-1} dry weight for fed and unfed animals respectively. Mean liver and kidney tissue Ti concentrations in fed 23 day old rats were also elevated compared to unfed rats, although this was not significant.

Fed young rats had significantly higher spleen and liver Ti concentration than fed older rats (ANOVA, $P < 0.05$). For example, Ti spleen concentrations were 54 nmol g^{-1} dry weight higher in young animals compared to 110 day old rats. In contrast to fed rats, unfed young rats had similar spleen, liver, kidney Ti tissue concentrations compared to unfed older rats. Older rats (110 and 172 days) demonstrated no

significant changes in spleen, liver or kidney Ti concentration associated with feed status.

The tissue moisture content of the spleen and kidney were also significantly higher in 23 day old rats in comparison to older rats irrespective of feed status (ANOVA, $P < 0.05$) (Table 5-2). Older rats (Day 110 and 169) demonstrated no differences in tissue % moisture.

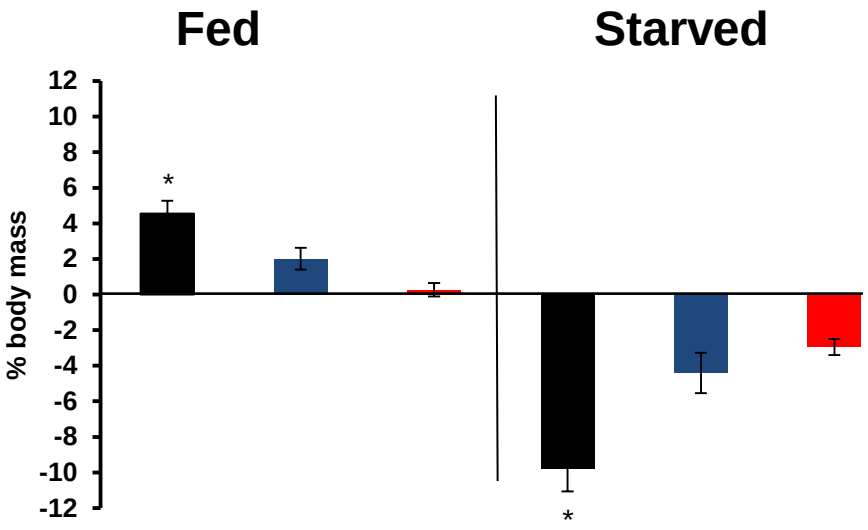

Fig. 5-2: Change in body mass following 48 h food deprivation or fed *ad libitum* (Mean ± S.E.M n = 6) until sampling Black, blue and red bars represent 23, 110, and 172 day old rats respectively. * indicates statistically significant changes in % body mass change within treatments between different aged rats (ANOVA, $P < 0.05$).

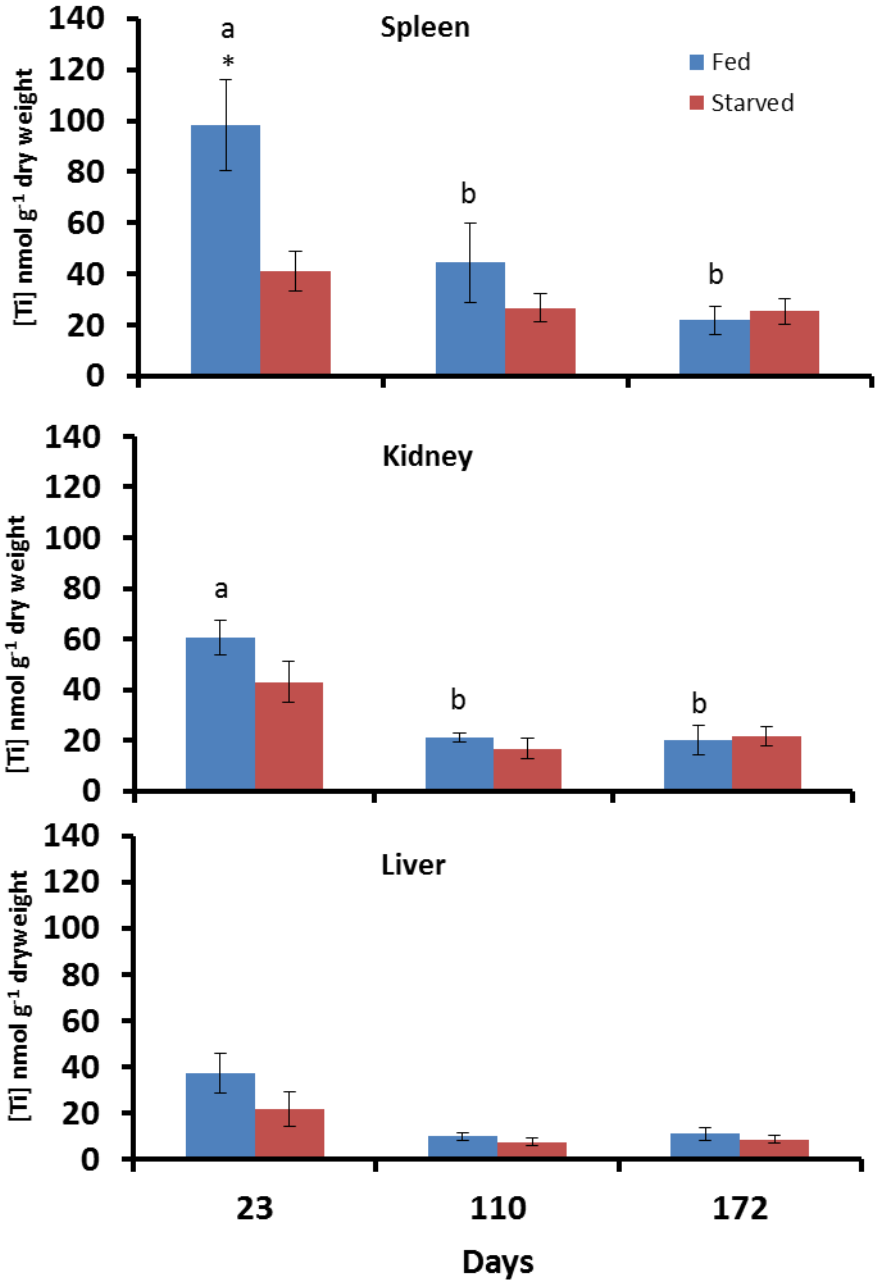

Fig. 5-3: Concentration of Ti nmol g^{-1} dry weight in Spleen (A), kidney (B) and liver (C) of different aged rats following food deprivation in comparison to fully fed individuals (n = 6) per treatment per time point. * indicate significant differences between treatment within age groups. Different letters indicate significance between animals of different ages within treatment (ANOVA, $P < 0.05$). Absence of symbols indicates no significant differences.

5.4.2 Feed status effects on tissue electrolytes

There were some age and feed status effects on tissue electrolyte concentrations in rats. For example mean spleen Na^+, Ca^{2+} and Mg^{2+} concentrations in 23 day old rats increased from (Mean ± S.E.M, n = 6) 78.9 ± 2.3, 3.8 ± 0.2 and 20.5 ± 0.3 µmol g^{-1} dry weight (fed animals) to 94.2 ± 1.5, 5.8 ± 0.4 and 23.5 ± 0.7 µmol g^{-1} dry weight for Na^+, Ca^{2+} and Mg^{2+}, respectively, for unfed animals (t-test or Mann Whitney U $P < 0.05$). This same pattern was observed in the kidney for 23 day old rats with electrolyte concentrations increasing from 149 ± 8.8 and 4.2 ± 0.2 (fed animals) to 189 ± 6.5.and 5.3 ± 0.2 µmol g^{-1} dry weight for Na^+ and Ca^{2+}, respectively, in unfed animals (Table 5-2). There were also some age-related differences in electrolyte concentration within treatments. For example older fed and starved rats had higher concentrations of Na^+ and lower concentrations of Ca^{2+} in the kidney liver and spleen in comparison to 23 day old rats (within treatments ANOVA or Kruskal Wallis, $P < 0.05$) (Table 5-2).

Table 5-2: Concentration of tissue Na^+, K^+, Ca^{2+} and Mg^{2+} (metal µmol g^{-1} dryweight) and % moisture of spleen liver and kidney in different aged rats subjected to 48 h food depravation or fed *ad libitum* until sampling

Rat age (Days) -	Organ	% Moisture	Na^+	K^+	Ca^{2+}	Mg^{2+}
23 S	Spleen	75.0 ± 0.5[a]	94.2 ± 1.5 *	280.0 ± 10.4	5.8 ± 0.4 *[a]	20.5 ± 0.3*
23 F	Spleen	76.4 ± 0.5[a]	78.9 ± 2.3 [a]	262.3 ± 5.7	3.8 ± 0.2[a]	23.5 ± 0.7[a]
110 S	Spleen	72.5 ± 0.5[b]	89.3 ± 2.5	261.1 ± 3.9	3.0 ± 0.2[b]	18.6 ± 0.6
110 F	Spleen	73.5 ±2.9[b]	94.6 ±0.8[b]	277.6 ± 6.6	3.1 ± 0.1[b]	19.7 ± 0.6[b]
172 S	Spleen	71.3 ± 1.2[b]	105.2 ± 11.4	240.1 ± 9.7	2.8 ± 0.3[b]	18.2 ± 1.3
172 F	Spleen	71.9 ± 1.3[b]	111.4 ±11.6[b]	254.6 ± 8.9	2.9 ± 0.2[b]	19.2 ± 1.2[b]
23 S	Liver	70.3 ± 0.3	63.3 ± 5.5	133.7 ± 5.4	2.1 ± 0.2*[a]	18.1 ±0.3*[a]
23 F	Liver	70.3 ± 0.2	66.6 ±2.7[a]	140.4 ± 5.0	1.6 ± 0.1	14.3 ± 0.2
110 S	Liver	70.5 ± 0.6	86.5 ± 9.6	123 ± 4.6	1.5 ± 0.1[b]	13.4 ± 0.4[b]
110 F	Liver	71.3 ± 0.9	91.7 ± 12.0[b]	131.2 ±7.4	1.6 ± 0.1	14.3 ± 0.7
172 S	Liver	70. 6 ± 0.7	86.8 ± 7.9	119.0 ± 6.0	1.4 ± 0.1[b]	14.2 ± 0.7[b]
172 F	Liver	70.9 ± 0.7	91.8 ± 7.6[b]	126.4 ± 6.1	1.4 ± 0.1	15.1 ± 1.0
23 S	Kidney	77.7 ±1.6[a]	189 ± 6.5*	164.0± 2.9[a]	5.3 ± 0.2*[a]	18.8 ± 0.2[a]
23 F	Kidney	75.7 ± 0.5[a]	149 ± 8.8[a]	153 ± 8.8	4.2 ± 0.2[a]	18.6 ± 0.8[a]
110 S	Kidney	73.6 ± 0.7[b]	167.8 ± 7.8	143.2 ± 4.1[b]	3.4 ± 0.2[b]	15.4 ± 0.5[b]
110 F	Kidney	72.6 ± 0.8[b]	179.5 ± 12.1[ab]	153.0 ±8.2	3.6 ±0.3[b]	16.4 ± 0.9[ab]
172 S	Kidney	71.8 ± 0.5[b]	147.1 ± 7.7	124.8 ± 5.2[c]	2.7 ± 0.1[c]	13.9 ± 0.7[b]
172 F	Kidney	71.2 ± 0.6[b]	156.9 ± 9.9[b]	132.7 ± 6.8	2.8 ± 0.1[c]	14.9 ± 0.8[b]

Values are means ± S.E.M (n = 6 for each group) and are expressed as µmol g^{-1} dryweight. Different letters represent differences between age within treatments, organs and electrolytes. The absence of letters indicated no differences.* indicates significant differences between fed (F) and starved (S) animals within age, organs and electrolytes. (ANOVA, Kruskal - Wallis, t-test or Mann Whitney U test $P < 0.05$).

5.4.3 Pilot study 2: Tissue and whole blood Ti concentrations in young rats: A comparison between fed and unfed animals

Following the first experiment, the most significant changes in tissue Ti and electrolyte concentrations occurred in 23 day old rats. This observation informed the next part of the study, which explored the effect of food deprivation (48 h without food) on Ti concentrations in tissue and whole blood in 23 day old rats in comparison to fed animals of the same age.

The mean tissue Ti concentrations are shown in Fig. 5-4. Animals fed *ad libitum* had higher mean concentrations of Ti in all tissues, except muscle (Fig. 5-4). Ti concentrations were significantly elevated in brain, lung, and jejunum of fed animals (t-test or Mann Whitney U, $P < 0.05$) and these increases were 64.3, 49.1 and 181.7 [Ti] nmol g^{-1} dry weight respectively. Spleen Ti concentrations were statistically different between treatments at the 90% confidence level ($P = 0.053$ (unlike the first pilot experiment). However, average Ti concentrations followed the same pattern as that found in the first experiment. Significant increases in whole blood Ti concentrations were demonstrated in fed rats compared to unfed animals ($P < 0.05$). For example mean whole blood Ti concentrations were 6.2 and 19.1 nmol mL^{-1} in unfed and fed animals respectively (Fig. 5-5, Panel H).

5.4.4 Feed status effects on tissue electrolytes

Similar to the first experiment, tissue electrolytes changed markedly between unfed and fed animals. Macro electrolyte concentrations (Na^+, K^+, Mg^{2+}, Ca^{2+} and Fe) increased in all the organs of starved animals with the majority being statistically significant (t-test, $P < 0.05$) (Table 5-4). This was probably due to changes in tissue

moisture content. For example, lung and spleen tissue in unfed animals had significantly lower water concentrations (69.4 ± 3.5 and 57.6 ± 1.3% compared to 75.3 ± 0.9 and 67.7 ± 1.1% for lung and spleen of fed animals, Mean ± S.E.M n = *5*) which would result in the increased concentration of tissue electrolytes when normalised to dry weight. Iron content of unfed animals increased in the liver by an average of 6.9 µmol g^{-1} dry weight compared to fed animals. Interestingly, the pattern was reversed in brain tissue with a mean Fe reduction of 10.9 µmol g^{-1} dry weight for unfed animals.

Trace elements (Cu, Zn) were also affected by food deprivation. For instance, Zn concentrations were elevated in all analysed tissues taken from unfed animals (Table 3 - ANOVA or Kruskal Wallis, $P < 0.05$). Cu concentrations were significantly increased in the spleen, liver and jejunum tissues (Table 5-4). In contrast, whole blood electrolyte levels exhibited a different distribution pattern (Fig. 5-5 Panel A-H) in unfed animals compared to fed animals. Whole blood Na^+, Ca^{2+}, Zn and Cu concentrations decreased significantly (t-test or Mann Whitney U $P < 0.05$) in unfed animals. Notably, average whole blood Na^+ and Ca^{2+} concentrations decreased from 223.2 and 6.6 µmol mL^{-1} for fed animals to 132.6 and 3.0 µmol mL^{-1} for unfed animals. Whole blood concentrations of Mg^{2+}, K^+ and Fe were not significantly affected by food deprivation (Fig. 5-5, Panel A-H).

5.4.5 Proximate composition

Mean values ± S.E.M (n = 5) for % moisture, % lipid, % crude protein, % carbohydrate and % ash in the remaining carcasses are summarized in Table 5-4. Acute starvation caused a significant increase in carcass % moisture and ash

content (t-test or Mann Whitney U, $P < 0.05$). The percentage moisture in the carcass increased from an average 68.08 ± 0.52% in fed animals to 73.03 ± 0.07% for starved animals. % Ash (mineral content) increased from 1.91 ± 0.01 for fed animals to 4.87 ± 0.01 for unfed animals. In contrast carcass % Lipid and % carbohydrate were significantly reduced in unfed animals (t-test or Mann Whitney U, $P < 0.05$). Average carcass gross energy was significantly less in unfed animals (Means ± S.E.M, n = 3; 21.2 ± 0.17 compared to 25.9 ± 0.13 MJ kg^{-1} for fed animals). This was probably due to the diminished carbohydrate and lipid stores in the starved animals. Carcass % protein remained unaffected by acute starvation (Table 5-3).

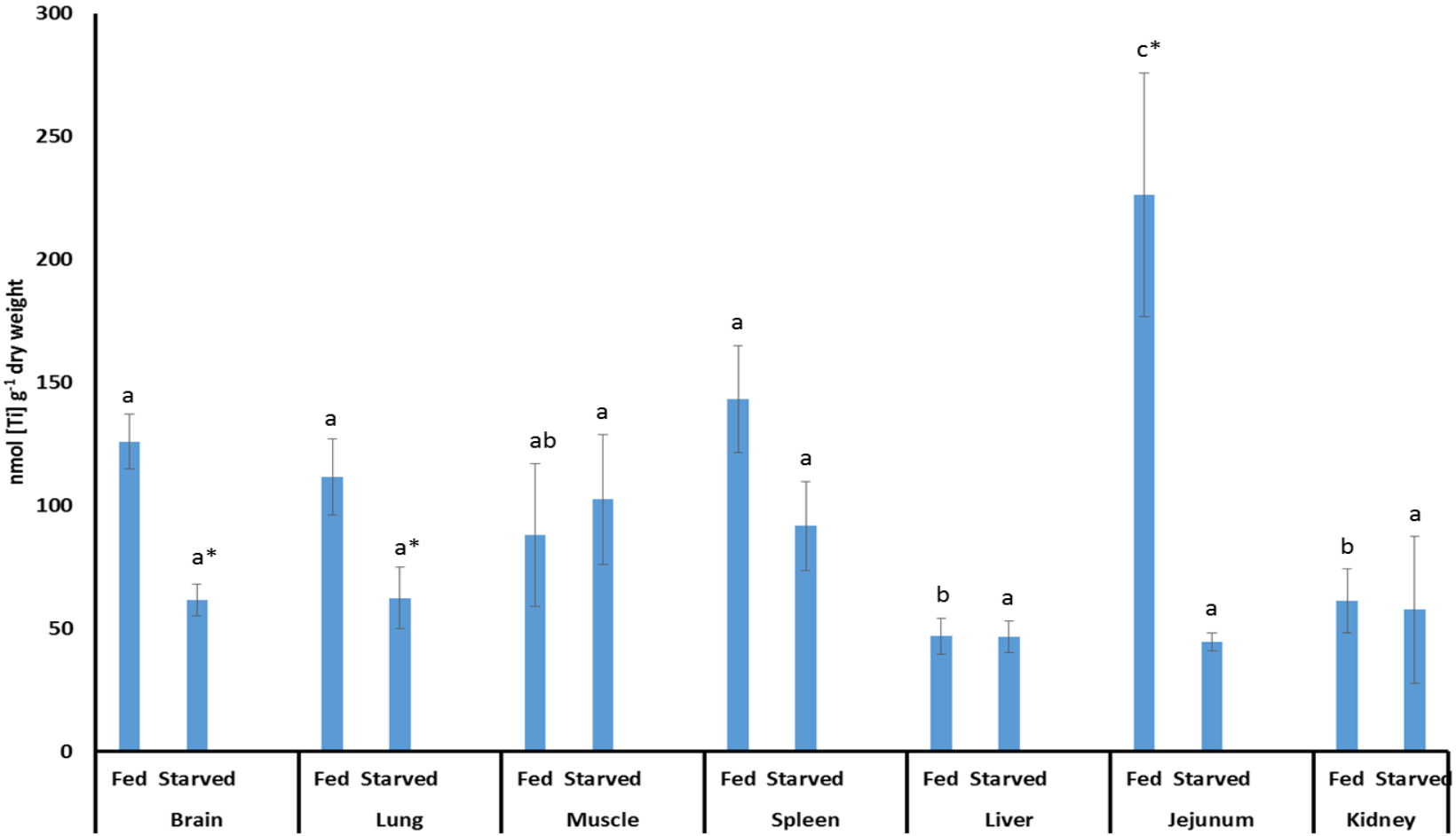

Fig. 5-4: Concentration of Ti nmol g^{-1} dry weight in young (23 day old) rat organs following 48 h food deprivation or fed *ad libitum* until sampling. Values are means ± S.E.M (n = 5 for each group). Letters represent significance between organs within treatments. * represents significance between treatments within tissues. ANOVA or Kruskal Wallis for between tissues and student's *t*-test or Mann Whitney *U* for between treatments within tissues ($P < 0.05$).

Table 5-3: Tissue moisture and electrolyte concentrations in 23 day old female Wistar rats fed *ad libitum* or starved for 48 h prior to sampling

			Tissue electrolytes µmol [Metal] g $^{-1}$ dry weight						
Treatment	**Organ**	**% moisture**	**Na^+**	**K^+**	**Ca^{2+}**	**Mg^{2+}**	**Fe**	**Cu**	**Zn**
F	Brain	78.3 ± 0.2^{a}	188.8 ± 4.2^{a}	238.4 ± 5.4^{a}	7.9 ± 0.4^{a}	14.6 ±0.3^{a}	15.3 ± 4.5^{a}	0.32 ± 0.07^{a}	1.07 ± 0.02^{a}
S	Brain	76.4 ± 0.26^{a}	288.7 ± 11.9^{a}*	297.5 ± 13.9^{a}*	32.8 ± 20.5^{a}	22.0 ± 0.7^{a}*	4.3 ± 0.9^{a}*	0.27 ± 0.01^{a}	1.82 ± 0.09^{a}*
F	Lung	75.3 ± 0.9^{a}	261.6 ± 24.6^{b}	135.8 ± 10.5^{b}	11.3 ± 1.0^{a}	9.8 ± 0.6^{b}	15.4 ± 4.4^{a}	0.11 ± 0.01^{b}	1.42 ± 0.24^{b}
S	Lung	69.4 ± 3.5^{b}*	390.9 ± 62.8^{b}*	201.7 ± 7.6^{b}*	21.2 ± 1.2^{b}*	17.0 ± 0.9^{b}*	17.6 ± 2.6^{b}	0.14 ± 0.03^{b}	2.27 ± 0.09^{b}*
F	Muscle	55.0 ± 5.8^{b}	81.9 ± 10.1^{c}	134.8 ± 30.1^{bc}	8.8 ± 0.9^{a}	14.1 ± 3.2^{abc}	4.7 ± 2.7^{b}	0.08 ± 0.01^{b}	0.67 ± 0.11^{c}
S	Muscle	49.5 ± 4.4^{c}*	225.4 ± 16.0^{a}*	202.2 ± 4.4^{b}	39.6 ± 16.3^{a}*	26.6 ± 1.1^{c}*	3.4 ± 0.6^{a}	0.10 ± 0.00^{b}	1.53 ± 0.06^{a}*
F	Spleen	67.7 ± 1.1^{b}	100.9 ± 5.0^{c}	245.3 ± 13.5^{a}	8.7 ± 0.5^{a}	18.4 ± 0.7^{c}	12.3 ± 3.3^{a}	0.09 ± 0.00^{b}	1.46 ± 0.07^{b}
S	Spleen	57.6 ± 1.3^{bc}*	234.8 ± 28.7^{a}	291.7 ± 17.4^{a}	21.6 ± 1.2^{b}*	25.4 ± 1.1^{c}*	16.1 ± 1.2^{b}	0.14 ± 0.01^{b}*	2.29 ± 0.13^{b}*
F	Liver	69.0 ± 0.3^{ab}	84.0 ± 4.5^{c}	136.7 ± 4.9^{b}	3.1 ± 0.3^{b}	13.7 ± 0.5^{a}	7.2 ± 1.1^{a}	0.42 ± 0.05^{a}	1.41 ± 0.06^{b}
S	Liver	67.0 ± 1.0^{b}	200.2 ± 8.3^{ac}*	186.4 ± 7.8^{b}*	4.9 ± 0.3^{c}*	24.1 ± 1.2^{ac}*	14.2 ± 2.2^{b}*	0.82 ± 0.11^{c}*	3.54 ± 0.38^{c}*
F	Jejunum	74.3 ± 0.9^{a}	286.6 ± 31.8^{b}	139.5 ± 17.7^{bc}	33.9 ± 5.8^{c}	19.6 ± 1.8^{c}	4.1 ± 0.9^{b}	0.11 ± 0.01^{b}	1.52 ± 0.11^{b}
S	Jejunum	76.5 ± 0.4^{a}	536.2 ± 52.5^{b}*	244.7 ± 5.2^{c}*	49.4 ± 14.8^{a}	33.6 ± 1.5^{d}*	2.7 ± 0.1^{a}	0.22 ± 0.01^{ab}*	3.70 ± 0.24^{c}*
F	Kidney	66.6 ± 1.7^{b}	129.2 ± 20.9^{c}	100.5 ± 17.7^{c}	6.7 ± 1.1^{ab}	11.2 ± 2.2^{ab}	20.6 ± 14.8^{ab}	0.18 ± 0.03^{ab}	0.92 ± 0.17^{abc}
S	Kidney	69.6 ± 0.6^{b}	204.4 ± 59.0^{ac}*	174.2 ± 39.1^{bc}	10.7 ± 2.4^{c}	18.3 ± 3.9^{abc}	24.6 ± 7.1^{b}	0.29 ± 0.06^{ab}	2.21 ± 0.52^{ab}*

Values are means ± S.E.M (n = 5 for each group) and are expressed as µmol g^{-1} dry weight. Different letters represent differences within treatments (starved (S) or Fed (F) between organs within columns. * indicate significant difference between treatments within organ columns and electrolytes (ANOVA, Kruskal Wallis, t-test or Mann Whitney U test, $P < 0.05$).

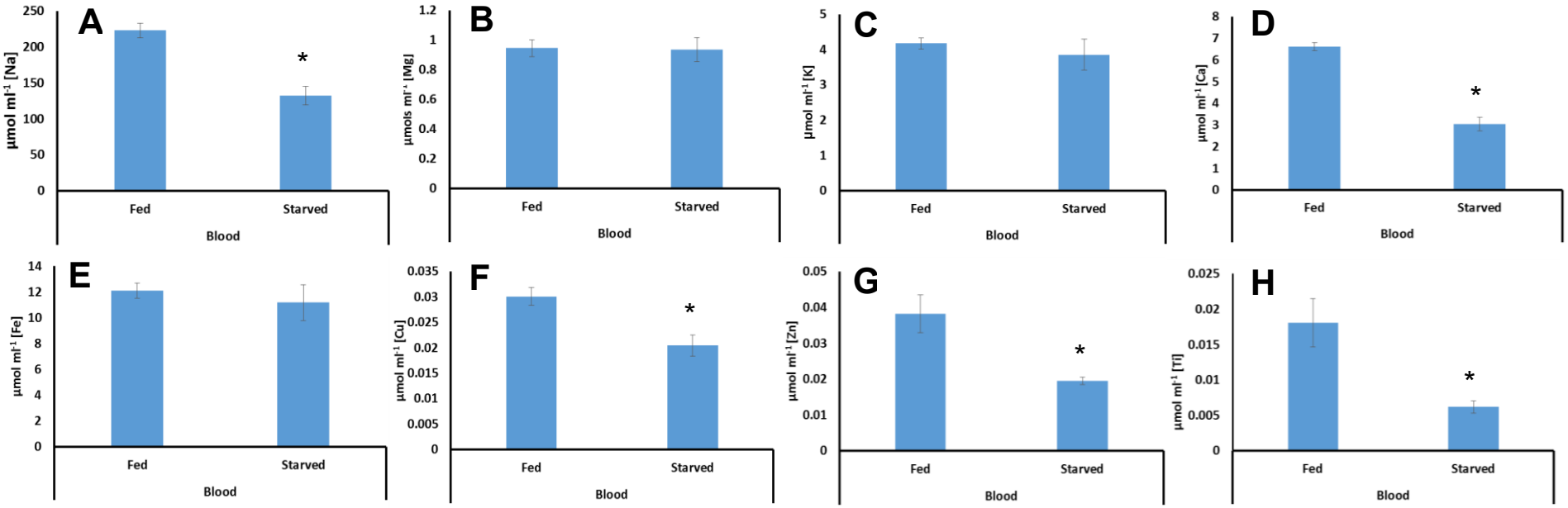

Fig. 5-5: Whole blood electrolyte concentrations for rats starved for 48 h or fed *ad libitum* until sampling. Values are means ± S.E.M (n = 5 for each group) and are expressed as µmol mL^{-1} Metal * indicates significance between treatments (student's t-test $P < 0.05$). Panels A-H represent whole blood concentrations of Na^{+}, Mg^{2+}, K^{+}, Ca^{2+}, Fe, Cu, Zn and Ti respectively.

Table 5-4: Proximate remaining carcass composition of 23 day old rats expressed as % wet weight

	Fed	Starved
% Moisture	68.08 ± 0.52	73.03 ± 0.07*
% Ash	1.91 ± 1.91	4.87 ± 0.01*
% Protein	17.22 ± 0.33	17.39 ± 0.04
% Lipid	10.63 ± 0.07	3.74 ± 0.03*
% Carbohydrate	2.15 ± 0.33	0.97 ± 0.12*

Values are means ± S.E.M (n = 5 for each group) and are expressed as % of wet eviscerated carcass.

5.5 Discussion

This pilot study is to our knowledge one of the first reports demonstrating changes in tissue Ti and electrolyte concentrations in rats of different ages, feeding on a commercially available standard rodent diet in comparison to rats acutely deprived of food. The present study demonstrated that the Ti concentrations in the blood and internal organs of young rats showed transient increases when the animals were fed a normal diet containing an incidental amount of Ti in comparison to unfed rats of the same age. No such differences were demonstrated in the tissues of older rats subjected to the same treatment. Moreover, older rats had lower Ti tissue concentrations than younger rats, regardless of the feeding status. Consequently, food intake and the age of the animals is likely to influence their Ti status with respect to initiating regulatory toxicity tests with bulk or nano forms of TiO_2 .

5.5.1 Effect of age and feed status on tissue Ti concentrations

The first pilot experiment investigated the effects of acute starvation on Ti and electrolyte concentrations in tissues that have been identified as primary target tissues for bulk and NP TiO_2 accumulation in rodents following intravenous exposures (Patri *et al*. 2009; van Ravenzwaay *et al*. 2009; Shinohara *et al*. 2012) and secondary targets following oral exposures (Jani *et al*. 1994; Tassinari *et al*. 2014).

This first pilot study shows that younger fed rats have higher mean Ti concentrations in the spleen liver and kidney per gram dry weight compared to fed older rats (Fig. 5-3). The standard rodent feed had a mean Ti concentration of 3.28 mg g^{-1}. Assuming

rats consume 5 g per 100 g of body weight (Bogdanske *et al*. 2011) they are exposed to 164 mg kg^{-1} bw day^{-1} Ti through their normal diet. In spite of this chronic oral exposure to high levels of Ti, fed older animals had considerably lower spleen and kidney Ti concentrations than fed young rats suggesting an organ dilution effect (Jovanovic *et al*. 2012) which would also imply low bioavailability and absorption of Ti from oral dietary exposures or that the rate of Ti absorption is matched by Ti depuration.

Unfortunately there is no clear pattern in the literature of this age effect on accumulation of Ti from TiO_2 NP or bulk exposures. For example Tassinari *et al*. (2014) showed 60 day old rats exposed to 2 mg kg^{-1} bw day^{-1} for 5 days had significant increases in spleen Ti concentrations; Geraets *et al*. (2014) showed 63 days old rats exposed to 8.6 mg kg^{-1} bw day^{-1} for 5 days demonstrated no effects; Cho *et al*. (2013) demonstrated no effects in 133 day old rats exposed to 1000 mg kg^{-1} bw day^{-1} for 13 weeks; Jani *et al*. (1994) showed 98 day old rats exposed to12.5 mg kg^{-1} day^{-1} for 10 days demonstrated increased liver spleen and lung Ti concentrations. A number of factors may be responsible for the discrepancies in the data, for example, rat strain, particle size, time of particle administration, feed status and duration of administration. It is difficult to tease apart the confounding variables which would allow for a true comparison between studies.

Spleen and kidney Ti tissue concentrations reported in this present study for fed young rats (23 days old) are higher than those reported in the Cho *et al*. (2013) study controls, but, the tissue Ti values reported for 6 month old rats in this present study are lower. Interestingly, the animals in Cho *et al*. (2013) study were 4 months old at the time of sampling and the tissue Ti values reported for the control animals fall in between the values reported for 23 day old and 6 month old animals in this present

study. For example Cho *et al*. (2013) reported tissue Ti values of 0.4 and 0.4, μg g^{-1} wet weight, equivalent to 42 and 42 nmol g^{-1} dry weight for spleen and kidney (figures are calculated from an assumed tissue moisture content of 80% and converted to nmol for convenience) and in this present study Ti tissue concentration values for fed 23 day old rats were 143 and 61 nmol g^{-1} dry weight, whilst for fed 6 month old rats the values were 21 and 20 nmol g^{-1} dry weight for spleen and kidney, respectively. This correlation may be a fortuitous; nevertheless, it is curious to see that tissue Ti concentrations appear to reduce with increasing age when comparing the results herein with other researcher's work. Historically it has been demonstrated that tissue metal concentrations for some metals (iron, copper) in young animals tend to be higher than older animals (Kello and Kostial 1977; Kostial *et al*. 1978) and the evidence presented herein suggests that Ti follows this pattern (at least in the kidney liver and spleen).

It is unclear why young animals have higher tissue Ti concentrations than older rats although there is a number of possible explanations based on our knowledge of physiological processes in young developing mammals. Young animals are likely to have a higher body burden of metals as a result of placental transfer (Kostial *et al*. 1978). This has been supported by Takeda *et al*. (2009) who showed subcutaneously administered TiO_2 in pregnant mice is transferred to the offspring. Another explanation could be ascribed to the higher metabolic rate young animals have compared to older animals (Roberts and Rosenberg 2006). Studies have demonstrated higher intestinal absorption rates and higher body retention in young animals (<1 month) for some metals e.g. Pb, Fe (Forbes and Reina 1972) Ce (Inaba and Lengemann 1972) TiO_2 (Wang *et al*. 2013), and this has been attributed to increased intestinal pinocytic activity in the GIT of developing animals (Lecce 1972;

Martinsson and Johnsson 1975). Finally, ration size per kg of tissue decreases with age, therefore, young animals are ingesting relatively more Ti containing food. Further research needs to examine the links between age and intestinal permeability to Ti/TiO_2 following oral exposures.

5.5.2 Tissue and whole blood Ti concentrations in young rats compared to acutely food deprived animals

Young rats demonstrated statistically significant increases (ANOVA or t-test, $P < 0.05$) in [Ti] in whole blood, brain, lung, spleen and jejunum compared to unfed rats of the same age. Given this, the data suggest that dietary Ti is absorbed and depurated quickly in young rats.

The increase in lung Ti concentrations following murine oral exposures to TiO_2 (oral gavage of a TiO_2 solution of bulk and NP) has been reported in a number studies (NP- Wang *et al*. (2007); Cho *et al*. (2013); bulk- Jani *et al*. (1994)). This may occur through incidental production of an aerosol stimulated by the gnawing action of the rat when feeding or simply due to the high blood flow infiltrating the lungs (intestinal absorption of Ti could end up in the lungs - Wang *et al*. 2007). The anatomy of the lung may play a role in preferentially accumulating particles of TiO_2. The high level of blood flow coupled with the intricate capillary network could act as a filter trapping particles (Li and Huang 2008). Elevated brain [Ti] may also be explained via incidental production of an aerosol. Wang *et al*. (2007) demonstrated intranasal instillation of TiO_2 NPs can enter the CNS via the olfactory system and accumulate in the brain or possibly via oral exposures (Wang *et al*. 2007); however, changes in blood brain barrier permeability associated with brain development in young rats

cannot be ruled out (Cremer *et al*. 1976). Jejunum levels of Ti are expected to be higher in fed animals due to undigested Ti containing food incidentally bound to the tissue.

Whole blood Ti concentrations varied in relation to feed status in young rats. In this pilot study mean blood [Ti] decreased by more than 50% in unfed young rats compared to fed rats suggesting rapid removal or redistribution of Ti. Geraets *et al*. (2014) demonstrated a similar rapid decline in rats intravenously administered 9.8 mg kg^{-1} bw TiO_2 NPs (< 30 min). After 24 h no Ti was detected in the blood (Geraets *et al*. 2014). Similar results were demonstrated by Fabian *et al*. (2008) who intravenously administered 5 mg kg^{-1} bw TiO_2 NPs. Unfortunately the mechanisms of Ti depuration are subject to debate and appear to be influenced by methods of administration. For example, Cho *et al*. (2013) detected high concentrations of Ti in the faeces following chronic oral exposure and this is also supported by Jani *et al* (1994) who calculated that 6.5% (12.5 mg kg^{-1} TiO_2 per day for 10 days 500 nm diameter primary particle size) of the dose is absorbed in rat small intestine whilst the rest is excreted through the bowel (Jani *et al*., 1994). Xie *et al*. (2011) demonstrated intravenously injected rutile TiO_2 radiolabelled with $_{125}$ I injected into mice and rats at 1 and10 mg kg^{-1} bw was mainly found in the urine indicating renal excretion. Whether renal excretion is responsible for already present systemic Ti and faecal excretion is merely a by product of a lack of absorption needs more research.

Once Ti is in the blood stream it is expected that levels of Ti would increase in organs such as the liver spleen and kidney. Surprisingly, there was no statistically significant increase in liver or kidney Ti concentrations in fed young animals. The reasons are unclear although this has been demonstrated in others work. For example, Geraets *et al*. (2014) showed repeated oral exposures of between 10.9 –

12 mg TiO_2 kg^{-1} bw day^{-1} for 5 days in female rats had no effect on kidney and liver [Ti]. Similar results were demonstrated by Cho *et al*. (2013) who administered a considerably larger dose of 1041.5 mg kg^{-1} bw day^{-1} TiO_2 for 13 weeks and demonstrated no changes in kidney and liver tissue Ti concentrations.

In contrast, Wang *et al* (2007) demonstrated considerable increase in kidney and liver tissue Ti concentrations in mice two weeks post exposure following a single oral administration of 5 g kg^{-1} (25 and 80 nm diameter) TiO_2 particles. This is likely related to the massive dose administered to the animals resulting in overloading the gut.

Mean spleen [Ti] was elevated in fed young animals although this was not regarded as significant in the 2nd pilot experiment. Interestingly, Tassinari *et al*. (2014) orally exposed 60 day old rats to TiO_2 NPs for 5 days at a concentration of 2 mg kg^{-1} bw day^{-1} and reported significant average Ti increases of 0.046 µg g^{-1} wet weight equivalent to 4.9 nmol g^{-1} dry weight in the spleen; however, Geraets *et al* (2014) demonstrated no changes in rats of similar ages (63 days) exposed to 8.6 mg kg^{-1} bw day^{-1} TiO_2 NPs for 5 days. It is surprising that the natural variation in 60 day old control animals in the Tassinari *et al*. (2014) study was so low. For example, in this present study, the standard error for mean spleen Ti concentrations for fed 3 month old rats was 15 nmol g^{-1} dry weight and for fed young rats (23 days) between 20-30 nmol g^{-1} dry weight .

Regrettably, many of the studies mentioned above (Wang *et al*. 2007; Cho *et al*. 2013; Geraets *et al*. 2014; Tassinari *et al*. 2014) state that all experimental animals were allowed to feed normally before and during the oral exposure experiments on standard laboratory feed, which was not characterized for [Ti], or in the case of the

Cho *et al*. (2013) study, explicitly stated that the [Ti] of the diet was unknown. This makes it difficult to draw any reasonable conclusions about TiO_2 ADME considering TiO_2 is present in food at mg kg^{-1} levels and if used as a food colouring the concentration will be considerably higher. This makes the concentrations used in low dose trials negligible in comparison to background exposures, which could be 20 - 50 times greater than the exposures being tested (Based on the Ti concentration of feed analysed in this present study).

5.5.3 Effect of food deprivation on tissue and blood electrolytes in young rats

Acute food deprivation caused significant increases in Na^+, K^+, Mg^{2+} and Ca^{2+} tissue electrolyte concentrations and decreases in whole blood Na^+ and Ca^{2+} concentrations compared to fed young rats. This is indicative of water movement from the tissue into the blood and is supported by the reduced carcass tissue moisture compared to fed animals (Table 5-4). A speculative explanation for these results may be related to starvation induced polydipsia (water consumption was not monitored during the study). Increasing water consumption is a well-documented reaction to food deprivation for some rodent species (Newcomer *et al*. 1987). The effect of increased water consumption causes a transient reduction in blood osmotic pressure, which is either quickly corrected by urine production (i.e., routine renal homeostasis of the drinking response), or in persistent situations, other solutes such as amino acids can be added to the blood to raise osmotic pressure. In animals, the release of amino acids from the tissues to the blood as osmolytes is a well-documented strategy. These can include proline, tyrosine, phenylalanine, leucine isoleucine and valine (Rankin and Davenport 1981). These amino acids diffuse into the blood down the concentration gradient thereby increasing blood osmotic

pressure. Water would be expected to follow this efflux of proteins out of the cell via solute drag (Van Bruggen *et al*. 1982), ultimately dehydrating the tissues and diluting extracellular whole blood electrolytes. Solute drag has been shown to exert considerable force on water movement (Van Bruggen *et al*. 1982) and could easily explain the moisture concentration asymmetry demonstrated in this present study. Whole blood Mg^{2+} K^{+} and Fe would not be expected to change because these elements are primarily regulated inside red cells (e.g. bound to haemoglobin or Mg ATP complexes) (Flatman 2002). This is in agreement with observations in this present study.

5.5.4 Weight loss and changes in proximal composition in starved juvenile rats

Weight loss is amplified in smaller endotherm animals subjected to acute food deprivation because they tend to have higher mass specific metabolic rates. Younger smaller rats have been shown to lose more mass per day than older larger rats subjected to food deprivation (Goodman *et al*. 1981) and this is in agreement with this present study. As expected, lipid and carbohydrate stores are the first to be depleted and used for energy metabolism. For example, glucose used in glycolysis and lipids used for ß-oxidation in the mitochondria (Murray *et al*. 2009). Carcass crude protein content was unaffected by acute food deprivation in young rats. Protein catabolism is considered to be a fuel of last resort and the switch from lipid catabolism to protein catabolism is thought to occur when an animal's lipid concentration reaches a critical threshold (Caloin 2004) which did not occur in 48 h suggesting the ramifications of food deprivation in this study were physiological and not pathological. Relative mineral content increased in the carcass of starved young

rats. This increase in mineral content has been reported to occur in starved vertebrates by a number of researchers (e.g. Cook *et al*. 2000; Shoemaker *et al*. 2003). The reasons are unclear although Prunescu *et al*. (2003) hypothesised that in the absence of food young animals would maintain or increase micronutrients in the body for building or rapidly turning over mineral rich tissues (e.g. bone, blood) (Prunescu *et al*. 2003).

5.5.5 Limitations of the study

Several limitations to this pilot study need to be acknowledged. The form and size of the Ti in the food was unknown. It may have been in the form of illumenite ($FeTiO_2$) or leucoxene ore ($TiO_2.FeO.H_2O$) or naturally occurring rutile rather than processed TiO_2. Only the kidney, liver and spleen were analysed for all age groups and feed statuses. There was no sham control e.g. animals being fed a Ti free diet.

5.5.6 Conclusion

This study shows that young rats are susceptible to transient increases in tissue and whole blood Ti concentrations when fed a standard laboratory diet containing Ti in comparison to unfed rats of the same age. Critically, there is an age effect with older rats demonstrating lower tissue [Ti] in liver kidney and spleen following long term chronic dietary exposures to relatively large concentrations of Ti in comparison to young rats.

TiO_2 particle (NP or Bulk) oral exposure studies need to explicitly analyse and report the concentrations and forms (if possible) of the control diet animals are fed,

especially, when trying to determine the effect of low dose oral exposures on accumulation, absorption and distribution of Ti/TiO_2 following TiO_2 NP particle exposures. There is a risk that conclusions drawn from TiO_2 NP oral exposures scenarios will misinterpret the ADME of administered Ti against the high background concentrations present in some standard laboratory feeds, especially when the technology used to determine tissue Ti concentrations is unable to differentiate between administered Ti and Ti already present.

Finally, age effects need to be considered when evaluating risk in the human population, considering, food with high [Ti] tends to be found in products that are predominantly marketed to children. Higher absorption and accumulation in children may lead to increased oral toxicity. More research is required in this field.

Chapter 6: General Discussion

There is limited information on the mechanisms of TiO_2 NP uptake via the mammalian intestine and the influence of crystal structure and particle size (bulk and nano) on these processes. The overarching hypothesis of this thesis is that TiO_2 particles are bioavailable and can translocate through gut epithelial cells and enter the serosal compartment mediated by vesicular energy dependent processes in mammalian intestinal epithelium. The physicochemical properties of the particles such as particle size and crystal structure will subsequently affect uptake rates and accumulation and exert different physiological effects on tissues relative to bulk versions of the same material. The body of work presented here has contributed to our knowledge of TiO_2 bulk and NP uptake and accumulation in mammalian models and goes on to offer some suggestions as to the mechanisms involved in this process. The data presented heirein can be used to inform hazard and risk assessments with regards to oral exposure of TiO_2 NPs.

6.1.1 Overview

In Caco-2 cells, uptake, accumulation and appearance of Ti/TiO_2 in the serosal compartment were demonstrated, and this was influenced by TiO_2 crystal morphology (Chapter 2, 3). The nano rutile form was taken up the least irrespective of cell maturation status and growth substrate (Chapter 2, 3). The bulk material demonstrated the greatest uptake and accumulation rates in cell culture, although appearance of Ti/TiO_2 from TiO_2 particle exposures in the serosal compartment from bulk TiO_2 exposures was delayed in comparison to nano P25 and nano anatase TiO_2 (Chapter 3). Incubating cells with pharmacological inhibitors caused significant changes in the cellular concentrations of Ti/TiO_2 at 24 h compared to no drug

treatments which implied an active process is responsible for uptake and accumulation rather than diffusional processes (Chapter 2). Moreover, differential accumulation of different crystal structures of TiO_2 in the pharmacological trials implies crystal structure influences uptake pathway in Caco-2 cells (Chapter 2).

In whole rat GIT the work presented herein reports regional differences in Ti/TiO_2 accumulation from both bulk and nano forms of TiO_2 by vertebrate mammalian intestine (Chapter 4), and demonstrates uptake of Ti/TiO_2 from TiO_2 particle exposures across jejunum segments of rat small intestine using the isolated perfused intestine technique (Chapter 4). The main findings are that Ti/TiO_2 from TiO_2 particle exposures (Bulk and nano P25) accumulate in the small intestine and large intestine in rats, with the Ti/TiO_2 mainly accumulating in the mucosa rather than the underlying muscularis. Initial rates of uptake and appearance of Ti/ TiO_2 from TiO_2 particle (bulk and nano) exposures in the serosal compartment are influenced by particle size. The nano TiO_2 exposures had significantly higher initial Ti flux rates (a measure of serosal appearance of Ti from apical exposures) than the bulk material (Chapter 4, Table 4-7). Addition of nystatin or vanadate caused the mean concentration of tissue Ti to increase for both bulk and nano TiO_2 exposures suggesting that export of Ti/TiO_2 is partly controlled by cholesterol and solute transport pathways. These results are in line with the results demonstrated in Caco-2 cells (Chapter 2).

Histopathology and ultrastructure analysis (TEM and SEM) of both cells and intestinal tissues demonstrated at least some of the administered TiO_2 remained in particulate form inside vesicles within cells and that TiO_2 irrespective of size and crystal structure had negligible effects on cell and tissue morphology compared to controls (Chapters 2 - 4).

In whole organisms, concentrations of Ti in secondary target organs following oral exposures of food containing Ti decreased with increasing age. Moreover, feed status had a negligible effect on Ti tissue concentrations in older animals. In contrast, younger animals demonstrated significant changes in tissue Ti relative to feed status (fed animals had higher tissue Ti concentrations) (Chapter 5). No concrete conclusions can be drawn from the pilot study in Chapter 5 although a number of ideas can be put forward to explain the data. Young animals may have increased intestinal permeability to Ti relative to older animals or older animals have more developed excretory mechanisms which may explain the disparity in tissue Ti concentration between animals of different ages. The latter may be a more likely explanation because the perfusion work used intestines of 12 week old rats and this data demonstrated uptake of TiO_2 occurs in this intestine. Unfortunately, drawing a comparison between this whole body work and the *in vitro* work described earlier is difficult due to a number of reasons. For example, the Ti in the feed was not adequately characterised. Food matrix effects, food transit times, changes in pH along the intestine and digesta composition were not analysed and likely play a role in the bioavailability of Ti from dietary exposures. Moreover, in the Caco-2 work and intestinal perfusions particles of TiO_2 were administered in a manner that facilitated direct contact of particles with apical epithelium.

The work described here significantly contributes to the field in terms of our understanding of particle physicochemical properties on uptake and accumulation in mammalian intestinal epithelium. For instance, particle crystal structure affects accumulation and uptake in intestinal cells. The rates of uptake and tissue accumulation in the perfused rat intestine are influenced by particle size and these rates are explicitly reported herein. Moreover, this work highlights some

methodological considerations with regards to *in vivo* dietary exposures. Finally the work presented herein contributes important information about the uptake hazard of bulk and nano TiO_2 in mammalian models and can be used to inform risk assessment and policy decisions with regards to the hazard presented by oral exposure to TiO_2 of various size and crystal structures.

6.1.2 Comparison between *in vitro* methods

Although *in vivo* studies are regarded as the "gold standard" for biological relevance with regards to TiO_2 uptake, systemic distribution, and toxicity; the mechanistic analysis of particle uptake is complicated by a considerable number of variables that inform on food intake, bioavailability and therefore oral dose (e.g. behavioural effects, animal social structure, stress etc.). These factors may in turn trigger, neuro-endocrine events that might alter blood flow and/or the metabolic activity of the gut epithelium. Performing experiments *in vitro* gives you control over these systemic signals in the blood, allowing for many variables to be accounted for and potential mechanisms to be tested.

In this present thesis, different *in vitro* methods were used to improve our understanding of TiO_2 uptake mechanisms, rates of Ti transport and the effects of TiO_2 exposures on biochemical markers and tissue and cell electrolytes in mammalian intestinal cells/tissue. Human intestinal Caco-2 cell culture is a useful tool to assess uptake and transport mechanisms of Ti/TiO_2 from apical exposure of TiO_2 across a monolayer of enterocyte like cells. Caco-2 cells have the advantage of being high throughput and being able to accurately control media/ material exposures. Disadvantages include a lack of realism in terms of metal uptake and

permeability when compared to an intact intestine. Given this, extrapolating uptake and accumulation rates to *in vivo* from cell line information should be applied with caution.

A more realistic *in vitro* model for assessing uptake and transport of Ti/TiO_2 from TiO_2 luminal exposures is the perfused intestine method. This is far closer to the real condition than those demonstrated by cell lines. Morphologically the structure of the gut consists of the four layers of intestinal tissues (mucosa, submucosa, muscularis, serosa) and the perfused intestine demonstrates good viability when removed from the organism and bathed in an appropriate physiological saline.

The results from these two *in vitro* methods (Chapters 2-4) show both similarities and differences with regards to particle accumulation and sub lethal physiological effects. Similarities include Ti/TiO_2 from TiO_2 exposures accumulated in the perfused intestine tissue and cell monolayer following mucosal/apical administrations. Mean tissue and cell Ca^{2+} concentrations both increased following TiO_2 exposures. Differences included mature cells grown on inserts (lowest accumulation for any of the cell culture experiments) demonstrated Ti concentrations at 4 h that were 15 times greater than the tissue Ti concentration for both bulk and nano P25 TiO_2 exposures. Overall rates of Ti/TiO_2 appearance in the basolateral compartment were 20 and 13 times higher in cells than perfused intestine for bulk and nano P25 TiO_2, respectively (Chapter 3, Fig. 3-10). Moreover, the electrolyte concentrations in control cells were 26, 14 and 8 times higher for Na^+, K^+ and Mg^{2+}, respectively, in comparison to control intestinal tissue electrolyte concentrations. These differences can be attributed to the phenotype of the Caco-2 immortalized cell lines (Chapter 2, Section 2.5.1d). Transport of Ti/TiO_2 is expected to be higher across a monolayer of cells in comparison to four tissue layers which comprise the intestine. Accumulation

rates would also be higher due to accelerated rates of membrane turnover associated with carcinogenic cells, lack of mucus and gravitational settling of particles on the apical membrane. Electrolyte concentrations are also expected to be higher because of the increased number of metal ion transporters associated with carcinogenic cells (Brookes *et al*. 2006).

The overall Ti flux rates in perfused rat intestine (Chapter 4, Table 4-7) presented in this thesis are 5 and 3 times greater than overall Ti flux rates demonstrated in the mid gut of trout (Al-Jubory and Handy 2012) using the same method, materials and administered concentrations of bulk and nano TiO_2. Trout mid intestine is considerable thicker than rat small intestine and it would be expected that this would slow Ti/TiO_2 transport from TiO_2 exposures from lumen to serosa. Moreover endotherms have higher metabolic rates which may increase the rate of energy dependent vesicular processes. Interestingly if the values from the trout perfusion are compared to the rat perfusion the Q10 for NP uptake is 1.7 and for bulk uptake 2.3 which would also support the idea that an energy-dependent process is responsible for particle uptake rather than diffusional processes.

6.1.3 Uptake and accumulation- Is there a material type affect?

Both *in vitro* methods demonstrated in this thesis showed Ti tissue and cell accumulation from bulk and nano P25 TiO_2 exposures. The tissue/cell TiO_2 accumulation for both forms (bulk and nano P25) was similar in both types of experiment and analysis of the basolateral medium/perfusate established the appearance of Ti from bulk TiO_2 exposures was slower than the appearance of Ti from nano P25 exposures (Chapters 3 - 4). It would be expected that slower efflux of

Ti from bulk TiO_2 exposures would result in higher tissue accumulation if the rates of apical uptake were the same. This occurred in cell culture (Chapter 2-3), but, in the perfused intestine this was not the case, suggesting the rate of apical uptake is different for the bulk TiO_2 relative to the nano P25 TiO_2 in the perfused rat intestine model. Another plausible explanation for the discrepancies in the data between both models could be due to the differences in experimental design. In the cell culture experiments the increased settling rate of the bulk material would have increased particle contact time with the apical cell surface possibly resulting in the increased accumulation observed. However, in the perfusion model the increased settling time of the bulk material would have resulted in less contact time with the epithelium whilst the more stable suspension of NPs would have resulted in an increased particle contact time with the intestinal epithelium.

Uptake and accumulation of Ti metal from TiO_2 exposures demonstrated in both *in vitro* methods can be most easily explained by apical uptake of TiO_2 particles rather than surface bound or dissolved Ti. This is evidenced by the low concentration of surface bound tissue Ti represented by the rapid solution dipping experiment (Chapter 4, Fig 4-10) and the low dissolution rates of TiO_2 demonstrated in 0.1 M NaCl solutions (Schmidt and Vogelsberger 2009), intracellular saline solution (Al-Jubory and Handy 2012) and inside Caco-2 cells (Brun *et al*. 2014). Moreover, TEM and SEM evidence has repeatedly demonstrated intact particles within vesicles in cells below the apical membrane (Brun *et al*. 2014; Gitrowski *et al*. 2014; Janer *et al*. 2014). In this present thesis characterisation of the material in cells was performed by X-ray energy dispersive spectrophotometry (EDS) (Chapter 2, Fig. 2-9, 2-10). In the gut perfusion, TEM sections of TiO_2 exposed tissues showed morphologically

similar particles to those characterised in the stock solutions within vesicles and these were absent from the controls. Although this is not definitive evidence of particles from exposures within tissues a number of previous studies have made inferences about putative TiO_2 particles within or on tissues without EDS measurements based on morphological similarities to stock solutions (Jani *et al*. 1994; Galloway *et al*. 2010; Janer *et al*. 2014). The evidence suggests that TiO_2 Bulk and nano enter mammalian cells through an apical endocytosis mechanism.

6.1.4 Mechanisms of TiO_2 uptake and accumulation

The evidence presented in this thesis implies that TiO_2 particle uptake occurs through vesicular endocytic processes. Sensitivity to pharmacological agents suggests diffusion alone cannot be responsible for the Ti accumulation in cells and tissues following exposure to TiO_2 particles. Chlorpromazine is arguably a selective inhibitor of clathrin-mediated endocytosis. Additions of this drug to cells caused a reduction in accumulated Ti from bulk and nano anatase TiO_2 exposures suggesting clathrin mediated endocytosis is at least partially responsible for apical uptake of some forms of TiO_2. Genistein, a tyrosine kinase inhibitor broadly reduces actin cytoskeletal movement, which would be a prerequisite to any endocytic processes and has been used as a calveolae-mediated endocytosis inhibitor (Le and Nabi 2003; Rejman *et al*. 2005; dos Santos *et al*. 2011) caused a significant reduction in Ti accumulation for all forms of TiO_2 (Chapter 2, Fig. 2-8). The rutile form was particularly affected, suggesting that rutile TiO_2 NPs are preferentially absorbed through calveolae based endocytic processes. Interestingly additions of nystatin a putative cholesterol inhibitor caused a marked increase in cell Ti concentrations. This

same effect was demonstrated in jejunum tissue exposed to bulk TiO_2, suggesting apical uptake of TiO_2 is cholesterol independent, but basal efflux has a cholesterol-dependent component (Chapter 2, 4). For example, the initial and overall rates of Ti efflux into the serosa for jejunum exposed to nano P25 TiO_2 were markedly reduced in the presence of nystatin (Chapter 4, Table 4-7). In the presence of vanadate (a p-type ATPase inhibitor) significant increases in tissue and cell Ti was demonstrated following exposure. This suggests that apical uptake continues, but basal efflux is interrupted. Curiously the effect of an ion transport inhibitor on Ti accumulation would imply that some of the TiO_2 undergoes dissolution and is subsequently incapable of efflux from the cell. Information regarding vanadate sensitive ATPases being involved in exocytosis is sparse. However, metal transporting ATPases have been known to be involved in loading metal ions into vesicles (e.g. Cu Dameron and Harrison (1998)) and subsequently trafficked to the serosal membrane (Handy *et al*. 2000).

6.1.5 Potential toxicity- Is there a nano effect?

An initial hypothesis of this thesis considered that TiO_2 NPs will exert different physiological effects in comparison to the bulk version of the material. In the cell culture experiments (Chapter 2, Table 2-2; Chapter 3, Table 3-1) the addition of TiO_2 NPs caused a greater mean increase in intracellular Ca^{2+} relative to the bulk version of the particles following 24 h incubation (although bulk TiO_2 exposures caused mean cell Ca^{2+} increases relative to controls). This effect was demonstrated irrespective of cell age or growth substrate. In the gut perfusion work this increase in tissue Ca^{2+} was also noted, with NPs causing a larger mean Ca^{2+} increase than the

bulk material (Chapter 4, Table 6). This effect has also been demonstrated in perfused trout intestine using the same materials described herein (Al-Jubory and Handy 2012). In contrast, the response *in vivo* is not so clear. For example, Ramsden *et al*. (2009) reported no effects of dietary TiO_2 (bulk and nano) on tissue electrolytes concentrations (Na^+, K^+ and Ca^{2+}) *in vivo*, although brain Na^+/K^+ ATPase activity was reduced by 50% following an 8 week exposure of 10 and 100 mg kg^{-1} day^{-1} nano TiO_2. Alternatively, Hu *et al*. (2010) demonstrated a reduction in brain Ca^{2+}/Mg^{2+} ATPase activity and an increase in brain tissue Ca^{2+} in mice following intragastric administration of anatase NPs (5-50 mg kg^{-1}) every day for 60 days. Unfortunately it was not possible to infer whether disturbances to Ca homeostasis occurred *in vivo* in this present thesis (Chapter 5) because there was no sham control and the Ti in the feed was not adequately characterised. Tissue and cell Ca^{2+} concentrations are tightly regulated and the evidence presented herein highlights a potential concern with regards to dietary TiO_2 exposures interfering with calcium homeostasis. In light of this, more research on the precise mechanisms of TiO_2 induced changes in electrolyte homeostasis is required.

In this present work, there was no effect of 1 mg L^{-1} TiO_2 exposures on medium LDH activity in Caco-2 cell culture regardless of cell maturity (Chapter 2, Table 2-1; Chapter 3, Fig. 3-11), nor in the perfused intestine serosal perfusate and mucosal solution (Chapter 4, Fig. 4-4) relative to controls, which is indicative of undamaged epithelium. Similar responses have been demonstrated in perfused trout intestine (Al-Jubory and Handy 2012). Moreover, there was no effect on cell and tissue morphology (Chapters 2, 3 and 4), nor were there any differences in TEER (Chapter 3, Fig. 3-9) following exposures to all forms of TiO_2 (bulk and nano) which suggests tight junction integrity remained unaffected. Similar results have been demonstrated

by Koeneman *et al*. (2010) in cell culture for similar exposure concentrations. *In vivo* the situation is inconsistent. A number of researchers have demonstrated dietary exposures to TiO_2 NPs causes detrimental changes to a number of secondary target organs (GIT/ Liver/ Kidney Wang *et al*. (2007); Kidney Gui *et al*. (2013); Spleen Wang *et al*. (2011) Spleen /ovaries Tassinari *et al*. (2014). In contrast, a number of researchers have demonstrated no pathological effects associated with oral TiO_2 exposure and tissue accumulation (Jani *et al*. 1994; Cho *et al*. 2013; Geraets *et al*. 2014). The situation is still unclear and more research needs to be done.

6.1.6 Hazard screening

Nanotechnology is an area with large potential benefits for consumers, workers, patients and the environment. However, it is important that the risk posed by ENMs/ NPs are appropriately mitigated in order to take advantage of the benefits of the technology (Handy *et al*. 2008). Within the food sector this same risk benefit balance needs to be achieved. Nevertheless, nanotechnology and ENMs may expose humans and the environment to new risks that are as of yet largely unknown. The lack of information about the impacts of such technologies on public safety, and the potential toxicity of ENMs require a precautionary stance to be adopted in the absence of suitable regulation (Chau *et al*. 2007).

Currently there are many different areas of legislation that apply to the food sector, and few of these give specific guidance on ENMs NMs and NPs. The production of new ENMs will be subject to the European REACH (Registration, Evaluation, Authorization and Restrictions of Chemicals) legislation, and NONS (Notification of New Substances) legislation (Hansen 2010). There are no provisions in REACH

referring explicitly to ENMs, but they are intended to be covered by the “substance” definition in REACH (European-Commission 2008). Under this legislation manufacturers and importers will have to submit a dossier for substances that they manufacture or import at or above 1 tonne a year. At or above 10 tonnes the registrant will be required to produce a chemical safety report (European-Commission 2008). There are some concerns that small manufacturers of ENMs may not reach the 1 tonne threshold in REACH, and that some ENMs will be made of existing chemical substances that already have a CAS number (Handy and Shaw, 2007). REACH therefore needs modification to include new physical forms of existing chemicals. Top down substances are nanomaterials that are made by grinding/milling an existing bulk chemical to the nano scale (<100 nm). Other legislation which is applicable to the use of nanotechnology in the food sector does not refer to the issue of particle size (Table 6-1).

Table 6-1: Food legislation that needs altering to account for NPs

EU Regulation/ Directive	What does it cover?	What are the gaps?	Website
EU 258/97 EU novel foods regulation 258/97	Foods and novel food ingredients not consumed before the 15/05/1997	Does not cover material that has an established history of food use Does not cover particle size	http://europa.eu/legislation_summaries/consumers/consumer_safety/l21119_en.htm
EU 178/2002 The general safety article of the EU Food Law Regulation	Food traceability Food safety	Too loose	http://ec.europa.eu/food/food/foodlaw/traceability/index_en.htm
EC 97/618 Framework for scientific assessment of novel foods	Scientific assessment procedures for Regulation (EC) No 258/97	Doctrine of substantial equivalence a concern	http://eur-lex.europa.eu/smartapi/cgi/sga_doc?smartapi!celexapi!prod!CELEXnumdoc&lg=EN&numdoc=31997H0618&model=guichett
Directive 89/107 EU Food Additive Use Directive	Food additive	List of permitted additives Does not specifically cover particle size	http://europa.eu.int/eur-lex/lex/LexUriServ/site/en/consleg/1989/L/01989L0107-20031120-en.pdf
EU 94/36 Regulation on colours for use in foodstuff	Colours for use in food stuff	List of permitted colours. Does not specifically cover particle size	http://eur-lex.europa.eu/smartapi/cgi/sga_doc?smartapi!celexdoc!prod!CELEXnumdoc&numdoc=31994L0036&model=lex&lg=en

EU 1935/2004 EU Food Packaging Regulation	Must comply with food labelling laws. Must not be misleading. Active ingredients must comply with 89/107.	Does not cover particle size	http://eur-lex.europa.eu/ LexUriServ/site/en/oj/2004/l_338/ l_33820041113en00040017.pdf
Directive 91/414 Directive 79/117 EC Regulation No 396/200	Pesticide regulations covering plant based products.	Needs to cover nanoformulations	http://ec.europa.eu/food/plant/ protection/index_en.htm
Directive 98/8/EC, Directive 76/769/EEC.	Regulations covering biocidal products	Needs to cover nanoformulations	http://ec.europa.eu/environment/ biocides/index.htm
Regulation (EC) No 1907/2006 REACH	Regulation applying to the manufacture, placing on the market and use of substances on their own, in preparations or in articles	Too loose. Does not cover nano material from already accepted bulk substances.	http://eur-lex.europa.eu/LexUriServ/LexUriServ.do?uri=COM:2008:0366:FIN:en:PDF

(European-Commission 2008; Miller and Senjen 2008)

This present thesis highlights the uptake hazard of TiO_2 via oral exposure scenarios and could be used to partially inform policy makers on risk assessments. For example, the legislation needs to be modified to account for particle size because the data presented herein demonstrated the uptake hazard of TiO_2 NPs into the serosal compartments is greater than the bulk material (Chapter 4, Table 4-7) and should be considered in risk assessments. The crystal structure of the material needs to be taken into account. The Caco-2 work (Chapter 2-3) suggests the rutile form would present less of an uptake hazard than the anatase form and this should be accounted for in legislation. Moreover, legislation does not take into account vulnerable groups such as children who may have higher exposure risk and therefore uptake risk in comparison to adults. Further investigations on the effects of TiO_2 on food related risk assessments and NP hazards are advisable.

6.1.7 Future work

A number of areas require further investigations, and some suggestions are indicated below.

- Research into the mechanisms underpinning the alteration of electrolyte homeostasis is required. Particularly with respect to changes in calcium. The first stage would be to assess the form of Ca^{2+} (free or bound) responsible for the detected increases. This could be explored using Fura 2 dye and confocal microscopy in conjunction with TiO_2 exposures.
- In intestinal cell culture, SiRNA could be used to specifically knock out proteins associated with particular endocytic (e.g. caveolin, dynamin) pathways which may allow for a more precise evaluation of the mechanisms mediating particle uptake rather than using pseudo-specific pharmacological inhibitors.
- More in depth pharmacological investigations in the perfused intestine. For example chlorpromazine (a clathrin mediated endocytosis inhibitor) and genistein (a tyrosine kinase inhibitor) have been shown to reduce accumulation in cell culture and it is uncertain whether this would occur in the more physiologically relevant perfused intestine model.
- Assessing the effect of TiO_2 crystal structure on uptake and accumulation in the perfused intestine model and definitively demonstrating the form of the Ti in the serosal compartment (intact particle or ion) thereby extending the work from cell culture to a more physiologically relevant model
- Assessing how food matrix affects impact on TiO_2 NP bioavailability. NPs are unlikely to be ingested alone; rather, they will be incorporated into a food/

liquid matrix which will influence abiotic factors which in turn will affect particle behaviour and perhaps, bioavailability.

- Chronic *in vivo* dietary exposures exploring the effect of TiO_2 particle size, crystal structure and animal age on GIT uptake, systemic accumulation and pathologies. TiO_2 containing products are preferentially consumed by children and the metals literature has demonstrated increased toxicological sensitivity in young animals in comparison to adults.

Research in all these areas will inform hazard assessment and bring us one a step closer to understanding mechanisms underpinning uptake and potential toxicity of TiO_2 NPs.

References

Abbott, L. C. & Maynard, A. D. 2010. Exposure assessment approaches for engineered nanomaterials. Risk Analysis, 30, 1634-1644.

Aitken, R. J., Chaudhry, M. Q., Boxall, A. B. A. & Hull, M. 2006. Manufacture and use of nanomaterials: current status in the UK and global trends. Occupational Medicine, 56, 300-306.

Akiyama, T., Ishida, J., Nakagawa, S., Ogawara, H., Watanabe, S.I., Itoh, N., Shibuya, M. & Fukami, Y. 1987. Genistein, a specific inhibitor of tyrosine-specific protein kinases. Journal of Biological Chemistry, 262, 5592-5595.

Al-Jubory, A. R. & Handy, R. D. 2012. Uptake of titanium from TiO_2 nanoparticle exposure in the isolated perfused intestine of rainbow trout: nystatin, vanadate and novel CO_2-sensitive components. Nanotoxicology, 7, 1282-1301.

Alberts, B., A. Johnson, J. Lewis., M. Raff., K. Roberts & P. Walter. 2008. Molecular Biology of the cell. New York, Garland Science, Taylor and Francis Group.

AOAC. 2007. Method 2007-04. Association of Official Analytical Chemists, Washington, DC.

Ando, M., Sasaki, H. & Huang, K. C. 1986. A new technique for measuring water transport across the seawater eel intestine. Journal of Experimental Biology, 122, 257-268.

Aquanova. 2006. Innovative liquid formulas for dietary supplements [Online]. Available: http://www.marcohi-tech.com/materials/NovaSOL_Technology.pdf [Accessed 19/10 2010].

Arredondo, M., Martinez, R., Nunez, M., Ruz, M. & Olivares, M. 2006. Inhibition of copper uptake by iron copper and zinc. Biological Research, 39, 95-102.

Arredondo, M., Uauy, R. & González, M. 2000. Regulation of copper uptake and transport in intestinal cell monolayers by acute and chronic copper exposure. Biochimica et Biophysica Acta (BBA) - General Subjects, 1474, 169-176.

Arrieta, M. C., Bistritz, L. & Meddings, J. B. 2006. Alterations in intestinal permeability. Gut, 55, 1512-1520.

Artursson, P., Palm, K. & Luthman, K. 2001. Caco-2 monolayers in experimental and theoretical predictions of drug transport. Advanced Drug Delivery Reviews, 46, 27-43.

Ashwood, P., Thompson, R. P. H. & Powell, J. J. 2007. Fine particles that adsorb lipopolysaccharide via bridging calcium cations may mimic bacterial pathogenicity towards cells. Experimental Biology and Medicine., 232, 107-117.

Au, A. P. & Reddy, M. B. 2000. Caco-2 cells can be used to assess human iron bioavailability from a semipurified meal. The Journal of nutrition, 130, 1329-1334.

Axel-Weiner, J. & Nylander, M. 1993. The relationship between mercury concentration in human organs and different predictor variables. Science of The Total Environment, 138, 101-115.

Baan, R., Straif, K., Grosse, Y., Secretan, B., El Ghissassi, F. & Cogliano, V. 2006. Carcinogenicity of carbon black, titanium dioxide, and talc. The Lancet Oncology, 7, 295 - 296.

Barksdale, J. 1950. Titanium, its occurrence, chemistry, and technology, New York, The Ronald Press Company.

Barrabin, H., Garrahan, P. J. & Rega, A. F. 1980. Vanadate inhibition of the Ca^{2+}-ATPase from human red cell membranes. Biochimica et Biophysica Acta (BBA)-Biomembranes, 600, 796-804.

Barteau, M. A. 1996. Organic reactions at well-defined oxide surfaces. Chemical Reviews, 96, 1413-1430.

Bergin, I. & Witzemabb, F. 2013. Nanoparticle toxicity by the gastrointestinal route: evidence and knowledge gaps. International journal of biomedical nanosciene and nanotechnology, 3, 163-210.

Bergmeyer, H. U. & Bernt, E. 1974. Lactate Dehydrogenase. In: Bergmeyer, H. U. (ed.) Methods of Enzymatic Analysis (Second Edition). Academic Press.

Bermudez, E., Mangum, J., Wong, B., Asgharian, B., Hext, P., Warheit, D. & Everitt, J. 2004. Pulmonary responses of mice, rats, and hamsters to subchronic inhalation of ultrafine titanium dioxide particles. Toxicological Sciences, 77, 347 - 357.

Bernard, B., Osheroff, M., Hofmann, A. & Mennear, J. 1990. Toxicology and carcinogenesis studies of dietary titanium dioxide-coated mica in male and female Fischer 344 rats. Journal of Toxicology and Environmental Health, 29, 417 - 429.

Blaustein, M. P. & Lederer, W. J. 1999. Sodium/Calcium Exchange: Its physiological implications. Physiological Reviews, 79, 763-854.

Böckmann, J., Lahl, H., Eckert, T. & Unterhalt, B. 2000. Blood titanium levels before and after oral administration titanium dioxide. Die Pharmazie, 55, 140-143.

Bogdanske, J. J., Stelle, S. H. V., Riley, M. R. & Schiffman, B. M. 2011. Laboratory rat procedural techniques, New York, Taylor and Francis.

Borm, P., Schins, R. & Albrecht, C. 2004. Inhaled particles and lung cancer, part B: paradigms and risk assessment. International Journal of Cancer, 110, 3 - 14.

Bouwmeester, H., Dekkers, S., Noordam, M. Y., Hagens, W. I., Bulder, A. S., De Heer, C., Ten Voorde, S. E. C. G., Wijnhoven, S. W. P., Marvin, H. J. P. & Sips, A. J. a. M. 2009. Review of health safety aspects of nanotechnologies in food production. Regulatory Toxicology and Pharmacology, 53, 52-62.

Boyle, J. F., Manas-Zloczower, I. & Feke, D. L. 2005. Hydrodynamic analysis of the mechanisms of agglomerate dispersion. Powder Technology, 153, 127-133.

Boylstein, R., Piacitelli, C., Grote, A., Kanwal, R., Kullman, G. & Kreiss, K. 2006. Diacetyl emissions and airborne dust from butter flavorings used in microwave popcorn production. Journal of occupational and environmental hygiene, 3, 530-535.

Brookes, M. J., Hughes, S., Turner, F. E., Reynolds, G., Sharma, N., Ismail, T., Berx, G., Mckie, A. T., Hotchin, N., Anderson, G. J., Iqbal, T. & Tselepis, C. 2006. Modulation of iron transport proteins in human colorectal carcinogenesis. Gut, 55, 1449-1460.

Brown, G. E., Henrich, V. E., Casey, W. H., Clark, D. L., Eggleston, C., Felmy, A., Goodman, D. W., Gratzel, M., Maciel, G., Mccarthy, M. I., Nealson, K. H., Sverjensky, D. A., Toney, M. F. & Zachara, J. M. 1998. Metal oxide surfaces and their interactions with aqueous solutions and microbial organisms. Chemical Reviews, 99, 77-174.

Brun, E., Barreau, F., Veronesi, G., Fayard, B., Sorieul, S., Chaneac, C., Carapito, C., Rabilloud, T., Mabondzo, A., Herlin-Boime, N. & Carriere, M. 2014. Titanium dioxide nanoparticle impact and translocation through *ex vivo*, *in vivo* and *in vitro* gut epithelia. Particle and Fibre Toxicology, 11, 13.

Buechter, D. 1988. Free radicals and oxygen toxicity. Pharmaceutical Research, 5, 253 - 260.

Burke, J. & Handy, R. 2005. Sodium-sensitive and-insensitive copper accumulation by isolated intestinal cells of rainbow trout *Oncorhynchus mykiss*. Journal of Experimental Biology, 208, 391-407.

Bury, N. & Handy, R. 2010. Copper and iron uptake in teleost fish. Surface chemistry, bioavailability and metal homeostasis in aquatic organisms:. An integrated approach. Essential Reviews in Experimental Biology, 2, 107-127.

Bu, Q., Yan, G., Deng, P., Peng, F., Lin, H., Xu, Y., Cao, Z., Zhou, T., Xue, A. & Wang, Y. 2010. NMR-based metabonomic study of the sub-acute toxicity of titanium dioxide nanoparticles in rats after oral administration. Nanotechnology, 21, 125105.

Caloin, M. 2004. Modeling of lipid and protein depletion during total starvation. American Journal of Physiology - Endocrinology and Metabolism, 287, 790-798.

Campbell, H., Handy, R. & Nimmo, M. 1999. Copper uptake kinetics across the gills of rainbow trout (*Oncorhynchus mykiss*) measured using an improved isolated perfused head technique. Aquatic Toxicology, 46, 177-190.

Campbell, P. 1995. Interactions between trace metals and aquatic organisms: A critique of the free-ion activity model. In: Tessier, A. & Turner, D. R. (eds.) Metal speciation and bioavailability in aquatic systems. Chichester UK: John Wiley and Sons.

Cantley, L. C., Resh, M. D. & Guidotti, G. 1978. Vanadate inhibits the red cell (Na^+/K^+;) ATPase from the cytoplasmic side.

Cartiera, M. S., Johnson, K. M., Rajendran, V., Caplan, M. J. & Saltzman, W. M. 2009. The uptake and intracellular fate of PLGA nanoparticles in epithelial cells. Biomaterials, 30, 2790-2798.

Chau, C. F., Wu, S. H. & Yen, G. C. 2007. The development of regulations for food and nanotechnology. Trends in Food Science & Technology, 18, 269-280.

Chaudhry, Q., Scotter, M., Blackburn, J., Ross, B., Boxall, A., Castle, L., Aitken, R. & Watkins, R. 2008. Applications and implications of nanotechnologies for the food sector. Food Additives & Contaminants: Part A: Chemistry, Analysis, Control, Exposure & Risk Assessment, 25, 241 - 258.

Chen, H.W., Su, S.F., Chien, C.T., Lin, W.H., Yu, S.L., Chou, C.C., Chen, J. J. W. & Yang, P.C. 2006. Titanium dioxide nanoparticles induce emphysema-like lung injury in mice. The FASEB Journal, 20, 2393-2395.

Chen, J., Dong, X., Zhao, J. & Tang, G. 2009. *In vivo* acute toxicity of titanium dioxide nanoparticles to mice after intraperitioneal injection. Journal of Applied Toxicology, 29, 330-337.

Chen, L., Remondetto, G. E. & Subirade, M. 2006. Food protein based materials as nutraceuticals delivery systems. Trends in Food Science & Technology, 17, 272-283.

Chen, X.X., Cheng, B., Yang, Y.X., Cao, A., Liu, J.H., Du, L.J., Liu, Y., Zhao, Y. & Wang, H. 2013. Characterization and preliminary toxicity assay of nano-titanium dioxide additive in sugar-coated chewing gum. Small, 9, 1765-1774.

Chen, X. & Mao, S. S. 2007. Titanium dioxide nanomaterials: synthesis, properties, modifications, and applications. Chemical Reviews, 107, 2891-2959.

Chen, Y., Wang, S., Lu, X., Zhang, H., Fu, Y. & Luo, Y. 2011. Cholesterol sequestration by nystatin enhances the uptake and activity of endostatin in endothelium via regulating distinct endocytic pathways. Blood, 117, 6392-6403.

Chen, Z., Meng, H., Xing, G., Chen, C., Zhao, Y., Jia, G., Wang, T., Yuan, H., Ye, C. & Zhao, F. 2006c. Acute toxicological effects of copper nanoparticles in vivo. Toxicology Letters, 163, 109-120.

Cheng, Z.-J., Singh, R. D., Sharma, D. K., Holicky, E. L., Hanada, K., Marks, D. L. & Pagano, R. E. 2006. Distinct mechanisms of clathrin-independent endocytosis have unique sphingolipid requirements. Molecular biology of the cell, 17, 3197-3210.

Chintagari, N. R., Jin, N., Wang, P., Narasaraju, T. A., Chen, J. & Liu, L. 2006. Effect of cholesterol depletion on exocytosis of alveolar type II cells. American journal of respiratory cell and molecular biology, 34, 677-687.

Cho, W.S., Kang, B.C., Lee, J. K., Jeong, J., Che, J.H. & Seok, S. H. 2013. Comparative absorption, distribution, and excretion of titanium dioxide and zinc oxide nanoparticles after repeated oral administration. Particle and Fibre Toxicology, 10, 9.

Chou, J.C. & Liao, L. P. 2005. Study on pH at the point of zero charge of TiO_2 pH ion-sensitive field effect transistor made by the sputtering method. Thin Solid Films, 476, 157-161.

Cientifica. 2006. Nanotechnologies in the food industry [Online]. Available: http://cientifica.eu/blog/white-papers/nanotechnologies-in-2009/ [Accessed 19/10 2010].

Cook, J., Sutterlin, A. & Mcniven, M. A. 2000. Effect of food deprivation on oxygen consumption and body composition of growth-enhanced transgenic Atlantic salmon (*Salmosalar*). Aquaculture, 188, 47-63.

Creeth, J. 1978. Constituents of mucus and their separation. British medical bulletin, 34, 17-24.

Cremer, J. E., Braun, L. D. & Oldendorf, W. H. 1976. Changes during development in transport processes of the blood-brain barrier. Biochimica et Biophysica Acta (BBA) - Biomembranes, 448, 633-637.

Cui, Y., Gong, X., Duan, Y., Li, N., Hu, R., Liu, H., Hong, M., Zhou, M., Wang, L., Wang, H. & Hong, F. 2010. Hepatocyte apoptosis and its molecular mechanisms in mice caused by titanium dioxide nanoparticles. Journal of Hazardous Materials, 183, 874-880.

Cui, Y., Liu, H., Zhou, M., Duan, Y., Li, N., Gong, X., Hu, R., Hong, M. & Hong, F. 2011. Signalling pathway of inflammatory responses in the mouse liver caused by TiO_2 nanoparticles. Journal of Biomedical Materials Research Part A, 96A, 221-229.

Dameron, C. T. & Harrison, M. D. 1998. Mechanisms for protection against copper toxicity. The American Journal of Clinical Nutrition, 67, 1091S-1097S.

Dankovic, D., Kuempel, E. & Wheeler, M. 2007. An approach to risk assessment for TiO_2. Inhalation Toxicology, 19, 205 - 212.

De Haar, C., Hassing, I., Bol, M., Bleumink, R. & Pieters, R. 2006. Ultrafine but not fine particulate matter causes airway inflammation and allergic airway sensitization to co‐administered antigen in mice. Clinical & Experimental Allergy, 36, 1469-1479.

Deng, Z., Mortimer, G., Schiller, T., Musumeci, A., Martin, D. & Minchin, R. 2009. Differential plasma protein binding to metal oxide nanoparticles. Nanotechnology, 20, 455101.

Des Rieux, A., Fievez, V., Garinot, M., Schneider, Y.J. & Préat, V. 2006. Nanoparticles as potential oral delivery systems of proteins and vaccines: A mechanistic approach. Journal of Controlled Release, 116, 1-27.

Dharmsathaphorn, K. & Madara, J. L. 1990. Established intestinal cell lines as model systems for electrolyte transport studies. Methods in enzymology, 192, 354-389.

Diebold, U. 2003. The surface science of titanium dioxide. Surface science reports, 48, 53-229.

Dos Santos, T., Varela, J., Lynch, I., Salvati, A. & Dawson, K. A. 2011. Effects of transport inhibitors on the cellular uptake of carboxylated polystyrene nanoparticles in different cell lines. PLoS ONE, 6, e24438.

Duan, Y., Liu, J., Ma, L., Li, N., Liu, H., Wang, J., Zheng, L., Liu, C., Wang, X., Zhao, X., Yan, J., Wang, S., Wang, H., Zhang, X. & Hong, F. 2010. Toxicological characteristics of nanoparticulate anatase titanium dioxide in mice. Biomaterials, 31, 894-899.

Eilam, Y. & Grossowicz, N. 1982. Nystatin effects on cellular calcium in Saccharomyces cerevisiae. Biochimica et Biophysica Acta (BBA)-Biomembranes, 692, 238-243.

European-Commission 2013. SCCS opinion on titanium dioxide (nano form). Scientific committee on consumer safety. Luxembourg.

European-Commission 2014. How to facilitate the use of alternative methods by regulators? 10th EPAA Annual Conference. Brussels.

European-Commission. 2011. Communication from the Commission to the European Parliament, the council and the European economic and social Committee, Regulatory aspects of nanomaterial's, [Online]. Available: http://ec.europa.eu/environment/chemicals/nanotech/faq/definition_en.htm [Accessed 20/06 2015].

European-Commission (2008) 'Communication from the Commission to the European Parliament, the council and the European economic and social Committee, Regulatory aspects of nanomaterial's, '[Online]. Available at: http://eur-

lex.europa.eu/LexUriServ/LexUriServ.do?uri=COM:2008:0366:FIN:en:PDF (Accessed: 20/10).

Fabian, E., Landsiedel, R., Ma-Hock, L., Wiench, K., Wohlleben, W. & Ravenzwaay, B. 2008. Tissue distribution and toxicity of intravenously administered titanium dioxide nanoparticles in rats. Archives of Toxicology, 82, 151-157.

FAO 2006. Titanium Dioxide: Chemical and Technical Assessment. Food and Agriculture Organisation.

FDA. 2014. Determining the Regulatory Status of a Food Ingredient [Online]. Available: http://www.fda.gov/Food/IngredientsPackagingLabeling/FoodAdditivesIngredients/ucm228269.htm [Accessed 29/06 2015].

Federici, G., Shaw, B. J. & Handy, R. D. 2007. Toxicity of titanium dioxide nanoparticles to rainbow trout (*Oncorhynchus mykiss*): Gill injury, oxidative stress, and other physiological effects. Aquatic Toxicology, 84, 415-430.

Feltz, A. 1987. R. J. D. Tilley. Defect crystal chemistry and its applications. Blackie and Sons Limited, Glasgow and London. Published in USA by Chapman and Hall, New York, 1987. Crystal Research and Technology, 22, 1210-1210.

Ferin, J. & Oberdörster, G. 1985. Biological effects and toxicity assessment of titanium dioxides: anatase and rutile. The American Industrial Hygiene Association Journal, 46, 69-72.

Ferin, J., Oberdorster, G. & Penney, D. 1992. Pulmonary retention of ultrafine and fine particles in rats. American Journal of Respiratory Cell and Molecular Biology, 6, 535 - 542.

Fisichella, M., Berenguer, F., Steinmetz, G., Auffan, M., Rose, J. & Prat, O. 2012. Intestinal toxicity evaluation of TiO_2 degraded surface-treated nanoparticles: a combined physico-chemical and toxicogenomics approach in Caco-2 cells. Particle and Fibre Toxicology, 9, 18.

Flatman, P. W. 2002. Regulation of Na–K–2Cl cotransport by phosphorylation and protein–protein interactions. Biochimica et Biophysica Acta (BBA)-Biomembranes, 1566, 140-151.

Forbes, G. B. & Reina, J. C. 1972. Effect of age on gastrointestinal absorbtion. Journal of Nutrition, 102, 647.

Frewer, L. J., Norde, W., Fischer, A. & Kampers, F. 2011. Nanotechnology in the agri-food sector, John Wiley & Sons.

Froment, D. P., Molitoris, B. A., Buddington, B., Miller, N. & Alfrey, A. C. 1989. Site and mechanism of enhanced gastrointestinal absorption of aluminum by citrate. Kidney international, 36, 978 -84.

Garnett, M. C. & Kallinteri, P. 2006. Nanomedicines and nanotoxicology: some physiological principles. Occupational Medicine, 56, 307-311.

Geraets, L., Oomen, A., Krystek, P., Jacobsen, N., Wallin, H., Laurentie, M., Verharen, H., Brandon, E. & De Jong, W. 2014. Tissue distribution and elimination after oral and intravenous administration of different titanium dioxide nanoparticles in rats. Particle and Fibre Toxicology, 11, 30.

Gerloff, K., Fenoglio, I., Carella, E., Kolling, J., Albrecht, C., Boots, A., Forster, I. & Schins, R. 2012. Distinctive toxicity of TiO_2 rutile/anatase mixed phase nanoparticles on Caco-2 cells. Chem Res Toxicol, 25, 646 - 655.

Gershbein, L. L. & Raikoff, K. G. 1977. Total lactate dehydrogenase and its isoenzymes in serum in the presence of penicillamine and other sulfhydryl compounds. Clinical chemistry, 23, 229-233.

Gitrowski, C., Al-Jubory, A. R. & Handy, R. D. 2014. Uptake of different crystal structures of TiO_2 nanoparticles by Caco-2 intestinal cells. Toxicology Letters, 226, 264-276.

Global-Industry-Analysts. 2012. Nanotechnology- A global industry outlook [Online]. Available: http://www.strategyr.com/GOS.asp?code=GOS-094 [Accessed 15/09/2013 2013].

González, R. C. & Woods, R. E. 2001. Digital Image Processing, Pearson Education.

Goodman, M. N., Mcelaney, M. A. & Ruderman, N. B. 1981. Adaptation to prolonged starvation in the rat: curtailment of skeletal muscle proteolysis. American Journal of Physiology - Endocrinology and Metabolism, 241, E321-E327.

Gopal, D. & Rosen, H. 2000. Abnormal findings on liver function tests: Interpreting results to narrow the diagnosis and establish a prognosis (vol 107, pg 100, 2000). Postgraduate Medicine, 107, 24-24.

Gui, S., Sang, X., Zheng, L., Ze, Y., Zhao, X., Sheng, L., Sun, Q., Cheng, Z., Cheng, J., Hu, R., Wang, L., Hong, F. & Tang, M. 2013. Intragastric exposure to titanium dioxide nanoparticles induced nephrotoxicity in mice, assessed by physiological and gene expression modifications. Particle and Fibre Toxicology, 10, 4.

Guo L.L., Liu X.H., Qin D.X., Gao L., Zhang H.M., Liu J.Y & YG., C. 2009. Effects of nanosized titanium dioxide on the reproductive system of male mice. National journal of andrology, 15, 517-522.

Gwinn, M. R. & Vallyathan, V. 2006. Nanoparticles: health effects: pros and cons. Environmental health perspectives, 1818-1825.

Hagens, W., Oomen, A., De Jong, W., Cassee, F. & Sips, A. 2007. What do we (need to) know about the kinetic properties of nanoparticles in the body? Regulatory Toxicology Pharmacology, 49, 217 - 229.

Handy, R., Eddy, F. & Baines, H. 2002. Sodium-dependent copper uptake across epithelia: a review of rationale with experimental evidence from gill and intestine. Biochimica et Biophysica Acta (BBA)-Biomembranes, 1566, 104-115.

Handy, R., Gow, I., Ellis, D. & Flatman, P. 1996. Na-dependent regulation of intracellular free magnesium concentration in isolated rat ventricular myocytes. Journal of molecular and cellular cardiology, 28, 1641-1651.

Handy, R., Henry, T., Scown, T., Johnston, B. & Tyler, C. 2008a. Manufactured nanoparticles: their uptake and effects on fish—a mechanistic analysis. Ecotoxicology, 17, 396-409.

Handy, R., Von Der Kammer, F., Lead, J., Hassellöv, M., Owen, R. & Crane, M. 2008b. The ecotoxicology and chemistry of manufactured nanoparticles. Ecotoxicology, 17, 287-314.

Handy, R. D. & Eddy, F. B. 2004. Transport of solutes across biological membranes in eukaryotes: an environmental perspective. IUPAC Sieries on analytical and physical chemistry of environmental systems, 9, 337-356.

Handy, R. D. & Maunder, R. J. 2009. The biological roles of mucus: Importance for osmoregulation and osmoregulatory disorders of fish health, London, Society for Experimental Biology.

Handy, R. D., Musonda, M. M., Phillips, C. & Falla, S. J. 2000. Mechanisms of gastrointestinal copper absorption in the African walking catfish: copper dose-effects and a novel anion-dependent pathway in the intestine. Journal of Experimental Biology, 203, 2365-2377.

Handy, R. D. & Shaw, B. J. 2007. Ecotoxicity of nanomaterials to fish: challenges for ecotoxicity testing. Integrated Environmental Assessment and Management, 3, 458-460.

Hansen, F. S., Larsen, B. H., Olsen, S. I. & Baun, A. 2007. Categorization framework to aid hazard identification of nanomaterials. Nanotoxicology, 1, 243-250.

Hansen, G. H., Rasmussen, K., Niels-Christiansen, L.L. & Danielsen, E. M. 2009. Endocytic trafficking from the small intestinal brush border probed with FM dye.

Hansen, S., Michelson, E., Kamper, A., Borling, P., Stuer-Lauridsen, F. & Baun, A. 2008. Categorization framework to aid exposure assessment of nanomaterials in consumer products. Ecotoxicology, 17, 438-447.

Hansen, S. F., Jensen, K. A. & Baun, A. 2014. NanoRiskCat: a conceptual tool for categorization and communication of exposure potentials and hazards of nanomaterials in consumer products. Journal of Nanoparticle Research, 16, 1-25.

Heinrich, U., Fuhst, R., Rittinghausen, S., Creutzenberg, O., Bellmann, B., Koch, W. & Levsen, K. 1995. Chronic Inhalation Exposure of Wistar Rats and two Different strains of mice to diesel engine exhaust, carbon black, and titanium dioxide. Inhalation Toxicology, 7, 533-556.

Henrich, V. & Cox, P. 1994. The surface science of metal oxides. Cambridge University Press, Cambridge

Hellstrand, E., Lynch, I., Andersson, A., Drakenberg, T., Dahlbäck, B., Dawson, K. A., Linse, S. & Cedervall, T. 2009. Complete high-density lipoproteins in nanoparticle corona. FEBS Journal, 276, 3372-3381.

Helmut-Kaiser-Consultancy. 2011. Nanotechnology in Food and Food Processing Industry Worldwide. [Online]. Available: http://www.hkc22.com/Nanofood.html [Accessed 19/10 2010].

Herold, G., Rogler, G., Rogler, D. & Stange, E. 1994. Morphology of Caco-2 cells varies in different cell batches. In Vitro Cellular & Developmental Biology - Animal, 30, 289-291.

Hillery, A. M., Jani, P. U. & Florence, A. T. 1994. Comparative, quantitative study of lymphoid and non-lymphoid uptake of 60 nm polystyrene particles. Journal of Drug Targeting, 2, 151 -156.

Hillyer, J. & Albrecht, R. 2001. Gastrointestinal persorption and tissue distribution of differently sized colloidal gold nanoparticles. Journal of Pharmaceutical Sciences, 90, 1927 - 1936.

Hirayama, T., Tamaki, Y., Takakubo, Y., Iwazaki, K., Sasaki, K., Ogino, T., Goodman, S. B., Konttinen, Y. T. & Takagi, M. 2011. Toll‐like receptors and their adaptors are regulated in macrophages after phagocytosis of lipopolysaccharide‐coated titanium particles. Journal of Orthopaedic Research, 29, 984-992.

Houba, R., Doekes, G. & Heederik, D. 1998. Occupational respiratory allergy in bakery workers: a review of the literature. American journal of industrial medicine, 34, 529-546.

Hoyle, I. & Handy, R. D. 2005. Dose-dependent inorganic mercury absorption by isolated perfused intestine of rainbow trout, *Oncorhynchus mykiss*, involves both amiloride-sensitive and energy-dependent pathways. Aquatic Toxicology, 72, 147-159.

Hu, L., Mao, Z., Zhang, Y. & Gao, C. 2011. Influences of size of silica particles on the cellular endocytosis, exocytosis and cell activity of HepG2 cells. Journal of Nanoscience Letters, 1.

Hu, R., Gong, X., Duan, Y., Li, N., Che, Y., Cui, Y., Zhou, M., Liu, C., Wang, H. & Hong, F. 2010. Neurotoxicological effects and the impairment of spatial recognition memory in mice caused by exposure to TiO_2 nanoparticles. Biomaterials, 31, 8043-8050.

Hubbs, A. F., Goldsmith, W. T., Kashon, M. L., Frazer, D., Mercer, R. R., Battelli, L. A., Kullman, G. J., Schwegler-Berry, D., Friend, S. & Castranova, V. 2008. Respiratory toxicologic pathology of inhaled diacetyl in Sprague-Dawley rats. Toxicologic pathology, 36, 330-344.

Huggins, C. & Froehlich, J. 1966. High concentration of injected titanium dioxide in abdominal lymph nodes. TheJournal of Experimental Medicine, 124, 1099 - 1106.

Inaba, J. & Lengemann, F. W. 1972. Intestinal uptake and whole body retention of 141Ce by suckling rats. Health Physics, 22, 169.

Iversen, T.G., Skotland, T. & Sandvig, K. 2011. Endocytosis and intracellular transport of nanoparticles: present knowledge and need for future studies. Nano Today, 6, 176-185.

Jacobs, J., Skipor, A., Black, J., Urban, R. & Galante, J. 1991. Release and excretion of metal in patients who have a total hip-replacement component made of titanium-base alloy. Journal of Bone and Joint Surgery American Volume, 73, 1475 - 1486.

Janer, G., Mas Del Molino, E., Fernández-Rosas, E., Fernández, A. & Vázquez-Campos, S. 2014. Cell uptake and oral absorption of titanium dioxide nanoparticles. Toxicology Letters, 228, 103-110.

Jani, P. U., Mccarthy, D. E. & Florence, A. T. 1994. Titanium dioxide (rutile) particle uptake from the rat GI tract and translocation to systemic organs after oral administration. International Journal of Pharmaceutics, 105, 157-168.

Jecfa 1969. Thirtieth report of the joint FAO/WHO expert committee on food additives. FAO nutrition meetings report series.

Johannessen, L. E., Spilsberg, B., Wiik-Nielsen, C. R., Kristoffersen, A. B., Holst-Jensen, A. & Berdal, K. G. 2013. DNA-fragments are transcytosed across Caco-2 cells by adsorptive endocytosis and vesicular mediated transport. PLoS ONE, 8, e56671.

Joseph, T. & Morrison, M. 2006. Nanoforum Report: Nanotechnology in Agriculture and Food. Institute of Nanotechnology.

Jovanović, B. 2014. Critical review of public health regulations of titanium dioxide, a human food additive. Integrated Environmental Assessment and Management, 11, 10-20.

Jovanovic, B. J., Jojic, S. G., Stanojevic, B. V., Adnadevic, V. & Vujosevic, M. 2012. Age differences in bioaccumulation of heavy metals in populations of th eblack-striped field mouse. International Journal of Environmental Research, 6, 1045-6865.

Julio, G., Merindano, M. D., Canals, M. & Ralló, M. 2008. Image processing techniques to quantify microprojections on outer corneal epithelial cells. Journal of anatomy, 212, 879-886.

Jüttner, R. & Ebel, H. 1998. Characterization of Mg^{2+} transport in brush border membrane vesicles of rabbit ileum studied with mag-fura-2. Biochimica et Biophysica Acta (BBA)-Biomembranes, 1370, 51-63.

Kalgaonkar, S. & Lönnerdal, B. 2009. Receptor-mediated uptake of ferritin-bound iron by human intestinal Caco-2 cells. The Journal of Nutritional Biochemistry, 20, 304-311.

Kanwal, R. 2008. Bronchiolitis obliterans in workers exposed to flavoring chemicals. Current opinion in pulmonary medicine, 14, 141-146.

Kaplan, J. H. & Lutsenko, S. 2009. Copper transport in mammalian cells: special care for a metal with special needs. Journal of Biological Chemistry, 284, 25461-25465.

Keller, A. A., Wang, H., Zhou, D., Lenihan, H. S., Cherr, G., Cardinale, B. J., Miller, R. & Ji, Z. 2010. Stability and aggregation of metal oxide nanoparticles in natural aqueous matrices. Environmental Science & Technology, 44, 1962-1967.

Kello, D. & Kostial, K. 1977. Influence of age on whole body retention and distribution of 115mCd in the rat. Environmental research, 14, 92-98.

Kirchhausen, T. 2009. Imaging endocytic clathrin structures in living cells. Trends in Cell Biology, 19, 596-605.

Kirkham, M. & Parton, R. G. 2005. Clathrin-independent endocytosis: new insights into caveolae and non-caveolar lipid raft carriers. Biochimica et Biophysica Acta (BBA)-Molecular Cell Research, 1745, 273-286.

Kiser, M., Westerhoff, P., Benn, T., Wang, Y., Perez-Rivera, J. & Hristovski, K. 2009. Titanium nanomaterial removal and release from wastewater treatment plants. Environmental Science & Technology, 43, 6757-6763.

Kiss, A. L. & Botos, E. 2009. Endocytosis via caveolae: alternative pathway with distinct cellular compartments to avoid lysosomal degradation? Journal of Cellular and Molecular Medicine, 13, 1228-1237.

Kobayashi, N., Naya, M., Endoh, S., Maru, J., Yamamoto, K. & Nakanishi, J. 2009. Comparative pulmonary toxicity study of nano-TiO_2 particles of different sizes and agglomerations in rats: Different short- and long-term post-instillation results. Toxicology, 264, 110-118.

Koeneman, B., Zhang, Y., Westerhoff, P., Chen, Y., Crittenden, J. & Capco, D. 2010. Toxicity and cellular responses of intestinal cells exposed to titanium dioxide. Cell Biology and Toxicology, 26, 225-238.

Koivusalo, M., Welch, C., Hayashi, H., Scott, C. C., Kim, M., Alexander, T., Touret, N., Hahn, K. M. & Grinstein, S. 2010. Amiloride inhibits macropinocytosis by lowering submembranous pH and preventing Rac1 and Cdc42 signaling. The Journal of cell biology, 188, 547-563.

Koodali, R. T. & Klabunde, K. J. 2006. Catalysis by metal oxides. In: Richards, R. (ed.) Surface and nanomeclucal catalysts. London: Taylor and Francis.

Kostial, K., Kello, D., Jugo, S., Rabar, I. & Maljkovic, T. 1978. Influence of age on metal metabolism and toxicity. Environmental health perspectives, 25, 81-86.

Kreyling, W., Semmler, M., Erbe, F., Mayer, P., Takenaka, S., Schulz, H., Oberdörster, G. & Ziesenis, A. 2002. Translocation of ultrafine insoluble iridium particles from lung epithelium to extrapulmonary organs is size dependent but very low. Journal of Toxicology and Environmental Health Part A, 65, 1513-1530.

Kühlbrandt, W. 2004. Biology, structure and mechanism of P-type ATPases. Nature Reviews Molecular Cell Biology, 5, 282-295.

Lademann, J., Weigmann, H., Rickmeyer, C., Barthelmes, H., Schaefer, H., Mueller, G. & Sterry, W. 1999. Penetration of titanium dioxide microparticles in a sunscreen formulation into the horny layer and the follicular orifice. Skin Pharmacology Applied Skin Physiology, 12, 247 - 256.

Larsen, S., Roursgaard, M., Jensen, K. & Nielsen, G. 2010. Nano titanium dioxide particles promote allergic sensitization and lung inflammation in mice. Basic Clin Pharmacol Toxicol, 106, 114 - 117.

Le, P. U. & Nabi, I. R. 2003. Distinct caveolae-mediated endocytic pathways target the Golgi apparatus and the endoplasmic reticulum. Journal of Cell Science, 116, 1059-1071.

Lead, J. R. & Wilkinson, K. J. 2006. Aquatic colloids and nanoparticles: current knowledge and future trends. Environmental Chemistry, 3, 159-171.

Lecce, J. G. 1972. Selective absorption of macromolecules into intestinal epithelium and blood by neonatal mice. Journal of Nutrition, 102, 69-76.

Lee, K., Trochimowicz, H. & Reinhardt, C. 1985. Pulmonary response of rats exposed to titanium dioxide (TiO_2) by inhalation for two years. Toxicology and Applied Pharmacology, 79, 179 - 192.

Lefevre, M. E., Olivo, R., Vanderhoff, J. W. & Joel, D. D. 1978. Accumulation of latex in Peyer's patches and its subsequent appearance in villi and mesenteric lymph nodes. Proceedings of the society for experimental biology and medicine, 159, 298 - 302.

Lewis, S. A., Eaton, D. C., Clausen, C. & Diamond, J. M. 1977. Nystatin as a probe for investigating the electrical properties of a tight epithelium. The Journal of General Physiology, 70, 427-440.

Li, N., Duan, Y., Hong, M., Zheng, L., Fei, M., Zhao, X., Wang, J., Cui, Y., Liu, H., Cai, J., Gong, S., Wang, H. & Hong, F. 2010. Spleen injury and apoptotic pathway in mice caused by titanium dioxide nanoparticules. Toxicology Letters, 195, 161-168.

Li, S.-D. & Huang, L. 2008. Pharmacokinetics and Biodistribution of Nanoparticles. Molecular Pharmaceutics, 5, 496-504.

Liang, G., Pu, Y., Yin, L., Liu, R., Ye, B., Su, Y. & Li, Y. 2009. Influence of different sizes of titanium dioxide nanoparticles on hepatic and renal functions in rats with correlation to oxidative stress. Journal of Toxicology and Environmental Health, Part A, 72, 740-745.

Linder, M. C., Moriya, M., Whon, A., Kassa, A. & Gilley, C. 2006. Vesicular transport of Fe and interaction with other metal ions in polarized Caco-2 Cell monolayers. Biological Research, 143-156.

Liu, Q., Hong, Z., Guo, B., Zhang, Y., Li, Y. & Liu, J. 2006. Experimental study on toxicity of nanosized titanium dioxide. Modern Preventive Medicine, 33, 1211 - 1212.

Liu, R., Yin, L., Pu, Y., Liang, G., Zhang, J., Su, Y., Xiao, Z. & Ye, B. 2009. Pulmonary toxicity induced by three forms of titanium dioxide nanoparticles via intra-tracheal instillation in rats. Progress in Natural Science, 19, 573-579.

Liu, H., Ma, L., Zhao, J., Liu, J., Yan, J., Ruan, J. & Hong, F. 2009. Biochemical Toxicity of Nano-anatase TiO_2 Particles in Mice. Biological Trace Element Research, 129, 170-180.

Lomer, M., Thompson, R. & Powell, J. 2002a. Fine and ultrafine particles of the diet: influence on the mucosal immune response and association with Crohn's disease. Proceedings of the Nutrition Society, 61, 123 - 130.

Lomer, M. C. E., Thompson, R. P. H., Commisso, J., Keen, C. L. & Powell, J. J. 2000. Determination of titanium dioxide in foods using inductively coupled plasma optical emission spectrometry. Analyst, 125, 2339-2343.

Lovestam, G., Rauscher, H., Roebben, G., Kluttgen, B., Gibson, N., Putaud, J. & Stamm, H. 2010. Considerations on a definition of nanomaterial for regulatory purposes. In: Joint-Research-Centre (ed.). Publications office of the European Union.

Luche, J. L. 1996. Synthetically useful sonochemical reaction in solution. Ultrasonics sonochemistry, 3, 215-221.

Ma, L., Liu, J., Li, N., Wang, J., Duan, Y., Yan, J., Liu, H., Wang, H. & Hong, F. 2010. Oxidative stress in the brain of mice caused by translocated nanoparticulate TiO_2 delivered to the abdominal cavity. Biomaterials, 31, 99-105.

Martinsson, K. & L, J. 1975. On the mechanism of intestinal absorption of macromolecules in piglats studies with dextran blue. Zentralbl Veterinarmed A, 22, 276-282.

Mcdonald, C. 2009. Methods of protein analysis and variation in protein results.

Mcwilliams, A. 2010. Nanotechnology: A realistic market assessment [Online]. Available: http://www.bccresearch.com/report/NAN031D.html [Accessed 13/10 2010].

Mebius, R. E. & Kraal, G. 2005. Structure and function of the spleen. Nature Reviews Immunology, 5, 606-616.

Medina, C., Santos-Martinez, M. J., Radomski, A., Corrigan, O. I. & Radomski, M. W. 2007. Nanoparticles: pharmacological and toxicological significance. British Journal of Pharmacology, 150, 552-558.

Meng Tang, Ting Zhang, Yuying Xue, Shu Wang, Mingming Huang, Yang Yang, Minyu Lu, Hao Lei, Lu Kong, Yiqing Wang & Pu, Y. 2011. Metabonomic studies of biochemical changes in the serum of rats by intratracheally instilled TiO_2 nanoparticles. Journal of Nanoscience and Nanotechnology, 11, 3065-74.

Miller, G. & Senjen, R. 2008. Out of the Laboratory and on to our Plate. 2nd ed.: Friends of the Earth.

Missiaen, L., Dode, L., Vanoevelen, J., Raeymaekers, L. & Wuytack, F. 2007. Calcium in the Golgi apparatus. Cell Calcium, 41, 405-416.

Moon, E.-Y., Yi, G.-H., Kang, J.-S., Lim, J.-S., Kim, H.-M. & Pyo, S. 2011. An increase in mouse tumor growth by an in vivo immunomodulating effect of titanium dioxide nanoparticles. Journal of immunotoxicology, 8, 56-67.

Moriya, M. & Linder, M. C. 2006. Vesicular transport and apotransferrin in intestinal iron absorption, as shown in the Caco-2 cell model. American Journal of Physiology-Gastrointestinal and Liver Physiology, 290, G301-G309.

Murray, R., Rodwell, V., Bender, D., Botham, K. M., Weil, P. A. & Kennelly, P. J. 2009. Harper's Illustrated Biochemistry, 28th Edition, McGraw-Hill Education.

Nazir, S., Hussain, T., Ayub, A., Rashid, U. & Macrobert, A. J. 2014. Nanomaterials in combating cancer: Therapeutic applications and developments. Nanomedicine: Nanotechnology, Biology and Medicine, 10, 19-34.

Nemmar, A., Hoet, P. M., Vanquickenborne, B., Dinsdale, D., Thomeer, M., Hoylaerts, M., Vanbilloen, H., Mortelmans, L. & Nemery, B. 2002. Passage of inhaled particles into the blood circulation in humans. Circulation, 105, 411-414.

Nemmar, A., Melghit, K., Al-Salam, S., Zia, S., Dhanasekaran, S., Attoub, S., Al-Amri, I. & Ali, B. H. 2011. Acute respiratory and systemic toxicity of pulmonary exposure to rutile Fe-doped TiO_2 nanorods. Toxicology, 279, 167-175.

Newcomer, C. E., Fitts, A. D., Goldman, B. D., Murphy, M. R., Rao, G. N., Shklar, G. & Schwartz, J. L. 1987. Experimental Biology: Other Research Uses of Syrian Hamsters, Orlando Florida, Academic Press.

Niwa, M., Hirayama, T., Okuda, K. & Nagasawa, H. 2014. A new class of high-contrast Fe (ii) selective fluorescent probes based on spirocyclized scaffolds for

visualization of intracellular labile iron delivered by transferrin. Organic & biomolecular chemistry, 12, 6590-6597.

Norris, D. A. & Sinko, P. J. 1997. Effect of size, surface charge, and hydrophobicity on the translocation of polystyrene microspheres through gastrointestinal mucin. Journal of Applied Polymer Science, 63, 1481-1492.

Nucifora, P. G. & Fox, A. P. 1999. Tyrosine phosphorylation regulates rapid endocytosis in adrenal chromaffin cells. The Journal of neuroscience, 19, 9739-9746.

Nurkiewicz, T., Porter, D., Hubbs, A., Cumpston, J., Chen, B., Frazer, D. & Castranova, V. 2008. Nanoparticle inhalation augments particle-dependent systemic microvascular dysfunction. Particle Fibre Toxicology, 5, 1.

O'hagan, D. 1996. The intestinal uptake of particles and the implications for drug and antigen delivery. Journal of anatomy, 189, 477.

Oberdorster, G., Ferin, J. & Jehnert, B. 1994. Correlation between particle size, in vivo particle persistence, and lung injury. Environmental Health Perspectives, 102, 173-179.

Oberdorster, G., Maynard, A., Donaldson, K., Castranova, V., Fitzpatrick, J., Ausman, K., Carter, J., Karn, B., Kreyling, W., Lai, D., Olin, S., Monteiro-Riviere, N., Warheit, D., Yang, H. 2005. Principles for characterizing the potential human health effects from exposure to nanomaterials: elements of a screening strategy. Particle and Fibre Toxicology, 2, 8.

Oberdörster, G., Sharp, Z., Atudorei, V., Elder, A., Gelein, R., Kreyling, W. & Cox, C. 2004. Translocation of inhaled ultrafine particles to the brain. Inhalation Toxicology, 16, 437-445.

Olmsted, S. S., Padgett, J. L., Yudin, A. I., Whaley, K. J., Moench, T. R. & Cone, R. A. 2001. Diffusion of macromolecules and virus-like particles in human cervical mucus. Biophysical journal, 81, 1930-1937.

Onishchenko, G., Erokhina, M., Abramchuk, S., Shaitan, K., Raspopov, R., Smirnova, V., Vasilevskaya, L., Gmoshinski, I., Kirpichnikov, M. & Tutelyan, V. 2012. Effects of titanium dioxide nanoparticles on small intestinal mucosa in rats. Bulletin of experimental biology and medicine, 154, 265-270.

Otberg, N., Patzelt, A., Rasulev, U., Hagemeister, T., Linscheid, M., Sinkgraven, R., Sterry, W. & Lademann, J. 2008. The role of hair follicles in the percutaneous absorption of caffeine. British journal of clinical pharmacology, 65, 488-492.

Otsu, N. 1979. A Threshold selection method from gray-Level histograms, 9, 62-66.

Pan, Y.H., Sader, K., Powell, J. J., Bleloch, A., Gass, M., Trinick, J., Warley, A., Li, A., Brydson, R. & Brown, A. 2009. 3D morphology of the human hepatic ferritin mineral core: New evidence for a subunit structure revealed by single particle analysis of HAADF-STEM images. Journal of Structural Biology, 166, 22-31.

Panessa-Warren, B., Warren, J., Wong, S. & Misewich, J. 2006. Biological cellular response to carbon nanoparticle toxicity. Journal of Physics: Condensed Matter, 18, S2185.

Palomäki, J., Karisola, P., Pylkkänen, L., Savolainen, K. & Alenius, H. 2010. Engineered nanomaterials cause cytotoxicity and activation on mouse antigen presenting cells. Toxicology, 267, 125-131.

Parton, R. G., Joggerst, B. & Simons, K. 1994. Regulated internalization of caveolae. The Journal of cell biology, 127, 1199-1215.

Parton, R. G. & Richards, A. A. 2003. Lipid rafts and caveolae as portals for endocytosis: new insights and common mechanisms. Traffic, 4, 724-738.

Parton, R. G. & Simons, K. 2007. The multiple faces of caveolae. Nature Review Molecular Cell Biology, 8, 185-194.

Patri, A., Umbreit, T., Zheng, J., Nagashima, K., Goering, P., Francke-Carroll, S., Gordon, E., Weaver, J., Miller, T. & Sadrieh, N. 2009. Energy dispersive X-ray analysis of titanium dioxide nanoparticle distribution after intravenous and subcutaneous injection in mice. Journal of Applied Toxicology, 29, 662 - 672.

Peterson, M. D., Bement, W. M. & Mooseker, M. S. 1993. An *in vitro* model for the analysis of intestinal brush border assembly. II. Changes in expression and localization of brush border proteins during cell contact-induced brush border assembly in Caco-2BBe cells. Journal of Cell Science, 105, 461-472.

Peterson, M. D. & Mooseker, M. S. 1992. Characterization of the enterocyte-like brush border cytoskeleton of the C2BBe clones of the human intestinal cell line, Caco-2. Journal of Cell Science, 102, 581-600.

Pflucker, F., Wendel, V., Hohenberg, H., Gartner, E., Will, T., Pfeiffer, S., Wepf, R. & Gers-Barlag, H. 2001. The human stratum corneum layer: an effective barrier against dermal uptake of different forms of topically applied micronised titanium dioxide. Skin Pharmacol Appl Skin Physiol, 14, 92 - 97.

Pohl, C., Hermanns, M. I., Uboldi, C., Bock, M., Fuchs, S., Dei-Anang, J., Mayer, E., Kehe, K., Kummer, W. & Kirkpatrick, C. J. 2009. Barrier functions and paracellular integrity in human cell culture models of the proximal respiratory unit. European Journal of Pharmaceutics and Biopharmaceutics, 72, 339-349.

Powell, J. J., Ainley, C. C., Harvey, R. S., Mason, I. M., Kendall, M. D., Sankey, E. A., Dhillion, A. P. & Thompson, R. P. 1996. Characterisation of inorganic microparticles in pigment cells of human gut associated lymphoid tissue. GUT, 38, 390-395.

Powell, J. J., Faria, N., Thomas-Mckay, E. & Pele, L. C. 2010. Origin and fate of dietary nanoparticles and microparticles in the gastrointestinal tract. Journal of Autoimmunity, 34, J226-J233.

Powell, J. J., Harvey, R. S. J., Ashwood, P., Wolstencroft, R., Gershwin, M. E. & Thompson, R. P. H. 2000. Immune potentiation of ultrafine dietary particles in normal subjects and patients with inflammatory bowel disease. Journal of Autoimmunity, 14, 99-105.

Prunescu, C.C., Serban-Parau, N., Brock, J. H., Vaughan, D. M. & Prunescu, P. 2003. Liver and kidney structure and iron content in romanian brown bears (Ursus arctos) before and after hibernation. Comparative Biochemistry and Physiology Part A: Molecular & Integrative Physiology, 134, 21-26.

Quant, C. A., Marla, K. T. & Meredith, J. C. 2008. Osmotic pressure and chemical potential of silica nanoparticles in aqueous poly(ethyleneoxide) solution. Colloids and Surfaces A: Physicochemical and Engineering Aspects, 317, 129-135.

Que, E. L., Domaille, D. W. & Chang, C. J. 2008. Metals in neurobiology: probing their chemistry and biology with molecular imaging. Chemical Reviews, 108, 1517-1549.

Ramsden, C., Smith, T., Shaw, B. & Handy, R. 2009. Dietary exposure to titanium dioxide nanoparticles in rainbow trout, (*Oncorhynchus mykiss*): no effect on growth, but subtle biochemical disturbances in the brain. Ecotoxicology, 18, 939-951.

Rankin, J. C. & Davenport, J. A. 1981. Animal Osmoregulation, London, Blackie and Son.

Rao, P. 2009. Influence of dietary calcium content on intestinal permeability in rat. Indian Journal of Medical Research, 129, 681-684.

Razani, B., Woodman, S. E. & Lisanti, M. P. 2002. Caveolae: from cell biology to animal physiology. Pharmacological reviews, 54, 431-467.

Rejman, J., Oberle, V., Zuhorn, I. S. & Hoekstra, D. 2004. Size-dependent internalization of particles via the pathways of clathrin- and caveolae-mediated endocytosis. Biochemical Journal, 377, 159-169.

Renwick, L. C., Brown, D., Clouter, A. & Donaldson, K. 2004. Increased inflammation and altered macrophage chemotactic responses caused by two ultrafine particle types. Occupational and Environmental Medicine, 61, 442-447.

Rivera Gil, P., Oberdörster, G., Elder, A., Puntes, V. & Parak, W. J. 2010. Correlating physico-chemical with toxicological properties of nanoparticles: The Present and the Future. ACS Nano, 4, 5527-5531.

Roberts, S. B. & Rosenberg, I. 2006. Nutrition and Aging: Changes in the regulation of energy metabolism with aging. Physiological Reviews, 86, 651-667.

Roco, M. & Bainbridge, W. 2001. Societal Implications of Nanoscience and Nanotechnology, Boston, Kluwer Academic.

Roco, M. C. 2007. National nanotechnology initiative-past, present, future. Handbook on nanoscience, engineering and technology, 2.

Romani, A. & Scarpa, A. 1992. Regulation of cell magnesium. Archives of biochemistry and biophysics, 298, 1-12.

Ros-Baró, A., López-Iglesias, C., Peiró, S., Bellido, D., Palacín, M., Zorzano, A. & Camps, M. 2001. Lipid rafts are required for GLUT4 internalization in adipose cells. Proceedings of the National Academy of Sciences, 98, 12050-12055.

Rossi, E., Koivisto, A., Vippopa, M., Jensen, K., Miettinen, M., Sirola, K., Nykasenoja, H., Karisola, P., Stjernvall, T., Vanhala, E., Kiilunen, M., Pasanen, P., Makinen, M., Hameri, K., Joutsensaari, J., Tuomi, T., Jokiniemi, J., Wolff, H., Savolainen, K., Matikainen, S. & Alenius, H. 2010. Airway exposure to silica-coated TiO_2 nanoparticles induces pulmonary neutrophilia in mice. Toxicological Sciences, 113, 422 - 433.

Rothen-Rutishauser, B., Schurch, S., Haenni, B., Kapp, N. & Gehr, P. 2006. Interaction of fine particles and nanoparticles with red blood cells visualized with advanced microscopic techniques. Environmental Science and Technology, 40, 4353 - 4359.

Ryabchikova, E. I., Mazurkova, N. A., Shikina, N. V. & Ismagilov, Z. R. 2010. The crystalline forms of titanium dioxide nanoparticles affect their interactions with individual cells. Journal of Medical Chemical, Biological and Radiological Defense, 8.

Sager, T., Kommineni, C. & Castranova, V. 2008. Pulmonary response to intratracheal instillation of ultrafine versus fine titanium dioxide: role of particle surface area. Particle and Fibre Toxicology, 5, 17.

Saladin, K. S. 2009. Anatomy and Physiology: The unit of form and function, McGraw-Hill.

Salaün, C., James, D. J. & Chamberlain, L. H. 2004. Lipid rafts and the regulation of exocytosis. Traffic, 5, 255-264.

Saltzman, W. M., Radomsky, M. L., Whaley, K. J. & Cone, R. A. 1994. Antibody diffusion in human cervical mucus. Biophysical journal, 66, 508-515.

Sanderson, I. R. & Walker, W. A. 1993. Uptake and transport of macromolecules by the intestine: possible role in clinical disorders (an update). Gastroenterology, 104, 622 - 639.

Sang, X., Fei, M., Sheng, L., Zhao, X., Yu, X., Hong, J., Ze, Y., Gui, S., Sun, Q., Ze, X., Wang, L. & Hong, F. 2013. Immunomodulatory effects in the spleen-injured mice following exposure to titanium dioxide nanoparticles. Journal of Biomedical Materials Research Part A, 102, 3562-3572.

Sayes, C., Wahi, R., Kurian, P., Liu, Y., West, J., Ausman, K., Warheit, D. & Colvin, V. 2006. Correlating nanoscale titania structure with toxicity: a cytotoxicity and inflammatory response study with human dermal fibroblasts and human lung epithelial cells. Toxicological Sciences, 92, 174 - 185.

Schaefer, A. E., Sassaman, H. L., Slocum, A. & Greene, R. D. 1955. Absorbtion of topically applied vitamins. Journal of Nutrition, 59, 171-179

Schmidt, J. & Vogelsberger, W. 2009. Aqueous long-term solubility of titania nanoparticles and titanium(IV) hydrolysis in a sodium chloride system studied by adsorptive stripping voltammetry. Journal of Solution Chemistry, 38, 1267-1282.

Selloni, A., Vittadini, A. & Grätzel, M. 1998. The adsorption of small molecules on the TiO_2 anatase (101) surface by first-principles molecular dynamics. Surface Science, 402–404, 219-222.

Shannon, R. T. 1976. Revised effective ionic radii and systematic studies of interatomic distances in halides and chalcogenides. Acta Crystallographica Section A: Crystal Physics, Diffraction, Theoretical and General Crystallography, 32, 751-767.

Shaw, B. J. & Handy, R. D. 2011. Physiological effects of nanoparticles on fish: A comparison of nanometals versus metal ions. Environment International, 37, 1083-1097.

Shaw, B. J., Ramsden, C. S., Turner, A. & Handy, R. D. 2013. A simplified method for determining titanium from TiO_2 nanoparticles in fish tissue with a concomitant multi-element analysis. Chemosphere, 92, 1136-1144.

Shi, H., Magaye, R., Castranova, V. & Zhao, J. 2013. Titanium dioxide nanoparticles: a review of current toxicological data. Particle and Fibre Toxicology, 10, 15.

Shimizu, M., Tainaka, H., Oba, T., Mizuo, K., Umezawa, M. & Takeda, K. 2009. Maternal exposure to nanoparticulate titanium dioxide during the prenatal period alters gene expression related to brain development in the mouse. Particle and Fibre Toxicology, 6, 20.

Shinohara, N., Danno, N., Ichinose, T., Sasaki, T., Fukui, H., Honda, K. & Gamo, M. 2012. Tissue distribution and clearance of intravenously administered titanium dioxide (TiO_2) nanoparticles. Nanotoxicology, 8, 132-141.

Schmid, R. & Sapunov, V. N. 1982. Non-formal kinetics: in search for chemical reaction pathways, Verlag Chemie.

Shoemaker, C., Klesius, P., Lim, C. & Yildirim, M. 2003. Feed deprivation of channel catfish, Ictalurus punctatus (Rafinesque), influences organosomatic indices,

chemical composition and susceptibility to Flavobacterium columnare. Journal of fish diseases, 26, 553-561.

Silva, L., Coutinho, A., Fedorov, A. & Prieto, M. 2006. Competitive Binding of Cholesterol and Ergosterol to the Polyene Antibiotic Nystatin. A Fluorescence Study. Biophysical journal, 90, 3625-3631.

Simon, M., Barberet, P., Delville, M.-H., Moretto, P. & Seznec, H. 2010. Titanium dioxide nanoparticles induced intracellular calcium homeostasis modification in primary human keratinocytes. Towards an *in vitro* explanation of titanium dioxide nanoparticles toxicity. Nanotoxicology, 5, 125-139.

Singh, S., Shi, T., Duffin, R., Albrecht, C., Van Berlo, D., Höhr, D., Fubini, B., Martra, G., Fenoglio, I. & Borm, P. J. 2007. Endocytosis, oxidative stress and IL-8 expression in human lung epithelial cells upon treatment with fine and ultrafine TiO_2: role of the specific surface area and of surface methylation of the particles. Toxicology and Applied Pharmacology, 222, 141-151.

Soldati, T. & Schliwa, M. 2006. Powering membrane traffic in endocytosis and recycling. Nature Reviews Molecular Cell Biology, 7, 897-908.

Sonnier, D. I., Bailey, S. R., Pritts, T. A. & Lentsch, A. B. 2011. TNF-α induced vectorial secretion of IL-8 corresponds to development of transepithelial electrical resistance in Caco-2 Cells. Gastroenterology, 140, S-1044-S-1045.

Stone, V., Nowack, B., Baun, A., Van Den Brink, N., Von Der Kammer, F., Dusinska, M., Handy, R., Hankin, S., Hassellöv, M., Joner, E. & Fernandes, T. F. 2010. Nanomaterials for environmental studies: Classification, reference material issues,

and strategies for physico-chemical characterisation. Science of The Total Environment, 408, 1745-1754.

Sukhija, P. S. & Palmquist, D. L. 1988. Rapid method for determination of total fatty acid content and composition of feedstuffs and faeces. Journal of Agricultural and Food Chemistry, 36, 1202-1206.

Sul, Y. 2010. Electrochemical growth behavior, surface properties, and enhanced in vivo bone response of TiO_2 nanotubes on microstructured surfaces of blasted, screw-shaped titanium implants. International Journal of Nanomedicine, 87-100.

Swirski, F. K., Nahrendorf, M., Etzrodt, M., Wildgruber, M., Cortez-Retamozo, V., Panizzi, P., Figueiredo, J.L., Kohler, R. H., Chudnovskiy, A., Waterman, P., Aikawa, E., Mempel, T. R., Libby, P., Weissleder, R. & Pittet, M. J. 2009. Identification of splenic reservoir monocytes and their deployment to inflammatory sites. Science, 325, 612-616.

Sycheva, L. P., Zhurkov, V. S., Iurchenko, V. V., Daugel-Dauge, N. O., Kovalenko, M. A., Krivtsova, E. K. & Durnev, A. D. 2011. Investigation of genotoxic and cytotoxic effects of micro- and nanosized titanium dioxide in six organs of mice *in vivo*. Mutation Research/ Genetic Toxicology and Environmental Mutagenesis, 726, 8-14.

Szentkuti, L. 1997. Light microscopical observations on luminally administered dyes, dextrans, nanospheres and microspheres in the pre epithelial mucus gel layer of the rat distal colon. Journal of Controlled Release, 46, 233-242.

Takeda, K. 2009. Nanoparticles transferred from pregnant mice to their offspring can damage the genital and cranial nerve systems. Journal of Health Science, 55, 95-102.

Tassinari, R., Cubadda, F., Moracci, G., Aureli, F., D'amato, M., Valeri, M., De Berardis, B., Raggi, A., Mantovani, A., Passeri, D., Rossi, M. & Maranghi, F. 2014. Oral, short-term exposure to titanium dioxide nanoparticles in Sprague-Dawley rat: focus on reproductive and endocrine systems and spleen. Nanotoxicology, 8, 654-662.

Terao, T. & Owen, C. A. 1977. Copper metabolism in pregnant and pospartum rat and pups. American Journal of Physiology - Endocrinology and Metabolism, 232, E172.

Thomsen, V., Schatzlein, D. & Mercuro, D. 2003. Limits of detection in spectroscopy. Spectroscopy, 18, 112-114.

Tiede, K., Boxall, A. B., Tear, S. P., Lewis, J., David, H. & Hassellöv, M. 2008. Detection and characterization of engineered nanoparticles in food and the environment. Food Additives and Contaminants, 25, 795-821.

Torgersen, M. L., Skretting, G., Van Deurs, B. & Sandvig, K. 2001. Internalization of cholera toxin by different endocytic mechanisms. Journal of Cell Science, 114, 3737-3747.

Trouiller, B., Reliene, R., Westbrook, A., Solaimani, P. & Schiestl, R. 2009. Titanium dioxide nanoparticles induce DNA damage and genetic instability in vivo in mice. Cancer Research, 69, 8784 - 8789.

European Union. 2003. Regulation (EC) No. 1831/2003 of the European Parliament and of the Council on additives for use in animal nutrition.

Ussing, H. H. 1982. Volume regulation of frog skin epithelium. Acta Physiologica Scandinavica, 114, 363-369.

Van Bruggen, J. T., Chalmers, B. & Muller, M. 1982. Effects of solvent and solute drag on transmembrane diffusion. Journal of General Physiology, 79, 507-528.

Van Der Aa, M., Huth, U., Häfele, S., Schubert, R., Oosting, R., Mastrobattista, E., Hennink, W., Peschka-Süss, R., Koning, G. & Crommelin, D. 2007. Cellular uptake of cationic polymer-DNA complexes via caveolae plays a pivotal role in gene transfection in COS-7 cells. Pharmaceutical research, 24, 1590-1598.

Van Ravenzwaay, B., Landsiedel, R., Fabian, E., Burkhardt, S., Strauss, V. & Ma-Hock, L. 2009. Comparing fate and effects of three particles of different surface properties: Nano-TiO_2, pigmentary TiO_2 and quartz. Toxicology Letters, 186, 152-159.

Vance, T. M., Su, J., Fontham, E. T. H., Koo, S. I. & Chun, O. K. 2013. Dietary Antioxidants and Prostate Cancer: A Review. Nutrition and Cancer, 65, 793-801.

Vittadini, A., Casarin, M. & Selloni, A. 2010. Hydroxylation of TiO_2-B: insights from density functional calculations. Journal of Materials Chemistry, 20, 5871-5877.

Vittadini, A., Selloni, A., Rotzinger, F. P. & Grätzel, M. 1998. Structure and Energetics of Water Adsorbed at TiO_2 anatase \(101) and (001) surfaces. Physical Review Letters, 81, 2954-2957.

Wang, B., Feng, W., Wang, M., Wang, T., Gu, Y., Zhu, M., Ouyang, H., Shi, J., Zhang, F. & Zhao, Y. 2008a. Acute toxicological impact of nano-and submicro-scaled zinc oxide powder on healthy adult mice. Journal of Nanoparticle Research, 10, 263-276.

Wang, J., Fan, Y.B., Gao, Y., Hu, Q.H. & Wang, T.C. 2009. TiO2 nanoparticles translocation and potential toxicological effect in rats after intraarticular injection. Biomaterials, 30, 4590-4600.

Wang, J., Chen, C., Liu, Y., Jia, F., Li, W., Lao, F., Lia, Y., Lia, B., Ge, C. & Zhou, G. 2008b. Potential neurological lesion after nasal instillation of TiO_2 nanoparticles in the anatase and rutile crystal phases. Toxicol Lett, 183, 72 - 80.

Wang, J., Li, N., Zheng, L., Wang, S., Wang, Y., Zhao, X., Duan, Y., Cui, Y., Zhou, M. & Cai, J. 2011. P38-Nrf-2 signaling pathway of oxidative stress in mice caused by nanoparticulate TiO_2. Biological Trace Element Research, 140, 186 - 197.

Wang, J., Li, Y., Zhou, G., Li, B., Jiao, F., Chen, C., Gao, Y., Zhao, Y. & Chai, Z. 2007a. Influence of intranasal instilled titanium dioxide nanoparticles on monoaminergic neurotransmitters of female mice at different exposure time. Chinese Journal of Preventitive medicine, 41, 91 - 95.

Wang, J., Zhou, G., Chen, C., Yu, H., Wang, T., Ma, Y., Jia, G., Gao, Y., Li, B. & Sun, J. 2007b. Acute toxicity and biodistribution of different sized titanium dioxide particles in mice after oral administration. Toxicology Letters, 168, 176 - 185.

Wang, L.H., Rothberg, K. G. & Anderson, R. 1993. Mis-assembly of clathrin lattices on endosomes reveals a regulatory switch for coated pit formation. The Journal of cell biology, 123, 1107-1117.

Wang, Y., Chen, Z., Ba, T., Pu, J., Chen, T., Song, Y., Gu, Y., Qian, Q., Xu, Y., Xiang, K., Wang, H. & Jia, G. 2013. Susceptibility of young and adult rats to the oral toxicity of titanium dioxide nanoparticles. Small, 9, 1742-52.

Wapnir, R. A. 1991. Copper-Sodium Linkage during Intestinal Absorption: Inhibition by Amiloride. Experimental Biology and Medicine, 196, 410-414.

Warheit, D., Webb, T., Reed, K., Frerichs, S. & Sayes, C. 2007. Pulmonary toxicity study in rats with three forms of ultrafine-TiO_2 particles: differential responses related to surface properties. Toxicology, 230, 90 - 104.

Weir, A., Westerhoff, P., Fabricius, L., Hristovski, K. & Von Goetz, N. 2012. Titanium dioxide nanoparticles in food and personal care products. Environmental Science and Technology, 46, 2242 - 2250.

Westerhoff, P., Song, G., Hristovski, K. & Kiser, M. A. 2011. Occurrence and removal of titanium at full scale wastewater treatment plants: implications for TiO_2 nanomaterials. Journal of Environmental Monitoring, 13, 1195-1203.

WHO. 1982. Environmental Health Criteria 24-Titanium. International Programme on Chemical Safety.

Wodnicka, M. C. & Burridge, K. 1994. Tyrosine phosphorylation is involved in reorganization of the actin cytoskeleton in response to serum or LPA stimulation. Journal of Cell Science, 107, 3643-3654.

Wong, K.L., Cachia, R. & Klaassen, C. D. 1980. Comparison of the toxicity and tissue distribution of cadmium in newborn and adult rats after repeated administration. Toxicology and Applied Pharmacology, 56, 317-325.

Wood, C. M., Gilmour, K. M. & Pärt, P. 1998. Passive and active transport Properties of a gill Model, the cultured branchial epithelium of the freshwater rainbow trout (*Oncorhynchus mykiss*). Comparative Biochemistry and Physiology Part A: Molecular & Integrative Physiology, 119, 87-96.

Woodrow-Wilson-Institute. 2014. The project on emerging nanotechnologies-Consumer products inventory [Online]. Available: http://www.nanotechproject.org/cpi/ [Accessed 13/09/2014 2014].

Wu, J., Liu, W., Xue, C., Zhou, S., Lan, F., Bi, L., Xu, H., Yang, X. & Zeng, F. 2009. Toxicity and penetration of TiO_2 nanoparticles in hairless mice and porcine skin after subchronic dermal exposure. Toxicology Letters, 191, 1 - 8.

Xia, T., Rome, L. & Nel, A. 2008. Nanobiology: Particles slip cell security. Nature Materials, 7, 519-520.

Xiao-E, L., Green, A. N., Haque, S. A., Mills, A. & Durrant, J. R. 2004. Light-driven oxygen scavenging by titania/polymer nanocomposite films. Journal of Photochemistry and Photobiology A: Chemistry, 162, 253-259.

Yamashita, K., Yoshioka, Y., Higashisaka, K., Mimura, K., Morishita, Y., Nozaki, M., Yoshida, T., Ogura, T., Nabeshi, H. & Nagano, K. 2011. Silica and titanium dioxide nanoparticles cause pregnancy complications in mice. Nature Nanotechnology, 6, 321-328.

Yamashita, S., Konishi, K., Yamazaki, Y., Taki, Y., Sakane, T., Sezaki, H. & Furuyama, Y. 2002. New and better protocols for a short term Caco-2 cell culture system. Journal of pharmaceutical sciences, 91, 669-679.

Yang, Y., Doudrick, K., Bi, X., Hristovski, K., Herckes, P., Westerhoff, P. & Kaegi, R. 2014. Characterization of food-grade titanium dioxide: The presence of nanosized particles. Environmental Science & Technology, 48, 6391-6400.

Zerounian, N. R. & Linder, M. C. 2002. Effects of copper and ceruloplasmin on iron transport in the Caco-2 cell intestinal model. The Journal of Nutritional Biochemistry, 13, 138-148.

Zhang, L. W. & Monteiro-Riviere, N. A. 2009. Mechanisms of quantum dot nanoparticle cellular uptake. Toxicological Sciences, 110, 138-155.

Zuskin, E., Kanceljak, B., Schachter, E. N., Godnic ‐ Cvar, J., Mustajbegovic, J. & Budak, A. 1998. Respiratory function and immunological status in cocoa and flour processing workers. American journal of industrial medicine, 33, 24-32.